An examination of default network organization, function, and pharmacological sensitivity

Manesh Girn
McGill University, Montreal
Integrated Program in Neuroscience

June 2023

A thesis submitted to McGill University in partial fulfillment of the requirements of the degree of Doctor of Philosophy.

Table of Contents

Abstract

The brain can be characterized as a set of large-scale functional networks which interact on multiple spatial and temporal scales to give rise to perception, cognition, and behaviour. Among the most studied of the large-scale networks is the so-called 'default network'. This distributed network, initially borne out of the observation of reduced activation during cognitive tasks and later characterized using resting-state functional connectivity (RSFC) methods, spans the frontal, parietal, and temporal lobes and is implicated in a variety of complex cognitive functions. Despite nearly two decades of research on the DN, however, there is still debate on (1) its precise organization, particularly as relates to its relationship to the putative 'limbic network', (2) the nature of its subsystem organization and subsystem-specific contributions to behaviour and cognition, and (3) the stability of the DN's functional organization and whole-brain RSFC in response to pharmacological manipulations. The present thesis is comprised by three studies, each of which tackles one of these outstanding questions.

Study 1 leveraged the superior temporal signal-to-noise ratio of multi-echo resting-state functional magnetic resonance imaging to evaluate the rightful inclusion of regions comprising the limbic network within the default network. Consistent with our hypotheses, data-driven modularity analyses indicated that a large proportion of regions within the limbic network may indeed be extensions of the DN. RSFC mapping and clustering analyses further revealed significant heterogeneity within the limbic network, with distinct clusters exhibiting distinct patterns of large-scale (sub)network connectivity.

Study 2 applied multivariate analyses to a resting-state multi-echo fMRI dataset with rich behavioural phenotyping in order to assess how DN subsystems – alongside limbic and temporoparietal networks, as motivated by the results of Study 1 – uniquely and differentially contribute to individual differences in a broad constellation of traits, behaviours, and cognitive processes. Multivariate analyses revealed complex associations between measures of DN subsystem, limbic, and temporoparietal structure and function, and behaviour. Consistent with our hypotheses, each axis of brain-behaviour covariance featured differential contributions from the

examined (sub)networks, with evidence for functional selectivity that converges with and goes beyond past task-based fMRI research.

Study 3 evaluated whether DN functional organization and relationship to other large-scale networks was significantly altered by psychedelic drug administration. This study leveraged two previously published pharmaco-fMRI datasets collected with serotonergic psychedelic drugs. A combination of novel gradient- and RSFC- mapping analyses were applied to assess changes in DN and macroscale cortical organization in the psychedelic state. Consistent with our hypotheses, results revealed that the principal axis of macroscale cortical organization – delineating a gradient from unimodal cortex (anchored in sensorimotor networks) to transmodal cortex (anchored within the DN) – was significantly attenuated in the psychedelic state. Analyses further indicated that this was underpinned by a break-down of intra-network RSFC in sensorimotor networks and increased RSFC between the DN and sensorimotor networks.

The studies of this thesis offer novel findings on multiple core aspects of the DN: its functional organization, relationship to individual differences in cognition and behaviour, and its pharmacological sensitivity. Collectively, the results provide a significant contribution towards the advancement of theoretical perspectives and empirical approaches on the DN and large-scale brain function more generally.

Résumé

Le cerveau peut être caractérisé comme un ensemble de réseaux fonctionnels à grande échelle qui interagissent à de multiples échelles spatiales et temporelles pour donner naissance à la perception, à la cognition et au comportement. Parmi les réseaux à grande échelle les plus étudiés, on trouve le "réseau par défaut". Ce réseau distribué, né initialement de l'observation d'une activation réduite lors de tâches cognitives et caractérisé par la suite à l'aide de méthodes de connectivité fonctionnelle à l'état de repos (RSFC), s'étend sur les lobes frontaux, pariétaux et temporaux et est impliqué dans une variété de fonctions cognitives complexes. Cependant, malgré près de deux décennies de recherche sur le DN, des débats subsistent sur (1) son organisation précise, en particulier en ce qui concerne sa relation avec le supposé "réseau limbique", (2) la nature de l'organisation de ses sous-systèmes et les contributions spécifiques de ces sous-systèmes au comportement et à la cognition, et (3) la stabilité de l'organisation fonctionnelle du DN et de la RSFC du cerveau entier en réponse à des manipulations pharmacologiques. La présente thèse comprend trois études, chacune abordant l'une de ces questions en suspens.

L'étude 1 s'est appuyée sur le rapport signal-bruit temporel supérieur de l'imagerie par résonance magnétique fonctionnelle multiéchogène à l'état de repos pour évaluer l'inclusion légitime des régions du réseau limbique dans le réseau par défaut. Conformément à nos hypothèses, les analyses de modularité basées sur les données ont indiqué qu'une grande partie des régions du réseau limbique peuvent en effet être des extensions du réseau par défaut. Les analyses de cartographie et de regroupement du RSFC ont en outre révélé une hétérogénéité significative au sein du réseau limbique, avec des regroupements distincts présentant des schémas distincts de connectivité (sous-)réseau à grande échelle.

L'étude 2 a appliqué des analyses multivariées à un ensemble de données d'IRMf multiéchogène à l'état de repos avec un phénotypage comportemental riche afin d'évaluer comment les sous-systèmes du DN - parallèlement aux réseaux limbiques et temporo-pariétaux, comme motivé par les résultats de l'étude 1 - contribuent de manière unique et différenciée aux différences individuelles dans une vaste constellation de traits, de comportements et de processus cognitifs. Les analyses multivariées ont révélé des associations complexes entre les mesures du sous-

système DN, la structure et la fonction limbique et temporo-pariétale, et le comportement. Conformément à nos hypothèses, chaque axe de covariance cerveau-comportement présentait des contributions différentielles des (sous-)réseaux examinés, avec des preuves de sélectivité fonctionnelle qui convergent avec les recherches antérieures sur l'IRMf basées sur les tâches et vont au-delà.

L'étude 3 a évalué si l'organisation fonctionnelle du DN et sa relation avec d'autres réseaux à grande échelle étaient significativement modifiées par l'administration de drogues psychédéliques. Cette étude s'est appuyée sur deux ensembles de données d'IRM-pharmacologie publiés antérieurement et recueillis avec des drogues psychédéliques sérotoninergiques. Une combinaison de nouvelles analyses de cartographie de gradient et de RSFC a été appliquée pour évaluer les changements dans le DN et l'organisation corticale à grande échelle dans l'état psychédélique. Conformément à nos hypothèses, les résultats ont révélé que l'axe principal de l'organisation corticale à grande échelle - délimitant un gradient du cortex unimodal (ancré dans les réseaux sensorimoteurs) au cortex transmodal (ancré dans le DN) - était significativement atténué dans l'état psychédélique. Les analyses ont en outre indiqué que ce phénomène était étayé par une rupture du RSFC intra-réseau dans les réseaux sensorimoteurs et une augmentation du RSFC entre le DN et les réseaux sensorimoteurs.

Les études menées dans le cadre de cette thèse offrent de nouvelles découvertes sur de multiples aspects fondamentaux du DN : son organisation fonctionnelle, sa relation avec les différences individuelles en matière de cognition et de comportement, et sa sensibilité pharmacologique. Collectivement, les résultats apportent une contribution significative à l'avancement des perspectives théoriques et des approches empiriques sur le DN et les fonctions cérébrales à grande échelle de manière plus générale.

Acknowledgements

Graduate school was an interesting time. The amount of academic learning was certainly secondary to the personal transformations I've undergone. From coming in as a highly motivated overachiever hellbent on a career in academia, to being pulled out of my usual social environments during the pandemic and connecting more deeply to myself, to spreading my wings as a public figure/content creator, industry executive, and well-known voice in psychedelic science. It's been a wild ride, and I couldn't have asked for things to have gone better.

I'm deeply grateful to my supervisor, Nathan Spreng. You trusted and had confidence in me from the very beginning – I always felt respected and deeply supported by you, and this was especially pivotal for my self-esteem and confidence as a researcher in my early years of grad school. Thank you for your no-bullshit style of feedback and your consistent accessibility when I needed you. Of course, thank you for the massive amount of freedom you gave me throughout my years in your lab (for better or for worse). Lastly, thank you for your top-calibre rigorous approach to science, which I absorbed through your feedback as well as via osmosis by seeing how you engage with research and explore ideas. It's been a pleasure to be a student in your lab.

Thank you to my parents who have always let me live my own life and craft my own journey – even though you might not fully understand it. Thanks for your unending support and trust in me. A huge thanks to the men in the weekly men's group that I had created and led during my 4 years living in Montreal. Having a weekly place to be supported and held accountable, and to escape my usual day to day life to immerse myself in targeted personal growth work, kept me sane during days of endless work and the cold harsh Montreal winters. Lastly, thank you to Robin Carhart-Harris – my soon-to-be postdoc supervisor – for being such an open collaborator and data sharer, and allowing for me to engage in my dream of being a psychedelic researcher even in the absence of working in a psychedelic lab. My continuing presence in academia would not be likely were it not for you and your generosity, not to mention your trust and confidence in me.

Contribution to Original Knowledge

Contemporary functional neuroimaging views the brain as a set of functionally specialized networks of regions that interact to mediate behaviour and cognition. Among the most studied of these is the so-called 'default network' (DN). This network exhibits a variety of unique functional and structural characteristics, is the most expanded in humans relative to other primates, and is thought to be the seat of complex behaviour and cognition. It has been implicated in a broad variety of complex cognitive processes, as well as neurological and neuropsychiatric conditions. The studies contained within this thesis apply cutting-edge neuroimaging approaches to investigate the DN from three interrelated angles: its functional organization and regional composition, its complex associations with a broad variety of traits and behaviours, and its sensitivity to a potent acute pharmacological manipulation.

Study 1 evaluated whether regions comprising the so-called 'limbic network' are more accurately construed as members of the DN. Importantly, this investigation was facilitated by an in-house dataset that features strong signal quality in limbic regions that exhibit signal drop-out in standard functional magnetic resonance imaging (fMRI) acquisitions. Data-driven modularity analyses indicated that a large proportion of regions within the limbic network may indeed be extensions of the DN. Resting-state functional connectivity mapping and clustering analyses further revealed significant heterogeneity within the limbic network, with distinct clusters exhibiting distinct patterns of large-scale (sub)network connectivity. Findings from Study 1 suggest that past work has neglected limbic membership in the DN as a result of poor signal quality, and that future conceptions and investigations of the DN may profit from greater acknowledgement of limbic regions and their associated functions.

Study 2 evaluated how DN subsystems uniquely and differentially contribute to individual differences in a broad constellation of traits, behaviours, and cognitive processes. Given the results of Study 1, we also included the limbic and temporoparietal networks in this study. Partial least squares multivariate analyses revealed complex associations between measures of DN subsystem, limbic, and temporoparietal structure and function, and behaviour. Results indicated several distinct axes of brain-behaviour covariance, each of which featured differential contributions from

the examined (sub)networks. Functional selectivity was present between particular networks and particular behaviours, broadly consistent with past task-based fMRI research. However, results also indicated significant shared variance across networks – particularly between the limbic network and DN, consistent with the results of Study 1. These findings offer novel evidence in support of functional heterogeneity within the DN, the DN's close association with the functionally related limbic and temporoparietal networks, and, more generally, the multifaceted and complex nature of brain-behaviour relationships involving the DN.

Study 3 evaluated whether DN functional organization and relationship to other large-scale networks was significantly altered by psychedelic drug administration. This study leveraged two previously published pharmaco-fMRI datasets collected with serotonergic psychedelic drugs. A combination of novel gradient- and RSFC- mapping analyses were applied to assess changes in DN and macroscale cortical organization in the psychedelic state. Results revealed that the principal axis of macroscale cortical organization – delineating a gradient from unimodal cortex (anchored in sensorimotor networks) to transmodal cortex (anchored within the DN) – was significantly attenuated in the psychedelic state. Analyses further indicated that this was underpinned by a break-down of intra-network RSFC in sensorimotor networks and increases in RSFC between the DN and sensorimotor networks. These findings provided novel evidence that a fundamental organizational property of macroscale organization can be significantly disrupted by an acute serotonergic manipulation and, moreover, that this is specifically due to a breakdown in the functional segregation between the DN and lower-order sensorimotor networks. This underscores the role of DN in global brain organization and the utility of psychedelics as scientific tools that uniquely enable a potent transient perturbation of this network.

Results across Study 1 and Study 2 collectively highlight that the DN is a complex and functionally heterogenous network with distinct subregions/subnetworks – including regions within limbic and temporoparietal networks – that jointly and differentially contribute to a variety of traits and behaviours. Study 3 adds to these findings by revealing that the fundamental organization of the DN within the context of macroscale cortical organization is sensitive to an acute serotonergic manipulation that has potent subjective effects. Study 3 further underscores the role of the DN and its functional segregation from other networks in ongoing conscious

experience. The studies of this thesis offer significant advances on our current understanding of the DN and pave the way forward for future theoretical perspectives and empirical approaches with respect to the DN and complex brain function more generally.

Contribution of Authors

Girn, M., Setton, R., Mwilambwe-Tshilobo, L., Turner, G.R., Spreng, R.N. (*In Preparation*) Limbic network inclusion within the default network: a multi-echo resting-state fMRI study.

Manesh Girn: proposed the idea and analytic approach, analyzed neuroimaging data, created visualizations, wrote and edited the manuscript; **Roni Setton:** managed, processed, and quality assessed all neuroimaging data; **Laetitia Mwilambwe-Tshilobo:** processed and quality assessed all neuroimaging data; **Gary R. Turner:** coordinated and supervised data collection; **R. Nathan Spreng:** assisted with study conceptualization, provided analysis feedback and guidance**,** coordinated and supervised data collection, provided funding, edited the manuscript

Girn, M., Bzdok, D., Lockrow, A., Setton, R., Mwilambwe-Tshilobo, L., Turner, G.R., Spreng, R.N., (*In preparation*). Default network subsystem-specific axes of multivariate brain-behaviour covariance revealed by deep behavioural phenotyping.

Manesh Girn: designed the analytic approach, analyzed neuroimaging data, created visualizations, wrote and edited the manuscript; **Danilo Bzdok:** assisted with study conceptualization, provided analysis feedback and guidance; **Amber Lockrow:** collected data, led questionnaire scoring and behavioural data management; **Roni Setton:** managed, processed, and quality assessed all neuroimaging data; **Laetitia Mwilambwe-Tshilobo:** led implementation of the individualized parcellation approach, processed and quality assessed all neuroimaging data; **Gary R. Turner:** coordinated and supervised data collection; **R. Nathan Spreng:** assisted with study conceptualization, provided analysis feedback and guidance**,** coordinated and supervised data collection, provided funding, edited the manuscript

Girn, M., Roseman, L., Bernhardt, B., Smallwood, J., Carhart-Harris, R., Spreng, R.N. (2022) Serotonergic psychedelic drugs LSD and psilocybin reduce the hierarchical differentiation of unimodal and transmodal cortex. *Neuroimage*

Manesh Girn: proposed the idea and analytic approach, analyzed neuroimaging data, created visualizations, wrote and edited the manuscript; **Leor Roseman:** led neuroimaging data management and pre-processing, edited the manuscript; **Boris Bernhardt**: assisted with study conceptualization, provided analysis feedback and guidance, edited the manuscript; **Jonathan Smallwood**: assisted with study conceptualization, provided analysis feedback and guidance, edited the manuscript; **Robin Carhart-Harris**: assisted with study conceptualization, supervised and coordinated neuroimaging data collection, edited the manuscript; **R. Nathan Spreng:** assisted with study conceptualization, provided analysis feedback and guidance**,** edited the manuscript

Chapter 1: General Introduction

Literature Review

Contemporary functional neuroimaging views the brain as a set of functionally specialized networks of regions that interact to mediate behaviour and cognition. Among the most studied of these is the so-called 'default network'. Originally discovered as a set of regions that consistently deactivate in response to most cognitive paradigms, the default network has now been implicated in a variety of complex cognitive processes, as well as neurological and neuropsychiatric conditions. Considered as the apex of the macroscale cortical processing hierarchy, regions comprising this network are considered to be critical for global brain function. The present thesis contributes to our growing understanding of this pivotal network by investigating the inclusion of additional regions within its functional organization, the role of its distinct subsystems in a broad constellation of traits and behaviours, and its sensitivity to a potent acute pharmacological manipulation. The following literature review is written to complement the reviews provided in the introduction of each manuscript.

Historical Overview

Functional neuroimaging has exploded as a discipline over the past three decades, spearheaded by a variety of technological, methodological, and analytical developments (Raichle, 2009). The initial kindling of this area can be attributed to the highly fruitful marrying of functional magnetic resonance imaging (fMRI) with the frameworks and paradigms of cognitive psychology (Posner & DiGirolamo, 2000; Raichle, 2009). This research – described under the heading of 'cognitive neuroscience' – has afforded an unprecedented window into the relations between brain function and cognition. Early research in cognitive neuroscience focused on contrast-based analyses of task-evoked activity (Friston et al., 1994). In such research, participants' brain activity while engaging in a cognitive task of interest is contrasted with their activity during a task or context that serves as a neutral baseline or active comparator. This serves to isolate task-evoked activity of interest, which is then interpreted as comprising the neural correlates of that given cognitive process. An interesting finding from this research was that although the activation maps widely varied based on the task paradigm in question, there appeared to be strong consistency in the set of regions

exhibiting task-induced deactivation (Shulman et al., 1997). Subsequent targeted analyses based on baseline oxygen consumption indicated that these regions comprised an organized baseline 'default mode' of brain function that is sustained while subjects are at rest, and which is temporarily suspended during goal-directed cognitive tasks (Raichle et al., 2001). This discovery helped stimulate interest in the 'intrinsic' activity of the awake resting brain and dovetailed with the then recent finding that low-frequency fluctuations of activity in the sensorimotor cortices were significantly correlated at rest (Biswal et al., 1995; Gusnard & Raichle, 2001). Soon thereafter, it was discovered that the regions comprising this default mode of brain function were also highly correlated at rest (Greicius et al., 2003).

Fast-forward two decades and this approach of characterizing correlations between regional timeseries – now referred to as 'resting-state functional connectivity (RSFC) – has transformed functional neuroimaging, shedding significant light on the intrinsic functional organization of the brain and opening the door to a wide variety of novel analytical techniques and associated findings (Bassett & Sporns, 2017; Buckner et al., 2013). Most notably, RSFC investigations have revealed that, within the structure of correlations between the low-frequency activity of distributed neural regions at rest, there exist functionally-dissociable large-scale networks that interact to mediate perception, cognition, and behaviour (Bassett & Sporns, 2017; Bressler & Menon, 2010; Uddin et al., 2019). These networks are reliable and consistent across time and context (Cole et al., 2014; Damoiseaux et al., 2006), exhibit strong correspondence to task-evoked activation patterns revealed by fMRI contrast-based approaches (Smith et al., 2009), and are thought to reflect underlying polysynaptic neuroanatomy (Fox & Raichle, 2007; Van Dijk et al., 2010). Of these large scale networks, the network initially found to comprise the 'default mode' of brain function – now referred to as the 'default network' (DN) – has been the focus of considerable research (Buckner & DiNicola, 2019; Smallwood, Bernhardt, et al., 2021).

The functional organization of the default network

RSFC studies have characterized the DN as a set of cortical regions spanning the frontal, temporal, and parietal lobes (Buckner et al., 2008; Buckner & DiNicola, 2019; Greicius et al., 2003; Smallwood, Bernhardt, et al., 2021; Yeo et al., 2011). These studies specifically describe it as

consisting of dorsal, anterior, and ventral medial prefrontal cortex, posterior cingulate/retrosplenial cortex, the inferior parietal lobule, lateral temporal cortex, as well as the parahippocampus and hippocampus. In earlier studies, this organization was revealed by placing a seed region within a putative core region of the DN (posterior cingulate) and examining its correlation with every other voxel of the brain (Buckner et al., 2008; Greicius et al., 2003). Subsequently, additional methods for characterizing the DN and the large-scale network organization of the brain were introduced, including clustering algorithms (Yeo et al., 2011), modularity algorithms derived from graph theory (Meunier et al., 2010; Sporns & Betzel, 2016), and dimensionality reduction techniques such as independent component analysis (Doucet et al., 2011).

The network parcellation scheme that has arguably been the most influential was proposed by Yeo and colleagues (2011). This investigation applied data-driven clustering analysis to resting-state fMRI data from two large (n=500) subsamples collected as part of the Human Connectome Project, and proposed that the brain can be reliably parcellated into 7 or 17 networks, depending on the spatial resolution desired (Yeo et al., 2011). Two important characteristics of this parcellation bear emphasis: (i) this was a cortex-only parcellation and did not examine the large-scale network memberships of subcortical regions, and (ii) the employed dataset featured poor signal quality in the regions described as comprising the 'limbic network', spanning the temporal poles (TPs), ventral anterior temporal lobes (vATL), and orbitofrontal cortex (OFC), rendering its designation as a distinct network suspect.

The former is pertinent as a variety of studies have highlighted the potential inclusion of subcortical regions within the DN, as well as the significant role of subcortical regions in modulating DN function (Alves et al., 2019; Buckner et al., 2011; Bzdok et al., 2013; Choi et al., 2012; Cunningham et al., 2017; Harrison et al., 2022). In particular, the basal forebrain and mediodorsal nucleus of the thalamus have been highlighted as critical drivers of the DN – wherein the former may play a role in the engagement of internally-directed cognitive processes, and the latter may be a driver of task-induced deactivation (Alves et al., 2019; Harrison et al., 2022). Strong evidence also exists for the inclusion of the amygdala within the DN (Alves et al., 2019; Bzdok et al., 2013), as well as the involvement of regions within the striatum (Alves et al., 2019; Choi et al., 2012; Li et al., 2021).

With regard to the so-called limbic network, multi-modal and multi-species evidence suggests a strong relationship between the regions comprising this network and the DN. Tract-tracing studies in non-human primates have found evidence for significant anatomical connections between the TPs, vATL, and OFC with DN regions (Barbas et al., 1999; Carmichael & Price, 1995, 1996; Kondo et al., 2003; Moran et al., 1987; Saleem et al., 2008). Consistent with this, RSFC investigations with modest but reliable signal quality in these regions has also found evidence for strong RSFC between them and the DN (Pascual et al., 2015) (Andrews-Hanna et al., 2010; Jackson et al., 2016; Simmons et al., 2010) (Jackson et al., 2018; Jackson et al., 2016; Simmons et al., 2010) (Du et al., 2020). (Andrews-Hanna et al., 2010; Vincent et al., 2006). Further support for the close relationship between the DN and LIM comes from task-based fMRI studies which have consistently found the co-recruitment of regions form these networks across a variety of semantic, social, and emotional tasks (Andrews-Hanna et al., 2014; Dixon et al., 2017; Kieran C.R. Fox et al., 2018; Frith & Frith, 2007; Spreng et al., 2009) (Chase et al., 2020; Zald et al., 2012) (Andrews-Hanna et al., 2014; Frith & Frith, 2007; Simmons et al., 2010; Spreng et al., 2009). Collectively, these findings – as well as the findings of subcortical involvement discussed above – suggest the possibility that the DN is an extended cortical-limbic-subcortical network, but this had yet to be studied in a targeted investigation. Study 1 of the present thesis seeks to resolve this gap.

The role of default network subsystems in cognition

Since its first characterization by RSFC studies, it was evident that correlations between DN regions are not uniform: certain subsets of regions have stronger correlations with each other relative to others (Buckner et al., 2008). Concordantly, research has provided evidence for a fractionation of the DN into distinct subsystems (Andrews-Hanna et al., 2010; Braga & Buckner, 2017; Buckner & DiNicola, 2019; DiNicola et al., 2020; Yeo et al., 2011). An influential fractionation of the DN into subsystems based on RSFC and meta-analytic task-based fMRI studies separates it into three networks: (i) the DN_A, which includes the anteromedial prefrontal cortex and dorsal posterior cingulate cortex, (ii) the DN_B, which includes the dorsomedial prefrontal cortex, anterior inferior parietal lobule/temporoparietal junction, and lateral temporal cortex, and

(iii) the DN_C, which includes ventromedial prefrontal cortex, posterior inferior parietal lobule, parahippocampus, and hippocampus (Andrews-Hanna et al., 2010; Yeo et al., 2011). Each of these networks have been linked to distinct, but partially overlapping, cognitive functions (Andrews-Hanna et al., 2014). DN_A has been most implicated in self-related processing and meaning creation, and is viewed as an integrative hub that interlinks the DN_B and DN_C – often acting in concert with each of them towards their associated cognitive functions (Andrews-Hanna et al., 2014; Qin & Northoff, 2011; Stawarczyk et al., 2019). DN_B has been linked predominantly to social cognitive processes and is also often recruited alongside the semantic system during linguistic-semantic tasks (Andrews-Hanna et al., 2014; Binder et al., 2009; Ralph et al., 2017; Spreng & Andrews-Hanna, 2015). Finally, DN_C is strongly implicated in episodic memory recollection and projection (Andrews-Hanna et al., 2014; Schacter et al., 2012).

An alternative fractionation proposes that the DN is comprised of two distinct networks: (i) $Default_A$, which includes the ventromedial prefrontal cortex, retrosplenial cortex/ventral posterior cingulate, posterior inferior parietal lobule, and parahippocampal cortex, and (ii) $Default_B$, which includes the anterior and dorsal ventromedial prefrontal cortex, dorsal posterior cingulate, anterior inferior parietal lobule/temporoparietal junction, and the temporal poles. This view argues that the DN_A's putative role as a hub that integrates the two other subsystems into a unified DN is a result of the blurring of individual differences in fine-scale functional neuroanatomy that occurs with group-level averaging (Braga & Buckner, 2017; Buckner & DiNicola, 2019; DiNicola et al., 2020). In contrast, it proposes that DN comprises two distinct networks that are spatially interdigitated throughout the frontal, temporal, parietal lobes, and that their functional separation requires consideration of differences in the spatial location of these regions across individuals (Braga & Buckner, 2017; Buckner & DiNicola, 2019; DiNicola et al., 2020). Within this view, $Default_A$ is linked to episodic memory processes, whereas $Default_B$ is linked to social cognition/theory of mind (DiNicola et al., 2020).

The 'correct' fractionation of the DN notwithstanding, the cognitive roles of these putative subsystems are based exclusively on findings from task-based fMRI investigations which examine one of these cognitive processes in isolation. While this approach has provided significant advances in mapping cognitive processes to functional neuroanatomy, it does not provide direct

evidence of functional specializations and dissociations in brain-behaviour associations. Rather, these must be inferred via cross-study comparisons. An alternative approach, which can allow a fuller characterization of the diverse functionality of the DN (and other networks) within a single study, is one that involves relating individual differences in brain structure and function to differences in a range of cognitive and behavioral variables (Bzdok & Yeo, 2017; Dubois & Adolphs, 2016; Smith et al., 2015). Notably, such an approach is afforded by the analysis of large, phenotypically rich neuroimaging datasets (Bzdok & Yeo, 2017; Dubois & Adolphs, 2016; Smith et al., 2015). Such datasets and associated analytic frameworks afford potential to go beyond circumscribed investigations of specific variables of interest, to assessments of complex multivariable relationships between the brain and rich suites of cognitive, emotional, social, personality, and lifestyle measures. This approach has gained increasing traction in recent years as a result of the coordinated collection of large-scale neuroimaging brain-behaviour datasets (Casey et al., 2018; Dubois & Adolphs, 2016; Mendes et al., 2019; Snoek et al., 2021; Sudlow et al., 2015; Van Essen et al., 2013). Research has yet to investigate whether and to what extent this approach convergences with the functionality of DN subsystems as revealed by task-based fMRI, as well as to what extent it offers novel insight into their roles and interrelationships. Study 2 is aimed at answering these questions.

Pharmacological manipulation of default network function

An application of fMRI that has become more prevalent over the past decade is the assessment of functional brain changes elicited by pharmacological challenges (i.e., drugs). This work – sometimes dubbed 'pharmaco-fMRI' – has often been applied in the context of drug development and discovery protocols, as a means of shedding additional light on drug efficacy, side effects, and neuropharmacological mechanisms (Nathan et al., 2014; Wandschneider & Koepp, 2016). Historically, neuropharmacological imaging had been carried out with positron emission tomography (PET), owing to the ability for this modality to assess receptor occupancy and affinity, as well as other neurochemical changes (Wang & Maurer, 2005). The advantage of fMRI is the ability to assess, with strong temporal and spatial resolution, the changes in distributed regional and large-scale network activity that occur as a downstream consequence of receptor-level alterations (Carmichael et al., 2018; Nathan et al., 2014; Wandschneider & Koepp, 2016). This

approach notably also allows direct comparison of drug effects to the patterns of pathological versus healthy neural phenotypes. To date, pharmaco -fMRI has been applied to study the acute effects of a wide variety of drugs on brain function, including anesthetics, stimulants, depressants/anxiolytics, anti-depressants, psychedelics, and cannabis (Fang et al., 2021; Flodin et al., 2012; Girn et al., 2023; Schrantee et al., 2016; Stamatakis et al., 2010; Wall et al., 2019). This work has suggested that the DN is particularly sensitive to serotonergic manipulations – whether it is in the form of tryptophan depletion (Zhang et al., 2019), serotonin reuptake inhibitors (Arnone et al., 2018; Dutta et al., 2019; Klaassens et al., 2017; Klaassens et al., 2015; van de Ven et al., 2013), or psychedelics drugs (Carhart-Harris et al., 2012; Carhart-Harris & Friston, 2019; Carhart-Harris, Muthukumaraswamy, et al., 2016; Girn et al., 2023; Girn et al., 2022; Vollenweider & Preller, 2020).

Among these manipulations, serotonergic psychedelic drugs – which includes psilocybin (the compound in so-called 'magic mushrooms'), lysergic acid diethylamide (LSD), and dimethyltryptiamine (DMT) – are a particularly interesting case. Known for their potent acute subjective effects, these drugs have seen a significant renewal of scientific interest over the past decade – spearheaded by clinical trials indicated that psychedelic-assisted psychotherapy can induce rapid and sustained symptom reductions across multiple disorders, including treatment-resistant depression, end-of-life anxiety, and substance use (Andersen et al., 2021; Johnson et al., 2019; McClure-Begley & Roth, 2022). Although each drug exhibits complex and unique neuropharmacological effects, the unifying mechanistic factor across serotonergic psychedelics is their role as partial agonists at the 5-HT2A receptor (Kwan et al., 2022; Nichols, 2016). Findings from both human and rodent studies have consistently found that pre-treatment with a 5-HT2A antagonist (e.g., ketanserin) abolishes nearly all subjective/behavioural and neural effects of these drugs (Kwan et al., 2022; Nichols, 2016). Notably, research from high-resolution *in vivo* PET imaging in humans has revealed that 5-HT2A densities are highest in regions comprising the DN (Beliveau et al., 2017). This distribution of 5-HT2A receptors, combined with their excitatory effects on highly influential layer 5 pyramidal neurons (Aghajanian & Marek, 1997; Aghajanian & Marek, 1999), *a priori* suggests a strong ability to modulate DN function. This has indeed been confirmed by a several pharmaco-fMRI investigations with serotonergic psychedelics, which have consistently found significant decreases in DN within-network RSFC and increases in the RSFC

between the DN and other networks (Carhart-Harris et al., 2012; Carhart-Harris, Muthukumaraswamy, et al., 2016; McCulloch et al., 2022; Müller et al., 2018; Preller et al., 2018; Preller et al., 2020; Roseman et al., 2014).

While this work has identified consistent alterations to DN RSFC, it has yet to directly assess whether and how these changes relate to broader properties of cortical functional organization. This question has direct relevance both in the context of recent 'gradient-mapping' characterizations of macroscale cortical organization (Margulies et al., 2016; Smallwood, Bernhardt, et al., 2021), as well as for a leading theoretical model of psychedelic drug effects (Carhart-Harris & Friston, 2019). In contrast to typical approaches which parcellate the brain into regions and networks and examine their relationships, gradient-mapping techniques characterize the brain as the superposition of multiple continuous axes of feature (dis)similarity (Haak & Beckmann, 2020; Huntenburg et al., 2018). These approaches have found that the principal axis of cortical organization is a gradient spanning from unimodal sensorimotor regions to transmodal association regions centered on the DN (Margulies et al., 2016). This gradient aligns with feature variation in a wide variety of structural, functional, and genetic measures (Sydnor et al., 2021), and represents a functional hierarchy from low-level sensorimotor processing to abstract, perceptually-decoupled cognition (Huntenburg et al., 2018; Margulies et al., 2016; Murphy et al., 2018). The presence of this gradient, which is founded on the functional differentiation of the DN from sensorimotor regions, is viewed as a fundamental organizational feature of the cortex. Interestingly, a leading theory of psychedelic drug effects has posited that a breakdown of this hierarchical organization and a concomitant blurring of DN-encoded abstract representations and low-level sensory inputs may be a core mechanism underlying the subjective effects of serotonergic psychedelics (Carhart-Harris & Friston, 2019). Study 3 brings these separate lines of research together and assesses psychedelic-induced alterations to the principal gradient of cortical organization, with a specific interest in alterations to the functional differentiation of the DN from unimodal sensorimotor cortices.

Rationale and Objectives

As described above, the literature on the DN spans several independent but interrelated lines of research, including on its functional organization, role in cognition, and sensitivity to

pharmacological perturbations. Each of these three research domains are critical to advancing our our understanding of the DN, and by extension, the neural processes that underlie complex cognition and behaviour in health and disease. The present thesis directly follows from the latest research in each of these three domains, consisting of projects designed to resolve critical gaps and thereby provide impactful insights that help advance our understanding of this network and guide future investigations.

Study 1 assesses the inclusion of limbic regions with the functional organization of the DN. Critically, this study will leverage an in-house multi-echo fMRI dataset which affords strong signal reliability in limbic regions which usually exhibit signal dropout in standard single-echo fMRI acquisitions. This affords a superior ability to reliably map the whole-brain and large-scale network RSFC of these regions. We apply data-driven modularity and clustering algorithms to comprehensively examine the structure of the data and evaluate how regions comprising the limbic network – as defined by the influential Yeo and colleagues 7 network parcellation – get grouped together and with other large-scale networks based on their whole-brain RSFC patterns. This RSFC mapping study explores the presence of functional heterogeneity within the limbic network, and interrelations between the limbic network, DN, and subcortical regions. Collectively, the results have potential to expand accounts of the functional organization of the DN and will shed novel light on the RSFC and large-scale network relationships of limbic regions.

Study 2 assesses the associations between DN subsystems and a broad variety of cognitive, emotional, social, and trait measures. Here, we again leverage the same in-house multi-echo fMRI dataset, this time making use of the rich suite of behavioural measures that were also assessed in these participants. In particular we apply multivariate analyses to examine relationships between individual differences in multiple measures of DN structure and function and a set of 85 behavioural variables. Critically, all analyses are stratified by DN subsystem, following the tripartite scheme of DN_A, DN_B, and DNc since it is more amenable to a large-scale group-level approach. Limbic and temporoparietal language networks were also included in the analyses, based on the results of Study 1. This analytic approach enabled us to assess whether the functionality of these (sub)networks as revealed by task-based fMRI converges with an individual differences approach, and also whether this approach reveals patterns of shared and unique

(sub)network-behaviour variance that is not afforded by task-based approaches. Results from this study will provide novel insights into the complex relations between DN subsystems, closely related networks, and behaviour. More specifically, it will shed light on the manner in which these (sub)networks selectively and jointly mediate complex behavioural phenotypes.

Study 3 assess whether serotonergic psychedelic drugs reduce the functional differentiation of the DN from unimodal sensory cortices and thereby alter the principal axis of macroscale cortical organization. In this study we collaborate with researchers from Imperial College London and conduct a re-analysis of two pharmaco-fMRI datasets, collected after administration of psilocybin and LSD, respectively. We apply a combination of cutting-edge gradient-mapping analyses and RSFC mapping to characterize psychedelic-induced changes to the principal gradient of macroscale cortical organization which spans from transmodal (DN) to unimodal (visual and somatomotor) cortex. We assess whether this core organizational feature of the brain is sensitive to a pharmacological challenge, and whether this is specifically driven by a reduction in functional segregation between the DN and unimodal sensory cortices. This study will offer findings with direct relevance to leading theoretical models of psychedelic drug effects and will provide novel insight into the stability (or lack thereof) of a core organizational feature of the cortex in which the DN plays a pre-eminent role.

Chapter 2: Evaluating the inclusion of limbic regions within the default network

Adapted from: Girn, M., Setton, R., Mwilambwe-Tshilobo, L., Turner, G., Spreng, R.N. (*In Preparation*) The limbic network is part of an extended default network: Evidence from multi-echo resting state fMRI

Abstract

Resting-state functional magnetic resonance imaging (fMRI) investigations have provided a view of the default network (DN) as composed of a specific set of frontal, parietal, and temporal cortical regions. This spatial topography is typically defined with reference to an influential network parcellation scheme which designated the DN as one of seven large-scale networks. However, the precise functional organization of the DN is still under debate, with studies arguing for varying subnetwork configurations and the inclusion of subcortical regions. In this vein, the so-called 'limbic network' – defined as a distinct large-scale network comprising the bilateral temporal poles, ventral anterior temporal lobes, and orbitofrontal cortex – is of particular interest. A large multi-modal and multi-species literature on the anatomical, functional, and cognitive properties of these limbic regions suggests a strong relationship to the DN. Notably, these regions have poor signal quality in conventional fMRI acquisitions; likely obscuring their precise large-scale network affiliation in most studies. Here, we leverage a multi-echo fMRI dataset with high temporal signal-to-noise ratio across the entire cortical mantle to examine the large-scale network resting-state functional connectivity of limbic regions and assess their associations with the DN. Consistent with our hypotheses, our results support the inclusion of the majority of the limbic network as part of the DN and reveal significant heterogeneity in limbic functional connectivity. We observed that left-lateralized regions within the temporal poles and ventral anterior temporal lobes, as well as medial orbitofrontal regions, exhibited the greatest resting-state functional connectivity with the DN, with different connectivity patterns across DN subnetworks. Overall, our findings suggest that, rather than being a functionally distinct network, the limbic network comprises a set of regions that are part of a larger, extended default network.

Introduction

Technological and methodological advances in functional magnetic resonance imaging (fMRI) research over the past three decades have afforded an unprecedented ability to characterize the functional organization of the human brain (Raichle, 2009). Chief among these approaches is resting-state functional connectivity (RSFC), which assesses the interregional correlation structure of the brain while an individual is not engaged in an explicit task (Biswal et al., 1995; Buckner et al., 2013). RSFC investigations have revealed that the brain is comprised by a set of reliable and consistent large-scale networks that interact to mediate perception, cognition, emotion, and behaviour (Bassett & Sporns, 2017; Bressler & Menon, 2010; Damoiseaux et al., 2006; Uddin et al., 2019). The rise of RSFC approaches led to the discovery that a set of regions that consistently deactivated during cognitive tasks were strongly positively correlated in the absence of any overt task (Raichle & Snyder, 2007). This set of regions, now referred to as the 'default network' (DN), has been the focus of a considerable amount of research and the DN has now been linked to a variety of complex cognitive processes (Andrews-Hanna et al., 2014; Buckner & DiNicola, 2019; Smallwood et al., 2021).

RSFC studies have characterized the DN as a set of regions spanning the frontal, temporal, and parietal lobes (Buckner et al., 2008; Buckner & DiNicola, 2019; Raichle et al., 2001; Smallwood et al., 2021; Yeo et al., 2011). These studies generally characterize the DN as consisting of dorsal, anterior, and ventral medial prefrontal cortex, posterior cingulate/retrosplenial cortex, the inferior parietal lobule, lateral temporal cortex, as well as the parahippocampus and hippocampus. RSFC and meta-analytic task findings have further supported a fractionation of the DN into three subnetworks: (i) the DN_A, which includes the anteromedial prefrontal cortex and dorsal posterior cingulate cortex, (ii) the DN_B, which includes the dorsomedial prefrontal cortex, anterior inferior parietal lobule/temporoparietal junction, and lateral temporal cortex, and (iii) the DN_C, which includes ventromedial prefrontal cortex, posterior inferior parietal lobule, parahippocampus, and hippocampus (Andrews-Hanna et al., 2010; Yeo et al., 2011).

Despite these advances, the precise organization of the DN is still a matter of debate (Uddin et al., 2019). For example, there is disagreement about whether the DN consists of the three partially

dissociable systems described above, or composed of two dissociable systems that are typically conflated as a result of group-level averaging and the obscuring influence of individual differences in functional neuroanatomy (Andrews-Hanna et al., 2010; Braga & Buckner, 2017; Buckner & DiNicola, 2019; DiNicola et al., 2020; Yeo et al., 2011). A line of work has also pushed back against the prevalence of corticocentric views of the DN and has provided evidence for the inclusion of subcortical regions as a core part of this network (Alves et al., 2019; Buckner et al., 2011; Bzdok et al., 2013; Choi et al., 2012; Cunningham et al., 2017). An additional area of interest with regard to the functional organization of the DN is the so-called limbic network (LIM; Yeo et al., 2011) and its potential inclusion as part of the DN (see Uddin et al., 2019).

The LIM was defined by the highly cited Yeo et al. (2011) network parcellation scheme as a distinct network that is composed of two subnetworks, LIM_A which encompasses the temporal pole (TP) and adjacent regions of the ventral anterior temporal lobe (vATL), and LIM_B which corresponds to orbitofrontal cortex (OFC). The reliability of these regions forming a distinct network, however, is unclear given that they have among the least reliable signal in conventional fMRI acquisition protocols. This is due to their close proximity to nasal airways and consequent vulnerability to susceptibility-related signal loss (Ojemann et al., 1997). Indeed, the Yeo et al. (2011) study featured poor temporal signal to noise ratio (TSNR~40) in most limbic regions, suggesting that the grouping of these regions into a distinct network may, at least partially, be driven by their shared property of poor signal.

Findings from tract-tracing work in non-human primates, as well as RSFC and task-based fMRI investigations where modestly reliable signal is present, suggest that regions within LIM – i.e., spanning the TP, vATL, and OFC – may be construed as extensions of the DN. Tract-tracing in non-human primates has found that the TP and vATL exhibit extensive anatomical connections to a broad variety of cortical and subcortical regions, many of which correspond to homologs of human DN regions (Barbas et al., 1999; Kondo et al., 2003; Moran et al., 1987; Saleem et al., 2008). Putative DN regions found to exhibit anatomical connectivity with subregions of the TP and vATL in macaque monkeys include the anteromedial and ventromedial prefrontal cortex (Barbas et al., 1999; Kondo et al., 2003), superior and inferior temporal gyrus (Kondo et al., 2003; Moran et al., 1987; Saleem et al., 2008), as well as the parahippocampal cortex and hippocampus

(Moran et al., 1987; Muñoz & Insausti, 2005; Saleem et al., 2008). Similarly, the OFC has also been found to exhibit anatomical connections to much of the brain, including regions corresponding to the DN. Putative DN regions found to exhibit anatomical connectivity with the OFC in macaque monkeys include the anteromedial and ventromedial prefrontal cortex (Carmichael & Price, 1996; Price, 2006; Saleem et al., 2008), anterior, mid, and posterior cingulate gyrus (Carmichael & Price, 1995, 1996), inferior frontal gyrus (Carmichael & Price, 1996), superior temporal gyrus (Carmichael & Price, 1995; Kondo et al., 2003; Saleem et al., 2008), as well as the parahippocampal cortex and hippocampus (Carmichael & Price, 1995; Kondo et al., 2005).

Consistent with these findings, RSFC investigations with modest but reliable signal quality (TSNR>50) in the TP, vATL, and OFC have found evidence for strong RSFC between each limbic network region and the DN. With regard to the TP, one RSFC-based parcellation study found that two anterolateral subdivisions of the left TP – spanning the anterior tip and the middle and inferior temporal gyri, and collectively comprising ~50% of total TP surface area – strongly recapitulated the full breadth of the DN (Pascual et al., 2015). This RSFC map also included the OFC – suggesting the presence of a combined DN-LIM network (Pascual et al., 2015). Another study parcellated the TP based on anatomical connectivity estimated by diffusion tensor imaging (DTI) and similarly found a bilateral anterolateral subregion that exhibited an RSFC pattern strongly resembling the DN (Fan et al., 2014). Additional studies have also supported the presence of RSFC between TP subregions and the DN (Andrews-Hanna et al., 2010; Jackson et al., 2016; Simmons et al., 2010). Similarly, strong RSFC between the vATL, particularly in the left hemisphere, and regions overlapping with the DN have also been found (Jackson et al., 2018; Jackson et al., 2016; Simmons et al., 2010). With regard to the OFC, a RSFC-based parcellation of this region revealed that medial subregions of the OFC in particular were significantly correlated with the mPFC and PCC – two core regions of the DN (Kahnt et al., 2012). This finding was consistent with earlier RSFC investigations which, in addition to the mPFC and PCC, also revealed RSFC between the OFC and medial temporal regions such as the parahippocampus and hippocampus (Andrews-Hanna et al., 2010; Vincent et al., 2006). A more recent study assessed OFC RSFC in 654 individuals and again found that multiple subregions – including the medial extent of OFC along the ventral frontal lobes – exhibited significant RSFC with the majority of the DN (Du et al., 2020).

Task-based fMRI investigations provide further evidence for strong linkages between each of the TP, vATL, and OFC, and the DN. A notable example is the common recruitment of the TP, vATL, and OFC alongside the DN in investigations of complex cognitive processes, including social cognition, spontaneous thought, episodic memory recollection and prospection, and self-referential processing (Andrews-Hanna et al., 2014; Dixon et al., 2017; Fox et al., 2018; Frith & Frith, 2007; Spreng et al., 2009). Among these, the coactivation of the TP with DN_B for social cognitive processes is a particularly consistent and robust finding (Andrews-Hanna et al., 2014; Frith & Frith, 2007; Simmons et al., 2010; Spreng et al., 2009). The TP and vATL are also central regions within a distributed conceptual processing/semantic memory network that highly overlaps with DN_B (Binder et al., 2009; Ralph et al., 2017). Further examples with respect to the OFC come from two meta-analytic connectivity modelling investigations of this region based on the Brain Map database (Chase et al., 2020; Zald et al., 2012). These studies revealed – directly in line with RSFC studies – that subregions of the OFC consistently exhibit significant task-based coactivation with the mPFC, PCC, and the medial temporal lobes (parahippocampus and hippocampus) across a variety of cognitive tasks (Chase et al., 2020; Zald et al., 2012).

Collectively, therefore, there is a strong body of evidence suggesting that the TP/vATL and OFC – or subregions thereof – may be regarded as part of the DN. However, this has yet to be evaluated in a targeted investigation. We leverage an open access multi-echo fMRI dataset (Spreng et al., 2023) that affords exceptional signal quality in LIM regions, thereby overcoming limitations concerning poor LIM tSNR in past work. Briefly, the signal of a given brain region at a given echo time (TE) is based on the transverse relaxation time (T2*) of brain tissue in that region. Brain regions vary in T2* and therefore a given TE will result in higher tSNR in some regions and lower tSNR in others. In typical fMRI acquisitions, data is collected at a single TE with the goal of maximizing signal quality across the entire brain – however, this results in notable trade-offs, such as poor signal in the TP/vATL and OFC. Critically, the multi-echo acquisitions used here collected data at three TEs, including a shorter TE that exhibits significantly less signal dropout in regions vulnerable to susceptibility distortions (Kundu et al., 2017). We optimally combined each TE timeseries in a manner that optimized for signal quality on a voxel-wise level, thereby mitigating signal dropout and significantly boosting whole-brain tSNR (see Figure 1). Moreover, the use of

multi-echo data enabled the use of multi-echo independent component analysis (ME-ICA) denoising, a biophysically-based noise-removal technique that separates BOLD from non-BOLD signal based on TE-dependence. This principled denoising technique has been found effective in removing motion and physiological artifacts in resting-state fMRI data (Kundu et al., 2013; Kundu et al., 2012; Lynch et al., 2020; Setton et al., 2023), including distant-dependent motion effects (Power et al., 2018; Spreng et al., 2019).

Combining multi-echo resting-state fMRI data and ME-ICA denoising affords the ability to map the RSFC and network organization of LIM_A (TP/vATL) and LIM_B (OFC). Leveraging these data, we sought to (i) determine whether data-driven network parcellation approaches assign LIM regions to the same network as DN regions, (ii) assess the whole-brain RSFC of LIM_A and LIM_B subnetworks, and (iii) assess the presence of functional heterogeneity within LIM_A and LIM_B via data-driven clustering. We hypothesize that (i) data-driven network parcellation approaches will assign the majority of LIM regions to the DN, (ii) data-driven clustering will delineate functionally heterogenous subregions within the LIM, and (iii) left-lateralized LIM_A and medial LIM_B regions will exhibit the greatest RSFC with the DN, given the former's overlap with the DN-overlapping semantic system (Binder et al., 2009; Ralph et al., 2017), and the latter's previously documented RSFC with DN regions (Du et al., 2020; Kahnt et al., 2012).

Methods

Participants

154 young adults (mean age 22.29, SD: 3.12; range: 18–34 years; 86 women) participated in the current study. All participants were healthy and had no history of psychiatric, neurological, or other medical illness that could compromise cognitive function.

Neuroimaging data acquisition

All imaging data were acquired on a 3T GE Discovery MR750 scanner (General Electric, Milwaukee, United States) with a 32-channel receive-only phased-array head coil at the

Cornell Magnetic Resonance Imaging Facility in Ithaca. High resolution structural images were acquired during one 5m25s run using a T1-weighted (T1w) volumetric MRI magnetization prepared rapid gradient echo (MPRAGE) sequence [repetition time (TR)=2530 ms; echo time (TE)=3.4 ms; inversion time (TI)=1100 ms; flip angle (FA)=7°; bandwidth=195 Hz/pixel; 1.0 mm isotropic voxels, 176 slices]. Structural scans were acquired with 2x acceleration with sensitivity encoding.

Participants completed two 10-minutes 6-seconds resting-state multi-echo BOLD functional scans with eyes open, blinking and breathing normally in the dimly lit scanner bay. These scans were acquired using a multi-echo echo planar imaging (ME-EPI) sequence with online reconstruction (TR = 3000 ms; TE's = 13.7, 30, 47 ms; FA = 83°; matrix size = 72 × 72; field of view (FOV) = 210 mm; 46 axial slices; 3.0 mm isotropic voxels). Resting-state functional scans were acquired with 2.5x acceleration with sensitivity encoding and were acquired prior to engagement in any cognitive task.

Neuroimaging preprocessing and denoising

Resting-state fMRI data were collected at three echo times (TEs), as afforded by the multi-echo fMRI acquisition. Timeseries data at each TE were first minimally preprocessed: the first 4 volumes were discarded, images were computed for de-obliquing, motion correction, and anatomical-functional coregistration, and volumes were brought into spatial alignment across TEs.

Given interregional differences in T_2* relaxation rates, volumes collected at each TE result in differential signal quality across regions. To exploit this, the resting-state fMRI data was averaged across TEs in a manner that was optimally weighted to maximize the temporal signal to noise ratio (TSNR) of each voxel. This significantly improves whole-brain TSNR and, critically, attenuates signal drop out in typically problematic regions along the ventral-anterior surface of the brain (i.e., orbitofrontal cortex and the temporal pole; (Kundu et al., 2013; Kundu et al., 2012; Lynch et al., 2020)).

In addition, a multi-echo acquisition facilitates the biophysically-based removal of noise components from resting fMRI datasets (Kundu et al., 2013; Kundu et al., 2012). This is because collecting data at multiple TEs allows the direct measurement of TE-dependent variability in the signal. The denoising method presently employed – multi-echo independent component analysis (ME-ICA) – exploits this information to distinguish BOLD signal from non-BOLD noise (Kundu et al., 2012). TE-dependent variability of the signal can be fit to models of changes in T_2* (i.e., the transverse relaxation rate; the basis for the BOLD contrast) or changes in baseline signal (S_0) which are the product of scanner artifacts, motion, and other sources of noise (Kundu et al., 2012). By comparing the relative goodness of fit of TE dependence to each of these models, one can separate BOLD signal from non-BOLD noise. Past work has supported the effectiveness of this technique in denoising BOLD signal of motion and physiological artifacts in resting-state fMRI (Kundu et al., 2013; Kundu et al., 2012; Lynch et al., 2020; Setton et al., 2023). Importantly, ME-ICA denoising has been found to remove distant dependent motion effects from RSFC data (Power et al., 2018; Spreng et al., 2019). ME-ICA outputs include: (i) spatial maps consisting of the BOLD-like components, (ii) reconstructed time series based on back-projecting the BOLD-like components only, and (iii) the BOLD-like component coefficient sets.

Quality assessments were performed on the reconstructed time series (ME-ICA output ii) in native space to identify and exclude participants with unsuccessful coregistration, residual noise (framewise displacement > 0.50-mm coupled with denoised time series showing DVARS > 1), temporal signal-to-noise ratio < 50, or fewer than 10 retained BOLD-like components. The denoised BOLD component coefficient sets (ME-ICA output iii) in native space, optimized for functional connectivity analyses (Kundu et al., 2013), were used in subsequent steps. We refer to these BOLD component coefficient sets as multi-echo functional connectivity (MEFC) data. Additional measures were taken to account for variation in the number of independent components from ME-ICA once connectivity matrices were estimated, as detailed below.

ME-ICA processing was run with ME-ICA version 3.2 beta; https://github.com/ME-ICA/ (Kundu et al., 2013; Kundu et al., 2012). Anatomical images were first skull stripped using the default parameters in FSL BET. ME-ICA processing was then run with the following options: -e 13.6, 29.79, 46.59; -b 12; --no_skullstrip; –space = Qwarp_meanE+tlrc. Here, the Qwarp_meanE+tlrc

file represented a site-specific MNI-space template (available here: https://zenodo.org/record/3575255). This template was created in AFNI using @toMNI_Qwarpar. MNI-space ME-ICA BOLD coefficient time series were resampled to 2mm isotropic. Timeseries were not smoothed, given that the parcel-wise timeseries extraction approach applied here represents a de facto form of smoothing (i.e., by averaging across spatially contiguous voxels).

Signal quality

In order to assess the whole-brain signal quality of the ME-ICA processed images, TSNR was calculated for each voxel as the mean signal intensity across its timeseries, divided by its standard deviation. Derived TSNR spatial maps were averaged across all subjects and thresholded at 50 (Figure 1). The results indicate strong whole-brain coverage, including within limbic areas which typically exhibit signal-drop out (i.e., orbitofrontal cortex and the temporal pole), consistent with prior reports of ME-ICA (e.g., DuPre et al., 2016; Setton et al., 2023; Spreng et al., 2017).

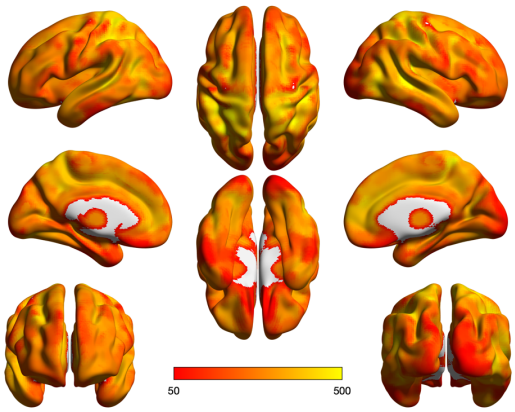

Figure 1. Parcel-wise (1000 parcels; Schaefer et al., 2017) temporal signal to noise ratio, thresholded at 50.

Neuroimaging Data Analysis

Resting-state functional connectivity

The MEFC denoised resting-state fMRI data (see Section 2.3 above) were parcellated into 1032 regions as follows: 1000 cortical regions following Schaefer et al. (2017) and 32 subcortical regions following (Tian et al., 2020). RSFC was computed as the product-moment correlation coefficient between all parcels, resulting in a 1032 × 1032 RSFC matrix for each subject. Given our use of MEFC data, RSFC was calculated as the correlation of the ME-ICA coefficients across parcels (parcel × coefficient vectors), rather than a correlation across BOLD signal time-series (parcel × timepoint vectors), as is typically done (see (Kundu et al., 2013)). The Fisher's r-to-z transformation was applied to normalize the distribution of correlation values and, importantly, account for variation in MEFC data degrees of freedom (as quantified by the number of BOLD ME-ICA components), across individuals (Kundu et al., 2013)):

$$Z = \text{arctanh}(\text{R}) \cdot \sqrt{df - 3}$$

where R is the product–moment correlation value and df is the number of BOLD ME-ICA components.

Modularity

Modularity is a measure derived from the subfield of mathematics referred to as graph theory. The application of graph theory to neuroimaging data formalizes the brain as a network of nodes (e.g., brain regions) which are connected by edges/links (e.g., functional correlations, white matter pathways; (Bassett & Sporns, 2017; Rubinov & Sporns, 2010)). This formalization enables the quantification of topological properties associated with the brain's graph (i.e., network) structure. Modularity in particular indexes the decomposability of a given network (in this case, whole-brain functional connectivity) into distinct modules.

Two modularity algorithms were applied: the Louvain algorithm and the InfoMap algorithm. The Louvain algorithm(Blondel et al., 2008) was implemented with the Network Community Toolbox (http://commdetect.weebly.com/). This algorithm finds modular partitions of the graph (synonymous with network) which optimize the modularity value, Q, by grouping nodes into non-

overlapping (sub)networks that maximize intra-modular and minimize inter-modular connections (Newman, 2004). The modularity value Q for a given modular partition is computed as follows:

$$Q = \frac{1}{l}\sum_{i,j\in N}\left[w_{ij} - \frac{k_i k_j}{l}\right]\delta_{m_i m_j}$$

where w is the edge weight (i.e., functional connectivity value) between nodes i and j, l^w is the sum of all weights in the graph, k_i is the weighted degree (edge weight summed across all edges) of node i, and m_i is a module containing node i. $\delta_{m_i m_j}$ =1 if nodes i and j belong to the same module, and = 0 otherwise. The Q value for a given partition therefore quantifies the strength of within-module edges relative to the strength of between-module edges, or, in other words, the extent to which distinct modules can be delineated in the data. This algorithm has a single free parameter, gamma (γ), which controls how many modules will be detected. Modularity was computed with three gamma values: 1 (the default), 1.25, and 1.5. The Louvain algorithm was run on the group-level mean RSFC matrix, using the Yeo 7 network assignments as the initial conditions. These initial assignments were used because our goal was to identify whether limbic regions remain assigned to a distinct 'limbic network', or get assigned to one or more of the other large-scale networks.

Clustering

Clustering analyses were applied as a data-driven assessment of subnetwork organization within the limbic network. To prepare the data for clustering, eta squared similarity was computed on matrices corresponding to RSFC between limbic regions (as defined based on the Schaefer-Yeo 17 network, 1000 region parcellation) and the rest of the brain (i.e., on subject-wise 61 × 1032 RSFC matrices). This yielded a 61 × 61 RSFC similarity matrix per subject, wherein each value represents the similarity between two given limbic regions in their whole-brain RSFC profile.

Clustering was performed on the group-level mean similarity matrix using Ward's agglomerative clustering. This clustering algorithm was chosen as past RSFC research has found that it produces results that are more accurate and reproducible than other popular algorithms (i.e., k-means

clustering or spectral clustering; (Thirion et al., 2014)). In addition, it does not require the *a priori* specification of number of clusters. Ward's clustering is an unsupervised algorithm that iteratively merges clusters in the data while seeking to minimize the "error sum of squares", which is computed as the sum of squares of the deviations from the cluster centroid. At initialization, all vectors (in this case, 1 × 61 vectors representing a given LIM parcel's similarity to all other LIM parcels) are their own cluster, and the algorithm stops after the further merging of clusters does not reduce the error sum of squares.

RSFC maps

We refer to the whole-brain interregional RSFC of a given parcel, subnetwork, or cluster as an 'RSFC map'. For a given parcel, this corresponds to a row of the whole-brain RSFC matrix (i.e., a 1 × 1032 vector). For a given subnetwork or cluster, this corresponds to the mean across the parcels comprising that subnetwork or cluster. Mass univariate one-sample t-tests were computed across subjects for all RSFC maps of interest ($p<0.01$ Bonferroni; 1032 comparisons). To highlight the unique topography of RSFC maps of interest, maps were further thresholded to include only the (absolute) top 25% of connections. Mass univariate paired-sample t-tests were computed to assess pair-wise differences between RSFC maps of interest ($p<0.01$ Bonferroni; 1032 comparisons). Contrasts were also computed on the mean values for subcortical regions of interest, as well as at the network-wise level for the 17 networks defined by the Yeo et al. 2011 parcellation. These networks include: visual network A (VIS_A), visual network B (VIS_B), somatomotor network A (SMN_A), somatomotor network B (SMN_B), dorsal attention network A (DAN_A), dorsal attention network B (DAN_B), salience network A (SAL_A), salience network B (SAL_B), LIM_A, LIM_B, frontoparietal network A (FPN_A), frontoparietal network B (FPN_B), frontoparietal network C (FPN_C), default network A (DN_A), default network B (DN_B), and default network C (DN_C).

Results

Modularity results

In order to assess, in a data-driven manner, whether limbic regions comprise a distinct large-scale network or may be more accurately construed as a part of the default network or other large-scale network, we applied two modularity algorithms (see *Section 2.4.2* above) to the group-level mean whole-brain RSFC data. These algorithms assign each parcel to a given module (broadly synonymous with network or cluster) based on their RSFC profile.

Modularity was first computed using the Louvain modularity algorithm (Figure 2A) This algorithm requires specification of a gamma parameter which controls the resolution of the output (i.e., number of modules). Three values for the gamma resolution parameter were examined: 1 (the default), 1.25, and 1.5. Results with gamma=1 parcellated the brain into putative visual (purple), somatomotor (blue), frontoparietal/executive (orange), and default networks (light red). Results with gamma=1.25 mirrored the results with gamma=1, with the further differentiation of the putative salience network (magenta). Finally, results with gamma=1.5 mirrored the results with gamma=1.25, with the further differentiation of the putative dorsal attention network (green). Critically – consistent with our hypothesis – LIM parcels were assigned to the putative DN across resolutions, with the single exception of parcels within the right medial temporal pole for gamma=1 and 1.5. Louvain results were consistent across runs with minor differences (Supplementary Figure 1).

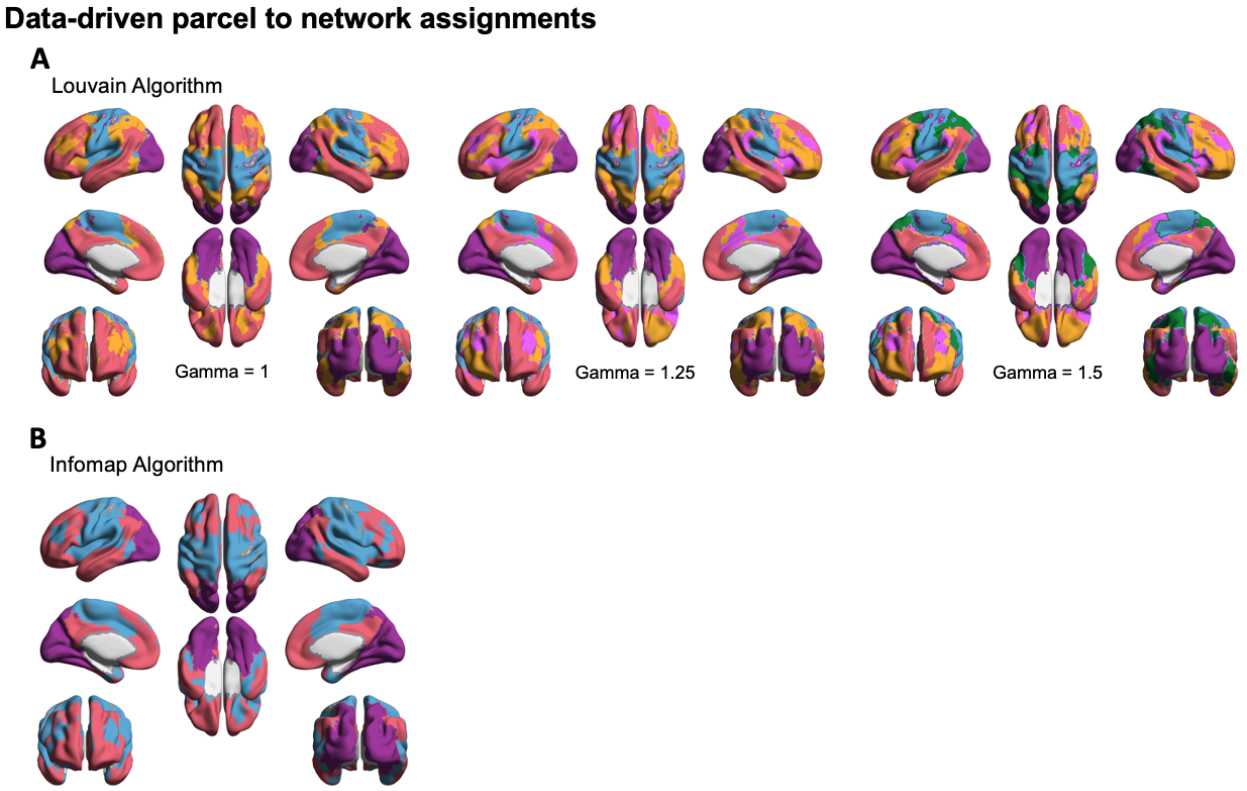

Figure 2. (A) Data-driven network assignments based on the Louvain modularity algorithm, at three values of the gamma resolution parameter. **(B)** Data-driven network assignments based on the Infomap modularity algorithm. Networks are colored according to their putative corresponding large-scale network according to the Yeo 7 network parcellation scheme (Yeo et al., 2011).

To assess the dependence of these results on the modularity algorithm, parcel to network assignments were also computed using the Infomap algorithm (Figure 2B). This algorithm parcellated the brain into three networks: a visual network (purple), a combined somatomotor/auditory/executive network (blue), and a putative default network (light red). Similar to the Louvain algorithm, the majority of LIM parcels were assigned to the DN. However, in this case several parcels within both OFC and the TP were assigned to the somatomotor/auditory/executive network. These parcels were primarily right-lateralized and included: the medial temporal poles, ventral-posterior OFC, and regions within the medial-posterior aspect of the ventral extent of the TP. Infomap were broadly consistent across runs, with the main difference being a greater assignment of left vATL parcels outside of the DN (Supplementary Figure 1).

RSFC map results

Having provided evidence that the LIM, or subregions thereof, are assigned to the DN in a data-driven manner, we next sought to examine the particular LIM RSFC patterns that underlie these assignments. In particular, we performed data-driven clustering on LIM-to-whole-brain RSFC to assess the presence of LIM subdivisions and examined the differential whole-brain RSFC of distinct clusters. Clustering was first performed on the full LIM (i.e., LIM_A and LIM_B combined) as defined by the Yeo et al. (2011) 17 network parcellation, and then each of LIM_A (TP/vATL) and LIM_B (OFC) separately. RSFC maps and contrasts for each of LIM_A and LIM_B as defined based on Yeo et al. (2011) are shown in Supplementary Figure 2.

LIM data-driven clusters

Data-driven clustering performed on the full LIM revealed the presence of multiple clusters and subclusters within this network, supporting our hypothesis of LIM functional heterogeneity (Figure 3B). Qualitative examination of the cluster dendrogram indicates the presence of three primary clusters. Cluster 1 RSFC maps thresholded for the absolute top 25% of connections revealed strong RSFC spanning regions within the bilateral medial prefrontal cortex, anterior, mid, and posterior cingulate, left temporal gyri extending through Wernicke's area into the supramarginal and angular gyri, right temporal pole, medial temporal lobes, left inferior frontal gyrus, and superior frontal gyrus. Cluster 2 RSFC maps thresholded for the absolute top 25% of connections revealed strong RSFC spanning regions within the bilateral anterior and mid cingulate, dorsomedial prefrontal cortex, inferior temporal gyri, medial temporal lobes, lateral prefrontal cortex, and superior and inferior parietal lobule. Cluster 3 RSFC maps thresholded for the absolute top 25% of connections revealed strong RSFC spanning regions within medial prefrontal cortex, bilateral anterior, mid, and dorsal posterior cingulate, bilateral middle and superior temporal gyri extending into Wernicke's area, bilateral inferior frontal gyri, and the medial temporal lobes.

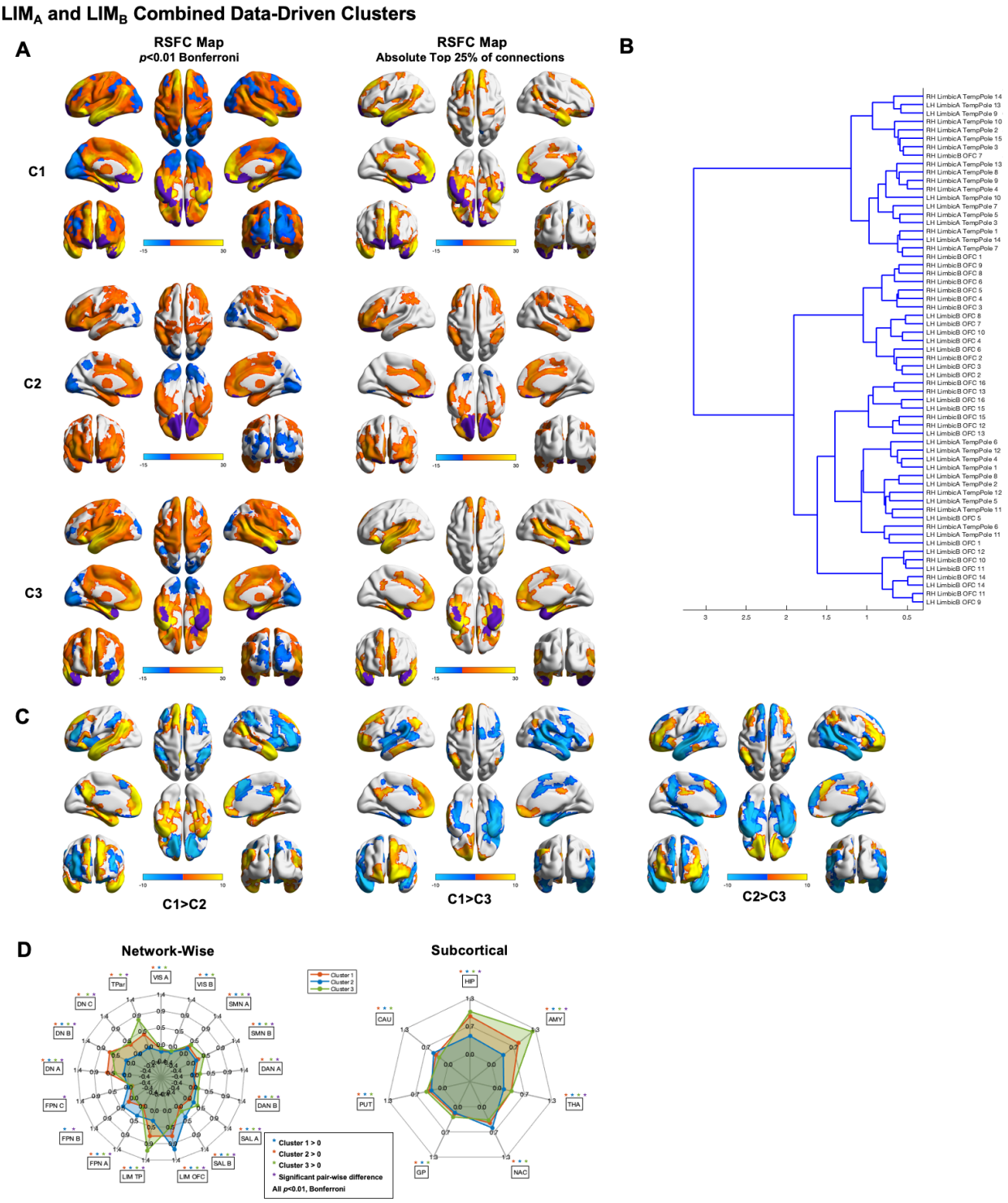

Figure 3. Data-driven clusters revealed by applying Ward clustering to all LIM parcels, spanning both LIM$_A$ and LIM$_B$ **(A) Left:** RSFC maps thresholded at p<0.01 Bonferroni for Cluster 1 (C1; Top), Cluster 2 (C2; Middle), and Cluster 3 (C3; Bottom). **Right:** RSFC maps thresholded at top absolute 25% of connections for Cluster 1 (C1; Top), Cluster 2 (C2; Middle), and Cluster 3 (C3; Bottom). **(B)** Cluster dendrogram. **(C)** Between-cluster contrasts. **(D)**

Spider plots displaying network-wise (Left) and subcortical (Right) between-cluster contrasts. Networks are defined based on the Yeo et al. 2011 17 network parcellation.

Between-subnetwork contrasts revealed a variety of significant differences between clusters. Cluster 1 exhibited significantly greater RSFC than Cluster 2 in the medial prefrontal cortex, posterior cingulate, medial temporal lobes, and primarily left lateralized superior and middle temporal gyri extending into Wernicke's area. Cluster 2 exhibited significantly greater RSFC than Cluster 1 in right lateral prefrontal cortex, bilateral inferior frontal gyrus, dorsomedial prefrontal/premotor cortex, and bilateral anterior parietal lobule. Network-wise contrasts between Cluster 1 and Cluster 2 revealed significantly different RSFC in SAL_A, SAL_B, LIM_A, LIM_B, DN_A, DN_B, DN_C, and TPar. Subcortical contrasts between Cluster 1 and Cluster 2 revealed significantly different RSFC in the hippocampus, amygdala, and thalamus.

Cluster 1 exhibited significantly greater RSFC than Cluster 3 in the medial prefrontal cortex, posterior cingulate, medial temporal lobes, and primarily left lateralized superior and middle temporal gyri extending into Wernicke's area. Cluster 3 exhibited significantly greater RSFC than Cluster 1 in the bilateral superior temporal gyrus and sulcus, bilateral inferior frontal gyrus, inferior somatosensory cortex, Wernicke's area, and the medial temporal lobes. Network-wise contrasts between Cluster 1 and Cluster 3 revealed significantly different RSFC in SAL_A, SAL_B, LIM_A, LIM_B, DN_A, DN_B, DN_C, and TPar. Subcortical contrasts between Cluster 1 and Cluster 3 revealed significantly different RSFC in the hippocampus (HIP), amygdala (AMY), and thalamus (THA).

Cluster 2 exhibited significantly greater RSFC than Cluster 3 in bilateral middle frontal gyrus, parietal lobule, posterior mid cingulate, and ventral OFC. Cluster 3 exhibited significantly greater RSFC than Cluster 2 in anterior/ventral medial prefrontal cortex, posterior cingulate and precuneus, temporal poles, and middle and super temporal gyri extending in Wernicke's area. Network-wise contrasts between Cluster 2 and Cluster 3 revealed significantly different RSFC in SMN_A, SMN_B, DAN_A, SAL_A, SAL_B, LIM_A, LIM_B, FPN_A, FPN_B, DN_A, DN_B, DN_C, and TPar. Subcortical contrasts between Cluster 1 and Cluster 3 revealed significantly different RSFC in the hippocampus, amygdala, and thalamus.

Results were predominantly consistent across runs (Supplementary Figure 3).

Temporal pole intra-subnetwork heterogeneity

Next, we sought to evaluate whether clustering performed separately on each of LIM_A and LIM_B allows greater sensitivity to finer subdivisions. Data-driven clustering performed on the LIM_A revealed the presence of multiple clusters and subclusters (Figure 4B). Qualitative examination of the cluster dendrogram indicates the presence of two primary clusters. Cluster 1 RSFC maps thresholded for the absolute top 25% of connections revealed strong RSFC spanning regions spanning the majority of bilateral temporal lobes excluding portions of the middle temporal gyri, anterior, mid, and dorsal-posterior and cingulate, bilateral inferior frontal gyri, and medial prefrontal cortex. Cluster 2 RSFC maps thresholded for the absolute top 25% of connections revealed strong RSFC spanning the majority of bilateral temporal lobes with a greater extent in the left hemisphere extending into Wernicke's area and the angular gyrus, medial prefrontal cortex, bilateral inferior, superior, and middle frontal gyri, and portions of anterior, mid, and dorsal-posterior cingulate.

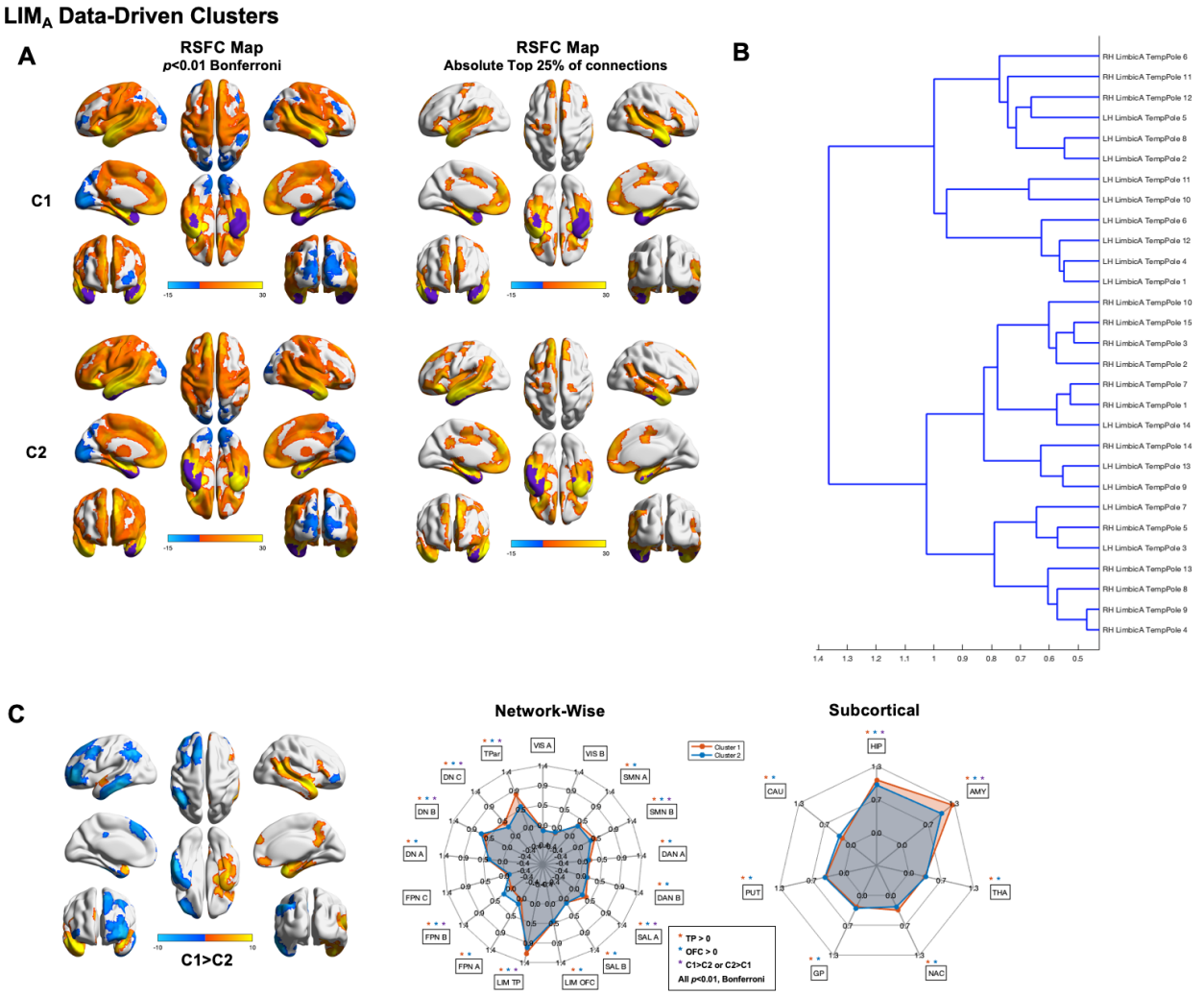

Figure 4. Data-driven clusters revealed by applying Ward clustering to LIM$_A$ parcels only **(A) Left:** RSFC maps thresholded at p<0.01 Bonferroni for Cluster 1 (C1; Top) and Cluster 2 (C2; Bottom). **Right:** RSFC maps thresholded at top absolute 25% of connections for Cluster 1 (C1; Top) and Cluster 2 (C2; Bottom **(B)** Cluster dendrogram. **(C)** Between-cluster C1>C2 contrast. **(D)** Spider plots displaying network-wise (Left) and subcortical (Right) between-cluster contrasts. Networks are defined based on the Yeo et al. 2011 17 network parcellation.

Between-cluster contrasts revealed highly lateralized differences between clusters. Cluster 1 exhibited significantly greater RSFC than Cluster 2 in the right superior temporal gyrus extending from the temporal pole to Wernicke's area and the angular gyrus, the right inferior temporal gyrus and temporal pole along the ventral surface, the right medial temporal lobe, the right dorsal posterior cingulate extending into the precuneus, and regions within ventromedial and dorsomedial prefrontal cortex. Cluster 2 exhibited significantly greater RSFC than Cluster 1 in left inferior, middle, and superior frontal gyri, left inferior temporal gyrus, left interior parietal

lobule/temporoparietal junction, and left dorsomedial prefrontal cortex. Network-wise contrasts between Cluster 1 and Cluster 2 revealed significantly different RSFC in SMN_A, SAL_A, LIM_A, FPN_B, DN_B, DN_C, and TPar. Subcortical contrasts between Cluster 1 and Cluster 2 revealed significantly different RSFC in the hippocampus, and amygdala.

Results were predominantly consistent across runs (Supplementary Figure 4).

Orbitofrontal intra-subnetwork heterogeneity

Data-driven clustering performed on the LIM_B revealed the presence of multiple clusters and subclusters (Figure 5B). Qualitative examination of the cluster dendrogram indicates the presence of three primary clusters. Cluster 1 RSFC maps thresholded for the absolute top 25% of connections revealed strong RSFC spanning regions within the bilateral medial prefrontal cortex, anterior and posterior cingulate, temporal poles, posterior inferior parietal lobule, medial temporal lobes, inferior and superior frontal gyri, and superior somatomotor cortex. Cluster 2 RSFC maps thresholded for the absolute top 25% of connections revealed strong RSFC spanning regions within the bilateral medial prefrontal cortex, bilateral anterior and mid cingulate, left dorsal posterior cingulate, temporal poles, left inferior parietal lobule, medial temporal lobes, and bilateral superior, middle, and inferior frontal gyri. Cluster 3 RSFC maps thresholded for the absolute top 25% of connections revealed strong RSFC spanning the cingulate gyrus extending from its subgenual portion to immediately anterior to its dorsal-posterior portion, bilateral inferior and middle frontal gyri, bilateral parietal lobules, dorsomedial prefrontal cortex, and medial temporal lobes.

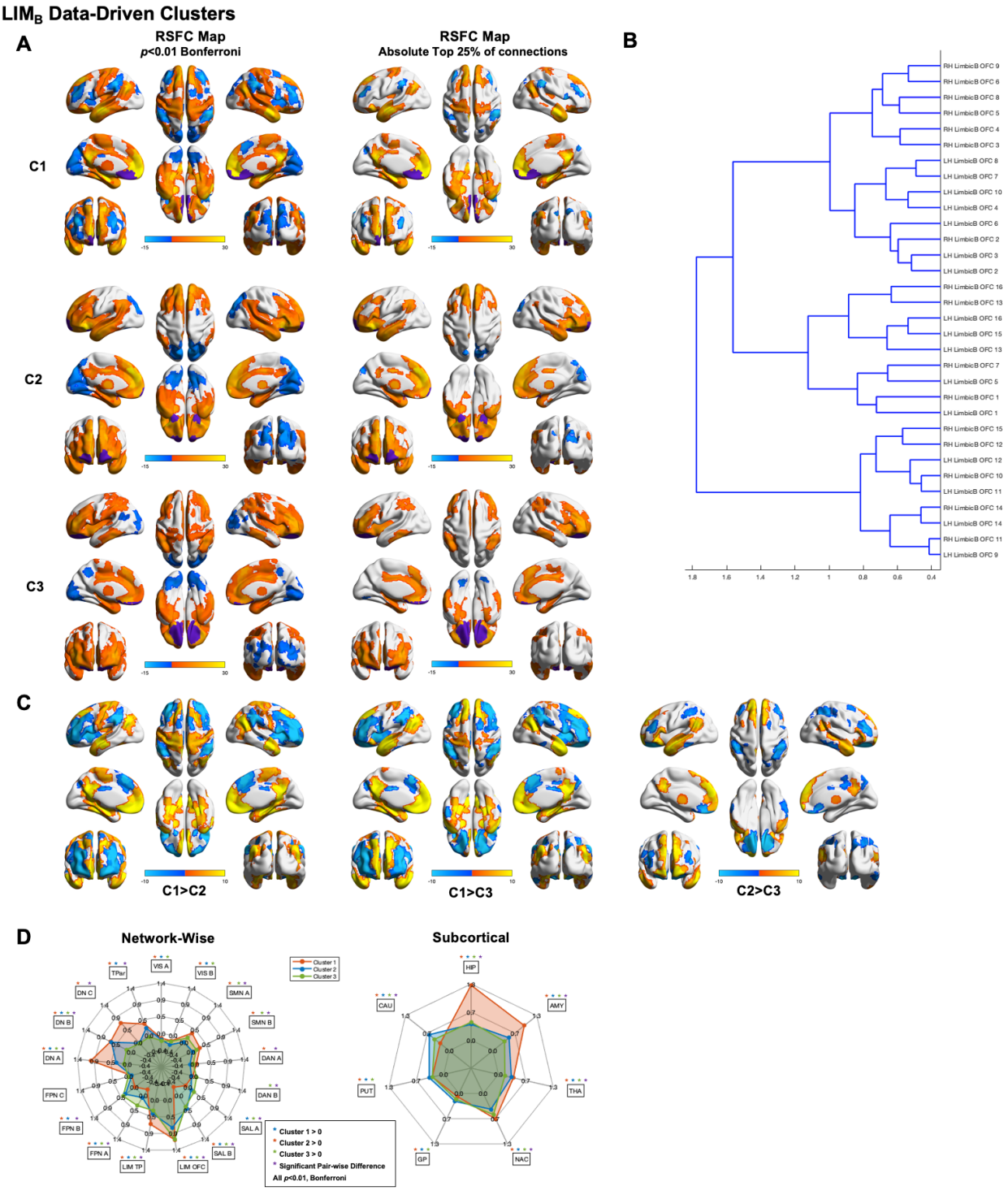

Figure 5. Data-driven clusters revealed by applying Ward clustering to LIM_B parcels **(A) Left:** RSFC maps thresholded at p<0.01 Bonferroni for Cluster 1 (C1; Top), Cluster 2 (C2; Middle), and Cluster 3 (C3; Bottom). **Right:** RSFC maps thresholded at top absolute 25% of connections for Cluster 1 (C1; Top), Cluster 2 (C2; Middle), and Cluster 3 (C3; Bottom). **(B)** Clustering dendrogram. **(C)** Between-cluster contrasts. **(D)** Spider plots displaying

network-wise (Left) and subcortical (Right) between-cluster contrasts. Networks are defined based on the Yeo et al. 2011 17 network parcellation.

Between-subnetwork contrasts revealed a variety of significant differences between clusters. Cluster 1 exhibited significantly greater RSFC than Cluster 2 in the medial prefrontal cortex, posterior cingulate, medial temporal lobes, bilateral somatomotor cortex, and bilateral temporal poles extending along the ventral surface of the temporal lobes/inferior frontal gyri. Cluster 2 exhibited significantly greater RSFC than Cluster 1 in bilateral superior, middle, and inferior frontal gyri, dorsomedial prefrontal/premotor cortex, and anterior superior parietal lobule. Network-wise contrasts between Cluster 1 and Cluster 2 revealed significantly different RSFC in SMN_A, SMN_B, DAN_A, SAL_A, SAL_B, LIM_A, LIM_B, FPN_A, FPN_B, DN_A, and DN_C. Subcortical contrasts between Cluster 1 and Cluster 2 revealed significantly different RSFC in the hippocampus, amygdala, and nucleus accumbens.

Cluster 1 exhibited significantly greater RSFC than Cluster 3 in the medial prefrontal cortex, posterior cingulate, medial temporal lobes, and bilateral temporal poles extending along the ventral surface of the temporal lobes/inferior frontal gyri. Cluster 3 exhibited significantly greater RSFC than Cluster 1 in bilateral superior, middle, and inferior frontal gyri, dorsomedial prefrontal/premotor cortex, and anterior superior parietal lobule. Network-wise contrasts between Cluster 1 and Cluster 3 revealed significantly different RSFC in SMN_A, SMN_B, DAN_A, SAL_A, SAL_B, LIM_A, LIM_B, FPN_A, FPN_B, DN_A, DN_B, and DN_C. Subcortical contrasts between Cluster 1 and Cluster 2 revealed significantly different RSFC in the hippocampus, amygdala, and thalamus.

Cluster 2 exhibited significantly greater RSFC than Cluster 3 in bilateral anterior and dorsal medial prefrontal cortex, dorsal posterior cingulate cortex, bilateral temporal poles, bilateral inferior parietal lobule/angular gyri, bilateral inferior frontal gyri, and the left superior frontal gyrus. Cluster 3 exhibited significantly greater RSFC than Cluster 2 in ventromedial and orbital prefrontal cortex, bilateral middle frontal gyri, bilateral superior parietal lobule, right precuneus, and right posterior-mid cingulate. Network-wise contrasts between Cluster 2 and Cluster 3 revealed significantly different RSFC in SMN_A, SMN_B, DAN_A, LIM_B, FPN_A, DN_A, DN_B, and TPar.

Subcortical contrasts between Cluster 1 and Cluster 3 revealed significantly different RSFC in the nucleus accumbens and caudate.

Results were predominantly consistent across runs (Supplementary Figure 5).

Discussion

In the present study, we leveraged a multi-echo resting-state fMRI dataset with whole-brain signal coverage, including within limbic regions, to characterize the large-scale network organization and whole-brain RSFC of the LIM as defined by the Yeo et al. 2011 17 network parcellation. This includes the two putative LIM subnetworks: LIM_A (comprising the TP and spatially adjacent vATL), and LIM_B (comprising the OFC). Our primary goal was to evaluate whether the LIM, or subregions thereof, may be plausibly construed as part of the DN, and, in addition, to examine intra-LIM heterogeneity in whole-brain RSFC via data-driven clustering and RSFC mapping. Data-driven modularity results with the Louvain algorithm supported the inclusion of the LIM within the DN: with the exception of parcels within the right medial temporal pole, all LIM parcels were assigned to the DN across the resolutions examined. Similarly, Infomap results also revealed that most LIM parcels were assigned to the DN, but revealed less uniformity wherein several most right lateralized parcels – particularly in the vATL – were assigned to a combined somatomotor-executive network. Data-driven clustering results indicated the presence of RSFC heterogeneity across the LIM as a whole, as well as within each of LIM_A and LIM_B separately. Distinct parcel clusters within the LIM exhibited differential RSFC with cortical and subcortical areas across the brain, with medial OFC and left-lateralized TP regions exhibiting the greatest RSFC with the DN, in a subnetwork-specific manner. Taken together, both the data-driven clustering and *a priori*, intra-LIM functional connectivity findings provide strong evidence that significant, and predominantly left lateralized, aspects of the LIM network may be more accurately characterized as the extended DN.

Modularity results from both algorithms assigned the majority of LIM parcels to the same module/network as putative DN regions. This indicates that most LIM regions exhibit strong RSFC with DN regions and that their RSFC with each other is not sufficiently greater to afford their segregation into a distinct network. LIM parcels assigned outside of the DN were assigned to

modules corresponding to executive (frontoparietal/ dorsal attention/salience) and/or somatomotor networks. These parcels were exclusively in the right medial TP for the Louvain algorithm and, for the Infomap algorithm, comprised bilateral medial TPs and a mostly right-lateralized set of parcels in the posterior OFC and an expanse of the right vATL spanning from its anterior-medial to posterior-lateral extent. This set of non-DN parcels within the vATL revealed by the Infomap algorithm was found to be more bilaterally localized for Run 2 (Supplementary Figure 1). Notably, the functional differentiation of the posteromedial versus anterolateral vATL has been highlighted in past task-based fMRI research (Binney et al., 2016; Humphreys et al., 2015; Jackson et al., 2016). This work has indicated that the vATL can be characterized in terms of a gradient from basic and modality-specific semantic representations within its posteromedial aspect, to complex and modality-general representations within its anterolateral aspect (Binney et al., 2016; Humphreys et al., 2015; Jackson et al., 2016). According to this work, the anterolateral vATL – which is the region of the vATL consistently assigned to the DN in the present study – represents the apex of the ATL's processing hierarchy, acting as a multi-modal integrative hub (Binney et al., 2016). As such, our finding that anterolateral vATL parcels were assigned to the DN across algorithms, whereas the remainder of the vATL was not, is consistent with past work indicating that the anterolateral vATL serves to integrate modality-specific inputs into complex abstract representations in a manner similar to regions comprising the DN (Smallwood et al., 2021). More generally, the present modularity findings do not support the differentiation of LIM regions into a large-scale network that is unified and functionally distinct from other networks.

The present clustering results provided deeper insight into the differential RSFC patterns of LIM subdivisions and how these might underpin the modularity assignments. Notably, the parcels assigned outside of the DN by the Infomap algorithm significantly overlap with Cluster 3 from the combined LIM_A-LIM_B clustering analysis and Cluster 1 from the LIM_A clustering analysis. These two clusters both comprise the majority of the right vATL, as well as portions of the bilateral medial TPs. In the case of the LIM_A-LIM_B clustering analysis, this cluster was differentiated from a cluster that combined the left TP and vATL with medial OFC regions, and which exhibited significantly greater RSFC with the DN. In the case of the LIM_A clustering analysis, this cluster was differentiated from a cluster that comprised the left medial TP and vATL, and which exhibited greater RSFC with a left-lateralized set of regions span the DN and the semantic control system

(Binder et al., 2009; Jackson, 2021). These clustering results therefore suggest that left lateralized TP/vATL regions may be more associated with the DN, potentially via their involvement in a DN-overlapping semantic processing network.

Interestingly, relative to left lateralized clusters dominated by LIM_A, the strongly right-lateralized LIM_A-LIM_B cluster comprising the TP, vATL, and posterior OFC exhibited greater RSFC with the bilateral superior temporal gyri and sulci, as well as the inferior frontal gyrus and insula. This pattern has notably been found in social and non-verbal semantic processing task-fMRI investigations that have argued for a right hemisphere bias in the ATL for the processing of social concepts and non-verbal stimuli (Kumfor et al., 2016; Skipper et al., 2011; Zahn et al., 2007). As such, the hemispheric dissociation in RSFC observed here – also partially mirrored in the modularity results – may reflect the distinction between a left-lateralized TP/vATL network that is closely related to the 'semantic system' as typically defined and predominantly involved in verbal and non-social semantic processing, and a right-lateralized TP/vATL network more involved in non-verbal and social semantic processing. It should be noted here, however, that previous studies of the RSFC of TP and vATL subdivisions have not found strong evidence for lateralization effects (Fan et al., 2014; Jackson et al., 2016), and multiple fMRI studies have found strong bilateral activation for social concepts and stimuli (Binney et al., 2016; Jackson et al., 2018). That said, it is likely that the former may be due to the relatively poor signal quality of LIM regions in past fMRI investigations. With respect to the latter, strong evidence from lesion studies and patients with lateralized semantic dementia suggests that some degree of right-lateralized specificity for social concepts have been observed (Pobric et al., 2016; Rice et al., 2018; Snowden et al., 2018), and it is likely that each hemisphere has a partially-specialized and graded contribution across semantic tasks (Ralph et al., 2017; Rice et al., 2018). The high tSNR in the present study may have provided greater sensitivity to hemispheric differences in TP/vATL RSFC.

DN-associated clusters of LIM_A and LIM_B did not exhibit uniform RSFC across the entire DN, but, rather, showed DN-subnetwork-specific patterns. Both LIM_A clusters were most associated with DN_B in particular, with strong RSFC also present for DN_A. The association between the TP/vATL and the DN_B is consistent with this subnetwork's spatial overlap with the semantic processing system, and its role in social cognitive processes for which the temporal lobes are

consistently co-recruited (Binder et al., 2009; Olson et al., 2013; Spreng & Andrews-Hanna, 2015). Indeed, the investigation which introduced the notion of tripartite subnetwork organization of the DN included the TP as a component of DN_B (Andrews-Hanna et al., 2010). LIM_A clusters were also particularly strongly connected to the TPar network (Yeo et al., 2011) which encompasses the superior temporal gyri and sulci, including primary auditory cortex and extending posteriorly into Wernicke's area and anterior visual association regions. TPar RSFC was particularly strong for the right-lateralized LIM_A Cluster 1 (which nonetheless includes a cluster within the left vATL). This can be seen as consistent with the findings discussed above, supporting a role for right superior temporal regions in right-lateralized social cognitive and non-verbal (i.e., pictorial) semantic processes (Kumfor et al., 2016; Pobric et al., 2016; Rice et al., 2018; Skipper et al., 2011; Snowden et al., 2018; Zahn et al., 2007). In contrast, LIM_B Cluster 1 (medial-most OFC) was most associated with DN_A and DN_C. This directly aligns with a recent large-scale RSFC study of the OFC which found that medial subregions exhibited RSFC patterns most overlapping with the DN midline (i.e., DN_A) and the medial temporal lobes (DN_C; (Du et al., 2020)). Moreover, the functional differentiation of medial versus lateral OFC is supported by a large multi-species literature of task-based studies (Kringelbach & Rolls, 2003; Rolls et al., 2020; Schultz et al., 2000; Xie et al., 2021), as well as additional functional and anatomical parcellation studies (Hsu et al., 2020; Rolls et al., 2020; Rolls et al., 2023). It remains unclear, however, why medial OFC regions in particular, which mediate positive reward value, should be more connected to the DN than lateral OFC regions which are involved in the negative reward value/the denial of an expected reward (Rolls et al., 2020). LIM_B Cluster 2, which comprised a small number of parcels within the most anterior and posterior aspects of the OFC, was most associated with DN_B. This also aligns with the results of the above-mentioned large scale RSFC study, in which similarly located parcels exhibited broadly similar RSFC patterns (Du et al., 2020). The results here extend these findings by highlighting how these spatially non-contiguous regions form a functionally dissociable subnetwork within the OFC, with a specific pattern of strong DN_B RSFC. Finally, Cluster 3 (the remainder of the OFC) was not significantly associated with the DN – exhibiting minimal RSFC across DN subsystems. Instead, Cluster 3 was most associated with FPCN and SAL subnetworks, potentially in line with the OFC's documented role in reward-based cognitive control (Dixon & Christoff, 2012; Dixon et al., 2017). Overall, results based on RSFC clustering indicate that several subdivisions of LIM exhibit significant RSFC with the DN in a subsystem-specific manner. These

results underscore the notion that the LIM is likely not a unified and distinct network, but is a collection of regions which show differential patterns of whole-brain RSFC – most prominently with particular DN subnetworks – to an extent that suggests membership in these subnetworks.

RSFC between LIM regions and subcortical regions was also assessed. All LIM subdivisions exhibited significant RSFC with the subcortical regions examined – which included the hippocampus, amygdala, nucleus accumbens, globus pallidus, putamen, and thalamus – indicating strong interconnectivity across limbic, cortical, and subcortical regions. Of note, the clusters which exhibited the greatest RSFC with the DN included the hippocampus, amygdala, thalamus, and to a lesser extent, the nucleus accumbens. Each of these regions correlate strongly with the DN, and recent studies have argued for their inclusion as part of the DN (Alves et al., 2019; Buckner & DiNicola, 2019; Bzdok et al., 2013; Li et al., 2021). This indicates the limitations of previous corticocentric – and non-limbic – conceptions of the DN and suggest that LIM regions may also join these regions in a combined cortical-limbic-subcortical extended DN.

In conclusion, by leveraging multi-echo fMRI data which provide strong tSNR in LIM regions, we found support for the hypothesis that the LIM is an extension of the DN. However, our results also highlighted the distributed and heterogenous nature of LIM RSFC, and indicated the presence of multiple subregions with distinct RSFC across DN subnetworks and the other large-scale networks of the brain. Among LIM regions, we found that the medial OFC and left TP/vATL were most associated with the DN and, more specifically, that medial OFC was primarily associated with DN_A and DN_C, while the left TP/vATL was primarily associated with DN_B. Our findings are consistent with and extend past task-based and RSFC investigations of the TP, vATL, and OFC, providing novel evidence on the precise large-scale network affiliations of these regions. This study contributes to the growing literature expanding the set of regions conceived of as constituents of the DN and suggests that past accounts of a distinct LIM may have been based on poor signal quality and relatively unreliable functional mapping.

References

Alves, P. N., Foulon, C., Karolis, V., Bzdok, D., Margulies, D. S., Volle, E., & de Schotten, M. T. (2019). An improved neuroanatomical model of the default-mode network reconciles previous neuroimaging and neuropathological findings. *Communications biology*, *2*(1), 1-14.

Andrews-Hanna, J. R., Reidler, J. S., Sepulcre, J., Poulin, R., & Buckner, R. L. (2010). Functional-anatomic fractionation of the brain's default network. *Neuron*, *65*(4), 550-562. https://doi.org/10.1016/j.neuron.2010.02.005

Andrews-Hanna, J. R., Smallwood, J., & Spreng, R. N. (2014). The default network and self-generated thought: Component processes and dynamic control. *Annals of the New York Academy of Sciences*, *1316*(1), 29-52.

Barbas, H., Ghashghaei, H., Dombrowski, S., & Rempel-Clower, N. (1999). Medial prefrontal cortices are unified by common connections with superior temporal cortices and distinguished by input from memory-related areas in the rhesus monkey. *Journal of Comparative Neurology*, *410*(3), 343-367.

Bassett, D. S., & Sporns, O. (2017). Network neuroscience. *Nat Neurosci*, *20*(3), 353-364.

Binder, J. R., Desai, R. H., Graves, W. W., & Conant, L. L. (2009). Where is the semantic system? A critical review and meta-analysis of 120 functional neuroimaging studies. *Cerebral Cortex*, *19*(12), 2767-2796.

Binney, R. J., Hoffman, P., & Lambon Ralph, M. A. (2016). Mapping the multiple graded contributions of the anterior temporal lobe representational hub to abstract and social concepts: evidence from distortion-corrected fMRI. *Cerebral Cortex*, *26*(11), 4227-4241.

Biswal, B., Zerrin Yetkin, F., Haughton, V. M., & Hyde, J. S. (1995). Functional connectivity in the motor cortex of resting human brain using echo-planar mri. *Magnetic resonance in medicine*, *34*(4), 537-541.

Blondel, V. D., Guillaume, J.-L., Lambiotte, R., & Lefebvre, E. (2008). Fast unfolding of communities in large networks. *Journal of statistical mechanics: theory and experiment*, *2008*(10), P10008.

Braga, R. M., & Buckner, R. L. (2017). Parallel interdigitated distributed networks within the individual estimated by intrinsic functional connectivity. *Neuron*, *95*(2), 457-471. e455.

Bressler, S. L., & Menon, V. (2010). Large-scale brain networks in cognition: emerging methods and principles [Research Support, U.S. Gov't, Non-P.H.S.

Review]. *Trends Cogn Sci*, *14*(6), 277-290. https://doi.org/10.1016/j.tics.2010.04.004

Buckner, R. L., Andrews-Hanna, J. R., & Schacter, D. L. (2008). The brain's default network: anatomy, function, and relevance to disease. *Ann N Y Acad Sci*, *1124*, 1-38. https://doi.org/10.1196/annals.1440.011

Buckner, R. L., & DiNicola, L. M. (2019). The brain's default network: updated anatomy, physiology and evolving insights. *Nature Reviews Neuroscience*, 1-16.

Buckner, R. L., Krienen, F. M., Castellanos, A., Diaz, J. C., & Yeo, B. T. (2011). The organization of the human cerebellum estimated by intrinsic functional connectivity. *American Journal of Physiology-Heart and Circulatory Physiology*.

Buckner, R. L., Krienen, F. M., & Yeo, B. T. T. (2013). Opportunities and limitations of intrinsic functional connectivity MRI. *Nat Neurosci*, *16*(7), 832-837.

Bzdok, D., Laird, A. R., Zilles, K., Fox, P. T., & Eickhoff, S. B. (2013). An investigation of the structural, connectional, and functional subspecialization in the human amygdala. *Human Brain Mapping*, *34*(12), 3247-3266.

Carmichael, S., & Price, J. (1995). Limbic connections of the orbital and medial prefrontal cortex in macaque monkeys. *Journal of Comparative Neurology*, *363*(4), 615-641.

Carmichael, S., & Price, J. (1996). Connectional networks within the orbital and medial prefrontal cortex of macaque monkeys. *Journal of Comparative Neurology*, *371*(2), 179-207.

Chase, H. W., Grace, A. A., Fox, P. T., Phillips, M. L., & Eickhoff, S. B. (2020). Functional differentiation in the human ventromedial frontal lobe: A data-driven parcellation. *Human Brain Mapping*.

Choi, E. Y., Yeo, B. T., & Buckner, R. L. (2012). The organization of the human striatum estimated by intrinsic functional connectivity. *J Neurophysiol*, *108*(8), 2242-2263.

Cunningham, S. I., Tomasi, D., & Volkow, N. D. (2017). Structural and functional connectivity of the precuneus and thalamus to the default mode network. *Human Brain Mapping*, *38*(2), 938-956.

Damoiseaux, J., Rombouts, S., Barkhof, F., Scheltens, P., Stam, C., Smith, S. M., & Beckmann, C. (2006). Consistent resting-state networks across healthy subjects. *Proceedings of the National Academy of Sciences*, *103*(37), 13848-13853.

DiNicola, L. M., Braga, R. M., & Buckner, R. L. (2020). Parallel distributed networks dissociate episodic and social functions within the individual. *Journal of neurophysiology*, *123*(3), 1144-1179.

Dixon, M. L., Thiruchselvam, R., Todd, R., & Christoff, K. (2017). Emotion and the prefrontal cortex: An integrative review. *Psychol Bull*, *143*(10), 1033.

Du, J., Rolls, E. T., Cheng, W., Li, Y., Gong, W., Qiu, J., & Feng, J. (2020). Functional connectivity of the orbitofrontal cortex, anterior cingulate cortex, and inferior frontal gyrus in humans. *Cortex*, *123*, 185-199.

DuPre, E., Luh, W.-M., & Spreng, R. N. (2016). Multi-echo fMRI replication sample of autobiographical memory, prospection and theory of mind reasoning tasks. *Scientific data*, *3*, 160116.

Fan, L., Wang, J., Zhang, Y., Han, W., Yu, C., & Jiang, T. (2014). Connectivity-based parcellation of the human temporal pole using diffusion tensor imaging. *Cerebral Cortex*, *24*(12), 3365-3378.

Fox, K. C. R., Andrews-Hanna, J. R., Mills, C., Dixon, M. L., Markovic, J., Thompson, E., & Christoff, K. (2018). Affective neuroscience of self-generated thought. *Ann NY Acad Sci*, *1426*, 25-51.

Frith, C. D., & Frith, U. (2007). Social cognition in humans. *Current Biology*, *17*(16), R724-R732.

Hsu, C.-C., Rolls, E. T., Huang, C.-C., Chong, S. T., Zac Lo, C.-Y., Feng, J., & Lin, C.-P. (2020). Connections of the human orbitofrontal cortex and inferior frontal gyrus. *Cerebral Cortex*, *30*(11), 5830-5843.

Humphreys, G. F., Hoffman, P., Visser, M., Binney, R. J., & Ralph, M. A. L. (2015). Establishing task-and modality-dependent dissociations between the semantic and default mode networks. *Proceedings of the National Academy of Sciences*, *112*(25), 7857-7862.

Jackson, R. L. (2021). The neural correlates of semantic control revisited. *Neuroimage*, *224*, 117444.

Jackson, R. L., Bajada, C. J., Rice, G. E., Cloutman, L. L., & Ralph, M. A. L. (2018). An emergent functional parcellation of the temporal cortex. *Neuroimage*, *170*, 385-399.

Jackson, R. L., Hoffman, P., Pobric, G., & Ralph, M. A. L. (2016). The semantic network at work and rest: differential connectivity of anterior temporal lobe subregions. *Journal of Neuroscience*, *36*(5), 1490-1501.

Kahnt, T., Chang, L. J., Park, S. Q., Heinzle, J., & Haynes, J.-D. (2012). Connectivity-based parcellation of the human orbitofrontal cortex. *Journal of Neuroscience*, *32*(18), 6240-6250.

Kondo, H., Saleem, K. S., & Price, J. L. (2003). Differential connections of the temporal pole with the orbital and medial prefrontal networks in macaque monkeys. *Journal of Comparative Neurology*, *465*(4), 499-523.

Kondo, H., Saleem, K. S., & Price, J. L. (2005). Differential connections of the perirhinal and parahippocampal cortex with the orbital and medial prefrontal networks in macaque monkeys. *Journal of Comparative Neurology*, *493*(4), 479-509.

Kringelbach, M. L., & Rolls, E. T. (2003). Neural correlates of rapid reversal learning in a simple model of human social interaction. *Neuroimage*, *20*(2), 1371-1383.

Kumfor, F., Landin-Romero, R., Devenney, E., Hutchings, R., Grasso, R., Hodges, J. R., & Piguet, O. (2016). On the right side? A longitudinal study of left-versus right-lateralized semantic dementia. *Brain*, *139*(3), 986-998.

Kundu, P., Brenowitz, N. D., Voon, V., Worbe, Y., Vértes, P. E., Inati, S. J., Saad, Z. S., Bandettini, P. A., & Bullmore, E. T. (2013). Integrated strategy for improving functional connectivity mapping using multiecho fMRI. *Proceedings of the National Academy of Sciences*, 201301725.

Kundu, P., Inati, S. J., Evans, J. W., Luh, W.-M., & Bandettini, P. A. (2012). Differentiating BOLD and non-BOLD signals in fMRI time series using multi-echo EPI. *Neuroimage*, *60*(3), 1759-1770.

Kundu, P., Voon, V., Balchandani, P., Lombardo, M. V., Poser, B. A., & Bandettini, P. A. (2017). Multi-echo fMRI: a review of applications in fMRI denoising and analysis of BOLD signals. *Neuroimage*, *154*, 59-80.

Li, J., Curley, W. H., Guerin, B., Dougherty, D. D., Dalca, A. V., Fischl, B., Horn, A., & Edlow, B. L. (2021). Mapping the subcortical connectivity of the human default mode network. *Neuroimage*, *245*, 118758. https://doi.org/10.1016/j.neuroimage.2021.118758

Lynch, C. J., Power, J. D., Scult, M. A., Dubin, M., Gunning, F. M., & Liston, C. (2020). Rapid precision functional mapping of individuals using multi-echo fMRI. *Cell reports*, *33*(12), 108540.

Moran, M., Mufson, E., & Mesulam, M. M. (1987). Neural inputs into the temporopolar cortex of the rhesus monkey. *Journal of Comparative Neurology*, *256*(1), 88-103.

Muñoz, M., & Insausti, R. (2005). Cortical efferents of the entorhinal cortex and the adjacent parahippocampal region in the monkey (Macaca fascicularis). *European Journal of Neuroscience*, *22*(6), 1368-1388.

Newman, M. E. (2004). Fast algorithm for detecting community structure in networks. *Physical review E*, *69*(6), 066133.

Ojemann, J. G., Akbudak, E., Snyder, A. Z., McKinstry, R. C., Raichle, M. E., & Conturo, T. E. (1997). Anatomic localization and quantitative analysis of gradient refocused echo-planar fMRI susceptibility artifacts. *Neuroimage*, *6*(3), 156-167.

Olson, I. R., McCoy, D., Klobusicky, E., & Ross, L. A. (2013). Social cognition and the anterior temporal lobes: a review and theoretical framework. *Social cognitive and affective neuroscience*, *8*(2), 123-133.

Pascual, B., Masdeu, J. C., Hollenbeck, M., Makris, N., Insausti, R., Ding, S.-L., & Dickerson, B. C. (2015). Large-scale brain networks of the human left temporal pole: a functional connectivity MRI study. *Cerebral Cortex*, *25*(3), 680-702.

Pobric, G., Lambon Ralph, M. A., & Zahn, R. (2016). Hemispheric specialization within the superior anterior temporal cortex for social and nonsocial concepts. *Journal of Cognitive Neuroscience*, *28*(3), 351-360.

Power, J. D., Plitt, M., Gotts, S. J., Kundu, P., Voon, V., Bandettini, P. A., & Martin, A. (2018). Ridding fMRI data of motion-related influences: Removal of signals with distinct spatial and physical bases in multiecho data. *Proceedings of the National Academy of Sciences*, *115*(9), E2105-E2114.

Price, J. L. (2006). Connections of orbital cortex. *The orbitofrontal cortex*, 39-55.

Raichle, M. E. (2009). A brief history of human brain mapping. *Trends Neurosci*, *32*(2), 118-126. https://doi.org/10.1016/j.tins.2008.11.001

Raichle, M. E., MacLeod, A. M., Snyder, A. Z., Powers, W. J., Gusnard, D. A., & Shulman, G. L. (2001). A default mode of brain function. *Proceedings of the National Academy of Sciences U.S.A.*, *98*(2), 678-682.

Raichle, M. E., & Snyder, A. Z. (2007). A default mode of brain function: A brief history of an evolving idea. *Neuroimage*, *37*(4), 1083-1090. https://doi.org/10.1016/j.neuroimage.2007.02.041

Ralph, M. A. L., Jefferies, E., Patterson, K., & Rogers, T. T. (2017). The neural and computational bases of semantic cognition. *Nature Reviews Neuroscience*, *18*(1), 42-55.

Rice, G. E., Caswell, H., Moore, P., Hoffman, P., & Lambon Ralph, M. A. (2018). The roles of left versus right anterior temporal lobes in semantic memory: a neuropsychological comparison of postsurgical temporal lobe epilepsy patients. *Cerebral Cortex*, *28*(4), 1487-1501.

Rolls, E. T., Cheng, W., & Feng, J. (2020). The orbitofrontal cortex: reward, emotion and depression. *Brain Communications*, *2*(2). https://doi.org/10.1093/braincomms/fcaa196

Rolls, E. T., Deco, G., Huang, C.-C., & Feng, J. (2023). The human orbitofrontal cortex, vmPFC, and anterior cingulate cortex effective connectome: emotion, memory, and action. *Cerebral Cortex*, *33*(2), 330-356.

Rubinov, M., & Sporns, O. (2010). Complex network measures of brain connectivity: uses and interpretations. *Neuroimage*, *52*(3), 1059-1069.

Saleem, K. S., Kondo, H., & Price, J. L. (2008). Complementary circuits connecting the orbital and medial prefrontal networks with the temporal, insular, and opercular cortex in the macaque monkey. *Journal of Comparative Neurology*, *506*(4), 659-693.

Schaefer, A., Kong, R., Gordon, E. M., Laumann, T. O., Zuo, X.-N., Holmes, A. J., Eickhoff, S. B., & Yeo, B. (2017). Local-global parcellation of the human cerebral cortex from intrinsic functional connectivity mri. *Cerebral Cortex*, 1-20.

Schultz, W., Tremblay, L., & Hollerman, J. R. (2000). Reward processing in primate orbitofrontal cortex and basal ganglia. *Cerebral Cortex*, *10*(3), 272-283.

Setton, R., Mwilambwe-Tshilobo, L., Girn, M., Lockrow, A. W., Baracchini, G., Hughes, C., Lowe, A. J., Cassidy, B. N., Li, J., & Luh, W.-M. (2023). Age differences in the functional architecture of the human brain. *Cerebral Cortex*, *33*(1), 114-134.

Simmons, W. K., Reddish, M., Bellgowan, P. S., & Martin, A. (2010). The selectivity and functional connectivity of the anterior temporal lobes. *Cerebral Cortex*, *20*(4), 813-825.

Skipper, L. M., Ross, L. A., & Olson, I. R. (2011). Sensory and semantic category subdivisions within the anterior temporal lobes. *Neuropsychologia*, *49*(12), 3419-3429.

Smallwood, J., Bernhardt, B. C., Leech, R., Bzdok, D., Jefferies, E., & Margulies, D. S. (2021). The default mode network in cognition: a topographical perspective. *Nature Reviews Neuroscience*, 1-11.

Snowden, J. S., Harris, J. M., Thompson, J. C., Kobylecki, C., Jones, M., Richardson, A. M., & Neary, D. (2018). Semantic dementia and the left and right temporal lobes. *Cortex*, *107*, 188-203.

Spreng, R. N., & Andrews-Hanna, J. (2015). The Default Network and Social Cognition. In A. W. Toga (Ed.), *Brain Mapping: An Encyclopedic Reference* (pp. 165-169). Academic Press.

Spreng, R. N., Fernández-Cabello, S., Turner, G. R., & Stevens, W. D. (2019). Take a deep breath: Multiecho fMRI denoising effectively removes head motion artifacts, obviating the need for global signal regression. *Proceedings of the National Academy of Sciences*, 201909848.

Spreng, R. N., Lockrow, A. W., DuPre, E., Setton, R., Spreng, K. A., & Turner, G. R. (2017). Semanticized autobiographical memory and the default–executive coupling hypothesis of aging. *Neuropsychologia*.

Spreng, R. N., Mar, R. A., & Kim, A. S. (2009). The common neural basis of autobiographical memory, prospection, navigation, theory of mind, and the default mode: a quantitative meta-analysis. *Journal of Cognitive Neuroscience*, *21*(3), 489-510.

Thirion, B., Varoquaux, G., Dohmatob, E., & Poline, J.-B. (2014). Which fMRI clustering gives good brain parcellations? *Frontiers in neuroscience*, *8*, 167.

Tian, Y., Margulies, D. S., Breakspear, M., & Zalesky, A. (2020). Topographic organization of the human subcortex unveiled with functional connectivity gradients. *Nat Neurosci*, *23*(11), 1421-1432.

Uddin, L. Q., Yeo, B., & Spreng, R. N. (2019). Towards a universal taxonomy of macro-scale functional human brain networks. *Brain topography*, *32*(6), 926-942.

Vincent, J. L., Snyder, A. Z., Fox, M. D., Shannon, B. J., Andrews, J. R., Raichle, M. E., & Buckner, R. L. (2006). Coherent spontaneous activity identifies a hippocampal-parietal memory network [Research Support, N.I.H., Extramural

Research Support, Non-U.S. Gov't

Research Support, U.S. Gov't, Non-P.H.S.]. *J Neurophysiol*, *96*(6), 3517-3531. https://doi.org/10.1152/jn.00048.2006

Xie, C., Jia, T., Rolls, E. T., Robbins, T. W., Sahakian, B. J., Zhang, J., Liu, Z., Cheng, W., Luo, Q., & Lo, C.-Y. Z. (2021). Reward versus nonreward sensitivity of the medial versus lateral orbitofrontal cortex relates to the severity of depressive symptoms. *Biological Psychiatry: Cognitive Neuroscience and Neuroimaging*, *6*(3), 259-269.

Yeo, B. T. T., Kirienen, F. M., Sepulcre, J., Sabuncu, M. R., Lashkari, D., Hollinshead, M., Roffman, J. L., Smoller, J. W., Zöllei, L., Polimeni, J. R., Fischl, B., Liu, H., & Buckner, R. L. (2011). The organization of the human cerebral cortex estimated by intrinsic functional connectivity. *J Neurophysiol*, *106*, 1125-1165. https://doi.org/10.1152/jn.00338.2011.-

Zahn, R., Moll, J., Krueger, F., Huey, E. D., Garrido, G., & Grafman, J. (2007). Social concepts are represented in the superior anterior temporal cortex. *Proceedings of the National Academy of Sciences*, *104*(15), 6430-6435.

Zald, D. H., McHugo, M., Ray, K. L., Glahn, D. C., Eickhoff, S. B., & Laird, A. R. (2012). Meta-analytic connectivity modeling reveals differential functional connectivity of the medial and lateral orbitofrontal cortex. *Cerebral Cortex*, *24*(1), 232-248.

Bridge to Chapter 3

Findings from Study 1 indicated that the majority of regions within the limbic network may be accurately construed as members of the DN. Moreover, RSFC-mapping revealed that distinct clusters within the limbic network exhibit distinct patterns of whole-brain RSFC, including differential patterns of RSFC with DN subsystems. Of note, the regions of limbic network A (temporal poles and ventral anterior temporal lobe) exhibited stronger RSFC with DN_B and the functionally related temporoparietal network, whereas the regions of limbic network B (particularly in medial orbitofrontal cortex) exhibited stronger RSFC with DN_A and DN_C. This suggests that subregions of the limbic network may differentially couple with subregions of the DN in the service of shared behaviours and cognitive processes.

In Study 2, we build on this study and assess how the structure and function of these networks (limbic, default, and temporoparietal) jointly and differentially covaries with individual differences in a broad variety of behavioural (in the sense of 'non-neural') variables. For this study, we leveraged the same multi-echo resting-state fMRI dataset as Study 1 and additionally included the rich set of behavioural measures that were collected in these same participants, which span social cognition, emotion, memory, executive function, and personality. Results from this study will extend the results of Study 1 and will provide insight into how the functional organization of the DN and related networks discovered at rest may relate to variation in complex behavioural phenotypes.

Chapter 3 – A multivariate examination of default network subsystem-specific brain-behaviour covariance

Adapted from: Girn, M., Bzdok, D., Lockrow, A., Setton, R., Mwilambwe-Tshilobo, L., Turner, G.R., Spreng, R.N., (*In preparation*). Brain-behaviour associations across default network subsystems as revealed by deep behavioural phenotyping

Abstract

Research over the last decades has extensively investigated the default network (DN), a large-scale brain network associated with a wide array of complex and human-defining cognitive processes. This network's diverse functionality is thought to be afforded by significant intra-network heterogeneity; wherein distinct subsystems mediate distinct cognitive processes. To date, the functional roles of DN subsystems have been primarily revealed via task-based neuroimaging studies examining one or two behavioral tasks in isolation. A more comprehensive characterization of the diverse functions mediated by the DN and their topographic distribution across subsystems is lacking. Large, phenotypically rich neuroimaging datasets make possible such characterizations by enabling assessments of complex multivariable relationships between the brain and a large number of behavioural (non-neural) measures. Here, we leverage a unique dataset and apply such an approach to examine multivariate associations between DN subsystem-specific measures of brain structure and function and a wide array of cognitive, emotional, social, and personality measures. Partial least squares (PLS) analyses revealed several axes of DN-behavior covariance which were distinct across neural measures, exhibited differential subsystem contributions, and which encompassed complex groupings between brain and behavior. These results underscore the subsystem organization of the DN and the multifaceted nature of its associations with behavior. More generally, the present study provides further evidence for the DN's complex role in traits and behaviors central to everyday human functioning.

Introduction

The brain comprises functionally specialized networks that interact to mediate complex human behaviors (Bassett & Sporns, 2017). Among the most studied of these networks is the 'default network' (DN) (Andrews-Hanna et al., 2014; Buckner et al., 2008; Buckner & DiNicola, 2019; Smallwood, Bernhardt, et al., 2021). Although initially characterized as a 'task negative' network involved in internally-directed processes which compete with task demands, investigations have now established the much broader functionality of the DN (Margulies & Smallwood, 2017; Smallwood, Bernhardt, et al., 2021; Stawarczyk et al., 2019). In addition to internally-directed processes such as spontaneous thought, social cognition/mentalizing, and prospection, the DN has also been implicated in a variety of externally- and goal-directed processes, including working memory, task updating, narrative/movie comprehension, and visual perception (Andrews-Hanna et al., 2014; Baldassano et al., 2017; Gonzalez-Garcia et al., 2018; Margulies & Smallwood, 2017; Smith et al., 2018; R Nathan Spreng et al., 2014; Stawarczyk et al., 2019; Vatansever, Manktelow, et al., 2017). Broadly, converging evidence suggests that the DN is recruited whenever access to internal representations (e.g., episodic and semantic memory, self/other knowledge, concepts etc.) is required for, or facilitates, a given cognitive/emotional/perceptual process or task (Margulies & Smallwood, 2017; Murphy et al., 2017; Smallwood, Bernhardt, et al., 2021; Smallwood, Turnbull, et al., 2021; Sormaz et al., 2018; R.N. Spreng et al., 2014; Spreng et al., 2010; Stawarczyk et al., 2019; Vatansever, Menon, et al., 2017; Vidaurre et al., 2017). This proposed functionality is consistent with findings indicating that the DN is situated at the apex of the macroscale cortical hierarchy, playing a critical role in spatially distributed transmodal processing that serves to integrate sensory and mnemonic information in the service of complex behaviors (Huntenburg et al., 2018; Margulies et al., 2016; Margulies & Smallwood, 2017; Smallwood, Bernhardt, et al., 2021).

The DN's diverse functionality is thought to be underpinned by significant heterogeneity within this network, wherein distinct regions are associated with dissociable functions (Andrews-Hanna et al., 2010; Andrews-Hanna et al., 2014; Braga & Buckner, 2017; DiNicola et al., 2020; Yeo et al., 2011). Past work has suggested that the DN has either a tripartite (Andrews-Hanna et al., 2010; Andrews-Hanna et al., 2014; Yeo et al., 2011) or bipartite (Braga & Buckner, 2017; DiNicola et

al., 2020; Dohmatob et al., 2020) subsystem organization. The tripartite scheme, revealed via standard group-level analyses and meta-analytic findings, separates the DN into (i) a self-related processing and meaning creation subsystem that runs along the DN midline and includes antero-medial prefrontal and posterior cingulate cortex (DN_A), (ii) a social cognition subsystem that includes dorsomedial prefrontal, lateral parietal, and lateral temporal cortex (DN_B), and (iii) an episodic memory subsystem that includes the medial temporal lobes and ventral posteromedial parietal cortex (DN_C; (Andrews-Hanna et al., 2010; Andrews-Hanna et al., 2014; Bzdok et al., 2015; Yeo et al., 2011). In contrast, the bipartite scheme, revealed via a 'precision mapping' approach that involves dense sampling of a small number of individuals, proposed two interdigitated subsystems: (i) an autobiographical/episodic memory subsystem that includes the medial temporal lobes and (ii) a social cognition subsystem that includes lateral temporal, as well as lateral and dorsomedial parietal cortex (Braga & Buckner, 2017; DiNicola et al., 2020). In addition, evidence from tract-tracing, as well as resting-state and task-based fMRI studies, suggest that the limbic network (LIM) and the temporoparietal network (TPar) may also be extensions of the DN. LIM consists of the bilateral temporal poles and ventral anterior temporal lobe, whereas TPar comprises the bilateral superior temporal gyrus and sulci, extending into Wernicke's area and the angular gyrus (Yeo et al., 2011). LIM regions typically exhibit signal drop out in conventional fMRI acquisitions, but several studies in which reliable signal is present provide evidence for significant RSFC between LIM and DN regions, and consistent task-based coactivation in semantic, social, and affective tasks (Andrews-Hanna et al., 2014; Du et al., 2020; Pascual et al., 2013; Rolls et al., 2020; Setton et al., 2022; Spreng & Andrews-Hanna, 2015; Zald et al., 2012). TPar regions are consistently co-recruited alongside DN and LIM regions in service of linguistic/semantic and social functions (Andrews-Hanna et al., 2014; Binder et al., 2009). Broadly, the studies supporting these schemes indicate that spatially distinct subsystems within the DN (conceived to include the LIM and TPar) make differential contributions to the functional domains of self-related processing, episodic memory, social cognition, emotion, and semantic-linguistic processing.

Multiple approaches have advanced our understanding of how specific regions of the brain mediate discrete cognitive processes (Poldrack & Farah, 2015; Yarkoni et al., 2010). Initial breakthroughs in the localization of function advanced primarily with lesion studies, which determine the brain

regions that are necessary for a cognitive function (Adolphs, 2016). Subsequently, task activation studies with fMRI came to dominate cognitive neuroscience, whereby regions involved in cognitive processes are mapped to the corresponding functional neuroanatomy (Poldrack, 2006; Poldrack & Farah, 2015; Yarkoni et al., 2010). A third approach involves examining inter-individual differences in behavior and determining the corresponding inter-individual variance in brain structure and function that predicts these behaviors (Bzdok & Yeo, 2017; Dubois & Adolphs, 2016; Smith et al., 2015). Characterization of individual differences according to this third approach can provide evidence that converges with findings from lesion-symptom mapping and task activation but can also reveal novel brain-behavior associations. This characterization may be afforded by the analysis of large, phenotypically rich neuroimaging datasets (Bzdok & Yeo, 2017; Dubois & Adolphs, 2016; Smith et al., 2015), which create potential to go beyond circumscribed investigations of specific variables of interest, to assessments of complex multivariable relationships between the brain and rich suites of cognitive, emotional, social, personality, and lifestyle measures. This approach has gained increasing traction in recent years as a result of the coordinated collection of large-scale neuroimaging brain-behavior datasets (Casey et al., 2018; Dubois & Adolphs, 2016; Mendes et al., 2019; Snoek et al., 2021; Sudlow et al., 2015; Van Essen et al., 2013).

Applying this data-driven individual differences approach, an influential large-scale investigation (n = 461) found that the DN was the most strongly implicated of all large-scale networks in a multivariate axis of brain-behavior covariance that linked whole-brain resting-state functional connectivity (RSFC) to a wide variety of cognitive, social, demographic, lifestyle, and neuropsychological factors collected for the Human Connectome Project (Smith et al., 2015). A pre-registered study replicated these findings and also demonstrated that the DN in particular shared the greatest variance with behaviour relative to other networks (Goyal et al., 2022). However, this study was not well-suited for detecting heterogeneities in brain-behaviour covariance *within* the DN. This study also exclusively focused on RSFC and did not examine associations involving brain structure (e.g., grey matter density or cortical thickness). Three outstanding questions, therefore, are (i) whether an individual differences approach focused on the DN can reveal DN subsystem-specific associations with behavior, (ii) whether these align with the

cognitive functions implicated by task-based investigations, and (iii) whether RSFC brain-behaviour relationships align with associations involving brain structure.

The present study seeks to address these questions by applying partial least squares (PLS) analyses to assess associations between the DN and a phenotypically rich set of behavioral measures. More specifically, we sought to examine the differential contributions of DN subnetworks, as well as LIM and TPar networks, to multivariate patterns of brain-behaviour covariance. To do so, RSFC and grey matter density (GMD) were computed within a mask that combines DN, LIM, and TPar (sub)networks as defined by the Schaefer-Yeo 17 network parcellation (Schaefer et al., 2017; Yeo et al., 2011). This parcellation follows the tripartite DN subsystem fractionation, which is more amenable to large-scale group-level analyses than the bipartite scheme, which had its genesis in a precision mapping approach in a small set of individuals (Braga & Buckner, 2017). RSFC connectomes for each participant were derived using an individualized parcellation approach which has been found to increase intra-parcel homogeneity and sensitivity to brain-behavior relationships (Chong et al., 2017). This affords a more precise mapping of RSFC patterns that can then be closely related to individual differences in behavior. We leverage a unique dataset that features a diverse array of cognitive, emotional, social, and personality variables to reveal complex multi-variable brain-behavior relationships involving the DN (Spreng et al., 2022). To facilitate identification of relationship with pre-established subnetwork functionality, behavioral variables were grouped into the categories of self, episodic memory, semantic memory/language, social, emotion, personality, and executive/other (Table 1, below).

We hypothesize that individual differences across these discrete behavioral categories will be robustly related to distinct DN subsystems for RSFC and GMD. Specifically, we predict that behaviour-subnetwork associations will be strongest for (1) DN_A and self variables (2) DN_B and social variables, (3) DN_C and episodic memory variables, (4) LIM and emotion variables (5) TPar and semantic memory/language variables. Our analytic approach will assess these hypotheses in terms of multivariate axes of brain-behaviour covariance, wherein each ‘axis’ pertains to a specific grouping of neural (connection-wise RSFC or voxel-wise GMD) and behavioural variables.

Methods

Participants

121 young adults (mean age 22.52, SD: 4.66; range: 18–32 years; 70 women) participated in the current study. All participants were healthy and had no history of psychiatric, neurological, or other medical illness that could compromise cognitive function. The present sample size is capable of detecting reliable associations between brain and behavior with a magnitude of $r > .20$ with 95% confidence intervals (CI's). 85 behavioural variables were included in the present analysis (Table 1).

Behavioural measures

Category	Measures	Relevant Citation(s)
Self	Meaning and Purpose (NIH) Self-Efficacy (NIH) SAWS Experience SAWS Emotions SAWS Reminiscence SAWS Openness SAWS Humor SLCSR Self-liking SLCSR Self-competence Spiritual Transcendence Index 3D-WS Cognitive 3D-WS Affective 3D-WS Reflective	(Gershon et al., 2013; Seidlitz et al., 2002; Tafarodi & Swann Jr, 2001; Webster, 2003)
Episodic Memory	Picture Sequence Memory (NIH) Autobiographical Interview Internal Density	(Akshoomoff et al., 2013; Levine et al., 2002)
Semantic Memory/Language	Associative Recall Autobiographical Interview External Density	(Brainerd et al., 2014; Levine et al., 2002; Moore & Gordon, 2015; Palombo et al., 2013; Shipley et al., 2009)

	Author Recognition Task Non-Fiction Author Recognition Task Fiction Shipley Vocab Oral Reading Recognition (NIH) Picture Vocabulary (NIH)	
Social	Emotional Support (NIH) Friendship (NIH) Instrumental Support (NIH) Loneliness (NIH) IRI Empathic Concern IRI Fantasy IRI Personal Distress IRI Perspective Taking Total Toronto Empathy Questionnaire ECR Close Relationships: Anxiety ECR Close Relationships: Avoid SNI Social Network Size SNI Social Network Diversity UCLA Loneliness Reading the Mind in the Eyes Moral Foundations Questionnaire (MFQ) Moral Competency Test (MCT) C Score	(Davis, 1983; Spreng* et al., 2009) (Baron-Cohen et al., 2001; Bickart et al., 2011; Davies et al., 2014; Fraley et al., 2000; Gerritsen et al., 2014; Graham et al., 2008; Russell, 1996)
Emotion	Anger-Affect (NIH) Anger-Hostility (NIH) Anger-Physical Aggression (NIH) Fear-Affect (NIH) Fear-Somatic Arousal (NIH) General Life Satisfaction (NIH) Perceived Hostility (NIH) Perceived Rejection (NIH) Perceived Stress (NIH) Sadness (NIH) Toronto Alexithymia DDF	(Gershon et al., 2013) (Bagby et al., 1994; Carver & White, 1994)

	Toronto Alexithymia DIF Toronto Alexithymia EOT Toronto Alexithymia Total Trait Boredom Scale BIS/BAS BAS Drive BIS/BAS BAS Fun BIS/BAS BAS Reward BIS/BAS BIS	
Personality	Volatility Withdrawal Neuroticism Compassion Politeness Agreeableness Industrious Orderliness Conscientiousness Enthusiasm Assertiveness Extraversion Openness Intellect Introverted	(DeYoung et al., 2007)
Executive/Other	Card Sort Flanker Inhibitory Control and Attention List Sorting Working Memory Pattern Comparison Process Speed Shipley Blocks DGI Delayed Gratification	(Akshoomoff et al., 2013; Hoerger et al., 2011; Lind, 2014)

Table 1. Abbreviations: NIH, National Institutes of Health; SAWS, Self-Assessed Wisdom Scale; 3D-WS, Three-Dimensional Wisdom Scale; SAM, Survey of Autobiographical Memory; AI, Autobiographical Interview; IRI, Interpersonal Reactivity Index; ECR, Experience in Close Relationships Revised; SNI, Social Network Index; DDF, Difficulty Describing Feelings; DIF, Difficulty Identifying Feelings; EOT, Externally Oriented Thinking; DGI, Delaying Gratification Inventory; SLCSR, Self-liking/Competence Scale Revised; MCT, Moral Competence Test.

Neuroimaging data acquisition

All imaging data were acquired on a 3T GE Discovery MR750 scanner (General Electric, Milwaukee, United States) with a 32-channel receive-only phased-array head coil at the Cornell Magnetic Resonance Imaging Facility in Ithaca. Participants completed two × 10 minutes 6 seconds resting-state multi-echo BOLD functional scans with eyes open, blinking and breathing normally in the dimly lit scanner bay. These scans were acquired using a multi-echo echo planar imaging (ME-EPI) sequence with online reconstruction (TR = 3000 ms; TE's = 13.7, 30, 47 ms; FA = 83°; matrix size = 72 × 72; field of view (FOV) = 210 mm; 46 axial slices; 3.0 mm isotropic voxels). Resting-state functional scans were acquired with 2.5x acceleration with sensitivity encoding and were acquired prior to engagement in any cognitive task fMRI experiment.

Anatomical images were acquired during one 5m25s run using a T1-weighted volumetric MRI magnetization prepared rapid gradient echo (MPRAGE) sequence (repetition time (TR)=2530 ms; echo time (TE)=3.4 ms; inversion time (TI)=1100 ms; flip angle (FA)=7°; bandwidth=195 Hz/pixel; 1.0 mm isotropic voxels, 176 slices). Anatomical scans were acquired with 2x acceleration with sensitivity encoding.

Neuroimaging preprocessing and denoising

The present multi-echo fMRI acquisition collected data at three echo times (TEs). Given interregional differences in T_2* relaxation rates, a given TE results in differential signal quality across regions. An acquisition with three TEs therefore allows the optimally-weighted voxel-wise averaging of data across echoes. This significantly improves whole-brain TSNR and attenuates signal drop out in typically problematic regions along the ventral-anterior surface of the brain (e.g., orbitofrontal cortex, temporal pole) (Kundu et al., 2013; Kundu et al., 2012; Lynch et al., 2020). In addition, a multi-echo acquisition facilitates the biophysically-based removal of noise components from resting fMRI datasets (Kundu et al., 2013; Kundu et al., 2012). This is because collecting data at multiple TEs allows the direct measurement of TE-dependent variability in the signal. The denoising method presently employed – multi-echo independent component analysis (ME-ICA) – exploits this information to distinguish BOLD signal from non-BOLD noise (Kundu et al., 2012). TE-dependent variability of the signal can be fit to models of changes in T_2* (i.e., the

transverse relaxation rate; the basis for the BOLD contrast) or changes in baseline signal (S_0) which are the product of scanner artifacts, motion, and other sources of noise (Kundu et al., 2012). By comparing the relative goodness of fit of TE dependence to each of these models, one can separate BOLD signal from non-BOLD noise. Past work has supported the effectiveness of this technique in denoising BOLD signal of motion and physiological artifacts in resting-state fMRI (Kundu et al., 2013; Kundu et al., 2012; Lynch et al., 2020; Setton et al., 2022). Importantly, ME-ICA denoising removes distant dependent motion effects from RSFC data (Power et al., 2018; Spreng et al., 2019). Resting-state fMRI data were preprocessed with ME-ICA version 2.7 (https://afni-nimh-nih-gov.proxy3.library.mcgill.ca/pub/dist/src/pkundu/meica.py). Anatomical images were first skull stripped using the default parameters in FSL BET. ME-ICA processing was then run with the following options: -e 13.6, 29.79, 46.59; -b 12; --no_skullstrip; –space = Qwarp_meanE+tlrc. Here, the Qwarp_meanE+tlrc file represented a site-specific MNI-space template (available here: https://zenodo.org/record/3575255). This template was created in AFNI using @toMNI_Qwarpar. Finally, ME-ICA denoised time series were resampled to 2mm isotropic and smoothed with a 6 mm FWHM kernel in SPM8.

Signal quality

In order to assess the signal quality of the ME-ICA processed images within the extended DN, we calculated tSNR on the data within a combined DN-LIM-TPar mask. This mask was defined based on the Yeo et al. (2011) 17 network parcellation, created by combining ROIs across these networks as parcellated by Schaefer and colleagues (Schaefer et al., 2017). tSNR, a measure of signal strength at the voxel level, was calculated as the mean signal intensity of a voxel across the timeseries divided by its standard deviation.

tSNR was calculated on the smoothed optimally combined (across TEs) timeseries following ME-ICA denoising. Derived tSNR spatial maps were averaged across all subjects, thresholded at 50, and projected onto a surface, as shown in Figure 1. tSNR was considered only within the combined DN-limbic mask used for analyses. The results display strong tSNR, including within areas that typically exhibit signal-drop out (e.g., orbitofrontal cortex and the temporal pole).

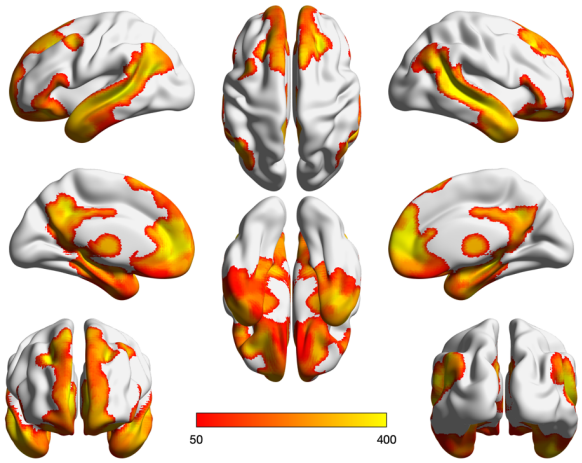

Figure 1. Mean TSNR for subjects of the current study within the combined DN-LIM-TPar mask, thresholded at 50.

Neural measures

Two PLS analyses were conducted to examine brain-behaviour relationships, each with distinct neural variables and identical behavioral variables. The first analysis featured GMD (Ashburner & Friston, 2000) as computed within the combined mask. The second analysis featured interregional RSFC between all regions corresponding to DN, LIM, and TPar based on the 400 region Schaefer cortical parcellation (119 individualized parcels collectively comprising these three networks). The measures are described in detail below.

Grey matter density (GMD)

GMD was calculated from the individual-subject T1-weighted images using voxel-based morphometry (VBM) as implemented in CAT12, a SPM12 add-on (Ashburner & Friston, 2000; Gaser & Dahnke, 2016). Raw T1-weighted images were first spatially normalized to a high-resolution stereotactic space using the DARTEL template and then underwent automated segmentation into gray matter, white matter, and cerebrospinal fluid (CSF). CAT12 uses a tissue probability map (TPM) prior to skull strip the data and initialize the segmentation, and segmentation is conducted using a hypothesis-free adaptive maximum *a posteriori* (AMAP) segmentation approach (Gaser & Dahnke, 2016). This approach estimates the amount of brain

tissue type within each voxel and allows for the control of partial volume effects. The resulting grey matter maps were visually inspected to ensure consistency in orientation across subjects. Once this was confirmed, the homogeneity of the total sample was evaluated in order to identify outliers. Homogeneity was determined to be high with average inter-subject spatial correlations of $r = >0.90$ and no significant outliers were identified. Prior to analysis, total intracranial volume was regressed from the grey matter maps to more reliably extract individual differences in relative gray matter proportions. The regressed grey matter maps were then smoothed with an 8mm Gaussian kernel prior to being used as input to the PLS analyses.

Individualized-parcel interregional resting-state functional connectivity (RSFC)

Recent years have seen great strides made in neuroimaging-based parcellations of the brain, which are generated in a data-driven fashion on the basis of functional or multimodal neuroimaging data (Eickhoff et al., 2018; Glasser et al., 2016; Gordon et al., 2014; Schaefer et al., 2017). As a result, certain group-level parcellations have been taken as reliable indicators of individual-subject neuroanatomy and have been employed in a wide-variety of studies (Eickhoff et al., 2018). However, neuroimaging research has increasingly revealed that the sizes, locations, and spatial arrangements of brain regions (parcels) vary across individuals (Braga & Buckner, 2017; Chong et al., 2017; Gordon et al., 2017; Kong et al., 2019; Laumann et al., 2015). The uniform application of a group-level parcellation to subjects with varying neuroanatomy, therefore, is likely to reduce correspondence across subjects, reduce intra-parcel homogeneity, and thereby reduce effect sizes. Consistent with this, individualized parcellation methods have been found to improve the homogeneity of BOLD signal within parcels and provide better estimates of task-related variance (Chong et al., 2017), as well as improve behavioral prediction (Kong et al., 2019).

Here we generated subject-specific parcels using a Group Prior Individual Parcellation (GPIP) approach (Chong et al., 2017). This approach is initialized by a pre-defined group parcellation, and then iteratively shifts parcel boundaries based on individual-specific resting-state fMRI data while preserving parcel label correspondence across subjects. More specifically, GPIP iterates between two primary steps. First, an initial pre-defined group parcellation atlas is refined to optimize each individual's parcel boundaries with respect to their resting state fMRI data. Second,

a group sparsity constraint is applied to model connectivity by leveraging the group similarities in connectivity between parcels while optimizing the parcel boundaries within individuals. With this two-step iterative process, parcel labels are continuously updated in order to converge upon the most optimal partition. Relative to group-based parcellations, GPIP has been shown to improve homogeneity of BOLD signal within parcels and delineation between regions of functional specialization (Chong et al., 2017). This approach therefore enables a more accurate estimation of subject-specific functional areas (Chong et al., 2017) and is more sensitive to detecting associations between RSFC and behaviour (Kong et al., 2019; Mwilambwe-Tshilobo et al., 2019; Setton et al., 2022).

In the present study, the GPIP algorithm was initialized with the Schaefer local-global 400 region parcellation (Schaefer et al., 2017) and run for 20 iterations of the two steps described above. Intra-parcel homogeneity (average correlation of intra-parcel vertex pairs) was calculated at each iteration for each subject and analyses confirmed increased homogeneity following the algorithm, as described in a previous paper (Setton et al., 2022). RSFC matrices for each subject were computed by calculating the product-moment correlation coefficient between each pair of individualized parcels. The Fisher's r-to-z transformation was then applied to account for variation in data degrees of freedom – in this case the number of de-noised ICA coefficients produced by ME-ICA – across individuals (Kundu et al., 2013):

$$Z = \text{arctanh}(\text{R}) \cdot \sqrt{df - 3}$$

where R is the correlation value and *df* refers to the number of de-noised ICA coefficients.

Partial least squares (PLS)

PLS is a multivariate statistical technique that assesses linear relationships between two variable sets/matrices (**X** and **Y**) in a data-driven manner (Wold et al., 1983). In the context of neuroimaging, PLS is commonly used to examine multivariate brain-behaviour relationships (McIntosh & Lobaugh, 2004). Given a set of neural variables **X** (e.g., voxel-wise patterns) and a

set of behavioural variables **Y**, PLS conducts a singular value decomposition of the cross-correlation matrix **X'Y** to identify the linear combinations of the individual variables which maximizes the covariance between **X** and **Y** across subjects. This process yields several mutually-orthogonal latent variables (LVs) which can be understood as covariance-maximized brain-behaviour groupings. Each LV is composed of three elements: (i) a left singular vector, containing weights for each of the behavioral measures ('behavioural saliences'); (ii) a right singular vector, containing weights for each of the functional connections ('neural saliences'); and (iii) a scalar singular value. Squared singular values reflect effect size: they are proportional to the covariance between connectivity and behavior that is accounted for by each latent variable. We refer to the whole-brain mean of neural saliences as a 'brain score' and the mean behavioural salience across all behavioural measures as a 'behaviour score'. The number of latent variables is equal to the rank of **X'Y**; in the present case, this is the number of behavioral measures.

Two distinct PLS analyses were conducted in the present study. Each included identical behavioral variables (**Y)** but differed in neural variables (**X)**, which pertained to either connection-wise RSFC or voxel-wise GMD values**.** For computational purposes and as a form of 'denoising', principal component analysis (PCA) was applied to the (79 variable) behavior matrix in order to reduce the dimensionality of the data (see Supplementary Table 1 for PCA component weightings for each behavioural variable). The top 20 principal components, representing 80% of cumulative explained variance, were used as the **Y** matrix. **X** for the first analysis consisted of the voxel-wise GMD vector for each subject. **X** for the second analysis consisted of the vectorized lower triangle of 119x119 Fisher-transformed DN-LIM-TPar interregional RSFC matrices for each subject.

The statistical significance of each LV was evaluated using permutation testing. This involved iteratively computing the PLS analysis 1000 times while permuting the rows of one of the data matrices **(X)** each time. This process generates a distribution of singular values under the null hypothesis that there is no relationship between the neural measures and behavior. The significance of each LV is then estimated by computing the proportion of times the permuted singular values is higher than the observed singular values (significance thresholded at $P < .05$). This step is required to determine whether a given LV likely reflects actual structure in the data as opposed to random noise.

In addition to computing the significance of a given LV, the reliability of the weights (saliences) for individual voxels and behavioural measures was assessed using bootstrap resampling. This step allows the identification of the variables (both neural and behavioural) which are likely core constituents of the given LV - as opposed to being more 'peripheral' and interchangeable - and enables more reliable interpretation. The rows of both data matrices (**X** and **Y**) were iteratively sampled with replacement and used as input to the PLS analysis 1000 times. This generated a sampling distribution for each neural and behavioural salience. To identify connections and behaviors that (i) make a large contribution to the overall multivariate pattern and (ii) are relatively insensitive to sub-sampling, the ratio between each weight and its bootstrap-estimated standard error was calculated. The resulting 'bootstrap ratios' (BSRs) are large for voxels/behaviors that have large weights and narrow confidence intervals. If the sampling distribution is approximately unit normal, BSRs are equivalent to z-scores. Voxels were considered reliable if the absolute value of the BSR > 2 (approximately $P < .05$). Thresholded neural BSR maps for each measure were projected to surface space and visualized using the BrainNet viewer software (Xia et al., 2013).

LV 'brainscores' were calculated as the dot product of the LV neural salience values with each subject's corresponding (input) neural measure values. Behavioural associations with a given LV were computed as the correlation between that LV's participant brainscores and the 79 input variables. We chose this approach rather than back-projecting the principal-component-wise behavioural loadings into the input variable space as it affords more direct interpretations of correlation values. For each LV and brain score-behaviour correlation, bootstrapped 95% confidence intervals were computed and behavioural measures with a confidence interval that crossed zero were excluded from visualization and interpretation.

Within-Sample Validation

Given concerns regarding the reliability of brain-behaviour associations, some form of validation is required. The present analyses were conducted on a unique in-house dataset with an idiosyncratic set of behavioural variables, therefore precluding an exact replication. Validation for RSFC findings was therefore conducted across runs within the current sample. For this within-

sample validation, functional neural measures and associated PLS analyses were first conducted on data from resting-state run 1 and then replicated on resting-state run 2 in the form of a direct replication. More specifically, each PLS analysis was applied to run 1 data, and, for each subject, the dot product was then computed between the neural salience maps of each resulting statistically significant LV and the corresponding input matrix computed on subject-level run 2 data. The dot product value therefore represents the extent to which the neural pattern associated with each run 1 LV is expressed in the run 2 data. The correlation between the dot product and the 79 behavioral measures was then computed for each LV, and reliability assessed, in the same manner as was done with run 1. Importantly, only the behavioral measures that were found as reliable in both runs are visualized and interpreted in the main text. The behavioral heatmaps for each LV shown in the main text represents the average correlation value across runs for these measures (correlations from each run were Fisher r-to-z transformed, averaged, and then reverse transformed). As such, all functional results were internally validated prior to interpretation. Within-validation was unfortunately not possible in the present dataset, given the availability of only one structural volume per subject.

Results

Behavioural Results

We first looked at descriptive statistics for the behavioral data to determine whether they were suitable for linear decomposition with PLS. Pair plots and box plots were created for each of the measures to confirm normality and spread in the distributions. Second, consistent with this, the pairwise correlations (product-moment correlation coefficients) were computed between all the measures, and the observed associations were consistent with hypothesized relationships based on the nature of the constructs (Supplementary Figure 1).

PLS Results

The PLS results revealed five significant LV for GMD and five for RSFC (all p's < 0.05, 1000 permutations). Each LV corresponds to a multivariate axis of covariance spanning multiple neural

(voxels or interregional connections) and behavioral variables (principal components). Note that the present manuscript uses the words ‘axis’ and ‘LV’ interchangeably. Each LV was represented as a set of neural and behavioral loadings (‘saliences’). For visualization and interpretation, neural loadings are expressed as bootstrap ratios (BSRs) of neural saliences (1000 bootstrap samples) and behavioral loadings are expressed as correlations between brainscores (subject-wise whole-brain mean of neural saliences) and the input behavioral variables. See *Section 2.6* for more details on the PLS approach**.**

GMD Results

Five statistically significant LVs of GMD-behaviour covariance are displayed in Figure 2 in descending order of covariance explained (see Supplementary Figure 2 for scree plot). GMD LVs did not exhibit significant sex differences (Supplementary Figure 3).

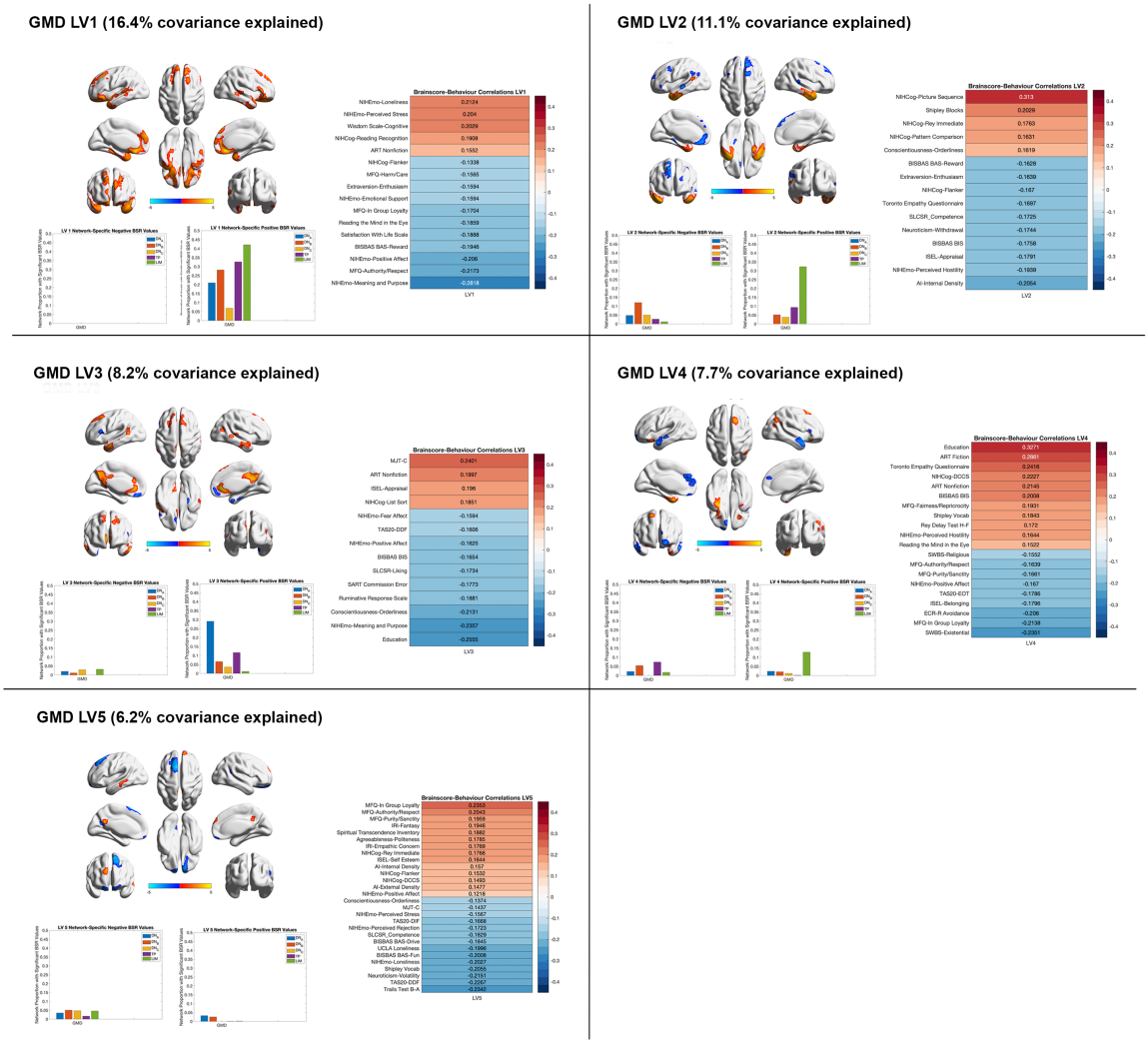

Figure 2. Statistically significant LVs each representing an axis of covariance between GMD and behaviour (p<0.05). For each LV: **(Top-left)** The most reliable neural weightings as determined by a voxel-wise BSR value ≥|2|, equivalent to p <0.05. **(Bottom-left)** Thresholded voxel-wise BSR values expressed as network proportions according to the Yeo et al. (2011) 17 network parcellation scheme, for positive (left) and negative (right) values. **(Right)** The correlation values of reliable brain-behaviour correlations pertaining to that LV (see *Methods*). For each LV, higher GMD values are depicted in warm colors and are: (i) positively associated with higher values of the positively weighted, warm-colored, behaviors, and (ii) negatively associated with lower values for the negatively weighted, cool colored, behaviors. Additionally, negative GMD values depicted in cooler colors are (i) positively associated with lower values of the negatively weighted, cool-colored, behaviors and (ii) negatively associated with higher values for the positively weighted, warm colored, behaviors.

Overall, results revealed multiple axes of GMD-behaviour covariance that map groupings of cognitive, emotional, personality, and social variables to brain structure. Each LV represents a complex latent brain-behaviour phenotype that is expressed to varying degrees across subjects.

On the brain side, LV 1 on the positive aspect loaded highest within bilateral ventral, dorsal, and orbital medial prefrontal cortex (PFC) as well as within temporopolar cortex extending ventrally. Clusters were also found in the bilateral inferior frontal junction, as well as along the superior temporal gyrus/temporal sulcus. Network-wise stratification indicated that LIM, TP, DN_B, and DN_A exhibited the greatest proportion of voxels with significant positive BSR values. No significant negative neural values were found for this LV. On the behavior side, LV 1 on the positive aspect loaded highly on measures of loneliness, stress, a tendency toward cognitive reflection, and two measures of crystallized cognition. Negatively, LV 1 loaded highly on measures of meaning and purpose, positive affect, and satisfaction with life, as well as a tendency towards recourse to authority/respect in moral judgments and reward-driven motivations. For each LV, higher values for the neural feature depicted in warm colored regions are associated with higher values for the positively weighted, warm colored, behaviors and lower values for the negatively weighted, cool colored, behaviors. For example, in this specific case, higher GMD in the anterior temporal poles is associated with greater loneliness and a lower sense of meaning and purpose in life.

On the brain side, LV 2 on the positive aspects loaded highly within bilateral temporopolar cortex extending ventrally. Of all the networks, this cluster predominantly overlapped with LIM. Negatively, LV 2 loads highest in left subgenual anterior cingulate/ventromedial PFC and right dorsomedial PFC, predominantly overlapping with DN_B. On the behaviour side, LV 2 on the positive aspect loaded highly on measures of episodic memory, executive function, and verbal learning, as well as the orderliness aspect of the personality domain of conscientiousness. Negatively, LV 2 loaded highly on measures of internal episodic memory detail, feelings of interpersonal hostility, perception of interpersonal appraisal, and a tendency toward neurotic withdrawal, as well as interpersonal unease, neurotic withdrawal, and behavioural inhibition, as well as self-assessed competence, empathy, reward-driven motivations, and trait enthusiasm.

On the brain side, LV 3 on the positive aspect loaded highly along the cortical midline encompassing bilateral anterior cingulate cortex and the PCC and precuneus, as well as within small clusters of lateral temporal cortex and the left superior frontal gyrus. Of all the networks, significant positive BSR values predominantly overlapped with DN_A. Negatively, LV 2 loaded highly within small clusters of anterior/ventromedial PFC, the left inferior frontal junction, and right temporal pole. On the behaviour side, LV 3 on the positive aspect loaded highly on measures of sophisticated moral reasoning, non-fiction knowledge, perception of interpersonal appraisal, and processing speed. Negatively, LV 3 loaded highly on measures of education, meaning and purpose, orderliness, a tendency towards rumination, and self-liking, as well as positive affect, fear affect, and a difficulty describing feelings.

On the brain side, LV 4 on the positive aspects loaded highly within a small cluster of the left temporal pole, extending ventromedially, as well as within the right inferior parietal lobule. Negatively, LV 4 loaded highly within the anterior superior temporal gyrus/temporal pol, as well as in left anterior/dorsomedial PFC. On the behaviour side, LV 4 on the positive aspect loaded highly on measures of education, crystallized cognition, empathy, and cognitive flexibility, as well as behavioural inhibition, moral judgments based on fairness and reciprocity, and perceived hostility. Negatively, LV 4 loaded highly on measures of existential and religious well-being, moral judgments based on in-group loyalty, purity, and authority, an avoidant relationship style, a sense of interpersonal belonging, and externally oriented thinking in relation to one's feelings.

On the brain side, LV 5 on the positive aspects loaded highly within small clusters in bilateral ventral PCC/retrosplenial cortex, and the left middle temporal gyrus. Negatively, LV 5 loaded highest within a large cluster of left superior temporal gyrus, extending in a dorsal-posterior direction. On the behaviour side, LV 5 on the positive aspect loaded highest on measures of moral judgments based on in group loyalty, authority, and purity, a style of fantasy and empathic concern style of interpersonal reactivity, as well as a tendency towards high agreeableness/politeness and interpersonal self-esteem. Negatively, LV 5 loads highly on measures of executive function, difficulty describing feelings, neuroticism-volatility, and loneliness, as well as crystallized knowledge, and behavioural activation driven by fun and drive.

RSFC Results

Five statistically significant LVs of RSFC-behaviour covariance are displayed in Figure 3 in descending order of covariance explained (see Supplementary Figure 2 for scree plot). RSFC LVs did not exhibit significant sex differences (Supplementary Figure 4). Overall, results revealed multiple axes of RSFC-behaviour covariance that map groupings of cognitive, emotional, personality, and social variables to brain functional connectivity. Each LV represents a complex latent brain-behaviour phenotype that is expressed to varying degrees across subjects.

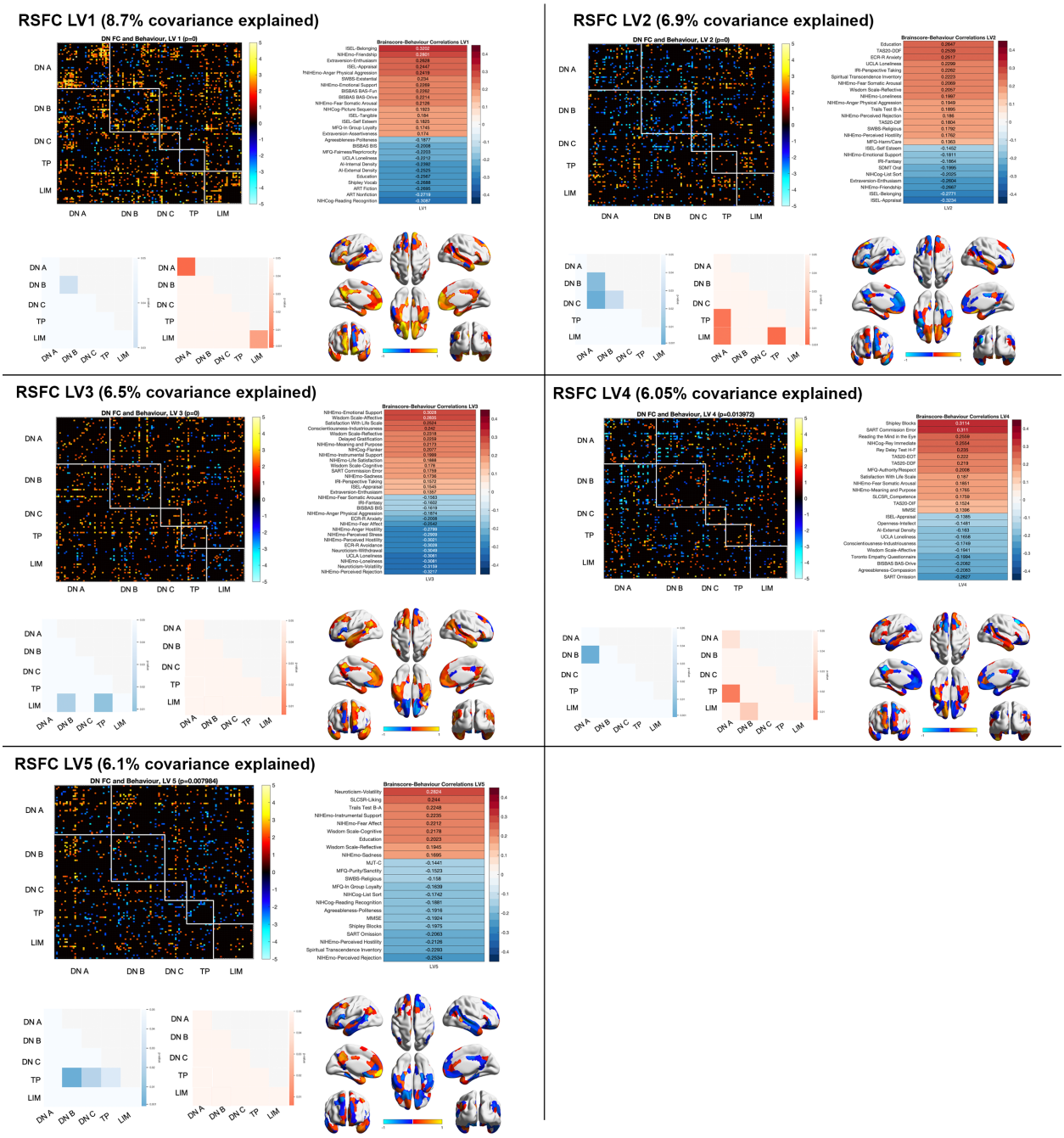

Figure 3. Statistically significant LVs each representing an axis of covariance between RSFC and behaviour (p<0.05). For each LV: **(Top-left)** the most reliable interregional neural weightings as determined by a voxel-wise BSR value ≥|2|, equivalent to p <0.05. **(Bottom-left)** Network-wise values according to the Yeo et al. (2011) 17 network parcellation scheme. Values are p values representing network-wise statistical significance based on permutation testing (see *Methods*), for negative (left) and positive (right) BSR values. **(Top-right)** The correlation values of reliable brain-behaviour correlations pertaining to that LV (see *Methods*). **(Bottom-right)** Mean whole-brain BSR value for each region (row-

wise mean based on top-left). For each LV, higher GMD values are depicted in warm colors and are: (i) positively associated with higher values of the positively weighted, warm-colored, behaviors, and (ii) negatively associated with lower values for the negatively weighted, cool colored, behaviors. Additionally, negative GMD values depicted in cooler colors are (i) positively associated with lower values of the negatively weighted, cool-colored, behaviors and (ii) negatively associated with higher values for the positively weighted, warm colored, behaviors.

On the brain side, LV 1 on the positive aspect displayed predominantly positive loadings across the examined networks, with the exception of TP within-network RSFC. Positive network loadings were most reliable for DN_A and LIM within-network RSFC. Negative loadings for LV 1 loads were scattered across the examined networks, with the most reliable loadings pertaining to DN_B within-network FC. On the behavior side, LV 1 on the positive aspect loaded highly on measures of interpersonal belonging and appraisal, friendship, and the enthusiastic aspect of extraversion, as well as physical aggression, somatic arousal, and behavioural activation based on fun and drive. Negatively, LV 1 loads highly on measures of crystallized cognition, education, episodic memory detail, loneliness, and moral judgments based on fairness/reciprocity.

On the brain side, LV 2 on the positive aspect loaded most consistently for RSFC between DN_A and each of TP and LIM, as well as between TP and LIM. Negatively, LV 2 loaded most consistently for RSFC between DN_A and each of DN_B and DN_C, as well as between DN_B and DN_C. On the behaviour side, LV 2 on the positive aspect loaded highly on measures of education, difficulty describing feelings, anxiety, and loneliness, as well as perspective taking interpersonal reactivity, spiritual transcendence, and self-assessed reflective wisdom. Negatively, LV 2 loaded highly on measures of interpersonal belonging and appraisal, friendship the enthusiasm aspect of extraversion, and measures of cognitive processing speed.

On the brain side, LV 3 on the positive aspect exhibited predominantly positive loadings across the networks examined, but a reliable pattern of RSFC did not emerge for any specific network or network-pair. Negatively, LV 3 loaded on connections between LIM and each of DN_B and TP. On the behaviour side, LV 3 on the positive aspect loaded highest on measures of emotional support, affective and reflective wisdom, satisfaction with life, and the industriousness aspect of conscientiousness. Negatively, LV 2 loaded highly on measures perceived rejection, the volatility

and withdrawal aspects of neuroticism, loneliness, avoidance tendences in relationships, and feelings of hostility, stress, anger, and fear.

On the brain side, LV 4 on the positive aspect loaded most reliably for RSFC within DN_A and between DN_A and TP, as well as between DN_B and LIM. Negatively, LV 4 loaded most reliably for RSFC between DN_A and DN_B. On the behaviour side, LV 4 on the positive aspect loaded highly on measures of fluid cognition, false positives on a sustained attention task, theory of mind, visuospatial memory, and a difficulty describing feelings and tendency to engage in externally oriented thinking. Negatively, LV 4 loads highly on measures of false negatives on a sustained attention task, the compassion aspect of agreeableness, drive-based behavioural activation, empathy, affective wisdom, and the industrious aspect of conscientiousness.

On the brain side, LV 5 on the positive aspect loaded highest on particular left lateralized connections within DN_A and between DN_A and DN_B, but these were not reliable at the level of the entire network/network pair. Negatively, LV 5 loaded most reliably for RSFC between TP and each od DN_B, DN_C, and TP. On the behaviour side, LV 5 on the positive aspect loads highly on measures of the volatility aspect of neuroticism, self-liking, executive control, and instrumental support, as well as fear affect and cognitive and reflective wisdom. Negatively, LV 5 loads highly on measures of perceived rejection and hostility, spiritual transcendence, false negatives on a sustained attention task, fluid cognition, mental state, and the politeness aspect of agreeableness.

Discussion

In the present study, we assessed individual differences in DN structure and function and related these to differences in a variety of human behaviors. More specifically, multivariate analyses were conducted for DN GMD (structure) and RSFC (function), linking each to 79 variables spanning measures of cognition, emotion, social behavior, and personality. Results revealed multiple statistically significant multivariate axes of brain-behavior covariance for each neural measure, wherein each axis represents a pattern that links a group of behavioral variables to a group of neural variables (voxel-wise GMD or connection-wise RSFC). As hypothesized, results indicated significant intra-DN heterogeneity in brain-behavior covariance, wherein each DN subsystem differentially contributed to each axis. Many, but not all, DN subsystem-specific associations

aligned with their putative cognitive/behavioral functions as revealed by task-based fMRI. This was particularly the case for axes which linked LIM to semantic memory/language and emotion, and DN_B to semantic memory/language and social variables. This study underscores the complexity of brain-behavior relationships involving the DN, and provides further evidence for DN subnetwork-specific roles in a variety of human traits and behaviors.

Based on previous findings, we hypothesized DN subsystem-specific associations with behavior. Our results revealed that DN subsystems indeed differentially contribute to axes of brain-behavior covariance, with certain axes exhibiting selectivity for a particular subsystem and others featuring joint contributions across subsystems. With marginal exceptions, DN subsystems did not uniformly contribute to the axes in which they were strongly implicated. More specifically, for GMD, in certain cases one or two subsystems/networks (out of five total) exhibited disproportionate contributions suggestive of DN subnetwork functional specificity. In other cases, three or more featured a sizeable number of significant voxels, indicative of domain generality across the DN. With respect to RSFC, each axis linked a distributed neural pattern to behavior, but evidence also indicated specific subnetwork-level associations more than others. These findings suggest that DN subnetworks exhibit a combination of unique and shared variance across participants in their association with behavior. This is consistent with the fact that the behavioral loadings for each axis cut across putative functional divides – often grouping together, for example, socio-emotional, personality, and cognitive variables. The brain-behavior axes revealed by our approach can, therefore, be said to represent complex behavioral phenotypes that span disparate functional domains, and which are accordingly underpinned by a selective mix of contributions across DN subsystems and functionally related networks – shedding light on the distributed nature of brain-behaviour associations. The intra-DN heterogeneity in brain-behaviour associations found here provides evidence against treating the DN as a unified system when evaluating associations with behavior (Andrews-Hanna et al., 2014; DiNicola et al., 2020; Kernbach et al., 2018).

A question of interest is to what extent the observed subsystem associations align with their putative contributions to behaviour and cognition based on task-based fMRI investigations. Across the observed brain-behavior axes, LIM – and/or a combination of LIM with DN_A or DN_B – was

the most commonly represented neural pattern. LIM comprises the bilateral temporal poles, ventral anterior temporal lobes, and orbitofrontal cortex and has been implicated in a variety of processes, most notably including linguistic-semantic processing, social cognition, and emotional/reward-related processing (Binder et al., 2009; Binney et al., 2016; Humphreys et al., 2015; Jackson, 2021; Jackson et al., 2016; Rolls et al., 2020). Important for the present context, the LIM has been reliably found to co-activate alongside regions comprising the DN – particularly DN_B – in the service of most of these processes (Andrews-Hanna et al., 2010; Andrews-Hanna et al., 2014; Binder et al., 2009; Fox et al., 2018; Olson et al., 2013). Consistent with this, we found that axes which featured strong contributions from LIM and/or LIM and DN_A or DN_B were most associated with semantic memory/language, social, and/or emotion variables. For example, GMD LV1 featured strongest weightings from voxels comprising LIM, with secondary strong weightings form TPar and DN_B, and was linked to five behavioral variables, two of which were semantic memory/language related and two of which social and emotional-related. Another example is RSFC LV1, which featured within-network RSFC for DN_A and LIM as the most reliable neural pattern. The behavioral variables linked to this pattern predominantly included social, emotion, and self-related variables. The present individual-differences findings, therefore, complement past task-based findings supporting the consistent recruitment of LIM and DN regions in the service of semantic, social, and emotional processes and, further, highlight the presence of DN-subsystem specific associations.

DN_A was associated with brain-behavior axes that spanned several behavioral categories, but was only loosely aligned with self-related measures as would be predicted from previous research. For example, GMD LV3 highly selectively features voxels overlapping with DN_A but its behavioral variables were distributed across executive/other, social, and semantic memory/language measures. The DN_A was also strongly implicated in RSFC LV1, in which case it was grouped alongside LIM and was predominantly associated with social and emotion variables. This functionality does not necessarily directly align with the DN_A's hypothesized primary involvement in self-related processes, but is does accord with the notion that it comprises a hub which not only integrates the other DN subsystems, but also other large-scale networks in general (Kernbach et al., 2018; Smallwood, Bernhardt, et al., 2021; Van Den Heuvel & Sporns, 2011). Indeed, regions within DN_A have been found to co-activate alongside the DN_B, DN_C, LIM, and TPar across their

diverse cognitive roles (Andrews-Hanna et al., 2014; Stawarczyk et al., 2019; Zald et al., 2012). Emerging evidence also suggests a role for DN_A, through connections with other large-scale brain systems, in executive cognitive processes, such as working memory and task-set shifting (Smith et al., 2018; Vatansever, Manktelow, et al., 2017; Vatansever, Menon, et al., 2017). Thus, the diverse behavioral associations of DN_A support its more general role as an integrative hub, as opposed to a specialized DN subsystem (Braga & Buckner, 2017; Smallwood, Bernhardt, et al., 2021; Stawarczyk et al., 2019; Van Den Heuvel & Sporns, 2011). Of the DN subsystems, DN_C was the least implicated in all observed brain-behaviour axes. This may be due to the small number (4 out of 79) of measures pertaining to episodic memory in the current study and the relatively selective specialization of DN_C for such processes (Andrews-Hanna et al., 2014). Overall, our results support the presence of functional specialization within each subsystem, while also indicating joint covariance in support of multi-variable behavioural phenotypes.

A comparable previous study leveraged data from the Human Connectome Project and assessed multivariate brain-behavior associations (Smith et al., 2015). This study found a multivariate axis of whole-brain brain-behavior covariance separating 'positive' behavioral variables – in the sense of being healthy or desirable – from 'negative' variables, with DN RSFC strongly positively weighted and exhibiting the strongest weighting of all networks (Goyal et al., 2022; Smith et al., 2015). The present results suggest considerably greater complexity in brain-behavior associations involving the DN by revealing groups of covarying behaviors that do not readily lend themselves to straightforward distinctions such as 'positive' versus 'negative'. Indeed, several of the behavioral LVs indicate covarying relationships with the brain that group together ostensibly desirable and undesirable characteristics. As an illustrative example, RSFC LV 1 groups together several 'positive' social variables, including measures of belonging, friendship, interpersonal appraisal, and emotional support, alongside measures of anger/physical aggression and fear-based somatic arousal – and separates them from several crystallized cognition and education-related variables, which themselves positively covary with a measure of loneliness. These groupings of behavior go beyond a simple positive-negative axis and may better reflect the complexities of real-world behavioral phenotypes. We note, however, that RSFC LV3 represents an axis that is broadly consistent with a positive-negative axis, and which may correspond to the axis found by Smith et al (2015). Similar to their earlier findings, RSFC LV3 implicates connections spanning much of

the DN, and these connections are positively associated with 'positive' behavioral measures, including measures of emotional support, interpersonal appraisal, satisfaction with life, self-efficacy, cognitive-affective wisdom, enthusiasm, and industriousness. In contrast, the opposing side of this axis encompasses measures of perceived rejection, neurotic volatility and withdrawal, loneliness, stress, anger, fear, and hostility. The neural pattern contributing to the negative side of axis predominantly implicates RSFC between LIM and each of DN_B and LIM – consistent with the role of these networks in social and emotional processing (Andrews-Hanna et al., 2014; Olson et al., 2013; Rolls et al., 2020; Rudebeck & Rich, 2018; Spreng & Andrews-Hanna, 2015). This latter neural finding is notable given that Smith et al. did not find within-DN connections which were associated with the negative side of the axis and can be attributed to the increased sensitivity of our DN-focused analyses (i.e., given the reduction of the feature space), as well as due to our inclusion of LIM and TPar.

More fundamentally, the present results suggest that characterizing brain-behavior associations based on a single behavioral measure alone may not provide an accurate portrayal of inter-individual variation. In particular, it was found that, across LVs, a given behavioral measure sometimes loaded strongly with a very different set of additional behavioral measures in its association with the brain. For example, in GMD LV1, loneliness loaded strongly with cognitive and reflective wisdom, perceived stress, and measures of crystallized cognition, whereas in RSFC LV3 loneliness loaded highly with measures such as perceived rejection, interpersonal avoidance, and the withdrawal and volatility aspects of neuroticism. Thus, a failure to consider the broader phenotypic context (i.e., co-occurring traits and tendencies) in which a particular behavior manifests may obscure multifaceted brain-behavior associations. In other words, the examination of multivariate interrelations across variables provides an important context that can help inform more subtle interpretations. This is because a given behavior or trait may be differentially expressed in brain structure and/or function depending on the constellation of behaviors with which it co-occurs. The present results therefore suggest that distinct 'phenotypic subtypes' might exist for particular brain-behavior associations.

An important limitation of the present study is a lack of an out-of-sample replication (Bzdok & Yeo, 2017). However, given that we used a unique dataset with a rich and idiosyncratic set of non-

neural variables, an independent replication is untenable. We believe that the use of unique datasets is critical for exploratory investigations which provide the foundation for novel discoveries. Comprehensive replications of the findings of such datasets by necessity will not be possible, but the intention is that they will serve to motivate future studies, inform the interpretation of previous ones, and potentially guide the inclusion of additional behavioral variables for larger future studies. To provide evidence of reliability in the present context, we conducted a within-sample replication for the RSFC results, using resting-state fMRI run 1 for discovery and run 2 for validation as described in the *Methods***.** RSFC results exhibited significant correspondence across runs and the results reported in the main text represent across-run overlap. It was not possible to conduct a within-sample replication for the GMD findings, as only one structural volume was available per participant. Concerns regarding reliability are particularly relevant given the poor replicability of findings within neuroimaging-based individual differences research (Button et al., 2013; Marek et al., 2022; Poldrack et al., 2017). This has been attributed predominantly to the use of underpowered datasets and overestimates of 'true' effect sizes (Yarkoni et al., 2009). A recent large-scale investigation of neuroimaging-based brain-behavior associations found that the effect sizes of the investigated univariate correlations continually decreased as a function of sample size, ultimately reaching $|r < 0.1|$ in the full sample of ~3000 subjects (Marek et al., 2022). In addition, this study found that with n=100 iterative subsampling from this full sample, univariate correlations ranged from approximately r = -0.3 to 0.3 within a 95% confidence interval (Marek et al., 2022). This raises an alarm given the abundance of individual differences studies that have used samples of n<100 (Schulz et al., 2020). Critically, however, three important points distinguish the current study from the Marek et al. study: (i) The above-mentioned estimates were based on univariate single-measure correlations, whereas we applied a multivariate approach spanning many behavioral variables. Moreover, Marek et al. (2022) notably found larger (and more replicable) effect sizes (r = 0.4 to 0.6, n = ~2000) when using canonical correlation analysis, a multivariate technique similar to the PLS approach adopted here. (ii) The above-mentioned estimates were based on whole-brain exploratory analyses ("brain wide association studies"; BWAS), whereas the present analyses were constrained to the DN and therefore afford increased sensitivity due to a hypothesis-driven reduction of the feature space. (iii) Marek et al. used single echo data, which has been found to exhibit significantly lower inter-scan RSFC reliability than multi-echo data (Lynch et al., 2020), and is therefore less likely to reveal large effect sizes. Taken together, the

present dataset and the analytical protocol implemented here affords confidence in the reliability of the findings, but future targeted analyses are needed to test specific hypotheses that emerge.

In conclusion, we applied PLS to assess multivariate axes of brain-behavior covariance involving the DN and found several complex mappings that group together sets of cognitive, social, emotional, and personality measures with subsystem-specific patterns of DN structure and function. Our findings support the presence of significant functional heterogeneity within the DN and this network's close association with the functionally related LIM and TPar networks. Consistent with our hypotheses, contributions from each DN subsystem (and each of LIM and TPar networks) were not uniform across the revealed brain-behaviour axes. Neural patterns involving the LIM, and the LIM in association with DN_A or DN_B, were the most common across the patterns observed and were most associated with semantic memory/language, social, and/or emotion variables. Broadly, the present results underscore the multifaceted and complex nature of brain-behavior relationships involving the DN and the value of deep behavioral phenotyping for a more comprehensive understanding of the functionality of large-scale networks, as revealed by taking an individual differences approach to identifying brain-behavior relationships.

References

Adolphs, R. (2016). Human lesion studies in the 21st century. *Neuron*, *90*(6), 1151-1153.

Akshoomoff, N., Beaumont, J. L., Bauer, P. J., Dikmen, S. S., Gershon, R. C., Mungas, D., Slotkin, J., Tulsky, D., Weintraub, S., & Zelazo, P. D. (2013). VIII. NIH Toolbox Cognition Battery (CB): composite scores of crystallized, fluid, and overall cognition. *Monographs of the Society for Research in Child Development*, *78*(4), 119-132.

Andrews-Hanna, J. R., Reidler, J. S., Sepulcre, J., Poulin, R., & Buckner, R. L. (2010). Functional-anatomic fractionation of the brain's default network. *Neuron*, *65*(4), 550-562. https://doi.org/10.1016/j.neuron.2010.02.005

Andrews-Hanna, J. R., Smallwood, J., & Spreng, R. N. (2014). The default network and self-generated thought: Component processes and dynamic control. *Annals of the New York Academy of Sciences*, *1316*(1), 29-52.

Arbabshirani, M. R., Damaraju, E., Phlypo, R., Plis, S., Allen, E., Ma, S., Mathalon, D., Preda, A., Vaidya, J. G., & Adali, T. (2014). Impact of autocorrelation on functional connectivity. *Neuroimage*, *102*, 294-308.

Ashburner, J., & Friston, K. J. (2000). Voxel-based morphometry—the methods. *Neuroimage*, *11*(6), 805-821.

Bagby, R. M., Parker, J. D., & Taylor, G. J. (1994). The twenty-item Toronto Alexithymia Scale—I. Item selection and cross-validation of the factor structure. *Journal of psychosomatic research*, *38*(1), 23-32.

Baldassano, C., Chen, J., Zadbood, A., Pillow, J. W., Hasson, U., & Norman, K. A. (2017). Discovering event structure in continuous narrative perception and memory. *Neuron*, *95*(3), 709-721. e705.

Baron-Cohen, S., Wheelwright, S., Hill, J., Raste, Y., & Plumb, I. (2001). The "Reading the Mind in the Eyes" Test revised version: a study with normal adults, and adults with Asperger syndrome or high-functioning autism. *The Journal of Child Psychology and Psychiatry and Allied Disciplines*, *42*(2), 241-251.

Bassett, D. S., & Sporns, O. (2017). Network neuroscience. *Nat Neurosci*, *20*(3), 353-364.

Bickart, K. C., Wright, C. I., Dautoff, R. J., Dickerson, B. C., & Barrett, L. F. (2011). Amygdala volume and social network size in humans. *Nat Neurosci*, *14*(2), 163.

Binder, J. R., Desai, R. H., Graves, W. W., & Conant, L. L. (2009). Where is the semantic system? A critical review and meta-analysis of 120 functional neuroimaging studies. *Cerebral Cortex*, *19*(12), 2767-2796.

Binney, R. J., Hoffman, P., & Lambon Ralph, M. A. (2016). Mapping the multiple graded contributions of the anterior temporal lobe representational hub to abstract and social concepts: evidence from distortion-corrected fMRI. *Cerebral Cortex*, *26*(11), 4227-4241.

Braga, R. M., & Buckner, R. L. (2017). Parallel interdigitated distributed networks within the individual estimated by intrinsic functional connectivity. *Neuron*, *95*(2), 457-471. e455.

Brainerd, C., Reyna, V., Gomes, C. F., Kenney, A., Gross, C., Taub, E., & Spreng, R. (2014). Dual-retrieval models and neurocognitive impairment. *Journal of Experimental Psychology: Learning, Memory, and Cognition*, *40*(1), 41.

Buckner, R. L., Andrews-Hanna, J. R., & Schacter, D. L. (2008). The brain's default network: anatomy, function, and relevance to disease. *Ann N Y Acad Sci*, *1124*, 1-38. https://doi.org/10.1196/annals.1440.011

Buckner, R. L., & DiNicola, L. M. (2019). The brain's default network: updated anatomy, physiology and evolving insights. *Nature Reviews Neuroscience*, 1-16.

Button, K. S., Ioannidis, J. P., Mokrysz, C., Nosek, B. A., Flint, J., Robinson, E. S., & Munafò, M. R. (2013). Power failure: why small sample size undermines the reliability of neuroscience. *Nature Reviews Neuroscience*, *14*(5), 365-376.

Bzdok, D., & Yeo, B. T. (2017). Inference in the age of big data: Future perspectives on neuroscience. *Neuroimage*, *155*, 549-564.

Carver, C. S., & White, T. L. (1994). Behavioral inhibition, behavioral activation, and affective responses to impending reward and punishment: the BIS/BAS scales. *Journal of personality and social psychology*, *67*(2), 319.

Casey, B., Cannonier, T., Conley, M. I., Cohen, A. O., Barch, D. M., Heitzeg, M. M., Soules, M. E., Teslovich, T., Dellarco, D. V., & Garavan, H. (2018). The adolescent brain cognitive development (ABCD) study: imaging acquisition across 21 sites. *Developmental cognitive neuroscience*, *32*, 43-54.

Chen, J., Leong, Y. C., Honey, C. J., Yong, C. H., Norman, K. A., & Hasson, U. (2017). Shared memories reveal shared structure in neural activity across individuals. *Nat Neurosci*, *20*(1), 115-125.

Chong, M., Bhushan, C., Joshi, A., Choi, S., Haldar, J., Shattuck, D., Spreng, R., & Leahy, R. (2017). Individual parcellation of resting fMRI with a group functional connectivity prior. *Neuroimage*, *156*, 87-100.

Davies, C. L., Sibley, C. G., & Liu, J. H. (2014). Confirmatory factor analysis of the Moral Foundations Questionnaire. *Social Psychology*.

Davis, M. H. (1983). Measuring individual differences in empathy: Evidence for a multidimensional approach. *Journal of personality and social psychology*, *44*(1), 113.

DeYoung, C. G., Quilty, L. C., & Peterson, J. B. (2007). Between facets and domains: 10 aspects of the Big Five. *Journal of personality and social psychology*, *93*(5), 880.

DiNicola, L. M., Braga, R. M., & Buckner, R. L. (2020). Parallel distributed networks dissociate episodic and social functions within the individual. *Journal of neurophysiology*, *123*(3), 1144-1179.

Du, J., Rolls, E. T., Cheng, W., Li, Y., Gong, W., Qiu, J., & Feng, J. (2020). Functional connectivity of the orbitofrontal cortex, anterior cingulate cortex, and inferior frontal gyrus in humans. *Cortex*, *123*, 185-199.

Dubois, J., & Adolphs, R. (2016). Building a Science of Individual Differences from fMRI. *Trends in Cognitive Sciences*, *20*(6), 425-443. https://doi.org/https://doi.org/10.1016/j.tics.2016.03.014

DuPre, E., Luh, W.-M., & Spreng, R. N. (2016). Multi-echo fMRI replication sample of autobiographical memory, prospection and theory of mind reasoning tasks. *Scientific data*, *3*, 160116.

Eickhoff, S. B., Yeo, B., & Genon, S. (2018). Imaging-based parcellations of the human brain. *Nature Reviews Neuroscience*, *19*(11), 672-686.

Fox, K. C. R., Andrews-Hanna, J. R., Mills, C., Dixon, M. L., Markovic, J., Thompson, E., & Christoff, K. (2018). Affective neuroscience of self-generated thought. *Ann NY Acad Sci*, *1426*, 25-51.

Fraley, R. C., Waller, N. G., & Brennan, K. A. (2000). An item response theory analysis of self-report measures of adult attachment. *Journal of personality and social psychology*, *78*(2), 350.

Garrett, D. D., Samanez-Larkin, G. R., MacDonald, S. W., Lindenberger, U., McIntosh, A. R., & Grady, C. L. (2013). Moment-to-moment brain signal variability: a next frontier in human brain mapping? *Neuroscience & Biobehavioral Reviews*, *37*(4), 610-624.

Gaser, C., & Dahnke, R. (2016). CAT-a computational anatomy toolbox for the analysis of structural MRI data. *Hbm*, *2016*, 336-348.

Gerritsen, C. J., Toplak, M. E., Sciaraffa, J., & Eastwood, J. (2014). I can't get no satisfaction: Potential causes of boredom. *Conscious Cogn*, *27*, 27-41.

Gershon, R. C., Wagster, M. V., Hendrie, H. C., Fox, N. A., Cook, K. F., & Nowinski, C. J. (2013). NIH toolbox for assessment of neurological and behavioral function. *Neurology*, *80*(11 Supplement 3), S2-S6.

Glasser, M. F., Coalson, T. S., Robinson, E. C., Hacker, C. D., Harwell, J., Yacoub, E., Ugurbil, K., Andersson, J., Beckmann, C. F., & Jenkinson, M. (2016). A multi-modal parcellation of human cerebral cortex. *Nature*, *536*(7615), 171-178.

Gonzalez-Garcia, C., Flounders, M. W., Chang, R., Baria, A. T., & He, B. J. (2018). Content-specific activity in frontoparietal and default-mode networks during prior-guided visual perception. *Elife*, *7*, e36068.

Gordon, E. M., Laumann, T. O., Adeyemo, B., Huckins, J. F., Kelley, W. M., & Petersen, S. E. (2014). Generation and evaluation of a cortical area parcellation from resting-state correlations. *Cerebral Cortex*, *26*(1), 288-303.

Gordon, E. M., Laumann, T. O., Adeyemo, B., & Petersen, S. E. (2017). Individual variability of the system-level organization of the human brain. *Cerebral Cortex*, *27*(1), 386-399.

Goyal, N., Moraczewski, D., Bandettini, P. A., Finn, E. S., & Thomas, A. G. (2022). The positive-negative mode link between brain connectivity, demographics, and behavior: A pre-registered replication of Smith et al. 2015. *arXiv preprint arXiv:2201.10598*.

Graham, J., Nosek, B. A., Haidt, J., Iyer, R., Spassena, K., & Ditto, P. H. (2008). Moral foundations questionnaire. *Journal of personality and social psychology*.

Hoerger, M., Quirk, S. W., & Weed, N. C. (2011). Development and validation of the Delaying Gratification Inventory. *Psychological assessment*, *23*(3), 725.

Humphreys, G. F., Hoffman, P., Visser, M., Binney, R. J., & Ralph, M. A. L. (2015). Establishing task-and modality-dependent dissociations between the semantic and default mode networks. *Proceedings of the National Academy of Sciences*, *112*(25), 7857-7862.

Huntenburg, J. M., Bazin, P.-L., & Margulies, D. S. (2018). Large-scale gradients in human cortical organization. *Trends in Cognitive Sciences*, *22*(1), 21-31.

Jackson, R. L. (2021). The neural correlates of semantic control revisited. *Neuroimage*, *224*, 117444.

Jackson, R. L., Hoffman, P., Pobric, G., & Ralph, M. A. L. (2016). The semantic network at work and rest: differential connectivity of anterior temporal lobe subregions. *Journal of Neuroscience*, *36*(5), 1490-1501.

Kernbach, J. M., Yeo, B. T., Smallwood, J., Margulies, D. S., De Schotten, M. T., Walter, H., Sabuncu, M. R., Holmes, A. J., Gramfort, A., & Varoquaux, G. (2018). Subspecialization within default mode nodes characterized in 10,000 UK Biobank participants. *Proceedings of the National Academy of Sciences*, *115*(48), 12295-12300.

Kong, R., Li, J., Orban, C., Sabuncu, M. R., Liu, H., Schaefer, A., Sun, N., Zuo, X.-N., Holmes, A. J., & Eickhoff, S. B. (2019). Spatial topography of individual-specific cortical networks predicts human cognition, personality, and emotion. *Cerebral Cortex*, *29*(6), 2533-2551.

Kundu, P., Brenowitz, N. D., Voon, V., Worbe, Y., Vértes, P. E., Inati, S. J., Saad, Z. S., Bandettini, P. A., & Bullmore, E. T. (2013). Integrated strategy for improving functional connectivity mapping using multiecho fMRI. *Proceedings of the National Academy of Sciences*, 201301725.

Kundu, P., Inati, S. J., Evans, J. W., Luh, W.-M., & Bandettini, P. A. (2012). Differentiating BOLD and non-BOLD signals in fMRI time series using multi-echo EPI. *Neuroimage*, *60*(3), 1759-1770.

Laumann, T. O., Gordon, E. M., Adeyemo, B., Snyder, A. Z., Joo, S. J., Chen, M.-Y., Gilmore, A. W., McDermott, K. B., Nelson, S. M., & Dosenbach, N. U. (2015). Functional system and areal organization of a highly sampled individual human brain. *Neuron*, *87*(3), 657-670.

Levine, B., Svoboda, E., Hay, J. F., Winocur, G., & Moscovitch, M. (2002). Aging and autobiographical memory: dissociating episodic from semantic retrieval. *Psychol Aging*, *17*(4), 677.

Lind, G. (2014). Moral competence test (MCT). In.

Lynch, C. J., Power, J. D., Scult, M. A., Dubin, M., Gunning, F. M., & Liston, C. (2020). Rapid precision functional mapping of individuals using multi-echo fMRI. *Cell reports*, *33*(12), 108540.

Marek, S., Tervo-Clemmens, B., Calabro, F. J., Montez, D. F., Kay, B. P., Hatoum, A. S., Donohue, M. R., Foran, W., Miller, R. L., & Hendrickson, T. J. (2022). Reproducible brain-wide association studies require thousands of individuals. *Nature*, *603*(7902), 654-660.

Margulies, D. S., Ghosh, S. S., Goulas, A., Falkiewicz, M., Huntenburg, J. M., Langs, G., Bezgin, G., Eickhoff, S. B., Castellanos, F. X., & Petrides, M. (2016). Situating the default-mode network along a principal gradient of macroscale cortical organization. *Proceedings of the National Academy of Sciences*, *113*(44), 12574-12579.

Margulies, D. S., & Smallwood, J. (2017). Converging evidence for the role of transmodal cortex in cognition. *Proceedings of the National Academy of Sciences*, *114*(48), 12641-12643.

McIntosh, A. R., & Lobaugh, N. J. (2004). Partial least squares analysis of neuroimaging data: applications and advances. *Neuroimage*, *23*, S250-S263.

Mendes, N., Oligschlaeger, S., Lauckner, M. E., Golchert, J., Huntenburg, J. M., Falkiewicz, M., Ellamil, M., Krause, S., Baczkowski, B. M., & Cozatl, R. (2019). A functional connectome phenotyping dataset including cognitive state and personality measures. *Scientific data*, *6*, 180307.

Moore, M., & Gordon, P. C. (2015). Reading ability and print exposure: Item response theory analysis of the author recognition test. *Behavior research methods*, *47*, 1095-1109.

Murphy, C., Jefferies, E., Rueschemeyer, S.-A., Sormaz, M., Wang, H.-t., Margulies, D., & Smallwood, J. (2017). Isolated from input: Transmodal cortex in the default mode network supports perceptually-decoupled and conceptually-guided cognition. *bioRxiv*, 150466.

Mwilambwe-Tshilobo, L., Ge, T., Chong, M., Ferguson, M. A., Misic, B., Burrow, A. L., Leahy, R. M., & Spreng, R. N. (2019). Loneliness and meaning in life are reflected in the intrinsic network architecture of the brain. *Social cognitive and affective neuroscience*, *14*(4), 423-433.

Olson, I. R., McCoy, D., Klobusicky, E., & Ross, L. A. (2013). Social cognition and the anterior temporal lobes: a review and theoretical framework. *Social cognitive and affective neuroscience*, *8*(2), 123-133.

Palombo, D. J., Williams, L. J., Abdi, H., & Levine, B. (2013). The survey of autobiographical memory (SAM): A novel measure of trait mnemonics in everyday life. *Cortex*, *49*(6), 1526-1540.

Pascual, B., Masdeu, J. C., Hollenbeck, M., Makris, N., Insausti, R., Ding, S.-L., & Dickerson, B. C. (2013). Large-scale brain networks of the human left temporal pole: a functional connectivity MRI study. *Cerebral Cortex*, *25*(3), 680-702.

Poldrack, R. A. (2006). Can cognitive processes be inferred from neuroimaging data? [Research Support, N.I.H., Extramural

Research Support, U.S. Gov't, Non-P.H.S.]. *Trends Cogn Sci*, *10*(2), 59-63. https://doi.org/10.1016/j.tics.2005.12.004

Poldrack, R. A., Baker, C. I., Durnez, J., Gorgolewski, K. J., Matthews, P. M., Munafò, M. R., Nichols, T. E., Poline, J.-B., Vul, E., & Yarkoni, T. (2017). Scanning the horizon: towards transparent and reproducible neuroimaging research. *Nature Reviews Neuroscience*, *18*(2), 115-126.

Poldrack, R. A., & Farah, M. J. (2015). Progress and challenges in probing the human brain. *Nature*, *526*(7573), 371-379.

Power, J. D., Plitt, M., Gotts, S. J., Kundu, P., Voon, V., Bandettini, P. A., & Martin, A. (2018). Ridding fMRI data of motion-related influences: Removal of signals with distinct spatial and physical bases in multiecho data. *Proceedings of the National Academy of Sciences*, *115*(9), E2105-E2114.

Rolls, E. T., Cheng, W., & Feng, J. (2020). The orbitofrontal cortex: reward, emotion and depression. *Brain Communications*, *2*(2). https://doi.org/10.1093/braincomms/fcaa196

Rudebeck, P. H., & Rich, E. L. (2018). Orbitofrontal cortex. *Current Biology*, *28*(18), R1083-R1088.

Russell, D. W. (1996). UCLA Loneliness Scale (Version 3): Reliability, validity, and factor structure. *Journal of personality assessment*, *66*(1), 20-40.

Schaefer, A., Kong, R., Gordon, E. M., Laumann, T. O., Zuo, X.-N., Holmes, A. J., Eickhoff, S. B., & Yeo, B. (2017). Local-global parcellation of the human cerebral cortex from intrinsic functional connectivity mri. *Cerebral Cortex*, 1-20.

Seidlitz, L., Abernethy, A. D., Duberstein, P. R., Evinger, J. S., Chang, T. H., & Lewis, B. b. L. (2002). Development of the spiritual transcendence index. *Journal for the scientific study of religion*, *41*(3), 439-453.

Setton, R., Mwilambwe-Tshilobo, L., Girn, M., Lockrow, A. W., Baracchini, G., Hughes, C., Lowe, A. J., Cassidy, B. N., Li, J., Luh, W.-M., Bzdok, D., Leahy, R. M., Ge, T., Margulies, D. S., Misic, B., Bernhardt, B. C., Stevens, W. D., De Brigard, F., Kundu, P., Turner, G. R., & Spreng, R. N. (2022). Age differences in the functional architecture of the human brain. *Cerebral Cortex*. https://doi.org/10.1093/cercor/bhac056

Shipley, W. C., Gruber, C. P., Martin, T. A., & Klein, A. M. (2009). Shipley-2. *Los Angeles, CA: Western Psychological Services*.

Smallwood, J., Bernhardt, B. C., Leech, R., Bzdok, D., Jefferies, E., & Margulies, D. S. (2021). The default mode network in cognition: a topographical perspective. *Nature Reviews Neuroscience*, 1-11.

Smallwood, J., Turnbull, A., Wang, H.-t., Ho, N. S., Poerio, G. L., Karapanagiotidis, T., Konu, D., Mckeown, B., Zhang, M., & Murphy, C. (2021). The neural correlates of ongoing conscious thought. *Iscience*, 102132.

Smith, S. M., Nichols, T. E., Vidaurre, D., Winkler, A. M., Behrens, T. E., Glasser, M. F., Ugurbil, K., Barch, D. M., Van Essen, D. C., & Miller, K. L. (2015). A positive-negative mode of population covariation links brain connectivity, demographics and behavior. *Nat Neurosci*, *18*(11), 1565.

Smith, V., Mitchell, D. J., & Duncan, J. (2018). Role of the default mode network in cognitive transitions. *Cerebral Cortex*, *28*(10), 3685-3696.

Snoek, L., van der Miesen, M. M., Beemsterboer, T., van der Leij, A., Eigenhuis, A., & Steven Scholte, H. (2021). The Amsterdam Open MRI Collection, a set of multimodal MRI datasets for individual difference analyses. *Scientific data*, *8*(1), 1-23.

Sormaz, M., Murphy, C., Wang, H.-t., Hymers, M., Karapanagiotidis, T., Poerio, G., Margulies, D. S., Jefferies, E., & Smallwood, J. (2018). Default mode network can support the level

of detail in experience during active task states. *Proceedings of the National Academy of Sciences*, *115*(37), 9318-9323.

Spreng, R. N., & Andrews-Hanna, J. (2015). The Default Network and Social Cognition. In A. W. Toga (Ed.), *Brain Mapping: An Encyclopedic Reference* (pp. 165-169). Academic Press.

Spreng, R. N., DuPre, E., Selarka, D., Garcia, J., Gojkovic, S., Mildner, J., Luh, W.-M., & Turner, G. R. (2014). Goal-Congruent Default Network Activity Facilitates Cognitive Control. *The Journal of Neuroscience*, *34*(42), 14108-14114.

Spreng, R. N., Fernández-Cabello, S., Turner, G. R., & Stevens, W. D. (2019). Take a deep breath: Multiecho fMRI denoising effectively removes head motion artifacts, obviating the need for global signal regression. *Proceedings of the National Academy of Sciences*, 201909848.

Spreng, R. N., Lockrow, A. W., DuPre, E., Setton, R., Spreng, K. A., & Turner, G. R. (2017). Semanticized autobiographical memory and the default–executive coupling hypothesis of aging. *Neuropsychologia*.

Spreng, R. N., Stevens, W. D., Chamberlain, J. P., Gilmore, A. W., & Schacter, D. L. (2010). Default network activity, coupled with the frontoparietal control network, supports goal-directed cognition [Research Support, N.I.H., Extramural]. *Neuroimage*, *53*(1), 303-317. https://doi.org/10.1016/j.neuroimage.2010.06.016

Spreng*, R. N., McKinnon*, M. C., Mar, R. A., & Levine, B. (2009). The Toronto Empathy Questionnaire: Scale development and initial validation of a factor-analytic solution to multiple empathy measures. *Journal of personality assessment*, *91*(1), 62-71.

Stawarczyk, D., Bezdek, M. A., & Zacks, J. M. (2019). Event Representations and Predictive Processing: The Role of the Midline Default Network Core. *Topics in cognitive science*.

Sudlow, C., Gallacher, J., Allen, N., Beral, V., Burton, P., Danesh, J., Downey, P., Elliott, P., Green, J., & Landray, M. (2015). UK biobank: an open access resource for identifying the causes of a wide range of complex diseases of middle and old age. *PLoS medicine*, *12*(3), e1001779.

Tafarodi, R. W., & Swann Jr, W. B. (2001). Two-dimensional self-esteem: Theory and measurement. *Personality and Individual Differences*, *31*(5), 653-673.

Van Den Heuvel, M. P., & Sporns, O. (2011). Rich-club organization of the human connectome. *The Journal of Neuroscience*, *31*(44), 15775-15786.

Van Essen, D. C., Smith, S. M., Barch, D. M., Behrens, T. E., Yacoub, E., Ugurbil, K., & Consortium, W.-M. H. (2013). The WU-Minn human connectome project: an overview. *Neuroimage*, *80*, 62-79.

Vatansever, D., Manktelow, A., Sahakian, B. J., Menon, D. K., & Stamatakis, E. A. (2017). Angular default mode network connectivity across working memory load. *Human Brain Mapping*, *38*(1), 41-52.

Vatansever, D., Menon, D. K., & Stamatakis, E. A. (2017). Default mode contributions to automated information processing. *Proceedings of the National Academy of Sciences*, *114*(48), 12821-12826.

Vidaurre, D., Smith, S. M., & Woolrich, M. W. (2017). Brain network dynamics are hierarchically organized in time. *Proceedings of the National Academy of Sciences*, *114*(48), 12827-12832.

Von Neumann, J., Kent, R., Bellinson, H., & Hart, B. t. (1941). The mean square successive difference. *The Annals of Mathematical Statistics*, *12*(2), 153-162.

Webster, J. D. (2003). An exploratory analysis of a self-assessed wisdom scale. *Journal of Adult Development*, *10*(1), 13-22.

Wold, S., Martens, H., & Wold, H. (1983). The multivariate calibration problem in chemistry solved by the PLS method. In *Matrix pencils* (pp. 286-293). Springer.

Xia, M., Wang, J., & He, Y. (2013). BrainNet Viewer: a network visualization tool for human brain connectomics. *PLoS One*, *8*(7), e68910.

Yarkoni, T., Poldrack, R. A., Van Essen, D. C., & Wager, T. D. (2010). Cognitive neuroscience 2.0: building a cumulative science of human brain function. *Trends Cogn Sci*, *14*(11), 489-496. https://doi.org/10.1016/j.tics.2010.08.004

Yeo, B. T. T., Kirienen, F. M., Sepulcre, J., Sabuncu, M. R., Lashkari, D., Hollinshead, M., Roffman, J. L., Smoller, J. W., Zöllei, L., Polimeni, J. R., Fischl, B., Liu, H., & Buckner, R. L. (2011). The organization of the human cerebral cortex estimated by intrinsic functional connectivity. *J Neurophysiol*, *106*, 1125-1165. https://doi.org/10.1152/jn.00338.2011.-

Zald, D. H., McHugo, M., Ray, K. L., Glahn, D. C., Eickhoff, S. B., & Laird, A. R. (2012). Meta-analytic connectivity modeling reveals differential functional connectivity of the medial and lateral orbitofrontal cortex. *Cerebral Cortex*, *24*(1), 232-248.

Zou, Q.-H., Zhu, C.-Z., Yang, Y., Zuo, X.-N., Long, X.-Y., Cao, Q.-J., Wang, Y.-F., & Zang, Y.-F. (2008). An improved approach to detection of amplitude of low-frequency fluctuation (ALFF) for resting-state fMRI: fractional ALFF. *Journal of neuroscience methods*, *172*(1), 137-141.

Bridge to Chapter 4

Findings from Study 2 built on Study 1 and provided evidence for several axes of covariance that link the structure and function of the default, limbic, and temporoparietal networks to a broad variety of behaviours. There was evidence for both (sub)network functional specialization, as well as for shared contributions across (sub)networks. A notable finding was that the limbic network and DN_B in particular were among the most consistently implicated neural regions, and multiple brain-behaviour axes displayed shared covariance across DN subnetworks and each of the limbic and temporoparietal networks. This offers further credence to the idea that regions within these two networks may actually be members of the DN, and that complex, distributed interactions between them may underlie complex real-world behavioural phenotypes.

Having assessed the DN's functional organization and relationship to limbic and temporoparietal networks, as well as their relationship to behavior, Study 3 switches gears assesses whether the DN's functional organization is sensitive to an acute pharmacological manipulation. A core property of the DN, supported by past work, is its role in high-level integrative and abstract cognitive processes, and its differentiation from low-level specialized and concrete sensory processes. Studie 3 examines whether 5-HT2A agonist psychedelic drugs are able to significantly alter functional organization of the DN in terms of its relationship to sensory regions and its embeddedment in macroscale hierarchical cortical organization. Given the potent subjective effects of psychedelic drugs, this also has implications for the DN's role in the maintenance of 'normal' ongoing conscious experience. Findings of this study will inform understanding of both DN organization and function, and can shed light on the usefulness of serotonergic psychedelic drugs as perturbational research tools.

Chapter 4 – Serotonergic psychedelic drugs reduce the functional differentiation of the default network from sensory cortices

Adapted from: Girn, M., Roseman, L., Bernhardt, B., Smallwood, J., Carhart-Harris, R., Spreng, R.N. (2022) Serotonergic psychedelic drugs LSD and psilocybin reduce the hierarchical differentiation of unimodal and transmodal cortex. *Neuroimage* (39 citations as of May 28, 2023)

Abstract

Lysergic acid diethylamide (LSD) and psilocybin are serotonergic psychedelic compounds with potential in the treatment of mental health disorders. Past neuroimaging investigations have revealed that both compounds can elicit significant changes to whole-brain functional organization and dynamics. A recent proposal linked past findings into a unified model and hypothesized reduced whole-brain hierarchical organization as a key mechanism underlying the psychedelic state, but this has yet to be directly tested. We applied a non-linear dimensionality reduction technique previously used to map hierarchical connectivity gradients to assess cortical organization in the LSD and psilocybin state from two previously published pharmacological resting-state fMRI datasets (N = 15 and 9, respectively). Results supported our primary hypothesis: The principal gradient of cortical connectivity, describing a hierarchy from unimodal to transmodal cortex, was significantly flattened under both drugs relative to their respective placebo conditions. Between-condition contrasts revealed that this was driven by a reduction of functional differentiation at both hierarchical extremes – default and frontoparietal networks at the upper end, and somatomotor at the lower. Gradient-based connectivity mapping indicated that this was underpinned by a disruption of modular unimodal connectivity and increased unimodal-transmodal crosstalk. Results involving the second and third gradient, which respectively represent axes of sensory and executive differentiation, also showed significant alterations across both drugs. These findings provide support for a recent mechanistic model of the psychedelic state relevant to therapeutic applications of psychedelics. More fundamentally, we provide the first evidence that macroscale connectivity gradients are sensitive to an acute pharmacological manipulation, supporting a role for psychedelics as scientific tools to perturb cortical functional organization.

Introduction

The past decade has seen a resurgence of scientific interest in serotonergic psychedelic compounds such as lysergic acid diethylamide (LSD), psilocybin, and dimethyltryptamine (DMT)/ayahuasca, primarily motivated by suggestive findings from preliminary clinical trials for depression, end-of-life-anxiety, alcoholism, and tobacco addiction (Bogenschutz et al., 2015; Carhart-Harris, Bolstridge, et al., 2016; Davis et al., 2020; Gasser et al., 2014; Griffiths et al., 2016; Johnson et al., 2014; Johnson et al., 2019). Mirroring their complex subjective effects (Preller & Vollenweider, 2016; Schmid et al., 2015; Studerus et al., 2011), functional neuroimaging investigations have shown significant alterations to whole-brain functional organization and dynamics following psychedelic administration (Carhart-Harris et al., 2012; Carhart-Harris & Friston, 2019; Carhart-Harris, Muthukumaraswamy, et al., 2016; McCulloch et al., 2021; Preller et al., 2018; Preller et al., 2020; Roseman et al., 2014; Tagliazucchi et al., 2016; Vollenweider & Preller, 2020). More specifically, findings suggest that psychedelic administration shifts the brain towards greater global functional integration, as reflected by the reduced functional segregation of large-scale brain networks and increased global functional connectivity (FC; Carhart-Harris, Muthukumaraswamy, et al., 2016; Müller et al., 2018; Preller et al., 2018; Roseman et al., 2014; Tagliazucchi et al., 2016). In addition, the complexity of brain dynamics has been shown to increase under psychedelics, as indexed by increases in regional and population-level entropy (Carhart-Harris, 2018; Carhart-Harris et al., 2014; Lebedev et al., 2016; Schartner et al., 2017; Varley et al., 2019), as well as increases in the diversity of functional connectivity (FC) states (Barnett et al., 2020; Lord et al., 2019; Luppi et al., 2021; Tagliazucchi et al., 2014; Varley et al., 2019).

Notably, the recently proposed RElaxed Beliefs Under Psychedelics (REBUS) model (Carhart-Harris & Friston, 2019) unifies past psychological and neural findings with psychedelics into a common theoretical framework based on hierarchical predictive coding and the Free Energy Principle (Friston, 2010). A primary hypothesis of this model is that psychedelics elicit their characteristic subjective effects by increasing the sensitivity of high-level representations (e.g., beliefs or assumptions) encoded within transmodal cortex to low-level inputs from sensory and/or limbic sources (Carhart-Harris & Friston, 2019). An acute reduction in the hierarchical

differentiation of transmodal versus unimodal cortex, consistent with increased crosstalk between these typically segregated functional zones, would provide support for this hypothesized effect. However, the impact of psychedelics on neural hierarchical organization has yet to be directly tested.

In parallel to research involving psychedelics, gradient-mapping techniques have emerged in recent years as valuable tools to characterize brain organization (de Wael et al., 2020; Haak et al., 2018; Huntenburg et al., 2018). In contrast to parcellation approaches which decompose the brain into discrete regions and networks, these approaches model the brain as the superposition of eigenmodes describing continuous axes of feature (dis)similarity (Haak & Beckmann, 2020; Huntenburg et al., 2018). Such techniques have consistently revealed a principal component describing a gradient of functional connectivity (FC) (dis)similarity spanning from unimodal sensorimotor regions to transmodal association regions centered on default and frontoparietal networks. This gradient is consistent with canonical tract-tracing work identifying hierarchical cortical organization in non-human primates (Mesulam, 1998), and fMRI investigations have indicated that it represents a functional hierarchy from low-level sensorimotor processing to abstract, perceptually-decoupled cognition (Huntenburg et al., 2018; Margulies et al., 2016; Murphy et al., 2018). In addition, recent multimodal gradient-mapping investigations have further found that a wide variety of cortical features vary along this hierarchical unimodal-transmodal axis, including myeloarchitecture, gene transcription, receptor densities, electrophysiology, metabolism, and cortical thickness (Burt et al., 2018; Huntenburg et al., 2017; Paquola, De Wael, et al., 2019; Sydnor et al., 2021). On the basis of this growing body of work, the unimodal-transmodal hierarchy has been highlighted as a central organizing principle of the cortex with direct links to neurodevelopmental and phylogenetic trajectories (Sydnor et al., 2021). Gradient-mapping has now been applied to characterize cortical hierarchy in diverse contexts, including autism (Hong et al., 2019), neonatal development (Larivière et al., 2019), schizophrenia (Dong et al., 2020), and lifespan development (Bethlehem, Paquola, Ronan, et al., 2020; Paquola, Bethlehem, et al., 2019).

Here, we leverage gradient-mapping approaches to investigate alterations to macroscale functional hierarchy in the psychedelic state. In particular, we apply gradient-mapping analyses to

interregional FC data from two previously published pharmacological fMRI datasets each collected with a different serotonergic psychedelic compound: LSD (Carhart-Harris, Muthukumaraswamy, et al., 2016) and psilocybin (Carhart-Harris et al., 2012). We apply cortex-wide and network-specific analyses to characterize psychedelic-dependent changes in cortical gradients. In addition, we leverage the organizational scheme provided by the hierarchical gradient to probe hierarchy-specific changes in whole-brain functional connectivity. We predicted that both LSD and psilocybin will be associated with a contraction of the principal gradient, reflecting reduced dissimilarity in the FC profiles of unimodal and transmodal cortices and dedifferentiation of these distinct processing zones. Further, we predicted that this hierarchical contraction would be specifically consistent with increased cross-talk between unimodal and transmodal cortices. In addition, we investigated psychedelic-induced changes to the second and third gradient, which have been shown, respectively, to differentiate visual from somatomotor/auditory cortex, and executive cortex from non-executive cortex. We also predicted gradient dedifferentiation along these axes, given past work which highlighted alterations to sensory and executive connectivity in the psychedelic state (Carhart-Harris et al., 2013; Carhart-Harris, Muthukumaraswamy, et al., 2016; Preller et al., 2018; Preller et al., 2020; Roseman et al., 2014). Collectively, this study provides a comprehensive assessment of whether serotonergic drugs LSD and psilocybin pharmacologically alter the primary axes of cortical functional organization. In addition, it constitutes the first direct assessment of whether cortical gradients are sensitive to acute pharmacological manipulation.

Methods

Participants

LSD. Neuroimaging data from an already published dataset (Carhart-Harris, Muthukumaraswamy, et al., 2016) was used for the present analyses. The acquisition protocol is described in greater detail in the original publication; we describe it in brief here. Twenty participants were recruited via word of mouth and provided written informed consent to participate after study briefing and screening for physical and mental health. The screening for physical health included electrocardiogram (ECG), routine blood tests, and urine test for recent drug use and pregnancy. A

psychiatric interview was conducted, and participants provided full disclosure of their drug use history. Key exclusion criteria included: < 21 years of age, personal history of diagnosed psychiatric illness, immediate family history of a psychotic disorder, an absence of previous experience with a classic psychedelic drug (e.g. LSD, mescaline, psilocybin/magic mushrooms or DMT/ayahuasca), any psychedelic drug use within 6 weeks of the first scanning day, pregnancy, problematic alcohol use (i.e. > 40 units consumed per week), or a medically significant condition rendering the volunteer unsuitable for the study

In a within-subjects design, resting-state BOLD fMRI data were acquired in 20 subjects for each of LSD and placebo conditions. Each condition occurred on separate scanning days (separated by 14 days), and the order was counterbalanced across subjects; subjects were blind to this order, but the researchers and those analyzing the data were not. The scans on each of the days were as follows: (1) resting-state eyes-closed with no music, (2) resting-state eyes-closed with music, (3) resting-state eyes-closed with no music. Scans featuring no music (scans 1 and 3) were used in the present analyses. For the placebo condition, subjects were given 10mL of saline and for the LSD condition they were given 75μg of LSD in 10-mL saline via intravenous injection. Ego-dissolution scores were collected via intra-scanner visual analogue scale ratings, whereas complex imagery scores were derived from the 11-factor altered states of consciousness (ASC) questionnaire (Dittrich, 1998; Studerus et al., 2010) which was completed at the end of each scan day.

Psilocybin. Neuroimaging data from an already published dataset (Carhart-Harris et al., 2012) was used for the present analyses. The acquisition protocol is described in detail in the original publication; we describe it in brief here. Fifteen healthy participants were recruited via word of mouth and provided written informed consent to participate after study briefing and screening for physical and mental health. The screening for physical health included electrocardiogram (ECG), routine blood tests, and urine test for recent drug use and pregnancy. A psychiatric interview was conducted, and participants provided full disclosure of their drug use history. Key exclusion criteria included: < 21 years of age, pregnancy, personal or immediate family history of psychiatric disorder, substance dependence, cardiovascular disease, claustrophobia, blood or needle phobia, or a significant adverse response to a hallucinogenic drug. All subjects had previous experience

with a ‘classic’ psychedelic drug (e.g., LSD, mescaline, psilocybin/magic mushrooms or DMT/ayahuasca) but not within 6 weeks of the study.

In a within-subjects design, resting-state BOLD fMRI data were acquired in 15 subjects for each of psilocybin and placebo conditions. Each condition occurred on separate scanning days (separated by ~14 days), and the order was counterbalanced across subjects; subjects were blind to this order, but the researchers and those analyzing the data were not. For the placebo condition, subjects were given 10mL of saline and for the psilocybin condition they were given 2mg of psilocybin in 10mL saline, via intravenous injection. Each scanning day consistent of one 12-minute scan with infusion beginning at 6 minutes following the start of the scan. The post-infusion half of the scan for each condition was used in the present analyses. Ego-dissolution scores were collected via intra-scanner visual analogue scale ratings, whereas complex imagery scores were derived from the 11-factor altered states of consciousness (ASC) questionnaire (Dittrich, 1998; Studerus et al., 2010) which was completed at the end of each scan day.

Ethics Statement

Data collection for both LSD and psilocybin datasets were approved by the National Research Ethics Service committee London-West London and was conducted in accordance with the revised declaration of Helsinki (2000), the International Committee on Harmonization Good Clinical Practice guidelines, and National Health Service Research Governance Framework. Imperial College London sponsored the research, which was conducted under a Home Office license for research with schedule 1 drugs.

Neuroimaging Data Preprocessing and Denoising

Both datasets underwent an identical preprocessing protocol, as described in detail elsewhere (Carhart-Harris, Muthukumaraswamy, et al., 2016). Subjects with excessive head motion were discarded from analyses (>15% volumes with FD >= 0.5). This resulted in 4 exclusions in the LSD dataset, and 6 exclusions in the psilocybin dataset. The excessive head motion was found in scans conducted during the drug conditions. One additional subject in the LSD dataset exited the scanner

due to intra-scanner anxiety, leaving a final sample of 15 for the LSD dataset and 9 for the psilocybin dataset.

The following pre-processing and denoising steps were performed on the BOLD resting-state fMRI data for each dataset: removal of the first three volumes, de-spiking (3dDespike, AFNI), slice time correction (3dTshift, AFNI), motion correction (3dvolreg, AFNI) by registering each volume to the volume most similar to all others, brain extraction (BET, FSL); rigid body registration to anatomical scans, non-linear registration to a 2mm MNI brain (Symmetric Normalization (SyN), ANTS), scrubbing (FD = 0.4), spatial smoothing (FWHM) of 6mm, band-pass filtering between [0.01 to 0.08] Hz, linear and quadratic de-trending (3dDetrend, AFNI), regression of 6 motion parameters, and regression of 3 anatomical nuisance regressors (ventricles, draining veins, and local white matter). Global signal regression was not performed. Quality control tests confirmed the lack of distance-dependent motion confounds in the denoised data (Carhart-Harris et al., 2012; Carhart-Harris, Muthukumaraswamy, et al., 2016).

Structural T1w images were processed using Freesurfer v5.3 (http://surfer.nmr.mgh.harvard.edu/). Structural processing included bias field correction, registration to stereotaxic space, intensity normalization, skull-stripping, and white matter segmentation. A deformable mesh model was fit on the white matter volume via a triangular surface tessellation. This resulted in >160,000 vertices which differentiate gray matter, white matter, and pial surfaces. Individual subject surfaces were fit to the fsaverage5 spherical surface template, which enables stronger inter-subject correspondence in gyral and sulcal folding patterns.

Statistical Analysis

Gradient-mapping. Cortical gradients were computed using the BrainSpace toolbox (https://github.com/MICA-MNI/BrainSpace; (de Wael et al., 2020)) as implemented in MATLAB. Surfaces were first downsampled from fsaverage 5 space (20,484 vertices) to 10,000 vertices for computational efficiency. For each subject, a 10,000 x 10,000 connectivity matrix was then computed by calculating the pairwise Pearson's correlation between all vertices. As has been done previously (e.g., Hong et al., 2019; Margulies et al., 2016), this matrix was z-transformed and

thresholded row-wise at 90% sparsity in order to retain only the strongest connections. Cosine similarity was then computed on the thresholded z-matrix in order to generate a similarity matrix which captures the similarity in whole-brain connectivity patterns between vertices. This similarity matrix is required as input to the diffusion map embedding algorithm we employed here. The use of cosine similarity as the similarity metric of choice is consistent with past work using this approach (Hong et al., 2019; Margulies et al., 2016; Paquola et al., 2020).

Diffusion map embedding (Coifman et al., 2005; Margulies et al., 2016), a non-linear manifold learning technique from the family of graph Laplacians, was applied to similarity matrices in order to identify gradient components at the individual subject level. The technique estimates a low-dimensional set of embedding components (gradients) from a high-dimensional similarity matrix, where each embedding can intuitively be viewed as a dimension of FC pattern similarity covariance. In the embedding space, vertices that are strongly connected (as weighted by FC pattern similarity) by many connections or a few very strong connections are closer together, whereas vertices with little or no connections are farther apart. Euclidean distance between two points in the embedding space is equivalent to the diffusion distance between probability distributions centered at those points (hence the name of the algorithm), each of which are equivalent to 'difference in gradient value' as referred to in the main text. The algorithm is controlled by a single parameter α, which controls the influence of density of sampling points on the manifold (α = 0, maximal influence; α = 1, no influence). Diffusion map embedding is specifically characterized by α = 0.5 (Coifman et al., 2005), which allows the influence of both global and local relationships between data points in the estimation of the embedding space. Following past work (Bethlehem, Paquola, Seidlitz, et al., 2020; Hong et al., 2019), to enable comparisons across subjects, Procrustes rotation was performed to align individual-subject embedding (gradient) components to an all-subjects group average embedding component template. This rotation ensures that gradient axes are matched across subjects. Group contrasts and behavioural associations were conducted using surface-based linear models, as implemented in the SurfStat toolbox (http://www.math.mcgill.ca/keith/surfstat; Worsley et al., 2009).

Gradient-based connectivity mapping. In order to further explicate how observed gradient differences related to interregional FC, we examined unimodal versus transmodal functional

connectivity changes as stratified by gradient scores. More specifically, we wanted to determine whether unimodal regions (as defined based on the hierarchical gradient) preferentially exhibited increased FC with transmodal regions, as opposed to non-specific global increases. To do this, we first separated vertex-wise gradient scores into 10 percentile bins (0-10, 11-20, 21-30, etc.) for each subject. These 10 bins were then used as ROIs in FC analyses. We were interested in whether each bin preferentially increased its connectivity with unimodal versus transmodal cortex after psychedelic administration. A combined unimodal cortex ROI was created as the combination of the first three percentile bins and a combined transmodal cortex ROI was defined as the last three percentile bins. Unimodal-specific FC and transmodal-specific FC was computed for each of the 10 bins, by computing the Pearson's correlation (r) between each bin and the combined unimodal ROI and the combined transmodal ROI. T-tests were applied to evaluate drug vs. placebo differences at each bin for each of unimodal-specific and transmodal-specific FC.

To complement this analysis and examine the spatial distribution of FC associated with each gradient percentile bin, we additionally computed seedmaps for each bin and compared across drug and placebo conditions at both vertex-wise and network-wise levels. This enabled a more detailed look at unimodal-specific versus transmodal-specific changes in whole-brain FC.

Data and code availability

All analyses were conducted in MATLAB using custom code and included functions within the BrainSpace and SurfStat toolboxes described above. Data is freely available at https://openneuro.org/datasets/ds003059/versions/1.0.0.

Results

We applied gradient-mapping techniques to characterize differences in macroscale cortical gradients in each of LSD and psilocybin states relative to their respective placebo states. The diffusion-map embedding algorithm used here is, compared to other gradient-mapping approaches, robust to noise, computationally inexpensive, and governed by a single parameter controlling the influence of the sampling density on the manifold (see *Methods* for details). Applying this

algorithm with standard settings revealed 98 mutually orthogonal gradient components per subject in each of the LSD dataset and psilocybin dataset. We presently include discussion of the first three gradients revealed by this approach, given that these explain the greatest variance and have been highlighted in past work (Margulies et al., 2016).

Principal ***gradient***

The principal gradient of cortical connectivity revealed in the present datasets replicates past findings (Hong et al., 2019; Margulies et al., 2016) of a putatively hierarchical axis of FC similarity variance spanning from unimodal regions centered in somatomotor cortex on one end to transmodal regions centered on the default network and superior frontal gyrus on the other (Figure 1). Lower principal gradient values reflect greater FC similarity to unimodal cortex, whereas higher principal gradient values reflect greater FC similarity to transmodal cortex. This gradient explained the greatest amount of variance in each of LSD placebo (mean 12.9% variance explained), LSD (mean 12.6% variance explained), psilocybin placebo (mean 13.1% variance explained**)**, and psilocybin **(**mean 11.9% variance explained**)** conditions. T-tests revealed significantly greater explained variance in respective placebo conditions: LSD-placebo (t^{28} = -2.17, p=0.047), psilocybin-placebo (t^{17} = -2.93, p<0.01).

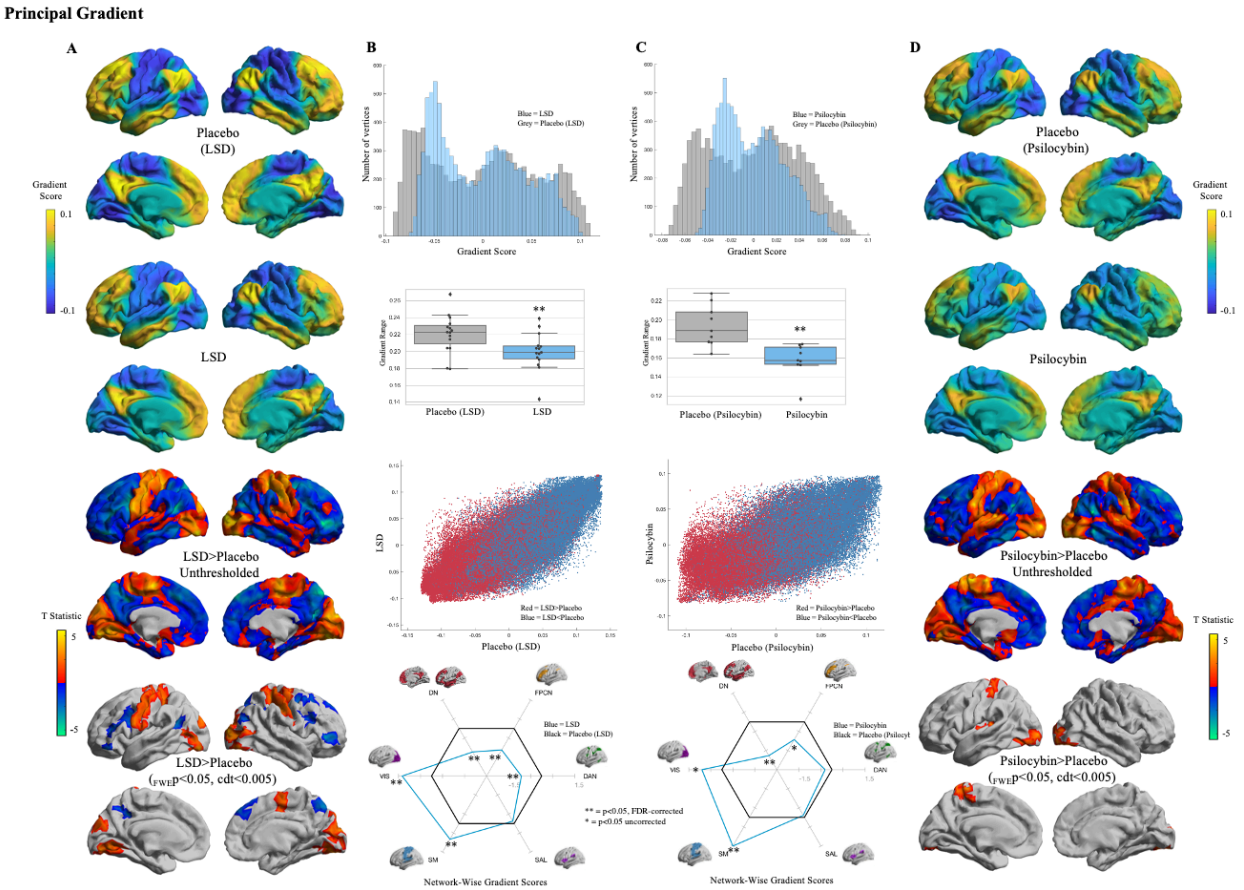

Figure 1. Figures are arranged vertically**. A.** Mean principal gradients representing an axis from unimodal to transmodal cortex, and unthresholded and thresholded vertex-wise contrasts in the LSD dataset **B:** (Top) Histogram showing number of occurrences for principal gradient values for each of LSD and placebo (LSD) conditions. (Mid-Top) Principal gradient range. Between-condition comparisons indicate a significant contraction in the LSD state (t^{28} = -2.5, p=0.01). (Mid-Bottom) The principal gradient manifold for both LSD (y-axis) and placebo (LSD) (x-axis) conditions, color coded for overall trends in between-condition differences (see inset). (Bottom) Spider plot displaying mean intra-network principal gradient scores for each of six functional networks, following the (Yeo et al., 2011) parcellation. Network-wise values indicate the mean gradient value of vertices within that network. Values are normalized to the placebo (LSD) condition (black lines). **C:** (Top) Histogram showing the number of occurrences of principal gradient values for each of psilocybin and placebo (psilocybin) conditions. (Mid-Top) Principal gradient range. Between-condition comparisons indicate a significant contraction in the psilocybin state (t^{28} = -3.9, p=0.001). (Mid-Bottom) The principal gradient manifold for both psilocybin (y-axis) and placebo (psilocybin) (x-axis) conditions, color coded for overall trends in between-condition differences (see inset). (Bottom) Spider plot displaying mean intra-network principal gradient scores for each of six functional networks, following the (Yeo et al., 2011) parcellation. Network-wise values indicate the mean gradient value of vertices within that network. Values are normalized to the placebo (psilocybin) condition (black lines). **D:** Mean principal gradients representing an axis from unimodal to transmodal cortex, and unthresholded and thresholded vertex-wise contrasts in the psilocybin dataset. Abbreviations: DN = default network; FPCN = frontoparietal control network; DAN = dorsal attention network; SAL = salience network; SM = somatomotor network; VIS = visual network

Principal gradient histograms for both datasets suggest a contraction on both sides of this gradient in the drug conditions relative to the respective placebo conditions, providing qualitative support for our hypothesis of reduced differentiation along this putatively hierarchical axis in the

psychedelic state (Figure 1B and 1C Top). To quantitatively assess this, we calculated the difference between each subject's maximum and minimum principal gradient value and compared these differences across conditions (Figure 1B and 1C Mid-Top). Results confirmed the presence of a significant contraction in both LSD (t^{28} = -2.5, p=0.01) and psilocybin (t^{16} = -3.9, p=0.001) conditions, reflective of reduced functional differentiation along this axis. We additionally evaluated left and right tail contractions separately, this indicated a contraction for the left (unimodal) and right (transmodal) tail for psilocybin (t^{16} = -3.4, p=0.01, right t^{16} = -3.7, p=0.01) and only for the left tail for LSD (left t^{28} = -3.9, p=0.09, right t^{28} = -1.27, p=0.22). This indicates that unimodal contractions may be more prominent or consistent. Finally, we also conducted a Brown-Forsythe test to evaluate whether drug and placebo distributions exhibit unequal variances, which was confirmed for both datasets (p<0.001). Similar results were also found with alternative tests of unequal variance (Bartlett's test and the Levene's test). In order to examine overall trends in psychedelic-dependent changes in hierarchical differentiation, we then visualized the principal gradient for each dataset as a scatter plot, color coded for increases (red) and decreases (blue) in each drug condition relative to placebo (Figure 1D). This revealed that both unimodal-proximal regions and transmodal-proximal regions become less differentiated along this axis, suggesting a contraction on both sides of the gradient.

Next, we quantitatively assessed between-condition differences in gradient score values at a vertex- (Figure 1A and 1D Mid-Bottom/Bottom) and network-wise (Figure 1B and 1C Bottom) level. Unthresholded maps at the vertex level are included to display the overall consistency in topology between LSD and psilocybin states, indicating that these distinct serotonergic drugs affect the principal gradient in a similar manner (Figure 1A and 1D Mid-Bottom). LSD vertex-wise contrasts revealed LSD-dependent principal gradient increases in somatomotor cortex, as well as in both medial and lateral visual regions. LSD-dependent principal gradient decreases were found in the precuneus, premotor cortex, superior and inferior frontal gyrus, superior parietal lobule, and Wernicke's area ($_{FWE}p$<0.05, cdt<0.01). Psilocybin vertex-wise contrasts revealed psilocybin-dependent principal gradient increases in somatomotor and auditory cortex, as well in visual cortex predominantly on the lateral surface. Psilocybin-dependent gradient decreases were found in the superior frontal gyrus and inferior parietal lobule ($_{FWE}p$<0.05, cdt<0.01).

Network-wise differences were assessed according to the Yeo et al. (2011) network parcellation scheme. Our use of FDR correction for network-wise contrasts is because FWE (e.g., Bonferroni) is unduly stringent at this sample size and likely to produce false negatives. We contend that FDR-correction with a 5% chance of a false positive is more appropriate for the current datasets and the number of tests performed. We also emphasize that the network-wise contrasts are predominantly aimed at facilitating the interpretation of the vertex-wise findings. LSD results indicated a significant increase in gradient score within visual and somatomotor networks, and a significant decrease within default, frontoparietal control, and dorsal attention networks ($p<0.05$ FDR corrected, critical t-value = |2.7|). Psilocybin results indicated a significant increase in gradient score within the somatomotor network and decrease in the default network ($p<0.05$ FDR corrected, critical t-value = |3.3|) All between-condition differences were consistent with the gradient scores of significant regions and networks approaching zero, indicating reductions in FC pattern similarity to corresponding extremes along this axis. These results therefore offer further quantitative support for the qualitative trend seen in Figure 1B and 1C Mid-Bottom. Namely, that the LSD state is characterized by a pulling-together of both unimodal (visual and somatomotor) and transmodal (default, frontoparietal control, and dorsal attention) networks in gradient space – reflective of relatively symmetrical reduction in differentiation along this hierarchical axis of cortical connectivity. Control analyses indicate that principal gradient score differences are not significantly correlated with motion (Supplementary Figure 1).

Gradient-Based Connectivity Mapping

In order to further explicate the observed reduction in hierarchical organization in the psychedelic state, we sought to determine whether the observed changes in gradient values were specifically consistent with increased cross-talk between unimodal and transmodal cortices, as hypothesized by the abovementioned REBUS model (Carhart-Harris & Friston, 2019). This interest was further motivated by the fact that the principal gradient changes found in both datasets each represent a movement towards zero. As such, the results are consistent with the changes simply corresponding to less of a loading on this gradient in general and not necessarily to increases/decreases in unimodal- or transmodal-specific connectivity. To evaluate whether the gradient changes are indicative of structured and hierarchically specific changes in FC, we applied a gradient-based

connectivity mapping approach. We constructed ROIs based on percentile bins along the principal gradient and evaluated drug-induced unimodal versus transmodal changes in FC. In particular, bin ROIs were correlated with each of a combined unimodal cortex ROI (three lowest bins) and combined transmodal cortex ROI (three highest bins; see Methods for more details).

Between-condition comparisons of unimodal versus transmodal-specific FC supported our hypotheses of increased crosstalk between unimodal and transmodal cortices. For both LSD and placebo, multiple lower percentile bins (corresponding to the unimodal side of the gradient) showed significantly reduced FC with unimodal cortex and less negative FC with transmodal cortex ($p<0.05$, FDR-corrected or uncorrected; Figure 2). In addition, higher percentile bins (corresponding to the transmodal side of the gradient) displayed significantly increased FC with unimodal cortex but not with transmodal cortex. This suggests that the observed gradient changes have their basis in structured, hierarchically specific changes in FC that are consistent with increased unimodal-transmodal crosstalk.

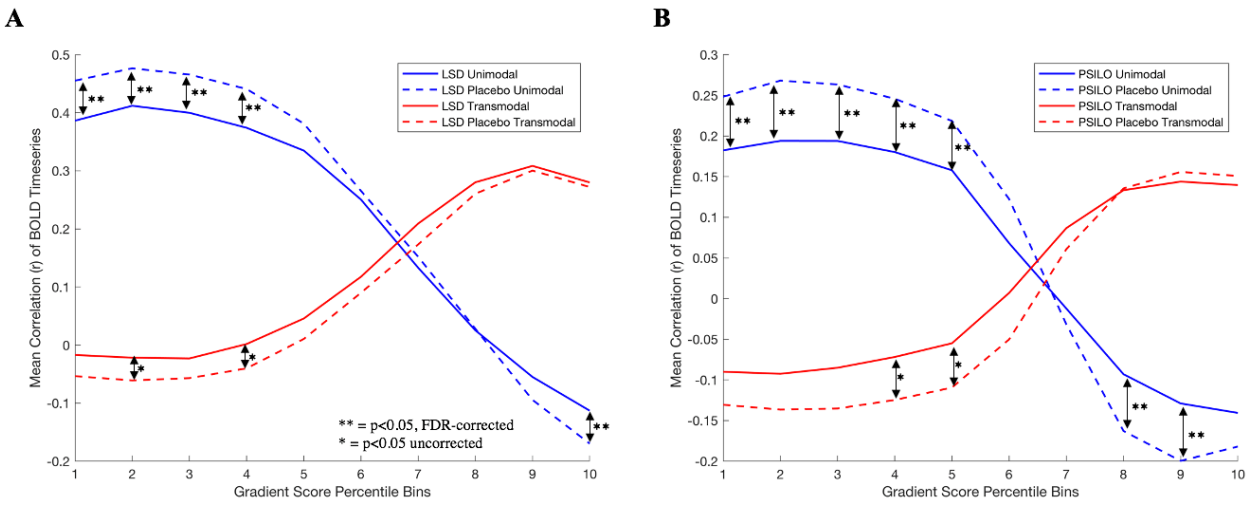

Figure 2. Line plots for each of LSD (A) and psilocybin (B) datasets, indicating FC between 10 percentile bins along the principal gradient and unimodal (blue) and transmodal (red) cortex. Solid lines indicate drug conditions, while dotted lines indicate corresponding placebo conditions. ** = $p<0.05$, FDR-corrected, * = $p<0.05$, uncorrected.

To further probe this effect, we also examined the spatial distribution of hierarchically specific changes in FC. In particular, we computed whole-brain seedmaps based on each gradient bin ROI and compared across conditions at both the vertex-wise and network-wise level (Figure 3). Results were largely consistent across drugs and indicate that lower percentile bins exhibit significantly

reduced FC with somatosensory and visual networks and increased connectivity with the frontoparietal control network, particularly in lateral prefrontal and lateral parietal cortex ($_{FWE}p<0.05$, cdt<0.05 vertex-wise, p<0.05 FDR or uncorrected network-wise). This effect was largely sustained in the median percentile bin, with greater differences involving the default and limbic networks for LSD. With respect to higher percentile bins, with the exception of the default network for the eighth bin of psilocybin, results indicated more of a trend toward increased FC, particularly involving visual, dorsal attention, and salience networks ($_{FWE}p<0.05$, cdt<0.05 vertex-wise, p<0.05 FDR or uncorrected network-wise).

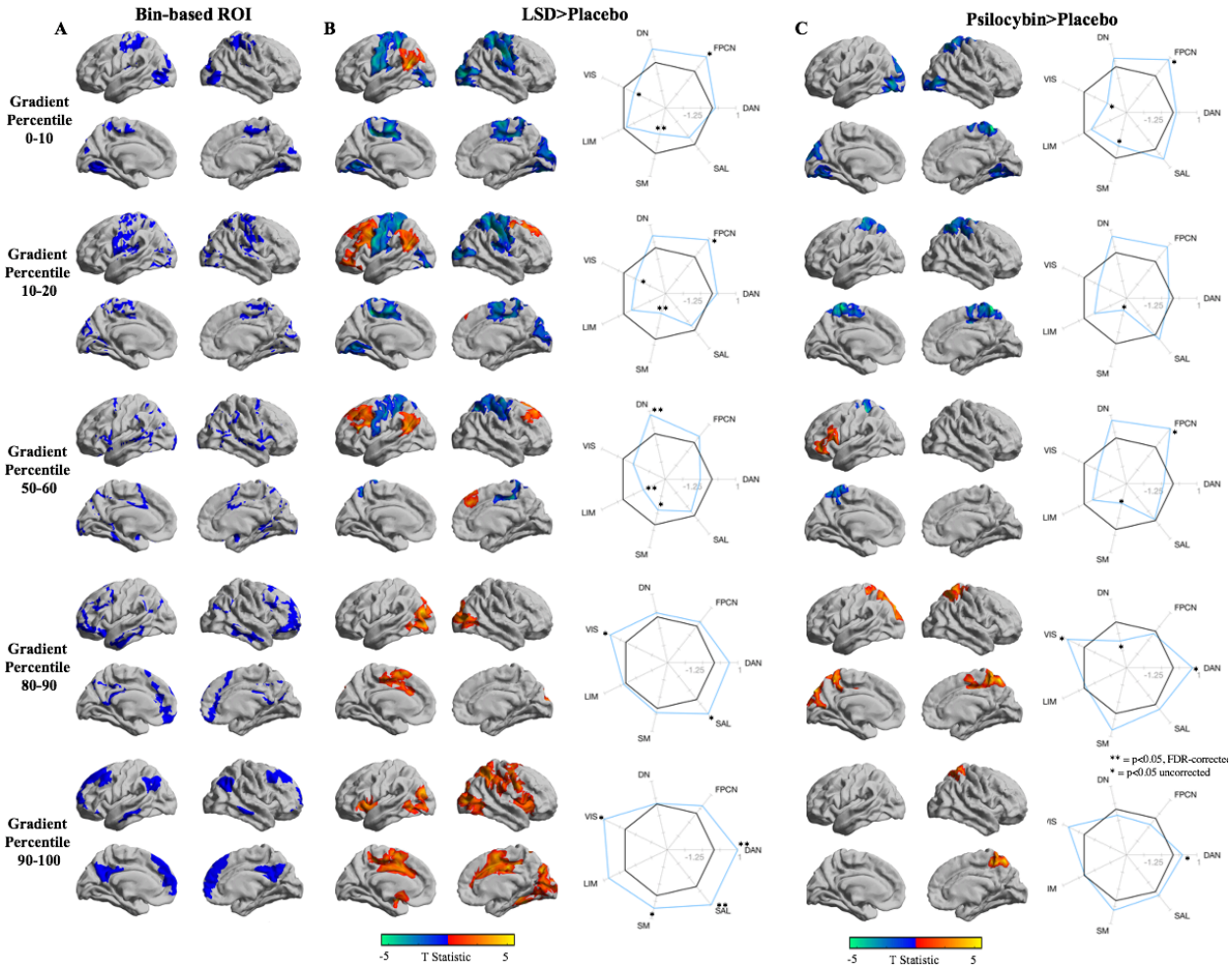

Figure 3. Vertex-wise and network-wise seedmap contrasts for the two lowest, median, and two highest percentile bins. Seeds/ROIs were defined based on percentile bins along the principal gradient. (A) The spatial distribution of each bin-based ROI. (B) LSD>Placebo contrasts: (left) vertex-wise contrast at $_{FWE}p<0.05$, cdt<0.05, (right) network-wise contrast, significance indicated. (C) Psilocybin>Placebo contrasts: (left) vertex-wise contrast at $_{FWE}p<0.05$, cdt<0.05, right network-wise contrast, significance indicated. **=p<0.05, FDR-corrected, *=p<0.05 uncorrected.

Second and third gradient

Having found support for our hypothesis of a contraction in macroscale functional hierarchy in the LSD state that is consistent with greater unimodal-transmodal crosstalk, we additionally examined the second and third gradient of macroscale functional organization. The second gradient represents an axis of FC similarity variance that separates the visual cortex on one end from the somatosensory/auditory on the other (Figure 4A and 4B). Lower second gradient values reflect greater FC similarity to visual cortex, whereas higher principal gradient values reflect greater FC similarity to somatomotor/auditory cortex. This gradient explained the second most variance in each of LSD placebo (mean 8.8% variance explained), LSD (8.6 variance explained**),** psilocybin placebo (9.8% variance explained**),** and psilocybin (mean 10.3% variance explained**)** conditions. T-tests revealed significantly greater explained variance in respective placebo conditions: LSD-placebo (t^{28} = -2.58, p=0.02), psilocybin-placebo (t^{17} = -2.68, p=0.02).

The third gradient represents an axis of FC similarity variance that separates executive control from the rest of cortex (Figure 4C and 4D). Lower third gradient values reflect greater FC similarity to executive networks, whereas higher principal gradient values reflect greater FC similarity to non-executive networks. This gradient explained the third most variance in each of LSD placebo **(**mean 7.7% variance explained**)**, LSD **(**mean 6% variance explained**)**, psilocybin placebo (mean 8.4% variance explained), and psilocybin (mean 7.5% variance explained**)** conditions. T-tests revealed significantly greater explained variance in psilocybin placebo (t^{28} = -2.36, p=0.03) conditions and a trend-level effect for LSD-placebo (t^{17} = -1.94, p=0.073).

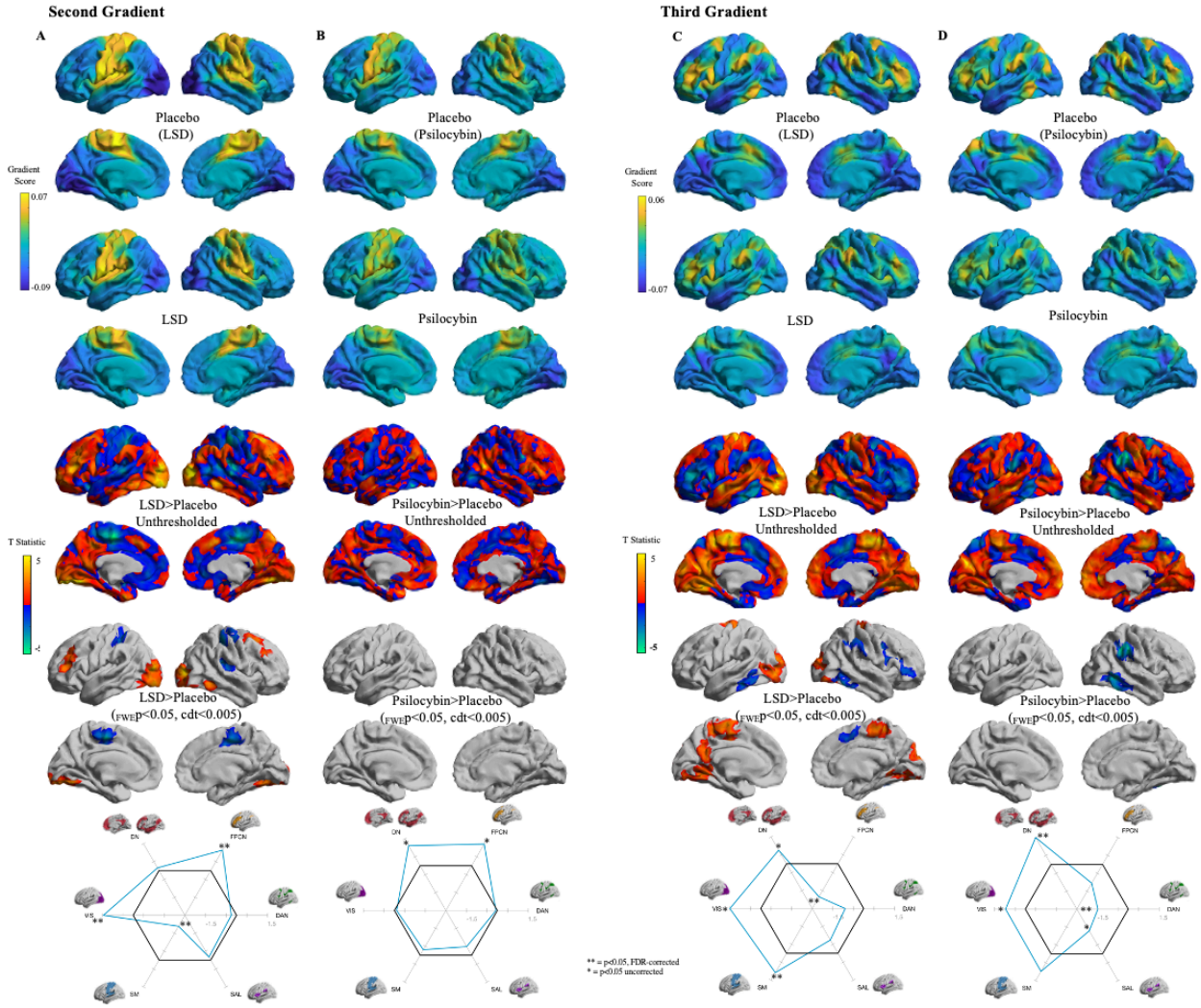

Figure 4. Mean second gradients representing an axis from visual to somatomotor cortex, unthresholded and thresholded vertex-wise contrasts, and network-wise contrasts in the LSD dataset (A) and (B) the psilocybin dataset. (C) Mean third gradients representing an axis from executive control regions to the rest of the cortex, unthresholded and thresholded vertex-wise contrasts, and network-wise contrasts in the LSD dataset and (D) the psilocybin dataset. Network-wise contrasts display mean intra-network gradient values for each of six functional networks, following the (Yeo et al., 2011) parcellation. Values are normalized to the respective placebo conditions (black lines). Blue lines indicate drug condition. Abbreviations: DN = default network; FPCN = frontoparietal control network; DAN = dorsal attention network; SAL = salience network; SMN = somatomotor network; VIS = visual network.

LSD second gradient vertex-wise contrasts revealed LSD-dependent increases in lateral and ventral visual cortex and the middle and superior frontal gyrus bilaterally, while decreases were found in somatomotor and auditory cortex (p_{FWE}<0.05, cdt<0.01). Network-wise contrasts revealed significant increases in frontoparietal control and visual networks and decreases in the somatomotor network (FDR p<0.05, critical t-value = |2.9|). Psilocybin vertex ($_{FWE}$p<0.05, cdt<0.01) and network-wise (FDR p<0.05, critical t-value = |3.4| contrasts revealed no significant differences), likely due to a lack of power in this dataset. Visual inspection of the unthresholded

contrast maps indicates overlap in topology between psilocybin and LSD-induced changes predominantly within lateral prefrontal cortex and posteromedial cortex. Control analyses indicate that second gradient score differences are not significantly correlated with motion (Supplementary Figure 2).

LSD third gradient vertex-wise contrasts revealed LSD-dependent increases in clusters within somatomotor vortex, lateral and medial visual cortex, and the retrosplenial/posterior cingulate cortex, while decreases were found in bilateral posterior middle temporal gyrus, bilateral inferior frontal gyrus, left premotor cortex, and right supramarginal gyrus ($_{FWE}p<0.05$, cdt<0.01). Network-wise contrasts revealed significant increases in visual and somatomotor networks and decreases in the frontoparietal control network (FDR $p<0.05$, critical t-value = |2.6}). Psilocybin third gradient vertex-wise contrasts revealed significant decreases in the right supramarginal gyrus and right posterior middle temporal gyrus ($p<0.05$, cdt<0.01). Network-wise contrasts revealed a significant decrease within the dorsal attention network (FDR $p<0.05$, critical t-value = |3.1|). Control analyses indicate that third gradient score differences are not significantly correlated with motion (Supplementary Figure 3).

Gradient manifolds

To visualize the relationship between the three gradients examined in this study and how they differ across drug and placebo conditions, we created gradient manifold scatter plots, color coded for each of the Yeo et al. 2011 7 networks (Figure 4). Qualitative examination of the LSD manifold plots (Figure 5A and 5B) reveals an overall less diffuse embedding space distribution in the LSD state, marked by notable contractions on the unimodal aspect of the principal gradient and the visual aspect of the second gradient. Qualitative examination of the psilocybin manifold plots (Figure 5C and 5D) similarly shows a significant contraction on the unimodal side of the principal gradient, but less contraction of the visual network along the second gradient relative to LSD. Psilocybin also displays a greater contraction of transmodal (default and frontoparietal control network) nodes in the principal gradient, and, interestingly, a greater contraction of the third gradient primarily involving regions within salience and dorsal attention networks.

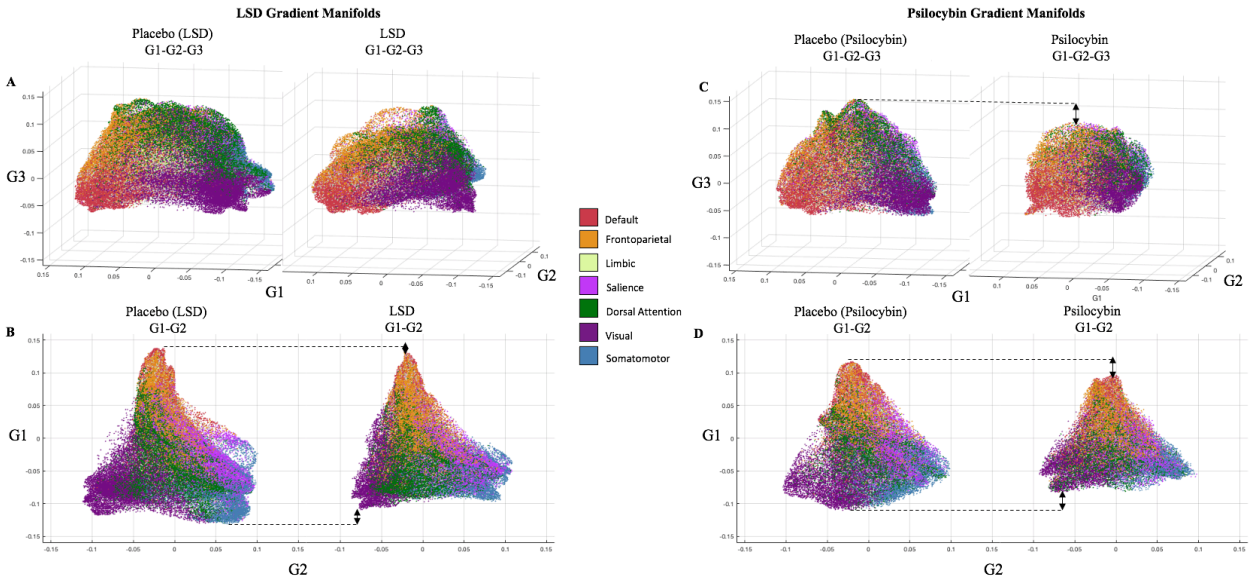

Figure 5. (A) Scatterplots representing the gradient embedding space across the first three gradients, for LSD placebo (left) and LSD (right) conditions. **(B)** Scatterplots representing the gradient embedding space across the principal and second gradient, for LSD placebo (left) and LSD (right) conditions. **(C)** Scatterplots representing the gradient embedding space across the first three gradients, for psilocybin placebo (left) and psilocybin (right) conditions. **(D)** Scatterplots representing the gradient embedding space across the principal and second gradient, for psilocybin placebo (left) and psilocybin (right) conditions. Scatter plot colors indicate functional network as per the (Yeo et al., 2011) 7-network parcellation scheme (see inset for legend).. Black arrows indicate contractions along each gradient.

Control Analyses

To support the robustness and reliability of our results we conducted multiple control analyses. First, to further ascertain whether our results are robust to motion confounds, we conducted all analyses on the principal gradient following a more stringent pipeline which appplied the original denoising approach but included an expanded set of 24 motion regressors and global signal regression. Results shown the Supplementary Figure 1 indicate a replication of hierarchy contraction in both LSD and psilocybin datasets. Second, to ascertain whether the results are independent of placebo effects, we conducted analyses on the principal gradient contrasting a psilocybin pre-infusion scan to the post-infusion scan used in the primary analyses. Hierarchy contraction was indeed replicated (Supplementary Figure 2A). Finally, we also conducted principal gradient analyses on additional LSD and LSD placebo scans that were conducted with music. Hierarchy contraction was also replicated when contrasting these scans (Supplementary Figure 2B). These control analyses, along with fact of replication in two distinct datasets, offer considerable support for the robustness and reliability of the present findings.

Discussion

To investigate psychedelic-induced changes in cortical functional organization and test the hypothesis that serotonergic psychedelics attenuate brain hierarchical organization, we characterized macroscale cortical gradients after LSD and psilocybin administration. Our results for both LSD and psilocybin datasets replicated past findings (Hong et al., 2019; Margulies et al., 2016) of a hierarchical principal gradient which represents a pattern of FC (dis)similarity spanning from unimodal sensory to transmodal association cortex. Between-condition contrasts supported our primary hypothesis: relative to placebo conditions, this gradient exhibited a significant contraction in both LSD and psilocybin states, reflective of less differentiated hierarchical organization. This contraction was more prominent on the unimodal side of the gradient, particularly with LSD, but was also evident on the transmodal axis as evidenced by vertex- and network-wise findings with both drugs. This suggests that both somatomotor regions on the unimodal aspect and default and frontoparietal regions on the transmodal aspect both became less differentiated along this hierarchical axis. Gradient-based connectivity mapping indicated that this contraction has its basis in hierarchically specific changes in FC that are consistent with increased crosstalk between unimodal and transmodal cortices and a disruption of specialized sensory processing. Overall, there was strong convergence in the topographical changes across the LSD and psilocybin datasets, providing important support for the robustness of our findings given the small sample sizes. Results with the second and third gradient indicate alterations to axes of cortical organization related to sensory differentiation and executive region differentiation, respectively. The topography of changes for these two gradients showed strong overlap across datasets, but with greater significant changes with LSD, likely owing to power differences. Second gradient findings with LSD extend previous work suggesting significant alterations to whole-brain visual FC in the LSD state (Carhart-Harris, Muthukumaraswamy, et al., 2016; Preller et al., 2018). Collectively, these results provide evidence for significant alterations of macroscale cortical gradients following psychedelic administration, marked by attenuation of hierarchical differentiation between unimodal and transmodal cortices as well as dedifferentiation along sensory and executive axes of cortical organization.

Past neuroimaging investigations with LSD and psilocybin, including past analyses of the present datasets, have revealed that they elicit a complex set of changes to both static and dynamic FC, as well as to regional and interregional entropy/complexity (Barnett et al., 2020; Carhart-Harris, 2018; Carhart-Harris, Muthukumaraswamy, et al., 2016; Lebedev et al., 2016; Lord et al., 2019; Luppi et al., 2021; Müller et al., 2018; Preller et al., 2018; Roseman et al., 2014; Schartner et al., 2017; Tagliazucchi et al., 2014; Tagliazucchi et al., 2016; Varley et al., 2019). This work has often attempted to manage this complexity by describing results either in terms of a focus on specific large-scale network interactions (e.g., involving the default network) or in terms of general trends (e.g., towards global integration; Carhart-Harris, Muthukumaraswamy, et al., 2016; Preller et al., 2018; Preller et al., 2020; Roseman et al., 2014; Tagliazucchi et al., 2016). This approach, while useful and necessary given the infancy of the field, can obscure important nuances in the structure of the datasets in question. For example, although decreased within-network and increased between-network FC is often listed as a consistent finding with serotonergic psychedelics, the effects with respect to specific networks and network pairs has limited overlap across drugs and datasets (Carhart-Harris, Muthukumaraswamy, et al., 2016; Müller et al., 2018; Roseman et al., 2014). Although this is to be somewhat expected given small sample sizes and analytical discrepancies, it suggests the need for approaches which can help organize findings and facilitate comparisons. The cortical gradient approach used here provides a novel perspective on the neural effects of serotonergic psychedelics by collapsing the complex mosaic of increases and decreases in FC into a low-dimensional set of macroscale axes which suggest specific alterations in cortical information processing. This approach can facilitate both functional interpretation (as described below) and the identification of effects specific to this class of drugs, which, evidently, decreased network segregation (or decreased default mode network integration) is not. As an example, healthy aging is also characterized by decreased within-network and increased between-network FC, yet gradient analyses comparing young and older adults have revealed qualitatively very different effects than those observed here (Bethlehem, Paquola, Seidlitz, et al., 2020; Setton et al., 2021).

Our results indicate that the FC profiles of unimodal and transmodal cortices are less dissimilar in the serotonergic psychedelic state, and that this is largely driven by a disintegration of unimodal cortices and greater unimodal-transmodal integration. This points to important systems-level

alterations in the psychedelic state. During regular functioning, the hierarchical axis spanning from unimodal to transmodal cortex represents a central organizing principle of the cortex which allows for the functional segregation and integration of concrete sensory and abstract cognitive information (Margulies et al., 2016; Mesulam, 1998; Murphy et al., 2018; Vézquez-Rodríguez et al., 2020). Consistent with segregation, meta-analytic and task-based fMRI studies have provided evidence that lower levels of the hierarchy pertain to behaviours that are coupled to immediate sensory input, while higher hierarchical zones pertain to perceptually-decoupled, abstract cognitive processes (Margulies et al., 2016; Mckeown et al., 2020; Murphy et al., 2018). Consistent with integration, increasing resting-state fMRI evidence indicates that cortical signals tend to propagate through the macroscale processing hierarchy from specialized sensory processing, to multi-modal integration, to higher-order, integrative processing within a distributed network of transmodal hubs (Hong et al., 2019; Paquola et al., 2020; Park et al., 2020; Sepulcre et al., 2012; Vézquez-Rodríguez et al., 2020). Understood in light of this research, our findings provide novel evidence that serotonergic psychedelics reduce the intervening processing steps between unimodal and transmodal cortex and further suggest that this may be related to a disruption of functionally specialized unimodal processing. In line with the REBUS model (Carhart-Harris & Friston, 2019), this pattern of results suggests decreased functional differentiation between sensory and abstract cognitive processing in the psychedelic state – a notion in line with reports that psychedelics can elicit a blurring of the internal-external/subject-object distinction and an increased influence of internal mentation on perceptual processing (Fox et al., 2018; Girn & Christoff, 2018; Girn et al., 2020; Kraehenmann et al., 2017; Millière, 2017).

Intriguingly, a contraction in cortical hierarchy was recently observed in patients suffering from schizophrenia (Dong et al., 2021) – a condition long considered to feature phenomenological similarities to the psychedelic state (Leptourgos et al., 2020; Mogar, 1970; Rucker et al., 2018). This study similarly found that the contraction in hierarchy was underpinned by a disruption of specialized unimodal processing and increased unimodal-transmodal cross-talk. The overlap found here suggests a common systems-level disruption in the relationship between concrete sensory and abstract cognitive processing in schizophrenia and the psychedelic state (Leptourgos et al., 2020; Mogar, 1970; Preller & Vollenweider, 2016). However, we note this disruption may occur via differential causal trajectories, with potentially different behavioural implications. Dong and

colleagues interpret their results in light of past schizophrenia research suggesting that "… [the disruption of] early regions of the sensory pathway may result in bottom-up dysregulation of higher cortical function" (Dong et al., 2021, p. 9). According to this 'bottom-up' view, the observed systems-level alterations of cortical hierarchy have their locus in dysfunctional sensory processing. A contrasting 'top-down' view posits that alterations in transmodal processing are the locus of changes in cortical hierarchy. One top-down interpretation is that increased global FC of transmodal cortex disrupts specialized unimodal sensory processing and increases the sensitivity of low-level sensory processing to high-level representations. An alternative top-down interpretation, proposed by the REBUS model, is that alterations of transmodal activity and connectivity lead to reduced top-down control of lower-order areas, leading to increased influence of unimodal sensory inputs on high-level transmodal representations. Although these interpretations cannot be adjudicated based on the current datasets (and may not be mutually exclusive), the top-down interpretations for psychedelic findings are consistent with evidence from *in vivo* PET molecular imaging that serotonin 2A receptor (the receptor most robustly linked to psychedelic effects (Nichols, 2016)) densities are highest in human transmodal cortices (Beliveau et al., 2017). However, we also note that the bottom-up view is consistent with thalamocortical models of psychedelic brain effects, which posit that agonism of presynaptic serotonin 2A receptors on thalamocortical afferents attenuates sensory gating, thereby producing cortical sensory overload and subsequent higher-order disruptions (Vollenweider & Preller, 2020). Future work should seek to evaluate these competing hypotheses of psychedelic action and their (dis)similarity to neural alterations in schizophrenia.

In addition to changes in cortical hierarchy, we examined changes in the second and third gradient of cortical connectivity. The second gradient represents the differentiation of visual versus somatomotor/auditory processing. We found multiple changes to this gradient with LSD which were not present with psilocybin, pertaining primarily to visual network differentiation along this axis. However, it is unclear given the limitations of the present datasets whether this is related to differential noise or 'true' drug-specific effects. The third gradient represents an axis which differentiates the so-called task positive (Fox et al., 2005)/multiple demand (Duncan, 2010)/executive network (Niendam et al., 2012; Seeley et al., 2007) from the rest of the cortex. Results with both drugs broadly indicate a contraction of this gradient consistent with reduced

differentiation of executive regions from the rest of cortex. Although speculative, this might relate to certain cognitive impairments present while under the influence of these drugs (Pokorny et al., 2020).

Finally, to our knowledge, this is the first investigation which has shown significant pharmacologically-induced alterations of macroscale cortical gradients. In particular, we have demonstrated that cortical gradients can be acutely altered by two distinct pharmacological manipulations. Although LSD and psilocybin exhibit a complex pharmacology, past investigations with LSD and psilocybin have consistently found that antagonist blockade of the 5-HT2A receptor abolishes the characteristic subjective and neural effects of these drugs, including changes to whole-brain functional connectivity (Kraehenmann et al., 2017; Nichols, 2016; Preller et al., 2018; Preller et al., 2017; Vollenweider et al., 1997; Vollenweider et al., 1998). As such, although strong conclusions cannot be made in the absence of explicit 5-HT2A antagonism, the present findings provide preliminary evidence that 5-HT2A agonism may modulate the functional differentiation of unimodal and transmodal systems, as well macroscale axes of cortical connectivity more generally. Targeted research is needed to investigate whether this is indeed the case and whether this effect generalizes to endogenous serotonergic 5-HT2A agonism.

An important limitation to the present results is the relatively small sample sizes. For this reason, we encourage cautious interpretation of our findings. However, the convergence across drugs and replication across multiple control analyses found here provides strong evidence for the robustness of the observed effects. Despite consistent evidence indicating their safety in controlled research settings (Johnson et al., 2008; Schmid et al., 2015), as well as their potential as both clinical and basic science tools (e.g., Carhart-Harris & Friston, 2019; Girn & Christoff, 2018; Girn et al., 2020; Johnson et al., 2019; Mason et al., 2021; Nour & Carhart-Harris, 2017), collecting large datasets with psychedelics is currently difficult due to persisting regulatory and financial hurdles (Nutt et al., 2013). We hope our findings serve as a foundational guide for future research in this nascent field and as motivation for replication in larger samples.

Another related limitation is that the principal gradient as derived from the psilocybin placebo condition features gradient values that are on the whole lower than the placebo condition of the

LSD dataset. Ideally, the two placebo conditions should be identical and form a baseline indicator of reliability. We note, however, that although gradient values are lower in psilocybin, the overall topography of the principal gradient highly convergent with LSD. This was confirmed quantitatively by an evaluation of the vertex-wise correlation between the mean LSD placebo and psilocybin placebo principal gradients (Spearman's rho = 0.96). As such, the difference in gradient values observed across placebo conditions is not expected to result in systematic differences in contrast results. Moreover, in further support of a lack of dependence of the results on idiosyncrasies within the placebo condition, the psilocybin results were replicated with a pre versus post infusion contrast (Supplementary Figure 2B).

The present study extends past findings on the neural underpinning of the psychedelic state by revealing that the whole-brain effects of LSD and psilocybin can be represented as a contraction the brain's macroscale functional hierarchy – directly in line with a recently proposed unified model of psychedelic brain action (Carhart-Harris & Friston, 2019). We also provided evidence of reductions in sensory and executive region differentiation following psychedelic administration. Future work is needed to ascertain whether reductions in cortical hierarchy in the acute psychedelic experience directly relate to findings of rapid and sustained symptom reductions observed via psychotherapeutically-mediated experiences with these drugs (Carhart-Harris & Friston, 2019; Johnson et al., 2019). The findings of this study lend further weight to the view that psychedelics can be powerful tools for investigating brain organization and dynamics.

Conflicts of Interest

MG reports receiving consulting fees from Psygen Labs Inc. and EntheoTech Bioscience. RLC-H reports receiving consulting fees from COMPASS Pathways, Entheon Biomedical, Mydecine, Synthesis Institute, Tryp Therapeutics, and Usona Institute. BB, JS, RNS, and LR report no conflicts of interest.

Acknowledgements

MG acknowledges funding from National Sciences and Engineering Research Council of Canada (NSERC; Alexander Graham Bell Canada Graduate Scholarships, CGS-D). JS is supported by a European Research Council Consolidator award (WANDERINGMINDS–646927). BB acknowledges research funding from the Canadian Institutes of Health Research (CIHR FDN-154298), the National Sciences and Engineering Research Council of Canada (NSERC; Discovery-1304413), and the Canada Research Chairsprogram (CRC-Tier 2 in Cognitive Neuroinformatics of Healthy and Diseased Brains). RLC-H is supported by the Alex Mosley Charitable Trust and supporters of the Centre for Psychedelic Research: https://www.imperial.ac.uk/psychedelic-research-centre. The original study received support from a Crowd Funding Campaign and the Beckley Foundation, as part of the Beckley-Imperial Research Programme.

References

Barnett, L., Muthukumaraswamy, S. D., Carhart-Harris, R. L., & Seth, A. K. (2020). Decreased directed functional connectivity in the psychedelic state. *Neuroimage, 209*, 116462.

Bethlehem, R. A., Paquola, C., Ronan, L., Seidlitz, J., Bernhardt, B., & Tsvetanov, K. A. (2020). Dispersion of functional gradients across the lifespan. *bioRxiv*.

Bethlehem, R. A., Paquola, C., Seidlitz, J., Ronan, L., Bernhardt, B., Tsvetanov, K. A., & Consortium, C.-C. (2020). Dispersion of functional gradients across the adult lifespan. *Neuroimage, 222*, 117299.

Bogenschutz, M. P., Forcehimes, A. A., Pommy, J. A., Wilcox, C. E., Barbosa, P., & Strassman, R. J. (2015). Psilocybin-assisted treatment for alcohol dependence: A proof-of-concept study. *Journal of Psychopharmacology, 29*(3), 289-299.

Burt, J. B., Demirtaş, M., Eckner, W. J., Navejar, N. M., Ji, J. L., Martin, W. J., . . . Murray, J. D. (2018). Hierarchy of transcriptomic specialization across human cortex captured by structural neuroimaging topography. *Nature Neuroscience, 21*(9), 1251-1259.

Carhart-Harris, R. L. (2018). The entropic brain-revisited. *Neuropharmacology, 142*, 167-178.

Carhart-Harris, R. L., Bolstridge, M., Rucker, J., Day, C. M., Erritzoe, D., Kaelen, M., . . . Feilding, A. (2016). Psilocybin with psychological support for treatment-resistant depression: an open-label feasibility study. *The Lancet Psychiatry, 3*(7), 619-627.

Carhart-Harris, R. L., Erritzoe, D., Williams, T., Stone, J. M., Reed, L. J., Colasanti, A., . . . Murphy, K. (2012). Neural correlates of the psychedelic state as determined by fMRI studies with psilocybin. *Proceedings of the National Academy of Sciences, 109*(6), 2138-2143.

Carhart-Harris, R. L., & Friston, K. J. (2019). REBUS and the Anarchic Brain: Toward a Unified Model of the Brain Action of Psychedelics. *Pharmacological Reviews, 71*(3), 316-344.

Carhart-Harris, R. L., Leech, R., Erritzoe, D., Williams, T. M., Stone, J. M., Evans, J., . . . Nutt, D. J. (2013). Functional connectivity measures after psilocybin inform a novel hypothesis of early psychosis. *Schizophrenia bulletin, 39*(6), 1343-1351.

Carhart-Harris, R. L., Muthukumaraswamy, S., Roseman, L., Kaelen, M., Droog, W., Murphy, K., . . . Nutt, D. J. (2016). Neural correlates of the LSD experience revealed by

multimodal neuroimaging. *Proceedings of the National Academy of Sciences, 113*(17), 4853-4858. doi:10.1073/pnas.1518377113

Coifman, R. R., Lafon, S., Lee, A. B., Maggioni, M., Nadler, B., Warner, F., & Zucker, S. W. (2005). Geometric diffusions as a tool for harmonic analysis and structure definition of data: Diffusion maps. *Proceedings of the National Academy of Sciences, 102*(21), 7426-7431.

D'Argembeau, A., Ruby, P., Collette, F., Degueldre, C., Balteau, E., Luxen, A., . . . Salmon, E. (2007). Distinct regions of the medial prefrontal cortex are associated with self-referential processing and perspective taking. *Journal of Cognitive Neuroscience, 19*(6), 935-944.

Davis, A. K., Barrett, F. S., May, D. G., Cosimano, M. P., Sepeda, N. D., Johnson, M. W., . . . Griffiths, R. R. (2020). Effects of psilocybin-assisted therapy on major depressive disorder: a randomized clinical trial. *JAMA Psychiatry*.

de Wael, R. V., Benkarim, O., Paquola, C., Lariviere, S., Royer, J., Tavakol, S., . . . Valk, S. (2020). BrainSpace: a toolbox for the analysis of macroscale gradients in neuroimaging and connectomics datasets. *Communications biology, 3*(1), 1-10.

Dittrich, A. (1998). The standardized psychometric assessment of altered states of consciousness (ASCs) in humans. *Pharmacopsychiatry*.

Dixon, M. L., Thiruchselvam, R., Todd, R., & Christoff, K. (2017). Emotion and the prefrontal cortex: An integrative review. *Psychological Bulletin, 143*(10), 1033.

Dong, D., Luo, C., Guell, X., Wang, Y., He, H., Duan, M., . . . Yao, D. (2020). Compression of Cerebellar Functional Gradients in Schizophrenia. *Schizophrenia bulletin*.

Duncan, J. (2010). The multiple-demand (MD) system of the primate brain: mental programs for intelligent behaviour. *Trends in Cognitive Sciences, 14*(4), 172-179.

Fox, K. C. R., Girn, M., Parro, C., & Christoff, K. (2018). Functional neuroimaging of psychedelic experience: An overview of psychological and neural effects and their relevance to research on creativity, daydreaming, and dreaming. *The cambridge handbook of the neuroscience of creativity*, 92-113.

Fox, M. D., Snyder, A. Z., Vincent, J. L., Corbetta, M., Van Essen, D. C., & Raichle, M. E. (2005). The human brain is intrinsically organized into dynamic, anticorrelated functional networks. *Proc Natl Acad Sci U S A, 102*(27), 9673-9678.

Friston, K. J. (2010). The free-energy principle: a unified brain theory? *Nature Reviews Neuroscience, 11*(2), 127.

Gasser, P., Kirchner, K., & Passie, T. (2014). LSD-assisted psychotherapy for anxiety associated with a life-threatening disease: A qualitative study of acute and sustained subjective effects. *Journal of Psychopharmacology, 29*(1), 57-68.

Girn, M., & Christoff, K. (2018). Expanding the Scientific Study of Self-Experience with Psychedelics. *Journal of Consciousness Studies, 25*(11-12), 131-154.

Girn, M., Mills, C., Roseman, L., Carhart-Harris, R. L., & Christoff, K. (2020). Updating the dynamic framework of thought: Creativity and psychedelics. *Neuroimage*, 116726.

Griffiths, R. R., Johnson, M. W., Carducci, M. A., Umbricht, A., Richards, W. A., Richards, B. D., . . . Klinedinst, M. A. (2016). Psilocybin produces substantial and sustained decreases in depression and anxiety in patients with life-threatening cancer: A randomized double-blind trial. *Journal of Psychopharmacology, 30*(12), 1181-1197.

Haak, K. V., & Beckmann, C. F. (2020). Understanding brain organisation in the face of functional heterogeneity and functional multiplicity. *Neuroimage, 220*, 117061.

Haak, K. V., Marquand, A. F., & Beckmann, C. F. (2018). Connectopic mapping with resting-state fMRI. *Neuroimage, 170*, 83-94.

Hong, S.-J., de Wael, R. V., Bethlehem, R. A., Lariviere, S., Paquola, C., Valk, S. L., . . . Smallwood, J. (2019). Atypical functional connectome hierarchy in autism. *Nature communications, 10*(1), 1022.

Huntenburg, J. M., Bazin, P.-L., Goulas, A., Tardif, C. L., Villringer, A., & Margulies, D. S. (2017). A systematic relationship between functional connectivity and intracortical myelin in the human cerebral cortex. *Cerebral Cortex, 27*(2), 981-997.

Huntenburg, J. M., Bazin, P.-L., & Margulies, D. S. (2018). Large-scale gradients in human cortical organization. *Trends in Cognitive Sciences, 22*(1), 21-31.

Johnson, M. W., Garcia-Romeu, A., Cosimano, M. P., & Griffiths, R. R. (2014). Pilot study of the 5-HT2AR agonist psilocybin in the treatment of tobacco addiction. *Journal of Psychopharmacology, 28*(11), 983-992.

Johnson, M. W., Hendricks, P. S., Barrett, F. S., & Griffiths, R. R. (2019). Classic psychedelics: An integrative review of epidemiology, therapeutics, mystical experience, and brain network function. *Pharmacology & therapeutics, 197*, 83-102.

Johnson, M. W., Richards, W. A., & Griffiths, R. R. (2008). Human hallucinogen research: guidelines for safety. *Journal of Psychopharmacology*.

Kraehenmann, R., Pokorny, D., Vollenweider, L., Preller, K. H., Pokorny, T., Seifritz, E., & Vollenweider, F. X. (2017). Dreamlike effects of LSD on waking imagery in humans depend on serotonin 2A receptor activation. *Psychopharmacology, 234*(13), 2031-2046.

Larivière, S., Vos de Wael, R., Hong, S.-J., Paquola, C., Tavakol, S., Lowe, A. J., . . . Bernhardt, B. C. (2019). Multiscale Structure–Function Gradients in the Neonatal Connectome. *Cerebral Cortex*.

Lebedev, A. V., Kaelen, M., Lövdén, M., Nilsson, J., Feilding, A., Nutt, D., & Carhart-Harris, R. (2016). LSD-induced entropic brain activity predicts subsequent personality change. *Human Brain Mapping*.

Lord, L.-D., Expert, P., Atasoy, S., Roseman, L., Rapuano, K., Lambiotte, R., . . . Kringelbach, M. L. (2019). Dynamical exploration of the repertoire of brain networks at rest is modulated by psilocybin. *Neuroimage, 199*, 127-142.

Luppi, A. I., Carhart-Harris, R. L., Roseman, L., Pappas, I., Menon, D. K., & Stamatakis, E. A. (2021). LSD alters dynamic integration and segregation in the human brain. *Neuroimage, 227*, 117653.

Margulies, D. S., Ghosh, S. S., Goulas, A., Falkiewicz, M., Huntenburg, J. M., Langs, G., . . . Petrides, M. (2016). Situating the default-mode network along a principal gradient of macroscale cortical organization. *Proceedings of the National Academy of Sciences, 113*(44), 12574-12579.

Mason, N., Kuypers, K., Reckweg, J., Müller, F., Tse, D., Da Rios, B., . . . Ramaekers, J. (2021). Spontaneous and deliberate creative cognition during and after psilocybin exposure. *Translational psychiatry, 11*(1), 1-13.

Mckeown, B., Strawson, W. H., Wang, H.-T., Karapanagiotidis, T., de Wael, R. V., Benkarim, O., . . . McCall, C. (2020). The relationship between individual variation in macroscale functional gradients and distinct aspects of ongoing thought. *Neuroimage, 220*, 117072.

Mesulam, M. (1998). From sensation to cognition. *Brain: A journal of neurology, 121*(6), 1013-1052.

Millière, R. (2017). Looking for the Self: Phenomenology, Neurophysiology and Philosophical Significance of Drug-induced Ego Dissolution. *Frontiers in Human Neuroscience, 11*, 245.

Müller, F., Dolder, P. C., Schmidt, A., Liechti, M. E., & Borgwardt, S. (2018). Altered network hub connectivity after acute LSD administration. *NeuroImage: Clinical, 18*, 694-701.

Murphy, C., Jefferies, E., Rueschemeyer, S.-A., Sormaz, M., Wang, H.-t., Margulies, D. S., & Smallwood, J. (2018). Distant from input: Evidence of regions within the default mode network supporting perceptually-decoupled and conceptually-guided cognition. *Neuroimage, 171*, 393-401.

Nichols, D. E. (2016). Psychedelics. *Pharmacological Reviews, 68*(2), 264-355.

Niendam, T. A., Laird, A. R., Ray, K. L., Dean, Y. M., Glahn, D. C., & Carter, C. S. (2012). Meta-analytic evidence for a superordinate cognitive control network subserving diverse executive functions. *Cognitive, Affective, & Behavioral Neuroscience, 12*(2), 241-268.

Nour, M. M., & Carhart-Harris, R. L. (2017). Psychedelics and the science of self-experience. *The British Journal of Psychiatry, 210*(3), 177-179.

Nour, M. M., Evans, L., Nutt, D., & Carhart-Harris, R. L. (2016). Ego-dissolution and psychedelics: Validation of the ego-dissolution inventory (EDI). *Frontiers in Human Neuroscience, 10*, 269.

Nutt, D. J., King, L. A., & Nichols, D. E. (2013). Effects of Schedule I drug laws on neuroscience research and treatment innovation. *Nature Reviews Neuroscience, 14*(8), 577-585.

Paquola, C., Bethlehem, R. A., Seidlitz, J., Wagstyl, K., Romero-Garcia, R., Whitaker, K. J., . . . Margulies, D. S. (2019). Shifts in myeloarchitecture characterise adolescent development of cortical gradients. *Elife, 8*.

Paquola, C., De Wael, R. V., Wagstyl, K., Bethlehem, R. A., Hong, S.-J., Seidlitz, J., . . . Margulies, D. S. (2019). Microstructural and functional gradients are increasingly dissociated in transmodal cortices. *PLoS biology, 17*(5), e3000284.

Paquola, C., Seidlitz, J., Benkarim, O., Royer, J., Klimes, P., Bethlehem, R. A., . . . Frauscher, B. (2020). The cortical wiring scheme of hierarchical information processing. *bioRxiv*.

Park, B.-y., de Wael, R. V., Paquola, C., Larivière, S., Benkarim, O., Royer, J., . . . Valk, S. L. (2020). Signal diffusion along connectome gradients and inter-hub routing differentially contribute to dynamic human brain function. *Neuroimage, 224*, 117429.

Pokorny, T., Duerler, P., Seifritz, E., Vollenweider, F. X., & Preller, K. H. (2020). LSD acutely impairs working memory, executive functions, and cognitive flexibility, but not risk-based decision-making. *Psychological medicine, 50*(13), 2255-2264.

Preller, K. H., Burt, J. B., Ji, J. L., Schleifer, C. H., Adkinson, B. D., Stämpfli, P., . . . Murray, J. D. (2018). Changes in global and thalamic brain connectivity in LSD-induced altered states of consciousness are attributable to the 5-HT2A receptor. *Elife, 7*, e35082.

Preller, K. H., Duerler, P., Burt, J. B., Ji, J. L., Adkinson, B., Stämpfli, P., . . . Murray, J. D. (2020). Psilocybin induces time-dependent changes in global functional connectivity: Psi-induced changes in brain connectivity. *Biological psychiatry*.

Preller, K. H., Herdener, M., Pokorny, T., Planzer, A., Kraehenmann, R., Stämpfli, P., . . . Vollenweider, F. X. (2017). The fabric of meaning and subjective effects in LSD-induced states depend on serotonin 2A receptor activation. *Current Biology, 27*(3), 451-457.

Preller, K. H., & Vollenweider, F. X. (2016). Phenomenology, structure, and dynamic of psychedelic states. In *Behavioral Neurobiology of Psychedelic Drugs* (pp. 221-256): Springer.

Roseman, L., Leech, R., Feilding, A., Nutt, D. J., & Carhart-Harris, R. L. (2014). The effects of psilocybin and MDMA on between-network resting state functional connectivity in healthy volunteers. *Frontiers in Human Neuroscience, 8*.

Schartner, M. M., Carhart-Harris, R. L., Barrett, A. B., Seth, A. K., & Muthukumaraswamy, S. D. (2017). Increased spontaneous MEG signal diversity for psychoactive doses of ketamine, LSD and psilocybin. *Scientific Reports, 7*, 46421.

Schmid, Y., Enzler, F., Gasser, P., Grouzmann, E., Preller, K. H., Vollenweider, F. X., . . . Liechti, M. E. (2015). Acute effects of lysergic acid diethylamide in healthy subjects. *Biological psychiatry, 78*(8), 544-553.

Seeley, W. W., Menon, V., Schatzberg, A. F., Keller, J., Glover, G. H., Kenna, H., . . . Greicius, M. D. (2007). Dissociable intrinsic connectivity networks for salience processing and executive control. *The Journal of Neuroscience, 27*(9), 2349-2356.

Sepulcre, J., Sabuncu, M. R., Yeo, T. B., Liu, H., & Johnson, K. A. (2012). Stepwise connectivity of the modal cortex reveals the multimodal organization of the human brain. *Journal of Neuroscience, 32*(31), 10649-10661.

Setton, R., Mwilambwe-Tshilobo, L., Girn, M., Lockrow, A. W., Baracchini, G., Lowe, A. J., . . . Nathan Spreng, R. (2021). Functional architecture of the aging brain. *bioRxiv*, 2021.2003.2031.437922. doi:10.1101/2021.03.31.437922

Studerus, E., Gamma, A., & Vollenweider, F. X. (2010). Psychometric evaluation of the altered states of consciousness rating scale (OAV). *PLoS ONE, 5*(8), e12412.

Studerus, E., Kometer, M., Hasler, F., & Vollenweider, F. X. (2011). Acute, subacute and long-term subjective effects of psilocybin in healthy humans: a pooled analysis of experimental studies. *Journal of Psychopharmacology, 25*(11), 1434-1452.

Tagliazucchi, E., Carhart-Harris, R., Leech, R., Nutt, D., & Chialvo, D. R. (2014). Enhanced repertoire of brain dynamical states during the psychedelic experience. *Human Brain Mapping, 35*(11), 5442-5456.

Tagliazucchi, E., Roseman, L., Kaelen, M., Orban, C., Muthukumaraswamy, S. D., Murphy, K., . . . Crossley, N. (2016). Increased global functional connectivity correlates with LSD-Induced ego dissolution. *Current Biology, 26*(8), 1043-1050.

Varley, T., Carhart-Harris, R., Roseman, L., Menon, D., & Stamatakis, E. (2019). Serotonergic Psychedelics LSD & Psilocybin Increase the Fractal Dimension of Cortical Brain Activity in Spatial and Temporal Domains. *bioRxiv*, 517847.

Vazquez-Rodriguez, B., Liu, Z.-Q., Hagmann, P., & Misic, B. (2020). Signal propagation via cortical hierarchies. *bioRxiv*.

Vollenweider, F. X., & Preller, K. H. (2020). Psychedelic drugs: neurobiology and potential for treatment of psychiatric disorders. *Nature Reviews Neuroscience*, 1-14.

Worsley, K. J., Taylor, J., Carbonell, F., Chung, M., Duerden, E., Bernhardt, B., . . . Evans, A. (2009). *A Matlab toolbox for the statistical analysis of univariate and multivariate surface and volumetric data using linear mixed effects models and random field theory.* Paper presented at the NeuroImage Organisation for Human Brain Mapping 2009 Annual Meeting.

Yeo, B. T. T., Kirienen, F. M., Sepulcre, J., Sabuncu, M. R., Lashkari, D., Hollinshead, M., . . . Buckner, R. L. (2011). The organization of the human cerebral cortex estimated by

intrinsic functional connectivity. *J Neurophysiol, 106*, 1125-1165. doi:10.1152/jn.00338.2011.-

Chapter 5: General Discussion

Collectively, these three studies offered novel findings on DN functional organization, role in cognition and behaviour, and sensitivity to pharmacological manipulation. In Study 1, we applied modularity, clustering, and RSFC-mapping analyses to assess whether limbic network (LIM) regions can be construed of as extensions of the DN, as well as to assess LIM heterogeneity in whole-brain RSFC. In support of our hypotheses, a large proportion of the LIM was assigned to the DN via modularity approaches, and clustering and RSFC-mapping analyses supported the presence of distinct LIM regions with varying patterns of DN subsystem RSFC. In Study 2, we assessed multivariate brain-behaviour associations involving DN subsystems, as well as LIM and temporoparietal (TPar) networks. We found evidence for complex mappings between the structure and function of DN subsystems and related networks, and behaviour. Our findings converged with and went beyond task-based investigations of these (sub)networks, providing evidence for selective and distributed contributions to complex behavioural phenotypes. Study 3 applied a combination of gradient- and RSFC- mapping analyses to assess whether DN functional organization and relationship to other large-scale networks was significantly altered by psychedelic drug administration. Results supported our hypotheses: there was a significant attenuation of the principal gradient of macroscale cortical organization in the psychedelic state, underpinned by reduced functional differentiation between transmodal (i.e., the DN) and unimodal cortices. These findings provided novel evidence that a fundamental organizational property of macroscale organization can be significantly disrupted by an acute serotonergic manipulation and support a leading theory of psychedelic brain action. In sum, the present thesis provides significant advances on multiple components of our current understanding of the DN and pave the way forward for future theoretical perspectives and empirical approaches.

The default network, limbic network, and emotional processing: the affect-laden nature of thought

Studies 1 and 2 underscore a close relationship between the DN and LIM – both in terms of RSFC and of associations with non-neural individual differences. As described in the *Literature Review* above, the DN was first identified as a set of regions that consistently deactivate in response to most canonical cognitive paradigms, and was later identified based on seed-based RSFC (Greicius et al., 2003; Raichle & Snyder, 2007; Shulman et al., 1997). These two approaches set the standard

for our understanding of the regional composition of the DN, and was later supported by the influential Yeo et al. (2011) network parcellation which applied clustering analyses to reveal a similar composition. These studies did not find consistent evidence that LIM regions – i.e., the temporal poles (TP), orbitofrontal cortex (OFC), and ventral anterior temporal lobe (vATL) – are a part of the DN. Critically, the data for these studies (and the majority of fMRI studies in general) were collected with conventional fMRI acquisitions which yield poor signal quality in LIM regions (Ojemann et al., 1997).

The notion that the exclusion of LIM regions from the DN in past work is likely a false negative due to a lack of sensitivity is supported by a large task-activation literature. This literature has consistently found evidence for the co-recruitment of DN and LIM regions across a variety of tasks (Andrews-Hanna et al., 2014; Dixon et al., 2017; Kieran C.R. Fox et al., 2018; Frith & Frith, 2007; Spreng et al., 2009). Each of these networks have been linked to distinct but likely highly interrelated functions. LIM regions have been strongly linked to processes at the intersection of memory, emotion, and (social) cognition (Binney et al., 2016; Herlin et al., 2021; Jackson et al., 2016; Olson et al., 2007; Rolls et al., 2020). In particular, the OFC has been linked to emotional appraisal, value attribution, and reward representations (Dixon et al., 2017; Rolls et al., 2020), and both the TP and vATL have been linked to the integration of emotional and perceptual information into multimodal abstract representations that are accessed and manipulated for semantic processing, language, and social cognition (Binder et al., 2009; Binney et al., 2016; Herlin et al., 2021; Jackson et al., 2016; Olson et al., 2007; Ralph et al., 2017; Rolls et al., 2020). In contrast, contemporary conceptions of the DN have highlighted its central role in all cognitive processes that rely on internal representations (i.e., memory) rather than (or in addition to) sensory information available in the here-and-now (Smallwood, Bernhardt, et al., 2021; Stawarczyk et al., 2019). Examples include social cognition/mentalizing, spontaneous thought/mind-wandering, episodic memory recall and projection, self-referential processing, and narrative comprehension (Andrews-Hanna et al., 2014; Smallwood, Bernhardt, et al., 2021; Stawarczyk et al., 2019).

The functional bridge connecting these two networks is that the various cognitive processes in which the DN is engaged in are usually, if not always, emotionally valenced (Kieran C.R. Fox et al., 2018). Consistent with the results of Study 1 which indicated high RSFC between medial OFC,

left TP, and the DN, a variety of studies have found activation within both the medial OFC and TP during internally-directed/self-generated thinking – which includes mentalizing, episodic recall/projection, and self-referential thinking – and correlations between medial OFC activity and the emotional valence of such thinking (D'Argembeau et al., 2005; D'Argembeau et al., 2007; Dixon et al., 2017; Kieran C.R. Fox et al., 2018; Koelsch et al., 2022; Spiers & Maguire, 2006; Taruffi et al., 2017; Tusche et al., 2014). It is further worth noting that high RSFC in Study 1 was found particularly between medial OFC and each of DN_A and DN_C, as well as the hippocampus and amygdala – all of which are involved in processes at the intersection of episodic memory, spontaneous thought, and emotion (Ellamil et al., 2012; Ellamil et al., 2016; Kieran C.R. Fox et al., 2018). The overlap in function between the DN and LIM was additionally supported by the results of Study 2, which found that LIM and DN_B were the strongest contributors to multiple axes of brain-behaviour covariance and, in particular, axes which featured a disproportionate number of social, emotional, and/or semantic variables. The present results and past task-based research, therefore, underscores the relatively neglected contribution of LIM-mediated emotional-semantic processing to DN function and self-generated cognition, and the likelihood that LIM regions may be accurately construed as extensions of the DN.

This notion of a close link between the DN and emotion aligns with multiple theoretical proposals on the neuroscience of emotion. Differences aside, these distinct proposals argue that, rather than cognition and emotions having their basis in discrete regions/networks, both are deeply intertwined and emerge from distributed interactions between multiple large-scale networks (Barrett, 2017; Dixon et al., 2017; Pessoa, 2008; Satpute & Lindquist, 2019). In this manner, cognition and emotion cannot be fully dissociated: abstract cognitive functions enable the appraisal of a particular viscerosomatic/interoceptive state as a particular emotional category, and this appraisal informs one's thought process and action selection (Barrett, 2017; Satpute & Lindquist, 2019). These proposals also highlight the manner in which valuation/emotional appraisal is intrinsic to perception and cognition – that is, all apprehended internal and external stimuli carry an affective tone (Dixon et al., 2017; Pessoa, 2008). This idea is supported, for example, by a variety of studies on internally-directed/self-generated thinking which have explicitly assessed and highlighted the affect-laden nature of cognition (Kieran C.R. Fox et al., 2018). The results of Study 1 and Study 2 therefore also dovetail with the latest theoretical perspectives on the neuroscience of emotion,

providing novel evidence in support of the DN's role in LIM-mediated emotional processing and the LIM's role in DN-mediated cognition. Future RSFC, task-based, and individual differences research should seek to employ acquisitions which afford reliable signal in LIM regions and further evaluate their relationship to the DN and complex cognition – with directly relevance for cases in which cognition goes awry in psychopathology, such as ruminative depression (Rolls et al., 2020).

Multivariate individual differences studies reveal the true complexity of brain-behaviour associations

The results of Study 2 revealed complex multivariable links between the brain and behaviour. A particularly interesting finding was that particular behavioural variables (e.g., loneliness) were found in multiple distinct axes and grouped alongside highly distinct variable sets in each case. This indicates that high scores in a given behavioural measure can occur in varying phenotypic contexts. For example, RSFC results from Study 2 found that, for one axis, high loneliness occurred along high neuroticism, emotional avoidance, and perceived hostility and rejection, while for another axis it co-occurred alongside measures of semantic memory/crystallized education and greater education. The former suggests a broader phenotype in which loneliness occurs in the context of poor mental health and interpersonal dysfunction, whereas the latter suggests the presence of loneliness in the context of a prioritization of solo academic/intellectual pursuits. A testable hypothesis that emerges from these results is whether high loneliness (or any other individual-differences measure) is differentially neurally expressed depending on the broader phenotypic context in which it is present.

The plausibility of this hypothesis is supported by neuropsychiatric research on data-driven phenotypic subtypes in the context of mental health disorders (Brucar et al., 2023; Drysdale et al., 2017; Feczko et al., 2019). In such approaches, data-driven analyses are applied to large datasets consisting of behavioural/clinical assessments and (neuro)biological data with the goal of extracting distinct and dissociable subtypes for a given disorder (e.g., depression) or across disorders (Brucar et al., 2023; Drysdale et al., 2017; Feczko et al., 2019). This process can disentangle intra-disorder heterogeneity, thereby facilitating targeted treatment options, helping clarify biological underpinnings, and improving future diagnoses (Brucar et al., 2023). Phenotypic subtyping research has indeed found evidence for behaviorally and biologically distinct subtypes

across multiple disorders, with direct clinical relevance (Brucar et al., 2023; Drysdale et al., 2017; Faraone et al., 1998; van Rentergem et al., 2021). This work highlights the limitations of univariate studies which seek to relate particular symptoms to the brain in isolation, and underscores the value of deep phenotyping and analysis of the interrelations between symptom clusters and brain clusters.

It is possible, therefore, – as suggested by Study 2 of the present thesis – that there are also distinct phenotypic subtypes of behavioural variation in healthy functioning and that the broader contextual embeddedment of a particular measure may be needed to accurately ascertain its neural basis. Speculatively, this may be most the case with complex measures which can ostensibly manifest in a variety of ways (e.g., socio-emotional measures such as loneliness, interpersonal support/appraisal/belonging, and perceived rejection, as well as personality measures). It is worth highlighting that the greater acknowledgement of how non-neural measures group together in complex ways in tandem with the brain is uniquely afforded by multivariate individual differences studies. While univariate brain-behaviour studies may reveal associations involving specific measures, they operate under the dubious statistical assumption that these associations occur in a vacuum. The results from such studies may therefore obscure important relationships between measures and, by extension, downplay interactions between functionally distinct regions/networks. This is also supported by the results of Study 2 – as well as previous similar investigations (Goyal et al., 2022; Smith et al., 2015) – which indicate the presence of complex behavioural variation that is underpinned by neural patterns that show some functional selectivity, but ultimately cut across functionally distinct large-scale (sub)networks. These suggest that regions comprising the DN and related networks collectively play graded and complex roles across a wide variety of shared traits, behaviours, and cognitive processes. Thus, it can be argued that, although task and univariate studies are able to isolate specific processes/measures and link them to functionally dissociable networks, this process of isolation will necessarily downplay the interactivity between networks and how they act in concert in varying was to give rise to variation in overall behavioural phenotypes. Future multivariate individual-differences studies are needed, therefore, to further illuminate how distinct networks – and/or the brain as a whole – jointly contribute to the complex behaviours that underlie day-to-day human life.

Psychedelic drugs, macroscale hierarchical predictive coding, and the default network

After a multi-decade research hiatus, psychedelic drugs such as psilocybin, LSD, and DMT have re-emerged as scientific and clinical tools of significant interest (Girn et al., 2023; Kwan et al., 2022; McClure-Begley & Roth, 2022; Nutt & Carhart-Harris, 2021). The value of psychedelics tools for basic (neuro)scientific research is driven by their ability to uniquely and potently alter multiple dimensions of conscious experience, spanning perception, cognition, emotion, and sense of self (Girn & Christoff, 2018; Girn et al., 2020; Girn et al., 2023; Girn et al., 2022; Preller & Vollenweider, 2016; Vollenweider & Preller, 2020). Important for the present context, empirical findings and theoretical models have highlighted changes to DN function as central to psychedelic brain action (Carhart-Harris, 2018; Carhart-Harris et al., 2012; Carhart-Harris & Friston, 2019; Carhart-Harris et al., 2014; Girn et al., 2022; Lebedev et al., 2015; Muthukumaraswamy et al., 2013).

The notion that psychedelics elicit their primary effects via a disruption of DN function and the downstream consequences thereof is supported by their neuropharmacological mechanisms. As mentioned in the manuscript for Study 3, the primary subjective and neural effects of serotonergic psychedelics can be largely attributed to agonism of 5-HT2A receptors - as evidenced by studies in humans and rodents with 5-HT2A antagonists (Kwan et al., 2022; Nichols, 2016). This receptor is the most abundant cortical serotonin receptor and, critically, has its highest density in transmodal association cortex centered on the default network, as well as in visual area V1 (Beliveau et al., 2017). Moreover, within transmodal cortex, 5-HT2A receptors are located specifically on the apical dendrites of layer 5 pyramidal cells (Aghajanian & Marek, 1997) – a neuron type that is critical for local (across cortical layers) and global (via long-range cortical and subcortical connections) information integration in the brain (Ramaswamy & Markram, 2015). The neuroanatomical localization of 5-HT2A receptors therefore suggests that they are poised to have a strong ability to modulate transmodal/DN function and, by extension, whole-brain RSFC and dynamics.

Further supporting this notion are the neuronal effects of 5-HT2A agonism. In particular, 5-HT2A agonism leads to a general increase in the excitability of layer 5 pyramidal neurons and the

activation of recurrent networks of deep layer 5 pyramidal neurons specifically (Aghajanian & Marek, 1997; Aghajanian, 2009; Aghajanian & Marek, 1999; Lambe & Aghajanian, 2006). This occurs via an increase in glutamatergic transmission, through a combination of synaptic and volume-transmission effects (Aghajanian, 2009; Aghajanian & Marek, 1999; Lambe & Aghajanian, 2006). Regarding the latter, there is evidence of 5-HT2A-receptor-induced 'glutamate spillover', where in glutamate spills into the extracellular space and alters the firing patterns of neurons in adjacent populations (Aghajanian, 2009; Aghajanian & Marek, 1999; Lambe & Aghajanian, 2006). Evidence suggests that this results in a disruption of local oscillatory dynamics in transmodal association cortices and, consequently, a disruption of functionally segregated, population-level information processing in these regions (Carhart-Harris & Friston, 2019; Carhart-Harris et al., 2014; Carhart-Harris, Muthukumaraswamy, et al., 2016; Muthukumaraswamy et al., 2013; Schartner et al., 2017; Timmermann et al., 2019). This, in turn, is thought to result in a cascade of brain-wide consequences which ultimately result in the potent effects of psychedelics on whole-brain RSFC and large-scale network dynamics as observed by functional neuroimaging (Alamia et al., 2020; Carhart-Harris, Muthukumaraswamy, et al., 2016; Girn et al., 2023; Girn et al., 2022; Lewis et al., 2017; Lord et al., 2019; Luppi et al., 2021; McCulloch et al., 2022; Müller et al., 2018; Preller et al., 2018; Roseman et al., 2014; Varley et al., 2020)

The centrality of the DN in the neuropharmacological effects of psychedelics, its relationship to psychedelic alterations of global brain function, and how all of this relates to psychedelic subjective effects can be fruitfully characterized in terms of hierarchical predicting coding accounts of brain function (Carhart-Harris & Friston, 2019; Clark, 2013; Girn et al., 2022; Rao & Ballard, 1999). These accounts posit that the brain represents the world via a multilevel cascade of dynamically updated predictive models, wherein a model at a given hierarchical level predicts and explains the models at lower levels (Clark, 2013). For example, in visual perception, this account proposes that object recognition neurons predict and explain the activity of neurons encoding low-level sensory features such as lines and edges. According to such accounts of brain function, the DN may represent the pinnacle of the brain's representational hierarchy, drawing from long-term and associative mnemonic information to generate high-level representations of ongoing experience in order to optimally predict and guide perception, cognition, and behaviour (Carhart-Harris & Friston, 2019; Smith et al., 2018; Stawarczyk et al., 2019; Vatansever, Menon,

et al., 2017). These high-level representations have variably referred to as scenes (Hassabis & Maguire, 2007), contexts (Bar, 2007; Ranganath & Ritchey, 2012; Smith et al., 2018), or event models (Baldassano et al., 2017; Stawarczyk et al., 2019). In relation to psychedelics, it may be that, via the 5-HT2A-based mechanisms described above, they disrupt the population-encoding of these high-level representations, thereby impairing the usual top-down prediction-based organization of experience and resulting in 'psychedelic' subjective effects. This perspective is consistent with the RElaxed Beliefs Under pSychedelics (REBUS) model of psychedelic effects (Carhart-Harris & Friston, 2019). A core idea of this model is that psychedelics impair the top-down constraining effect of association cortices on lower-level sensory and limbic networks, thereby liberating bottom-up information flow and increasing crosstalk between abstract (i.e., DN) and concrete (visual/somatosensory/auditory) processing (Carhart-Harris & Friston, 2019). As described above, Study 3 provided empirical support for this in two independent psychedelic datasets, one with LSD and one with psilocybin (Girn et al., 2022). A recently published study also found a similar pattern with DMT (Timmermann et al., 2023).

An often-discussed component of the psychedelic experience that may be plausibly explained from the above-described hierarchical predictive coding perspective is so-called 'ego dissolution', which pertains to an attenuation of one's sense of being distinct from others and the external world, and which coincides with a blurring between internal and external experience (Girn & Christoff, 2018; Nour & Carhart-Harris, 2017; Nour et al., 2016). Speculatively, this aspect of psychedelic phenomenology may be the result of a disruption of DN-mediated processes that underpin the 'high-level representations' that mediate the sense of individualized identity/self-hood that is characteristic of normal conscious experience. Another component of the psychedelic experience amenable to this perspective is the presence of complex visual imagery (Aqil & Roseman, 2022; Studerus et al., 2010). This refers to closed-eye imagery of complex scenes, landscapes, and vivified episodic memories (Preller & Vollenweider, 2016; Studerus et al., 2010). It may be that these subjective effects are a result of disruptions to the functional segregation of the DN – particularly the medial temporal lobe regions within DN_C – from visual regions, wherein high-level episodic representations spill into visual processing. Supporting this, functional neuroimaging research has found evidence for significant alterations in the RSFC between visual and medial temporal lobe regions (Carhart-Harris, Muthukumaraswamy, et al., 2016; Girn et al.,

2022; Kaelen et al., 2016; Lebedev et al., 2015; Roseman et al., 2014), and one study specifically found a relationship between increased parahippocampus-visual RSFC and increased music-evoked autobiographical imagery (Kaelen et al., 2016). Collectively, this further underscores an essential role for DN functional integrity and functional segregation from other networks in mediating fundamental aspects of conscious experience – including our experience of a coherent perceptual world 'out there' that is distinct from a sense of inhibiting an individualized identity 'in here'. By transiently perturbing the structures of consciousness in this manner, psychedelics represent unique and powerful tools for probing the large-scale brain functional connectivity and dynamics that undergird 'regular' human consciousness, as well as how these might relate to the functional roles of the DN in particular.

Conclusions

This thesis consisted of studies which set out to assess each of the DN's functional organization, relationship to non-neural individual differences, and sensitivity to pharmacological perturbation. In doing so, it sought to offer novel and impactful contributions to each of these domains so as to offer far-reaching influence on current understandings of the DN. This was accomplished: Study 1 revealed novel evidence supporting the inclusion of the limbic network as part of the DN and extended past findings exploring the functional heterogeneity of limbic network regions; Study 2 revealed multiple multivariate axes of DN-behaviour covariance, which underscored unique and overlapping contributions across DN subnetworks and related networks in relation to complex behavioural phenotypes; Study 3 revealed the significant sensitivity of the DN and macroscale cortical organization to the acute effects of psychedelic drugs, thereby supporting the DN's essential but malleable role in processes that are central to conscious experience. Collectively, these findings highlight the importance of limbic regions in understanding the DN's organization and role in cognition, the complex and distributed nature of relationships between the DN and behaviour/cognition, and the manner in which certain drugs can be used to probe fundamental aspects of DN organization and function and their relationship to ongoing conscious experience. In doing so, they offer impactful contributions with strong high potential to help revise and advance theoretical conceptions of the DN and to motivate future empirical investigations of this network.

Master References

Adolphs, R. (2016). Human lesion studies in the 21st century. *Neuron*, *90*(6), 1151-1153.

Aghajanian, G., & Marek, G. (1997). Serotonin induces excitatory postsynaptic potentials in apical dendrites of neocortical pyramidal cells. *Neuropharmacology*, *36*(4-5), 589-599.

Aghajanian, G. K. (2009). Modeling "psychosis" in vitro by inducing disordered neuronal network activity in cortical brain slices. *Psychopharmacology*, *206*(4), 575-585.

Aghajanian, G. K., & Marek, G. J. (1999). Serotonin, via 5-HT2A receptors, increases EPSCs in layer V pyramidal cells of prefrontal cortex by an asynchronous mode of glutamate release. *Brain Research*, *825*(1-2), 161-171.

Akshoomoff, N., Beaumont, J. L., Bauer, P. J., Dikmen, S. S., Gershon, R. C., Mungas, D., Slotkin, J., Tulsky, D., Weintraub, S., & Zelazo, P. D. (2013). VIII. NIH Toolbox Cognition Battery (CB): composite scores of crystallized, fluid, and overall cognition. *Monographs of the Society for Research in Child Development*, *78*(4), 119-132.

Alamia, A., Timmermann, C., Nutt, D. J., VanRullen, R., & Carhart-Harris, R. L. (2020). DMT alters cortical travelling waves. *Elife*, *9*. https://doi.org/10.7554/eLife.59784

Alves, P. N., Foulon, C., Karolis, V., Bzdok, D., Margulies, D. S., Volle, E., & de Schotten, M. T. (2019). An improved neuroanatomical model of the default-mode network reconciles previous neuroimaging and neuropathological findings. *Communications biology*, *2*(1), 1-14.

Andersen, K. A., Carhart-Harris, R., Nutt, D. J., & Erritzoe, D. (2021). Therapeutic effects of classic serotonergic psychedelics: A systematic review of modern-era clinical studies. *Acta Psychiatrica Scandinavica*, *143*(2), 101-118.

Andrews-Hanna, J. R., Reidler, J. S., Sepulcre, J., Poulin, R., & Buckner, R. L. (2010). Functional-anatomic fractionation of the brain's default network. *Neuron*, *65*(4), 550-562. https://doi.org/10.1016/j.neuron.2010.02.005

Andrews-Hanna, J. R., Smallwood, J., & Spreng, R. N. (2014). The default network and self-generated thought: Component processes and dynamic control. *Annals of the New York Academy of Sciences*, *1316*(1), 29-52.

Aqil, M., & Roseman, L. (2022). More than meets the eye: The role of sensory dimensions in psychedelic brain dynamics, experience, and therapeutics. *Neuropharmacology*, 109300.

Arbabshirani, M. R., Damaraju, E., Phlypo, R., Plis, S., Allen, E., Ma, S., Mathalon, D., Preda, A., Vaidya, J. G., & Adali, T. (2014). Impact of autocorrelation on functional connectivity. *Neuroimage*, *102*, 294-308.

Arnone, D., Wise, T., Walker, C., Cowen, P. J., Howes, O., & Selvaraj, S. (2018). The effects of serotonin modulation on medial prefrontal connectivity strength and stability: a pharmacological fMRI study with citalopram. *Progress in Neuro-Psychopharmacology and Biological Psychiatry*, *84*, 152-159.

Ashburner, J., & Friston, K. J. (2000). Voxel-based morphometry—the methods. *Neuroimage*, *11*(6), 805-821.

Bagby, R. M., Parker, J. D., & Taylor, G. J. (1994). The twenty-item Toronto Alexithymia Scale—I. Item selection and cross-validation of the factor structure. *Journal of psychosomatic research*, *38*(1), 23-32.

Baldassano, C., Chen, J., Zadbood, A., Pillow, J. W., Hasson, U., & Norman, K. A. (2017). Discovering event structure in continuous narrative perception and memory. *Neuron*, *95*(3), 709-721. e705.

Bar, M. (2007). The proactive brain: using analogies and associations to generate predictions. *Trends in Cognitive Sciences*, *11*(7), 280-289.

Barbas, H., Ghashghaei, H., Dombrowski, S., & Rempel-Clower, N. (1999). Medial prefrontal cortices are unified by common connections with superior temporal cortices and distinguished by input from memory-related areas in the rhesus monkey. *Journal of Comparative Neurology*, *410*(3), 343-367.

Barnett, L., Muthukumaraswamy, S. D., Carhart-Harris, R. L., & Seth, A. K. (2020). Decreased directed functional connectivity in the psychedelic state. *Neuroimage*, *209*, 116462.

Baron-Cohen, S., Wheelwright, S., Hill, J., Raste, Y., & Plumb, I. (2001). The "Reading the Mind in the Eyes" Test revised version: a study with normal adults, and adults with Asperger syndrome or high-functioning autism. *The Journal of Child Psychology and Psychiatry and Allied Disciplines*, *42*(2), 241-251.

Barrett, L. F. (2017). The theory of constructed emotion: an active inference account of interoception and categorization. *Social cognitive and affective neuroscience*, *12*(1), 1-23.

Bassett, D. S., & Sporns, O. (2017). Network neuroscience. *Nat Neurosci*, *20*(3), 353-364.

Beliveau, V., Ganz, M., Feng, L., Ozenne, B., Højgaard, L., Fisher, P. M., Svarer, C., Greve, D. N., & Knudsen, G. M. (2017). A high-resolution in vivo atlas of the human brain's serotonin system. *Journal of Neuroscience*, *37*(1), 120-128.

Bethlehem, R. A., Paquola, C., Ronan, L., Seidlitz, J., Bernhardt, B., & Tsvetanov, K. A. (2020). Dispersion of functional gradients across the lifespan. *bioRxiv*.

Bethlehem, R. A., Paquola, C., Seidlitz, J., Ronan, L., Bernhardt, B., Tsvetanov, K. A., & Consortium, C.-C. (2020). Dispersion of functional gradients across the adult lifespan. *Neuroimage*, *222*, 117299.

Bickart, K. C., Wright, C. I., Dautoff, R. J., Dickerson, B. C., & Barrett, L. F. (2011). Amygdala volume and social network size in humans. *Nat Neurosci*, *14*(2), 163.

Binder, J. R., Desai, R. H., Graves, W. W., & Conant, L. L. (2009). Where is the semantic system? A critical review and meta-analysis of 120 functional neuroimaging studies. *Cerebral Cortex*, *19*(12), 2767-2796.

Binney, R. J., Hoffman, P., & Lambon Ralph, M. A. (2016). Mapping the multiple graded contributions of the anterior temporal lobe representational hub to abstract and social concepts: evidence from distortion-corrected fMRI. *Cerebral Cortex*, *26*(11), 4227-4241.

Biswal, B., Zerrin Yetkin, F., Haughton, V. M., & Hyde, J. S. (1995). Functional connectivity in the motor cortex of resting human brain using echo-planar mri. *Magnetic resonance in medicine*, *34*(4), 537-541.

Blondel, V. D., Guillaume, J.-L., Lambiotte, R., & Lefebvre, E. (2008). Fast unfolding of communities in large networks. *Journal of statistical mechanics: theory and experiment*, *2008*(10), P10008.

Bogenschutz, M. P., Forcehimes, A. A., Pommy, J. A., Wilcox, C. E., Barbosa, P., & Strassman, R. J. (2015). Psilocybin-assisted treatment for alcohol dependence: A proof-of-concept study. *Journal of Psychopharmacology*, *29*(3), 289-299.

Braga, R. M., & Buckner, R. L. (2017). Parallel interdigitated distributed networks within the individual estimated by intrinsic functional connectivity. *Neuron*, *95*(2), 457-471. e455.

Brainerd, C., Reyna, V., Gomes, C. F., Kenney, A., Gross, C., Taub, E., & Spreng, R. (2014). Dual-retrieval models and neurocognitive impairment. *Journal of Experimental Psychology: Learning, Memory, and Cognition*, *40*(1), 41.

Bressler, S. L., & Menon, V. (2010). Large-scale brain networks in cognition: emerging methods and principles [Research Support, U.S. Gov't, Non-P.H.S.

Review]. *Trends Cogn Sci*, *14*(6), 277-290. https://doi.org/10.1016/j.tics.2010.04.004

Brucar, L. R., Feczko, E., Fair, D. A., & Zilverstand, A. (2023). Current approaches in computational psychiatry for the data-driven identification of brain-based subtypes. *Biological psychiatry*, *93*(8), 704-716.

Buckner, R. L., Andrews-Hanna, J. R., & Schacter, D. L. (2008). The brain's default network: anatomy, function, and relevance to disease. *Ann N Y Acad Sci*, *1124*, 1-38. https://doi.org/10.1196/annals.1440.011

Buckner, R. L., & DiNicola, L. M. (2019). The brain's default network: updated anatomy, physiology and evolving insights. *Nature Reviews Neuroscience*, 1-16.

Buckner, R. L., Krienen, F. M., Castellanos, A., Diaz, J. C., & Yeo, B. T. (2011). The organization of the human cerebellum estimated by intrinsic functional connectivity. *American Journal of Physiology-Heart and Circulatory Physiology*.

Buckner, R. L., Krienen, F. M., & Yeo, B. T. T. (2013). Opportunities and limitations of intrinsic functional connectivity MRI. *Nat Neurosci*, *16*(7), 832-837.

Burt, J. B., Demirtaş, M., Eckner, W. J., Navejar, N. M., Ji, J. L., Martin, W. J., Bernacchia, A., Anticevic, A., & Murray, J. D. (2018). Hierarchy of transcriptomic specialization across human cortex captured by structural neuroimaging topography. *Nat Neurosci*, *21*(9), 1251-1259.

Button, K. S., Ioannidis, J. P., Mokrysz, C., Nosek, B. A., Flint, J., Robinson, E. S., & Munafò, M. R. (2013). Power failure: why small sample size undermines the reliability of neuroscience. *Nature Reviews Neuroscience*, *14*(5), 365-376.

Bzdok, D., Laird, A. R., Zilles, K., Fox, P. T., & Eickhoff, S. B. (2013). An investigation of the structural, connectional, and functional subspecialization in the human amygdala. *Human Brain Mapping*, *34*(12), 3247-3266.

Bzdok, D., & Yeo, B. T. (2017). Inference in the age of big data: Future perspectives on neuroscience. *Neuroimage*, *155*, 549-564.

Carhart-Harris, R. L. (2018). The entropic brain-revisited. *Neuropharmacology*, *142*, 167-178.

Carhart-Harris, R. L., Bolstridge, M., Rucker, J., Day, C. M., Erritzoe, D., Kaelen, M., Bloomfield, M., Rickard, J. A., Forbes, B., & Feilding, A. (2016). Psilocybin with psychological support for treatment-resistant depression: an open-label feasibility study. *The Lancet Psychiatry*, *3*(7), 619-627.

Carhart-Harris, R. L., Erritzoe, D., Williams, T., Stone, J. M., Reed, L. J., Colasanti, A., Tyacke, R. J., Leech, R., Malizia, A. L., & Murphy, K. (2012). Neural correlates of the psychedelic state as determined by fMRI studies with psilocybin. *Proceedings of the National Academy of Sciences*, *109*(6), 2138-2143.

Carhart-Harris, R. L., & Friston, K. J. (2019). REBUS and the Anarchic Brain: Toward a Unified Model of the Brain Action of Psychedelics. *Pharmacological Reviews*, *71*(3), 316-344.

Carhart-Harris, R. L., Leech, R., Erritzoe, D., Williams, T. M., Stone, J. M., Evans, J., Sharp, D. J., Feilding, A., Wise, R. G., & Nutt, D. J. (2013). Functional connectivity measures after psilocybin inform a novel hypothesis of early psychosis. *Schizophrenia bulletin*, *39*(6), 1343-1351.

Carhart-Harris, R. L., Leech, R., Hellyer, P. J., Shanahan, M., Feilding, A., Tagliazucchi, E., Chialvo, D. R., & Nutt, D. (2014). The entropic brain: a theory of conscious states informed by neuroimaging research with psychedelic drugs. *Frontiers in Human Neuroscience*, *8*, 20.

Carhart-Harris, R. L., Muthukumaraswamy, S., Roseman, L., Kaelen, M., Droog, W., Murphy, K., Tagliazucchi, E., Schenberg, E. E., Nest, T., Orban, C., Leech, R., Williams, L. T., Williams, T. M., Bolstridge, M., Sessa, B., McGonigle, J., Sereno, M. I., Nichols, D., Hellyer, P. J., Hobden, P., Evans, J., Singh, K. D., Wise, R. G., Curran, H. V., Feilding, A., & Nutt, D. J. (2016). Neural correlates of the LSD experience revealed by multimodal neuroimaging. *Proceedings of the National Academy of Sciences*, *113*(17), 4853-4858. https://doi.org/10.1073/pnas.1518377113

Carmichael, O., Schwarz, A. J., Chatham, C. H., Scott, D., Turner, J. A., Upadhyay, J., Coimbra, A., Goodman, J. A., Baumgartner, R., & English, B. A. (2018). The role of fMRI in drug development. *Drug discovery today*, *23*(2), 333-348.

Carmichael, S., & Price, J. (1995). Limbic connections of the orbital and medial prefrontal cortex in macaque monkeys. *Journal of Comparative Neurology*, *363*(4), 615-641.

Carmichael, S., & Price, J. (1996). Connectional networks within the orbital and medial prefrontal cortex of macaque monkeys. *Journal of Comparative Neurology*, *371*(2), 179-207.

Carver, C. S., & White, T. L. (1994). Behavioral inhibition, behavioral activation, and affective responses to impending reward and punishment: the BIS/BAS scales. *Journal of personality and social psychology*, *67*(2), 319.

Casey, B., Cannonier, T., Conley, M. I., Cohen, A. O., Barch, D. M., Heitzeg, M. M., Soules, M. E., Teslovich, T., Dellarco, D. V., & Garavan, H. (2018). The adolescent brain cognitive development (ABCD) study: imaging acquisition across 21 sites. *Developmental cognitive neuroscience*, *32*, 43-54.

Chase, H. W., Grace, A. A., Fox, P. T., Phillips, M. L., & Eickhoff, S. B. (2020). Functional differentiation in the human ventromedial frontal lobe: A data-driven parcellation. *Human Brain Mapping*.

Chen, J., Leong, Y. C., Honey, C. J., Yong, C. H., Norman, K. A., & Hasson, U. (2017). Shared memories reveal shared structure in neural activity across individuals. *Nat Neurosci*, *20*(1), 115-125.

Choi, E. Y., Yeo, B. T., & Buckner, R. L. (2012). The organization of the human striatum estimated by intrinsic functional connectivity. *J Neurophysiol*, *108*(8), 2242-2263.

Chong, M., Bhushan, C., Joshi, A., Choi, S., Haldar, J., Shattuck, D., Spreng, R., & Leahy, R. (2017). Individual parcellation of resting fMRI with a group functional connectivity prior. *Neuroimage*, *156*, 87-100.

Clark, A. (2013). Whatever next? Predictive brains, situated agents, and the future of cognitive science. *Behavioral and Brain Sciences*, *36*(03), 181-204.

Coifman, R. R., Lafon, S., Lee, A. B., Maggioni, M., Nadler, B., Warner, F., & Zucker, S. W. (2005). Geometric diffusions as a tool for harmonic analysis and structure definition of data: Diffusion maps. *Proceedings of the National Academy of Sciences*, *102*(21), 7426-7431.

Cole, M. W., Bassett, D. S., Power, J. D., Braver, T. S., & Petersen, S. E. (2014). Intrinsic and task-evoked network architectures of the human brain. *Neuron*, *83*(1), 238-251.

Cunningham, S. I., Tomasi, D., & Volkow, N. D. (2017). Structural and functional connectivity of the precuneus and thalamus to the default mode network. *Human Brain Mapping*, *38*(2), 938-956.

D'Argembeau, A., Collette, F., Van der Linden, M., Laureys, S., Del Fiore, G., Degueldre, C., Luxen, A., & Salmon, E. (2005). Self-referential reflective activity and its relationship with rest: a PET study. *Neuroimage*, *25*(2), 616-624.

D'Argembeau, A., Ruby, P., Collette, F., Degueldre, C., Balteau, E., Luxen, A., Maquet, P., & Salmon, E. (2007). Distinct regions of the medial prefrontal cortex are associated with self-referential processing and perspective taking. *Journal of Cognitive Neuroscience*, *19*(6), 935-944.

Damoiseaux, J., Rombouts, S., Barkhof, F., Scheltens, P., Stam, C., Smith, S. M., & Beckmann, C. (2006). Consistent resting-state networks across healthy subjects. *Proceedings of the National Academy of Sciences*, *103*(37), 13848-13853.

Davies, C. L., Sibley, C. G., & Liu, J. H. (2014). Confirmatory factor analysis of the Moral Foundations Questionnaire. *Social Psychology*.

Davis, A. K., Barrett, F. S., May, D. G., Cosimano, M. P., Sepeda, N. D., Johnson, M. W., Finan, P. H., & Griffiths, R. R. (2020). Effects of psilocybin-assisted therapy on major depressive disorder: a randomized clinical trial. *JAMA Psychiatry*.

Davis, M. H. (1983). Measuring individual differences in empathy: Evidence for a multidimensional approach. *Journal of personality and social psychology*, *44*(1), 113.

de Wael, R. V., Benkarim, O., Paquola, C., Lariviere, S., Royer, J., Tavakol, S., Xu, T., Hong, S.-J., Langs, G., & Valk, S. (2020). BrainSpace: a toolbox for the analysis of macroscale gradients in neuroimaging and connectomics datasets. *Communications biology*, *3*(1), 1-10.

DeYoung, C. G., Quilty, L. C., & Peterson, J. B. (2007). Between facets and domains: 10 aspects of the Big Five. *Journal of personality and social psychology*, *93*(5), 880.

DiNicola, L. M., Braga, R. M., & Buckner, R. L. (2020). Parallel distributed networks dissociate episodic and social functions within the individual. *Journal of neurophysiology*, *123*(3), 1144-1179.

Dittrich, A. (1998). The standardized psychometric assessment of altered states of consciousness (ASCs) in humans. *Pharmacopsychiatry*.

Dixon, M. L., Thiruchselvam, R., Todd, R., & Christoff, K. (2017). Emotion and the prefrontal cortex: An integrative review. *Psychol Bull*, *143*(10), 1033.

Dong, D., Luo, C., Guell, X., Wang, Y., He, H., Duan, M., Eickhoff, S. B., & Yao, D. (2020). Compression of Cerebellar Functional Gradients in Schizophrenia. *Schizophrenia bulletin*.

Doucet, G., Naveau, M., Petit, L., Delcroix, N., Zago, L., Crivello, F., Jobard, G., Tzourio-Mazoyer, N., Mazoyer, B., & Mellet, E. (2011). Brain activity at rest: a multiscale hierarchical functional organization. *Journal of neurophysiology*, *105*(6), 2753-2763.

Drysdale, A. T., Grosenick, L., Downar, J., Dunlop, K., Mansouri, F., Meng, Y., Fetcho, R. N., Zebley, B., Oathes, D. J., & Etkin, A. (2017). Resting-state connectivity biomarkers define neurophysiological subtypes of depression. *Nature medicine*, *23*(1), 28-38.

Du, J., Rolls, E. T., Cheng, W., Li, Y., Gong, W., Qiu, J., & Feng, J. (2020). Functional connectivity of the orbitofrontal cortex, anterior cingulate cortex, and inferior frontal gyrus in humans. *Cortex*, *123*, 185-199.

Dubois, J., & Adolphs, R. (2016). Building a Science of Individual Differences from fMRI. *Trends in Cognitive Sciences*, *20*(6), 425-443. https://doi.org/https://doi.org/10.1016/j.tics.2016.03.014

Duncan, J. (2010). The multiple-demand (MD) system of the primate brain: mental programs for intelligent behaviour. *Trends in Cognitive Sciences*, *14*(4), 172-179.

DuPre, E., Luh, W.-M., & Spreng, R. N. (2016). Multi-echo fMRI replication sample of autobiographical memory, prospection and theory of mind reasoning tasks. *Scientific data*, *3*, 160116.

Dutta, A., McKie, S., Downey, D., Thomas, E., Juhasz, G., Arnone, D., Elliott, R., Williams, S., Deakin, J. W., & Anderson, I. M. (2019). Regional default mode network connectivity in major depressive disorder: modulation by acute intravenous citalopram. *Translational psychiatry*, *9*(1), 116.

Eickhoff, S. B., Yeo, B., & Genon, S. (2018). Imaging-based parcellations of the human brain. *Nature Reviews Neuroscience*, *19*(11), 672-686.

Ellamil, M., Dobson, C., Beeman, M., & Christoff, K. (2012). Evaluative and generative modes of thought during the creative process. *Neuroimage*, *59*(2), 1783-1794. https://doi.org/10.1016/j.neuroimage.2011.08.008

Ellamil, M., Fox, K. C., Dixon, M. L., Pritchard, S., Todd, R. M., Thompson, E., & Christoff, K. (2016). Dynamics of neural recruitment surrounding the spontaneous arising of thoughts in experienced mindfulness practitioners. *Neuroimage*, *136*, 186-196.

Fan, L., Wang, J., Zhang, Y., Han, W., Yu, C., & Jiang, T. (2014). Connectivity-based parcellation of the human temporal pole using diffusion tensor imaging. *Cerebral Cortex*, *24*(12), 3365-3378.

Fang, X., Deza-Araujo, Y. I., Petzold, J., Spreer, M., Riedel, P., Marxen, M., O'Connor, S. J., Zimmermann, U. S., & Smolka, M. N. (2021). Effects of moderate alcohol levels on default mode network connectivity in heavy drinkers. *Alcoholism: Clinical and Experimental Research*, *45*(5), 1039-1050.

Faraone, S. V., Biederman, J., Weber, W., & Russell, R. L. (1998). Psychiatric, neuropsychological, and psychosocial features of DSM-IV subtypes of attention-deficit/hyperactivity disorder: results from a clinically referred sample. *Journal of the American Academy of Child & Adolescent Psychiatry*, *37*(2), 185-193.

Feczko, E., Miranda-Dominguez, O., Marr, M., Graham, A. M., Nigg, J. T., & Fair, D. A. (2019). The heterogeneity problem: approaches to identify psychiatric subtypes. *Trends in Cognitive Sciences*, *23*(7), 584-601.

Flodin, P., Gospic, K., Petrovic, P., & Fransson, P. (2012). Effects of L-dopa and oxazepam on resting-state functional magnetic resonance imaging connectivity: a randomized, cross-sectional placebo study. *Brain Connectivity*, *2*(5), 246-253.

Fox, K. C. R., Andrews-Hanna, J. R., Mills, C., Dixon, M. L., Markovic, J., Thompson, E., & Christoff, K. (2018). Affective neuroscience of self-generated thought. *Ann NY Acad Sci*, *1426*, 25-51.

Fox, K. C. R., Girn, M., Parro, C., & Christoff, K. (2018). Functional neuroimaging of psychedelic experience: An overview of psychological and neural effects and their relevance to research on creativity, daydreaming, and dreaming. *The cambridge handbook of the neuroscience of creativity*, 92-113.

Fox, M. D., & Raichle, M. E. (2007). Spontaneous fluctuations in brain activity observed with functional magnetic resonance imaging. *Nature Reviews Neuroscience*, *8*(9), 700-711. https://doi.org/10.1038/nrn2201

Fox, M. D., Snyder, A. Z., Vincent, J. L., Corbetta, M., Van Essen, D. C., & Raichle, M. E. (2005). The human brain is intrinsically organized into dynamic, anticorrelated functional networks. *Proc Natl Acad Sci U S A*, *102*(27), 9673-9678.

Fraley, R. C., Waller, N. G., & Brennan, K. A. (2000). An item response theory analysis of self-report measures of adult attachment. *Journal of personality and social psychology*, *78*(2), 350.

Friston, K. J. (2010). The free-energy principle: a unified brain theory? *Nature Reviews Neuroscience*, *11*(2), 127.

Friston, K. J., Jezzard, P., & Turner, R. (1994). Analysis of functional MRI time-series. *Human Brain Mapping*, *1*(2), 153-171.

Frith, C. D., & Frith, U. (2007). Social cognition in humans. *Current Biology*, *17*(16), R724-R732.

Garrett, D. D., Samanez-Larkin, G. R., MacDonald, S. W., Lindenberger, U., McIntosh, A. R., & Grady, C. L. (2013). Moment-to-moment brain signal variability: a next frontier in human brain mapping? *Neuroscience & Biobehavioral Reviews*, *37*(4), 610-624.

Gaser, C., & Dahnke, R. (2016). CAT-a computational anatomy toolbox for the analysis of structural MRI data. *Hbm*, *2016*, 336-348.

Gasser, P., Kirchner, K., & Passie, T. (2014). LSD-assisted psychotherapy for anxiety associated with a life-threatening disease: A qualitative study of acute and sustained subjective effects. *Journal of Psychopharmacology*, *29*(1), 57-68.

Gerritsen, C. J., Toplak, M. E., Sciaraffa, J., & Eastwood, J. (2014). I can't get no satisfaction: Potential causes of boredom. *Conscious Cogn*, *27*, 27-41.

Gershon, R. C., Wagster, M. V., Hendrie, H. C., Fox, N. A., Cook, K. F., & Nowinski, C. J. (2013). NIH toolbox for assessment of neurological and behavioral function. *Neurology*, *80*(11 Supplement 3), S2-S6.

Girn, M., & Christoff, K. (2018). Expanding the Scientific Study of Self-Experience with Psychedelics. *Journal of Consciousness Studies*, *25*(11-12), 131-154.

Girn, M., Mills, C., Roseman, L., Carhart-Harris, R. L., & Christoff, K. (2020). Updating the dynamic framework of thought: Creativity and psychedelics. *Neuroimage*, 116726.

Girn, M., Rosas, F. E., Daws, R. E., Gallen, C. L., Gazzaley, A., & Carhart-Harris, R. L. (2023). A complex systems perspective on psychedelic brain action. *Trends in Cognitive Sciences*.

Girn, M., Roseman, L., Bernhardt, B., Smallwood, J., Carhart-Harris, R., & Spreng, R. N. (2022). Serotonergic psychedelic drugs LSD and psilocybin reduce the hierarchical differentiation of unimodal and transmodal cortex. *Neuroimage*, 119220. https://doi.org/https://doi.org/10.1016/j.neuroimage.2022.119220

Glasser, M. F., Coalson, T. S., Robinson, E. C., Hacker, C. D., Harwell, J., Yacoub, E., Ugurbil, K., Andersson, J., Beckmann, C. F., & Jenkinson, M. (2016). A multi-modal parcellation of human cerebral cortex. *Nature*, *536*(7615), 171-178.

Gonzalez-Garcia, C., Flounders, M. W., Chang, R., Baria, A. T., & He, B. J. (2018). Content-specific activity in frontoparietal and default-mode networks during prior-guided visual perception. *Elife*, *7*, e36068.

Gordon, E. M., Laumann, T. O., Adeyemo, B., Huckins, J. F., Kelley, W. M., & Petersen, S. E. (2014). Generation and evaluation of a cortical area parcellation from resting-state correlations. *Cerebral Cortex*, *26*(1), 288-303.

Gordon, E. M., Laumann, T. O., Adeyemo, B., & Petersen, S. E. (2017). Individual variability of the system-level organization of the human brain. *Cerebral Cortex*, *27*(1), 386-399.

Goyal, N., Moraczewski, D., Bandettini, P. A., Finn, E. S., & Thomas, A. G. (2022). The positive-negative mode link between brain connectivity, demographics, and behavior: A pre-registered replication of Smith et al. 2015. *arXiv preprint arXiv:2201.10598*.

Graham, J., Nosek, B. A., Haidt, J., Iyer, R., Spassena, K., & Ditto, P. H. (2008). Moral foundations questionnaire. *Journal of personality and social psychology*.

Greicius, M. D., Krasnow, B., Reiss, A. L., & Menon, V. (2003). Functional connectivity in the resting brain: a network analysis of the default mode hypothesis. *Proceedings of the National Academy of Sciences*, *100*(1), 253-258.

Griffiths, R. R., Johnson, M. W., Carducci, M. A., Umbricht, A., Richards, W. A., Richards, B. D., Cosimano, M. P., & Klinedinst, M. A. (2016). Psilocybin produces substantial and sustained decreases in depression and anxiety in patients with life-threatening cancer: A randomized double-blind trial. *Journal of Psychopharmacology*, *30*(12), 1181-1197.

Gusnard, D. A., & Raichle, M. E. (2001). Searching for a baseline: functional imaging and the resting human brain. *Nature Reviews Neuroscience*, *2*(10), 685-694.

Haak, K. V., & Beckmann, C. F. (2020). Understanding brain organisation in the face of functional heterogeneity and functional multiplicity. *Neuroimage*, *220*, 117061.

Haak, K. V., Marquand, A. F., & Beckmann, C. F. (2018). Connectopic mapping with resting-state fMRI. *Neuroimage*, *170*, 83-94.

Harrison, B. J., Davey, C. G., Savage, H. S., Jamieson, A. J., Leonards, C. A., Moffat, B. A., Glarin, R. K., & Steward, T. (2022). Dynamic subcortical modulators of human default mode network function. *Cerebral Cortex*, *32*(19), 4345-4355.

Hassabis, D., & Maguire, E. A. (2007). Deconstructing episodic memory with construction. *Trends in Cognitive Sciences*, *11*(7), 299-306.

Herlin, B., Navarro, V., & Dupont, S. (2021). The temporal pole: From anatomy to function—A literature appraisal. *J Chem Neuroanat*, *113*, 101925.

Hoerger, M., Quirk, S. W., & Weed, N. C. (2011). Development and validation of the Delaying Gratification Inventory. *Psychological assessment*, *23*(3), 725.

Hong, S.-J., de Wael, R. V., Bethlehem, R. A., Lariviere, S., Paquola, C., Valk, S. L., Milham, M. P., Di Martino, A., Margulies, D. S., & Smallwood, J. (2019). Atypical functional connectome hierarchy in autism. *Nature communications*, *10*(1), 1022.

Hsu, C.-C., Rolls, E. T., Huang, C.-C., Chong, S. T., Zac Lo, C.-Y., Feng, J., & Lin, C.-P. (2020). Connections of the human orbitofrontal cortex and inferior frontal gyrus. *Cerebral Cortex*, *30*(11), 5830-5843.

Humphreys, G. F., Hoffman, P., Visser, M., Binney, R. J., & Ralph, M. A. L. (2015). Establishing task-and modality-dependent dissociations between the semantic and default mode networks. *Proceedings of the National Academy of Sciences*, *112*(25), 7857-7862.

Huntenburg, J. M., Bazin, P.-L., Goulas, A., Tardif, C. L., Villringer, A., & Margulies, D. S. (2017). A systematic relationship between functional connectivity and intracortical myelin in the human cerebral cortex. *Cerebral Cortex*, *27*(2), 981-997.

Huntenburg, J. M., Bazin, P.-L., & Margulies, D. S. (2018). Large-scale gradients in human cortical organization. *Trends in Cognitive Sciences*, *22*(1), 21-31.

Jackson, R. L. (2021). The neural correlates of semantic control revisited. *Neuroimage*, *224*, 117444.

Jackson, R. L., Bajada, C. J., Rice, G. E., Cloutman, L. L., & Ralph, M. A. L. (2018). An emergent functional parcellation of the temporal cortex. *Neuroimage*, *170*, 385-399.

Jackson, R. L., Hoffman, P., Pobric, G., & Ralph, M. A. L. (2016). The semantic network at work and rest: differential connectivity of anterior temporal lobe subregions. *Journal of Neuroscience*, *36*(5), 1490-1501.

Johnson, M. W., Garcia-Romeu, A., Cosimano, M. P., & Griffiths, R. R. (2014). Pilot study of the 5-HT2AR agonist psilocybin in the treatment of tobacco addiction. *Journal of Psychopharmacology*, *28*(11), 983-992.

Johnson, M. W., Hendricks, P. S., Barrett, F. S., & Griffiths, R. R. (2019). Classic psychedelics: An integrative review of epidemiology, therapeutics, mystical experience, and brain network function. *Pharmacology & therapeutics*, *197*, 83-102.

Johnson, M. W., Richards, W. A., & Griffiths, R. R. (2008). Human hallucinogen research: guidelines for safety. *Journal of Psychopharmacology*.

Kaelen, M., Roseman, L., Kahan, J., Santos-Ribeiro, A., Orban, C., Lorenz, R., Barrett, F. S., Bolstridge, M., Williams, T., & Williams, L. (2016). LSD modulates music-induced imagery via changes in parahippocampal connectivity. *European neuropsychopharmacology*.

Kahnt, T., Chang, L. J., Park, S. Q., Heinzle, J., & Haynes, J.-D. (2012). Connectivity-based parcellation of the human orbitofrontal cortex. *Journal of Neuroscience*, *32*(18), 6240-6250.

Kernbach, J. M., Yeo, B. T., Smallwood, J., Margulies, D. S., De Schotten, M. T., Walter, H., Sabuncu, M. R., Holmes, A. J., Gramfort, A., & Varoquaux, G. (2018). Subspecialization within default mode nodes characterized in 10,000 UK Biobank participants. *Proceedings of the National Academy of Sciences*, *115*(48), 12295-12300.

Klaassens, B. L., Rombouts, S. A., Winkler, A. M., van Gorsel, H. C., van der Grond, J., & van Gerven, J. M. (2017). Time related effects on functional brain connectivity after serotonergic and cholinergic neuromodulation. *Human Brain Mapping*, *38*(1), 308-325.

Klaassens, B. L., van Gorsel, H. C., Khalili-Mahani, N., van der Grond, J., Wyman, B. T., Whitcher, B., Rombouts, S. A., & van Gerven, J. M. (2015). Single-dose serotonergic stimulation shows widespread effects on functional brain connectivity. *Neuroimage*, *122*, 440-450.

Koelsch, S., Andrews-Hanna, J. R., & Skouras, S. (2022). Tormenting thoughts: The posterior cingulate sulcus of the default mode network regulates valence of thoughts and activity in the brain's pain network during music listening. *Human Brain Mapping*, *43*(2), 773-786.

Kondo, H., Saleem, K. S., & Price, J. L. (2003). Differential connections of the temporal pole with the orbital and medial prefrontal networks in macaque monkeys. *Journal of Comparative Neurology*, *465*(4), 499-523.

Kondo, H., Saleem, K. S., & Price, J. L. (2005). Differential connections of the perirhinal and parahippocampal cortex with the orbital and medial prefrontal networks in macaque monkeys. *Journal of Comparative Neurology*, *493*(4), 479-509.

Kong, R., Li, J., Orban, C., Sabuncu, M. R., Liu, H., Schaefer, A., Sun, N., Zuo, X.-N., Holmes, A. J., & Eickhoff, S. B. (2019). Spatial topography of individual-specific cortical networks predicts human cognition, personality, and emotion. *Cerebral Cortex*, *29*(6), 2533-2551.

Kraehenmann, R., Pokorny, D., Vollenweider, L., Preller, K. H., Pokorny, T., Seifritz, E., & Vollenweider, F. X. (2017). Dreamlike effects of LSD on waking imagery in humans depend on serotonin 2A receptor activation. *Psychopharmacology*, *234*(13), 2031-2046.

Kringelbach, M. L., & Rolls, E. T. (2003). Neural correlates of rapid reversal learning in a simple model of human social interaction. *Neuroimage*, *20*(2), 1371-1383.

Kumfor, F., Landin-Romero, R., Devenney, E., Hutchings, R., Grasso, R., Hodges, J. R., & Piguet, O. (2016). On the right side? A longitudinal study of left-versus right-lateralized semantic dementia. *Brain*, *139*(3), 986-998.

Kundu, P., Brenowitz, N. D., Voon, V., Worbe, Y., Vértes, P. E., Inati, S. J., Saad, Z. S., Bandettini, P. A., & Bullmore, E. T. (2013). Integrated strategy for improving functional connectivity mapping using multiecho fMRI. *Proceedings of the National Academy of Sciences*, 201301725.

Kundu, P., Inati, S. J., Evans, J. W., Luh, W.-M., & Bandettini, P. A. (2012). Differentiating BOLD and non-BOLD signals in fMRI time series using multi-echo EPI. *Neuroimage*, *60*(3), 1759-1770.

Kundu, P., Voon, V., Balchandani, P., Lombardo, M. V., Poser, B. A., & Bandettini, P. A. (2017). Multi-echo fMRI: a review of applications in fMRI denoising and analysis of BOLD signals. *Neuroimage*, *154*, 59-80.

Kwan, A. C., Olson, D. E., Preller, K. H., & Roth, B. L. (2022). The neural basis of psychedelic action. *Nat Neurosci*, 1-13.

Lambe, E. K., & Aghajanian, G. K. (2006). Hallucinogen-induced UP states in the brain slice of rat prefrontal cortex: role of glutamate spillover and NR2B-NMDA receptors. *Neuropsychopharmacology*, *31*(8), 1682-1689.

Larivière, S., Vos de Wael, R., Hong, S.-J., Paquola, C., Tavakol, S., Lowe, A. J., Schrader, D. V., & Bernhardt, B. C. (2019). Multiscale Structure–Function Gradients in the Neonatal Connectome. *Cerebral Cortex*.

Laumann, T. O., Gordon, E. M., Adeyemo, B., Snyder, A. Z., Joo, S. J., Chen, M.-Y., Gilmore, A. W., McDermott, K. B., Nelson, S. M., & Dosenbach, N. U. (2015). Functional system and areal organization of a highly sampled individual human brain. *Neuron*, *87*(3), 657-670.

Lebedev, A. V., Kaelen, M., Lövdén, M., Nilsson, J., Feilding, A., Nutt, D., & Carhart-Harris, R. (2016). LSD-induced entropic brain activity predicts subsequent personality change. *Human Brain Mapping*.

Lebedev, A. V., Lövdén, M., Rosenthal, G., Feilding, A., Nutt, D. J., & Carhart-Harris, R. L. (2015). Finding the self by losing the self: Neural correlates of ego-dissolution under psilocybin. *Human Brain Mapping*, *36*(8), 3137-3153.

Levine, B., Svoboda, E., Hay, J. F., Winocur, G., & Moscovitch, M. (2002). Aging and autobiographical memory: dissociating episodic from semantic retrieval. *Psychol Aging*, *17*(4), 677.

Lewis, C. R., Preller, K. H., Kraehenmann, R., Michels, L., Staempfli, P., & Vollenweider, F. X. (2017). Two dose investigation of the 5-HT-agonist psilocybin on relative and global cerebral blood flow. *Neuroimage*, *159*, 70-78.

Li, J., Curley, W. H., Guerin, B., Dougherty, D. D., Dalca, A. V., Fischl, B., Horn, A., & Edlow, B. L. (2021). Mapping the subcortical connectivity of the human default mode network. *Neuroimage*, *245*, 118758. https://doi.org/10.1016/j.neuroimage.2021.118758

Lind, G. (2014). Moral competence test (MCT). In.

Lord, L.-D., Expert, P., Atasoy, S., Roseman, L., Rapuano, K., Lambiotte, R., Nutt, D. J., Deco, G., Carhart-Harris, R. L., & Kringelbach, M. L. (2019). Dynamical exploration of the repertoire of brain networks at rest is modulated by psilocybin. *Neuroimage*, *199*, 127-142.

Luppi, A. I., Carhart-Harris, R. L., Roseman, L., Pappas, I., Menon, D. K., & Stamatakis, E. A. (2021). LSD alters dynamic integration and segregation in the human brain. *Neuroimage*, *227*, 117653.

Lynch, C. J., Power, J. D., Scult, M. A., Dubin, M., Gunning, F. M., & Liston, C. (2020). Rapid precision functional mapping of individuals using multi-echo fMRI. *Cell reports*, *33*(12), 108540.

Marek, S., Tervo-Clemmens, B., Calabro, F. J., Montez, D. F., Kay, B. P., Hatoum, A. S., Donohue, M. R., Foran, W., Miller, R. L., & Hendrickson, T. J. (2022). Reproducible brain-wide association studies require thousands of individuals. *Nature*, *603*(7902), 654-660.

Margulies, D. S., Ghosh, S. S., Goulas, A., Falkiewicz, M., Huntenburg, J. M., Langs, G., Bezgin, G., Eickhoff, S. B., Castellanos, F. X., & Petrides, M. (2016). Situating the default-mode network along a principal gradient of macroscale cortical organization. *Proceedings of the National Academy of Sciences*, *113*(44), 12574-12579.

Margulies, D. S., & Smallwood, J. (2017). Converging evidence for the role of transmodal cortex in cognition. *Proceedings of the National Academy of Sciences*, *114*(48), 12641-12643.

Mason, N., Kuypers, K., Reckweg, J., Müller, F., Tse, D., Da Rios, B., Toennes, S., Stiers, P., Feilding, A., & Ramaekers, J. (2021). Spontaneous and deliberate creative cognition during and after psilocybin exposure. *Translational psychiatry*, *11*(1), 1-13.

McClure-Begley, T. D., & Roth, B. L. (2022). The promises and perils of psychedelic pharmacology for psychiatry. *Nature Reviews Drug Discovery*, 1-11.

McCulloch, D. E. W., Knudsen, G. M., Barrett, F. S., Doss, M. K., Carhart-Harris, R. L., Rosas, F. E., Deco, G., Kringelbach, M. L., Preller, K. H., Ramaekers, J. G., Mason, N. L., Müller, F., & Fisher, P. M. (2022). Psychedelic Resting-state Neuroimaging: A Review and Perspective on Balancing Replication and Novel Analyses. *Neuroscience & Biobehavioral Reviews*, 104689. https://doi.org/https://doi.org/10.1016/j.neubiorev.2022.104689

McIntosh, A. R., & Lobaugh, N. J. (2004). Partial least squares analysis of neuroimaging data: applications and advances. *Neuroimage*, *23*, S250-S263.

Mckeown, B., Strawson, W. H., Wang, H.-T., Karapanagiotidis, T., de Wael, R. V., Benkarim, O., Turnbull, A., Margulies, D., Jefferies, E., & McCall, C. (2020). The relationship between

individual variation in macroscale functional gradients and distinct aspects of ongoing thought. *Neuroimage*, *220*, 117072.

Mendes, N., Oligschlaeger, S., Lauckner, M. E., Golchert, J., Huntenburg, J. M., Falkiewicz, M., Ellamil, M., Krause, S., Baczkowski, B. M., & Cozatl, R. (2019). A functional connectome phenotyping dataset including cognitive state and personality measures. *Scientific data*, *6*, 180307.

Mesulam, M. (1998). From sensation to cognition. *Brain: A journal of neurology*, *121*(6), 1013-1052.

Meunier, D., Lambiotte, R., Fornito, A., Ersche, K. D., & Bullmore, E. T. (2010). Hierarchical modularity in human brain functional networks. *Hierarchy and dynamics in neural networks*, *1*, 2.

Millière, R. (2017). Looking for the Self: Phenomenology, Neurophysiology and Philosophical Significance of Drug-induced Ego Dissolution. *Frontiers in Human Neuroscience*, *11*, 245.

Moore, M., & Gordon, P. C. (2015). Reading ability and print exposure: Item response theory analysis of the author recognition test. *Behavior research methods*, *47*, 1095-1109.

Moran, M., Mufson, E., & Mesulam, M. M. (1987). Neural inputs into the temporopolar cortex of the rhesus monkey. *Journal of Comparative Neurology*, *256*(1), 88-103.

Müller, F., Dolder, P. C., Schmidt, A., Liechti, M. E., & Borgwardt, S. (2018). Altered network hub connectivity after acute LSD administration. *NeuroImage: Clinical*, *18*, 694-701.

Muñoz, M., & Insausti, R. (2005). Cortical efferents of the entorhinal cortex and the adjacent parahippocampal region in the monkey (Macaca fascicularis). *European Journal of Neuroscience*, *22*(6), 1368-1388.

Murphy, C., Jefferies, E., Rueschemeyer, S.-A., Sormaz, M., Wang, H.-t., Margulies, D., & Smallwood, J. (2017). Isolated from input: Transmodal cortex in the default mode network supports perceptually-decoupled and conceptually-guided cognition. *bioRxiv*, 150466.

Murphy, C., Jefferies, E., Rueschemeyer, S.-A., Sormaz, M., Wang, H.-t., Margulies, D. S., & Smallwood, J. (2018). Distant from input: Evidence of regions within the default mode network supporting perceptually-decoupled and conceptually-guided cognition. *Neuroimage*, *171*, 393-401.

Muthukumaraswamy, S. D., Carhart-Harris, R. L., Moran, R. J., Brookes, M. J., Williams, T. M., Errtizoe, D., Sessa, B., Papadopoulos, A., Bolstridge, M., & Singh, K. D. (2013). Broadband cortical desynchronization underlies the human psychedelic state. *The Journal of Neuroscience*, *33*(38), 15171-15183.

Mwilambwe-Tshilobo, L., Ge, T., Chong, M., Ferguson, M. A., Misic, B., Burrow, A. L., Leahy, R. M., & Spreng, R. N. (2019). Loneliness and meaning in life are reflected in the intrinsic network architecture of the brain. *Social cognitive and affective neuroscience*, *14*(4), 423-433.

Nathan, P. J., Phan, K. L., Harmer, C. J., Mehta, M. A., & Bullmore, E. T. (2014). Increasing pharmacological knowledge about human neurological and psychiatric disorders through functional neuroimaging and its application in drug discovery. *Current opinion in pharmacology*, *14*, 54-61.

Newman, M. E. (2004). Fast algorithm for detecting community structure in networks. *Physical review E*, *69*(6), 066133.

Nichols, D. E. (2016). Psychedelics. *Pharmacological Reviews*, *68*(2), 264-355.

Niendam, T. A., Laird, A. R., Ray, K. L., Dean, Y. M., Glahn, D. C., & Carter, C. S. (2012). Meta-analytic evidence for a superordinate cognitive control network subserving diverse executive functions. *Cognitive, Affective, & Behavioral Neuroscience*, *12*(2), 241-268.

Nour, M. M., & Carhart-Harris, R. L. (2017). Psychedelics and the science of self-experience. *The British Journal of Psychiatry*, *210*(3), 177-179.

Nour, M. M., Evans, L., Nutt, D., & Carhart-Harris, R. L. (2016). Ego-dissolution and psychedelics: Validation of the ego-dissolution inventory (EDI). *Frontiers in Human Neuroscience*, *10*, 269.

Nutt, D., & Carhart-Harris, R. (2021). The Current Status of Psychedelics in Psychiatry. *JAMA Psychiatry*, *78*(2), 121-122. https://doi.org/10.1001/jamapsychiatry.2020.2171

Nutt, D. J., King, L. A., & Nichols, D. E. (2013). Effects of Schedule I drug laws on neuroscience research and treatment innovation. *Nature Reviews Neuroscience*, *14*(8), 577-585.

Ojemann, J. G., Akbudak, E., Snyder, A. Z., McKinstry, R. C., Raichle, M. E., & Conturo, T. E. (1997). Anatomic localization and quantitative analysis of gradient refocused echo-planar fMRI susceptibility artifacts. *Neuroimage*, *6*(3), 156-167.

Olson, I. R., McCoy, D., Klobusicky, E., & Ross, L. A. (2013). Social cognition and the anterior temporal lobes: a review and theoretical framework. *Social cognitive and affective neuroscience*, *8*(2), 123-133.

Olson, I. R., Plotzker, A., & Ezzyat, Y. (2007). The enigmatic temporal pole: a review of findings on social and emotional processing. *Brain*, *130*(7), 1718-1731.

Palombo, D. J., Williams, L. J., Abdi, H., & Levine, B. (2013). The survey of autobiographical memory (SAM): A novel measure of trait mnemonics in everyday life. *Cortex*, *49*(6), 1526-1540.

Paquola, C., Bethlehem, R. A., Seidlitz, J., Wagstyl, K., Romero-Garcia, R., Whitaker, K. J., de Wael, R. V., Williams, G. B., Vértes, P. E., & Margulies, D. S. (2019). Shifts in myeloarchitecture characterise adolescent development of cortical gradients. *Elife*, *8*.

Paquola, C., De Wael, R. V., Wagstyl, K., Bethlehem, R. A., Hong, S.-J., Seidlitz, J., Bullmore, E. T., Evans, A. C., Misic, B., & Margulies, D. S. (2019). Microstructural and functional gradients are increasingly dissociated in transmodal cortices. *PLoS Biology*, *17*(5), e3000284.

Paquola, C., Seidlitz, J., Benkarim, O., Royer, J., Klimes, P., Bethlehem, R. A., Lariviere, S., de Wael, R. V., Hall, J. A., & Frauscher, B. (2020). The cortical wiring scheme of hierarchical information processing. *bioRxiv*.

Park, B.-y., de Wael, R. V., Paquola, C., Larivière, S., Benkarim, O., Royer, J., Tavakol, S., Cruces, R. R., Li, Q., & Valk, S. L. (2020). Signal diffusion along connectome gradients and inter-hub routing differentially contribute to dynamic human brain function. *Neuroimage*, *224*, 117429.

Pascual, B., Masdeu, J. C., Hollenbeck, M., Makris, N., Insausti, R., Ding, S.-L., & Dickerson, B. C. (2013). Large-scale brain networks of the human left temporal pole: a functional connectivity MRI study. *Cerebral Cortex*, *25*(3), 680-702.

Pascual, B., Masdeu, J. C., Hollenbeck, M., Makris, N., Insausti, R., Ding, S.-L., & Dickerson, B. C. (2015). Large-scale brain networks of the human left temporal pole: a functional connectivity MRI study. *Cerebral Cortex*, *25*(3), 680-702.

Pessoa, L. (2008). On the relationship between emotion and cognition. *Nature Reviews Neuroscience*, *9*(2), 148-158.

Pobric, G., Lambon Ralph, M. A., & Zahn, R. (2016). Hemispheric specialization within the superior anterior temporal cortex for social and nonsocial concepts. *Journal of Cognitive Neuroscience*, *28*(3), 351-360.

Pokorny, T., Duerler, P., Seifritz, E., Vollenweider, F. X., & Preller, K. H. (2020). LSD acutely impairs working memory, executive functions, and cognitive flexibility, but not risk-based decision-making. *Psychological medicine*, *50*(13), 2255-2264.

Poldrack, R. A. (2006). Can cognitive processes be inferred from neuroimaging data? [Research Support, N.I.H., Extramural

Research Support, U.S. Gov't, Non-P.H.S.]. *Trends Cogn Sci*, *10*(2), 59-63. https://doi.org/10.1016/j.tics.2005.12.004

Poldrack, R. A., Baker, C. I., Durnez, J., Gorgolewski, K. J., Matthews, P. M., Munafò, M. R., Nichols, T. E., Poline, J.-B., Vul, E., & Yarkoni, T. (2017). Scanning the horizon: towards transparent and reproducible neuroimaging research. *Nature Reviews Neuroscience*, *18*(2), 115-126.

Poldrack, R. A., & Farah, M. J. (2015). Progress and challenges in probing the human brain. *Nature*, *526*(7573), 371-379.

Posner, M. I., & DiGirolamo, G. J. (2000). Cognitive neuroscience: origins and promise. *Psychol Bull*, *126*(6), 873.

Power, J. D., Plitt, M., Gotts, S. J., Kundu, P., Voon, V., Bandettini, P. A., & Martin, A. (2018). Ridding fMRI data of motion-related influences: Removal of signals with distinct spatial and physical bases in multiecho data. *Proceedings of the National Academy of Sciences*, *115*(9), E2105-E2114.

Preller, K. H., Burt, J. B., Ji, J. L., Schleifer, C. H., Adkinson, B. D., Stämpfli, P., Seifritz, E., Repovs, G., Krystal, J. H., & Murray, J. D. (2018). Changes in global and thalamic brain connectivity in LSD-induced altered states of consciousness are attributable to the 5-HT2A receptor. *Elife*, *7*, e35082.

Preller, K. H., Duerler, P., Burt, J. B., Ji, J. L., Adkinson, B., Stämpfli, P., Seifritz, E., Repovs, G., Krystal, J. H., & Murray, J. D. (2020). Psilocybin induces time-dependent changes in global functional connectivity: Psi-induced changes in brain connectivity. *Biological psychiatry*.

Preller, K. H., Herdener, M., Pokorny, T., Planzer, A., Kraehenmann, R., Stämpfli, P., Liechti, M. E., Seifritz, E., & Vollenweider, F. X. (2017). The fabric of meaning and subjective effects in LSD-induced states depend on serotonin 2A receptor activation. *Current Biology*, *27*(3), 451-457.

Preller, K. H., & Vollenweider, F. X. (2016). Phenomenology, structure, and dynamic of psychedelic states. In *Behavioral Neurobiology of Psychedelic Drugs* (pp. 221-256). Springer.

Price, J. L. (2006). Connections of orbital cortex. *The orbitofrontal cortex*, 39-55.

Qin, P., & Northoff, G. (2011). How is our self related to midline regions and the default-mode network? *Neuroimage*, *57*(3), 1221-1233.

Raichle, M. E. (2009). A brief history of human brain mapping. *Trends Neurosci*, *32*(2), 118-126. https://doi.org/10.1016/j.tins.2008.11.001

Raichle, M. E., MacLeod, A. M., Snyder, A. Z., Powers, W. J., Gusnard, D. A., & Shulman, G. L. (2001). A default mode of brain function. *Proceedings of the National Academy of Sciences U.S.A.*, *98*(2), 678-682.

Raichle, M. E., & Snyder, A. Z. (2007). A default mode of brain function: A brief history of an evolving idea. *Neuroimage*, *37*(4), 1083-1090. https://doi.org/10.1016/j.neuroimage.2007.02.041

Ralph, M. A. L., Jefferies, E., Patterson, K., & Rogers, T. T. (2017). The neural and computational bases of semantic cognition. *Nature Reviews Neuroscience*, *18*(1), 42-55.

Ramaswamy, S., & Markram, H. (2015). Anatomy and physiology of the thick-tufted layer 5 pyramidal neuron. *Frontiers in cellular neuroscience*, *9*, 233.

Ranganath, C., & Ritchey, M. (2012). Two cortical systems for memory-guided behaviour. *Nature Reviews Neuroscience*, *13*(10), 713-726.

Rao, R. P., & Ballard, D. H. (1999). Predictive coding in the visual cortex: a functional interpretation of some extra-classical receptive-field effects. *Nat Neurosci*, *2*(1), 79.

Rice, G. E., Caswell, H., Moore, P., Hoffman, P., & Lambon Ralph, M. A. (2018). The roles of left versus right anterior temporal lobes in semantic memory: a neuropsychological comparison of postsurgical temporal lobe epilepsy patients. *Cerebral Cortex*, *28*(4), 1487-1501.

Rolls, E. T., Cheng, W., & Feng, J. (2020). The orbitofrontal cortex: reward, emotion and depression. *Brain Communications*, *2*(2). https://doi.org/10.1093/braincomms/fcaa196

Rolls, E. T., Deco, G., Huang, C.-C., & Feng, J. (2023). The human orbitofrontal cortex, vmPFC, and anterior cingulate cortex effective connectome: emotion, memory, and action. *Cerebral Cortex*, *33*(2), 330-356.

Roseman, L., Leech, R., Feilding, A., Nutt, D. J., & Carhart-Harris, R. L. (2014). The effects of psilocybin and MDMA on between-network resting state functional connectivity in healthy volunteers. *Frontiers in Human Neuroscience*, *8*.

Rubinov, M., & Sporns, O. (2010). Complex network measures of brain connectivity: uses and interpretations. *Neuroimage*, *52*(3), 1059-1069.

Rudebeck, P. H., & Rich, E. L. (2018). Orbitofrontal cortex. *Current Biology*, *28*(18), R1083-R1088.

Russell, D. W. (1996). UCLA Loneliness Scale (Version 3): Reliability, validity, and factor structure. *Journal of personality assessment*, *66*(1), 20-40.

Saleem, K. S., Kondo, H., & Price, J. L. (2008). Complementary circuits connecting the orbital and medial prefrontal networks with the temporal, insular, and opercular cortex in the macaque monkey. *Journal of Comparative Neurology*, *506*(4), 659-693.

Satpute, A. B., & Lindquist, K. A. (2019). The default mode network's role in discrete emotion. *Trends in Cognitive Sciences*, *23*(10), 851-864.

Schacter, D. L., Addis, D. R., Hassabis, D., Martin, V. C., Spreng, R. N., & Szpunar, K. K. (2012). The future of memory: remembering, imagining, and the brain. *Neuron*, *76*(4), 677-694.

Schaefer, A., Kong, R., Gordon, E. M., Laumann, T. O., Zuo, X.-N., Holmes, A. J., Eickhoff, S. B., & Yeo, B. (2017). Local-global parcellation of the human cerebral cortex from intrinsic functional connectivity mri. *Cerebral Cortex*, 1-20.

Schartner, M. M., Carhart-Harris, R. L., Barrett, A. B., Seth, A. K., & Muthukumaraswamy, S. D. (2017). Increased spontaneous MEG signal diversity for psychoactive doses of ketamine, LSD and psilocybin. *Scientific Reports*, *7*, 46421.

Schmid, Y., Enzler, F., Gasser, P., Grouzmann, E., Preller, K. H., Vollenweider, F. X., Brenneisen, R., Müller, F., Borgwardt, S., & Liechti, M. E. (2015). Acute effects of lysergic acid diethylamide in healthy subjects. *Biological psychiatry*, *78*(8), 544-553.

Schrantee, A., Ferguson, B., Stoffers, D., Booij, J., Rombouts, S., & Reneman, L. (2016). Effects of dexamphetamine-induced dopamine release on resting-state network connectivity in recreational amphetamine users and healthy controls. *Brain imaging and behavior*, *10*, 548-558.

Schultz, W., Tremblay, L., & Hollerman, J. R. (2000). Reward processing in primate orbitofrontal cortex and basal ganglia. *Cerebral Cortex*, *10*(3), 272-283.

Seeley, W. W., Menon, V., Schatzberg, A. F., Keller, J., Glover, G. H., Kenna, H., Reiss, A. L., & Greicius, M. D. (2007). Dissociable intrinsic connectivity networks for salience processing and executive control. *The Journal of Neuroscience*, *27*(9), 2349-2356.

Seidlitz, L., Abernethy, A. D., Duberstein, P. R., Evinger, J. S., Chang, T. H., & Lewis, B. b. L. (2002). Development of the spiritual transcendence index. *Journal for the scientific study of religion*, *41*(3), 439-453.

Sepulcre, J., Sabuncu, M. R., Yeo, T. B., Liu, H., & Johnson, K. A. (2012). Stepwise connectivity of the modal cortex reveals the multimodal organization of the human brain. *Journal of Neuroscience*, *32*(31), 10649-10661.

Setton, R., Mwilambwe-Tshilobo, L., Girn, M., Lockrow, A. W., Baracchini, G., Hughes, C., Lowe, A. J., Cassidy, B. N., Li, J., & Luh, W.-M. (2023). Age differences in the functional architecture of the human brain. *Cerebral Cortex*, *33*(1), 114-134.

Setton, R., Mwilambwe-Tshilobo, L., Girn, M., Lockrow, A. W., Baracchini, G., Hughes, C., Lowe, A. J., Cassidy, B. N., Li, J., Luh, W.-M., Bzdok, D., Leahy, R. M., Ge, T., Margulies, D. S., Misic, B., Bernhardt, B. C., Stevens, W. D., De Brigard, F., Kundu, P., Turner, G. R., & Spreng, R. N. (2022). Age differences in the functional architecture of the human brain. *Cerebral Cortex*. https://doi.org/10.1093/cercor/bhac056

Setton, R., Mwilambwe-Tshilobo, L., Girn, M., Lockrow, A. W., Baracchini, G., Lowe, A. J., Cassidy, B. N., Li, J., Luh, W.-M., Bzdok, D., Leahy, R. M., Ge, T., Margulies, D. S., Misic, B., Bernhardt, B. C., Dale Stevens, W., Brigard, F. D., Kundu, P., Turner, G. R., & Nathan Spreng, R. (2021). Functional architecture of the aging brain. *bioRxiv*, 2021.2003.2031.437922. https://doi.org/10.1101/2021.03.31.437922

Shipley, W. C., Gruber, C. P., Martin, T. A., & Klein, A. M. (2009). Shipley-2. *Los Angeles, CA: Western Psychological Services*.

Shulman, G. L., Fiez, J. A., Corbetta, M., Buckner, R. L., Miezin, F. M., Raichle, M. E., & Petersen, S. E. (1997). Common blood flow changes across visual tasks: II. Decreases in cerebral cortex. *Journal of Cognitive Neuroscience*, *9*(5), 648-663.

Simmons, W. K., Reddish, M., Bellgowan, P. S., & Martin, A. (2010). The selectivity and functional connectivity of the anterior temporal lobes. *Cerebral Cortex*, *20*(4), 813-825.

Skipper, L. M., Ross, L. A., & Olson, I. R. (2011). Sensory and semantic category subdivisions within the anterior temporal lobes. *Neuropsychologia*, *49*(12), 3419-3429.

Smallwood, J., Bernhardt, B. C., Leech, R., Bzdok, D., Jefferies, E., & Margulies, D. S. (2021). The default mode network in cognition: a topographical perspective. *Nature Reviews Neuroscience*, 1-11.

Smallwood, J., Turnbull, A., Wang, H.-t., Ho, N. S., Poerio, G. L., Karapanagiotidis, T., Konu, D., Mckeown, B., Zhang, M., & Murphy, C. (2021). The neural correlates of ongoing conscious thought. *Iscience*, 102132.

Smith, S. M., Fox, P. T., Miller, K. L., Glahn, D. C., Fox, P. M., Mackay, C. E., Filippini, N., Watkins, K. E., Toro, R., & Laird, A. R. (2009). Correspondence of the brain's functional architecture during activation and rest. *Proceedings of the National Academy of Sciences*, *106*(31), 13040-13045.

Smith, S. M., Nichols, T. E., Vidaurre, D., Winkler, A. M., Behrens, T. E., Glasser, M. F., Ugurbil, K., Barch, D. M., Van Essen, D. C., & Miller, K. L. (2015). A positive-negative mode of population covariation links brain connectivity, demographics and behavior. *Nat Neurosci*, *18*(11), 1565.

Smith, V., Mitchell, D. J., & Duncan, J. (2018). Role of the default mode network in cognitive transitions. *Cerebral Cortex*, *28*(10), 3685-3696.

Snoek, L., van der Miesen, M. M., Beemsterboer, T., van der Leij, A., Eigenhuis, A., & Steven Scholte, H. (2021). The Amsterdam Open MRI Collection, a set of multimodal MRI datasets for individual difference analyses. *Scientific data*, *8*(1), 1-23.

Snowden, J. S., Harris, J. M., Thompson, J. C., Kobylecki, C., Jones, M., Richardson, A. M., & Neary, D. (2018). Semantic dementia and the left and right temporal lobes. *Cortex*, *107*, 188-203.

Sormaz, M., Murphy, C., Wang, H.-t., Hymers, M., Karapanagiotidis, T., Poerio, G., Margulies, D. S., Jefferies, E., & Smallwood, J. (2018). Default mode network can support the level of detail in experience during active task states. *Proceedings of the National Academy of Sciences*, *115*(37), 9318-9323.

Spiers, H., & Maguire, E. (2006). Spontaneous mentalizing during an interactive real world task: An fMRI study. *Neuropsychologia*, *44*(10), 1674-1682. https://doi.org/http://dx.doi.org/10.1016/j.neuropsychologia.2006.03.028

Sporns, O., & Betzel, R. F. (2016). Modular brain networks. *Annu Rev Psychol*, *67*, 613-640.

Spreng, R. N., & Andrews-Hanna, J. (2015). The Default Network and Social Cognition. In A. W. Toga (Ed.), *Brain Mapping: An Encyclopedic Reference* (pp. 165-169). Academic Press.

Spreng, R. N., DuPre, E., Selarka, D., Garcia, J., Gojkovic, S., Mildner, J., Luh, W.-M., & Turner, G. R. (2014). Goal-Congruent Default Network Activity Facilitates Cognitive Control. *The Journal of Neuroscience*, *34*(42), 14108-14114.

Spreng, R. N., Fernández-Cabello, S., Turner, G. R., & Stevens, W. D. (2019). Take a deep breath: Multiecho fMRI denoising effectively removes head motion artifacts, obviating the need for global signal regression. *Proceedings of the National Academy of Sciences*, 201909848.

Spreng, R. N., Lockrow, A. W., DuPre, E., Setton, R., Spreng, K. A., & Turner, G. R. (2017). Semanticized autobiographical memory and the default–executive coupling hypothesis of aging. *Neuropsychologia*.

Spreng, R. N., Mar, R. A., & Kim, A. S. (2009). The common neural basis of autobiographical memory, prospection, navigation, theory of mind, and the default mode: a quantitative meta-analysis. *Journal of Cognitive Neuroscience*, *21*(3), 489-510.

Spreng, R. N., Stevens, W. D., Chamberlain, J. P., Gilmore, A. W., & Schacter, D. L. (2010). Default network activity, coupled with the frontoparietal control network, supports goal-directed cognition [Research Support, N.I.H., Extramural]. *Neuroimage*, *53*(1), 303-317. https://doi.org/10.1016/j.neuroimage.2010.06.016

Spreng*, R. N., McKinnon*, M. C., Mar, R. A., & Levine, B. (2009). The Toronto Empathy Questionnaire: Scale development and initial validation of a factor-analytic solution to multiple empathy measures. *Journal of personality assessment*, *91*(1), 62-71.

Stamatakis, E. A., Adapa, R. M., Absalom, A. R., & Menon, D. K. (2010). Changes in resting neural connectivity during propofol sedation. *PLoS One*, *5*(12), e14224.

Stawarczyk, D., Bezdek, M. A., & Zacks, J. M. (2019). Event Representations and Predictive Processing: The Role of the Midline Default Network Core. *Topics in cognitive science*.

Studerus, E., Gamma, A., & Vollenweider, F. X. (2010). Psychometric evaluation of the altered states of consciousness rating scale (OAV). *PLoS One*, *5*(8), e12412.

Studerus, E., Kometer, M., Hasler, F., & Vollenweider, F. X. (2011). Acute, subacute and long-term subjective effects of psilocybin in healthy humans: a pooled analysis of experimental studies. *Journal of Psychopharmacology*, *25*(11), 1434-1452.

Sudlow, C., Gallacher, J., Allen, N., Beral, V., Burton, P., Danesh, J., Downey, P., Elliott, P., Green, J., & Landray, M. (2015). UK biobank: an open access resource for identifying the causes of a wide range of complex diseases of middle and old age. *PLoS medicine*, *12*(3), e1001779.

Sydnor, V. J., Larsen, B., Bassett, D. S., Alexander-Bloch, A., Fair, D. A., Liston, C., Mackey, A. P., Milham, M. P., Pines, A., & Roalf, D. R. (2021). Neurodevelopment of the association cortices: Patterns, mechanisms, and implications for psychopathology. *Neuron*, *109*(18), 2820-2846.

Tafarodi, R. W., & Swann Jr, W. B. (2001). Two-dimensional self-esteem: Theory and measurement. *Personality and Individual Differences*, *31*(5), 653-673.

Tagliazucchi, E., Carhart-Harris, R., Leech, R., Nutt, D., & Chialvo, D. R. (2014). Enhanced repertoire of brain dynamical states during the psychedelic experience. *Human Brain Mapping*, *35*(11), 5442-5456.

Tagliazucchi, E., Roseman, L., Kaelen, M., Orban, C., Muthukumaraswamy, S. D., Murphy, K., Laufs, H., Leech, R., McGonigle, J., & Crossley, N. (2016). Increased global functional connectivity correlates with LSD-Induced ego dissolution. *Current Biology*, *26*(8), 1043-1050.

Taruffi, L., Pehrs, C., Skouras, S., & Koelsch, S. (2017). Effects of sad and happy music on mind-wandering and the default mode network. *Scientific Reports*, *7*(1), 14396.

Thirion, B., Varoquaux, G., Dohmatob, E., & Poline, J.-B. (2014). Which fMRI clustering gives good brain parcellations? *Frontiers in neuroscience*, *8*, 167.

Tian, Y., Margulies, D. S., Breakspear, M., & Zalesky, A. (2020). Topographic organization of the human subcortex unveiled with functional connectivity gradients. *Nat Neurosci*, *23*(11), 1421-1432.

Timmermann, C., Roseman, L., Haridas, S., Rosas, F. E., Luan, L., Kettner, H., Martell, J., Erritzoe, D., Tagliazucchi, E., & Pallavicini, C. (2023). Human brain effects of DMT assessed via EEG-fMRI. *Proceedings of the National Academy of Sciences*, *120*(13), e2218949120.

Timmermann, C., Roseman, L., Schartner, M., Milliere, R., Williams, L. T., Erritzoe, D., Muthukumaraswamy, S., Ashton, M., Bendrioua, A., & Kaur, O. (2019). Neural correlates of the DMT experience assessed with multivariate EEG. *Scientific Reports*, *9*(1), 1-13.

Tusche, A., Smallwood, J., Bernhardt, B. C., & Singer, T. (2014). Classifying the wandering mind: Revealing the affective content of thoughts during task-free rest periods. *Neuroimage*, *97*, 107-116.

Uddin, L. Q., Yeo, B., & Spreng, R. N. (2019). Towards a universal taxonomy of macro-scale functional human brain networks. *Brain topography*, *32*(6), 926-942.

van de Ven, V., Wingen, M., Kuypers, K. P., Ramaekers, J. G., & Formisano, E. (2013). Escitalopram decreases cross-regional functional connectivity within the default-mode network. *PLoS One*, *8*(6), e68355.

Van Den Heuvel, M. P., & Sporns, O. (2011). Rich-club organization of the human connectome. *The Journal of Neuroscience*, *31*(44), 15775-15786.

Van Dijk, K. R., Hedden, T., Venkataraman, A., Evans, K. C., Lazar, S. W., & Buckner, R. L. (2010). Intrinsic functional connectivity as a tool for human connectomics: theory, properties, and optimization. *J Neurophysiol*, *103*(1), 297.

Van Essen, D. C., Smith, S. M., Barch, D. M., Behrens, T. E., Yacoub, E., Ugurbil, K., & Consortium, W.-M. H. (2013). The WU-Minn human connectome project: an overview. *Neuroimage*, *80*, 62-79.

van Rentergem, J. A. A., Deserno, M. K., & Geurts, H. M. (2021). Validation strategies for subtypes in psychiatry: A systematic review of research on autism spectrum disorder. *Clin Psychol Rev*, *87*, 102033.

Varley, T., Carhart-Harris, R., Roseman, L., Menon, D., & Stamatakis, E. (2019). Serotonergic Psychedelics LSD & Psilocybin Increase the Fractal Dimension of Cortical Brain Activity in Spatial and Temporal Domains. *bioRxiv*, 517847.

Varley, T. F., Carhart-Harris, R., Roseman, L., Menon, D. K., & Stamatakis, E. A. (2020). Serotonergic psychedelics LSD & psilocybin increase the fractal dimension of cortical brain activity in spatial and temporal domains. *Neuroimage*, *220*, 117049.

Vatansever, D., Manktelow, A., Sahakian, B. J., Menon, D. K., & Stamatakis, E. A. (2017). Angular default mode network connectivity across working memory load. *Human Brain Mapping*, *38*(1), 41-52.

Vatansever, D., Menon, D. K., & Stamatakis, E. A. (2017). Default mode contributions to automated information processing. *Proceedings of the National Academy of Sciences*, *114*(48), 12821-12826.

Vazquez-Rodriguez, B., Liu, Z.-Q., Hagmann, P., & Misic, B. (2020). Signal propagation via cortical hierarchies. *bioRxiv*.

Vidaurre, D., Smith, S. M., & Woolrich, M. W. (2017). Brain network dynamics are hierarchically organized in time. *Proceedings of the National Academy of Sciences*, *114*(48), 12827-12832.

Vincent, J. L., Snyder, A. Z., Fox, M. D., Shannon, B. J., Andrews, J. R., Raichle, M. E., & Buckner, R. L. (2006). Coherent spontaneous activity identifies a hippocampal-parietal memory network [Research Support, N.I.H., Extramural
Research Support, Non-U.S. Gov't
Research Support, U.S. Gov't, Non-P.H.S.]. *J Neurophysiol*, *96*(6), 3517-3531. https://doi.org/10.1152/jn.00048.2006

Vollenweider, F. X., & Preller, K. H. (2020). Psychedelic drugs: neurobiology and potential for treatment of psychiatric disorders. *Nature Reviews Neuroscience*, 1-14.

Von Neumann, J., Kent, R., Bellinson, H., & Hart, B. t. (1941). The mean square successive difference. *The Annals of Mathematical Statistics*, *12*(2), 153-162.

Wall, M. B., Pope, R., Freeman, T. P., Kowalczyk, O. S., Demetriou, L., Mokrysz, C., Hindocha, C., Lawn, W., Bloomfield, M. A., & Freeman, A. M. (2019). Dissociable effects of cannabis with and without cannabidiol on the human brain's resting-state functional connectivity. *Journal of Psychopharmacology*, *33*(7), 822-830.

Wandschneider, B., & Koepp, M. J. (2016). Pharmaco fMRI: determining the functional anatomy of the effects of medication. *NeuroImage: Clinical*, *12*, 691-697.

Wang, J., & Maurer, L. (2005). Positron emission tomography: applications in drug discovery and drug development. *Current topics in medicinal chemistry*, *5*(11), 1053-1075.

Webster, J. D. (2003). An exploratory analysis of a self-assessed wisdom scale. *Journal of Adult Development*, *10*(1), 13-22.

Wold, S., Martens, H., & Wold, H. (1983). The multivariate calibration problem in chemistry solved by the PLS method. In *Matrix pencils* (pp. 286-293). Springer.

Worsley, K. J., Taylor, J., Carbonell, F., Chung, M., Duerden, E., Bernhardt, B., Lyttelton, O., Boucher, M., & Evans, A. (2009). A Matlab toolbox for the statistical analysis of univariate and multivariate surface and volumetric data using linear mixed effects models and random field theory. NeuroImage Organisation for Human Brain Mapping 2009 Annual Meeting,

Xia, M., Wang, J., & He, Y. (2013). BrainNet Viewer: a network visualization tool for human brain connectomics. *PLoS One*, *8*(7), e68910.

Xie, C., Jia, T., Rolls, E. T., Robbins, T. W., Sahakian, B. J., Zhang, J., Liu, Z., Cheng, W., Luo, Q., & Lo, C.-Y. Z. (2021). Reward versus nonreward sensitivity of the medial versus lateral orbitofrontal cortex relates to the severity of depressive symptoms. *Biological Psychiatry: Cognitive Neuroscience and Neuroimaging*, *6*(3), 259-269.

Yarkoni, T., Poldrack, R. A., Van Essen, D. C., & Wager, T. D. (2010). Cognitive neuroscience 2.0: building a cumulative science of human brain function. *Trends Cogn Sci*, *14*(11), 489-496. https://doi.org/10.1016/j.tics.2010.08.004

Yeo, B. T. T., Kirienen, F. M., Sepulcre, J., Sabuncu, M. R., Lashkari, D., Hollinshead, M., Roffman, J. L., Smoller, J. W., Zöllei, L., Polimeni, J. R., Fischl, B., Liu, H., & Buckner, R. L. (2011). The organization of the human cerebral cortex estimated by intrinsic functional connectivity. *J Neurophysiol*, *106*, 1125-1165. https://doi.org/10.1152/jn.00338.2011.-

Zahn, R., Moll, J., Krueger, F., Huey, E. D., Garrido, G., & Grafman, J. (2007). Social concepts are represented in the superior anterior temporal cortex. *Proceedings of the National Academy of Sciences*, *104*(15), 6430-6435.

Zald, D. H., McHugo, M., Ray, K. L., Glahn, D. C., Eickhoff, S. B., & Laird, A. R. (2012). Meta-analytic connectivity modeling reveals differential functional connectivity of the medial and lateral orbitofrontal cortex. *Cerebral Cortex*, *24*(1), 232-248.

Zhang, X., Huettel, S. A., O'Dhaniel, A., Guo, H., & Wang, L. (2019). Exploring common changes after acute mental stress and acute tryptophan depletion: Resting-state fMRI studies. *Journal of Psychiatric Research*, *113*, 172-180.

Zou, Q.-H., Zhu, C.-Z., Yang, Y., Zuo, X.-N., Long, X.-Y., Cao, Q.-J., Wang, Y.-F., & Zang, Y.-F. (2008). An improved approach to detection of amplitude of low-frequency fluctuation (ALFF) for resting-state fMRI: fractional ALFF. *Journal of neuroscience methods*, *172*(1), 137-141.

Appendix A: Supplementary Material to "Evaluating the inclusion of limbic regions within the default network"

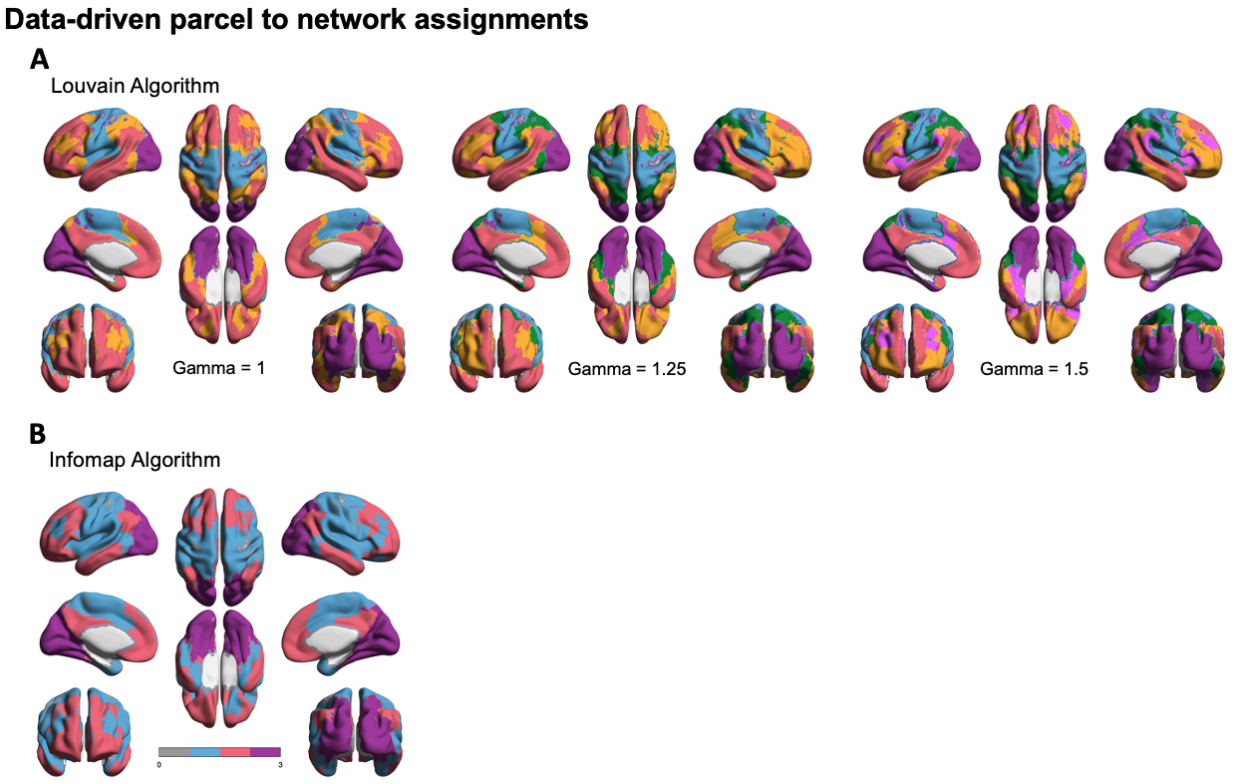

Supplementary Figure 1. Modularity results for Run 2. **(A)** Data-driven network assignments based on the Louvain modularity algorithm, at three values of the gamma resolution parameter. **(B)** Data-driven network assignments based on the Infomap modularity algorithm. Networks are colored according to their putative corresponding large-scale network according to the Yeo 7 network parcellation scheme (Yeo et al., 2011).

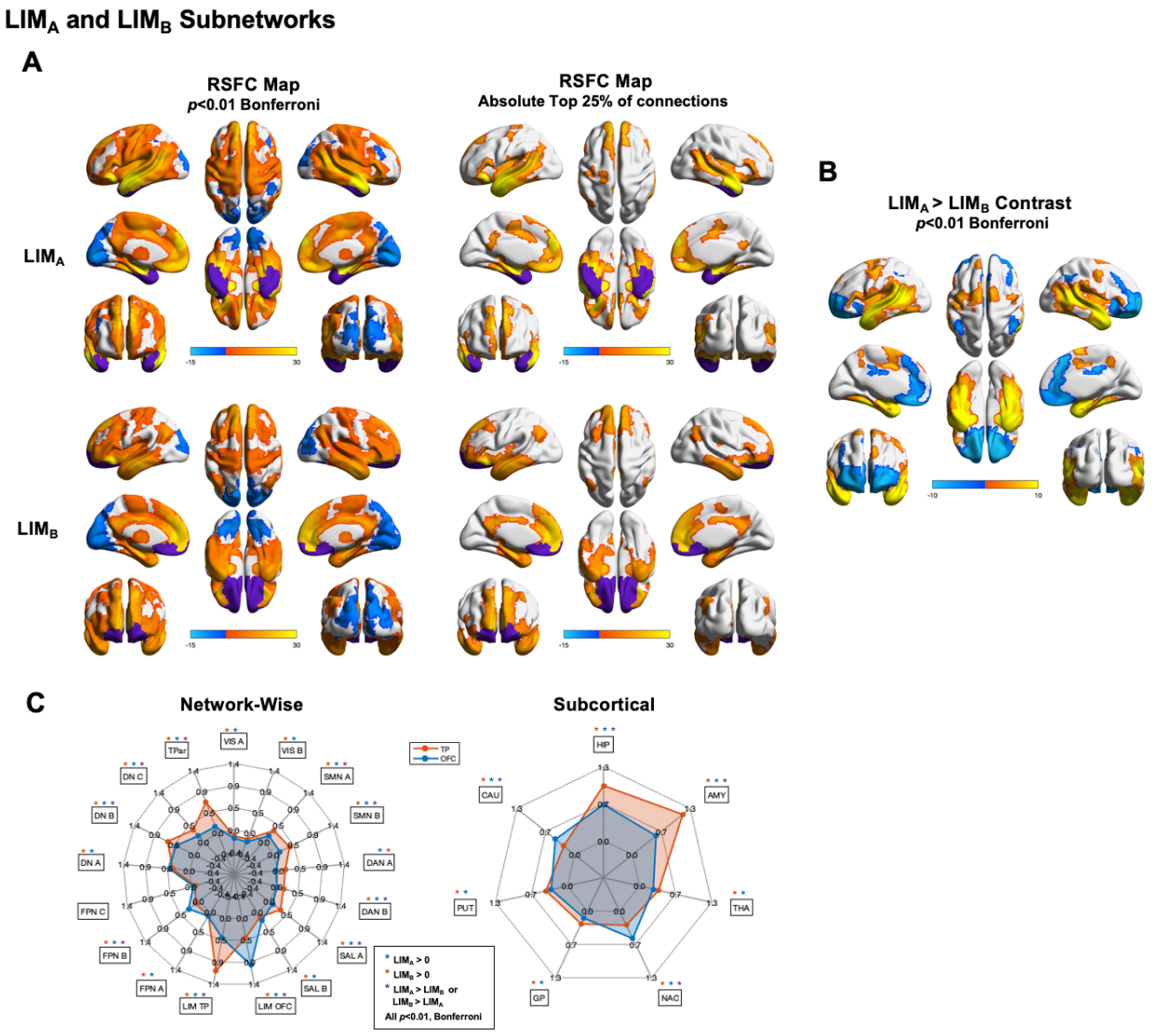

Supplementary Figure 2. RSFC maps for LIM_A and LIM_B, as defined by the Yeo et al. 2011 17 network parcellation **(A) Left:** RSFC maps thresholded at p<0.01 Bonferroni for Cluster 1 (C1; Top) and Cluster 2 (C2; Bottom). **Right:** RSFC maps thresholded at top absolute 25% of connections for Cluster 1 (C1; Top) and Cluster 2 (C2; Bottom **(B)** Cluster dendrogram. **(C)** Between-cluster C1>C2 contrast. **(D)** Spider plots displaying network-wise (Left) and subcortical (Right) between-cluster contrasts. Networks are defined based on the Yeo et al. 2011 17 network parcellation.

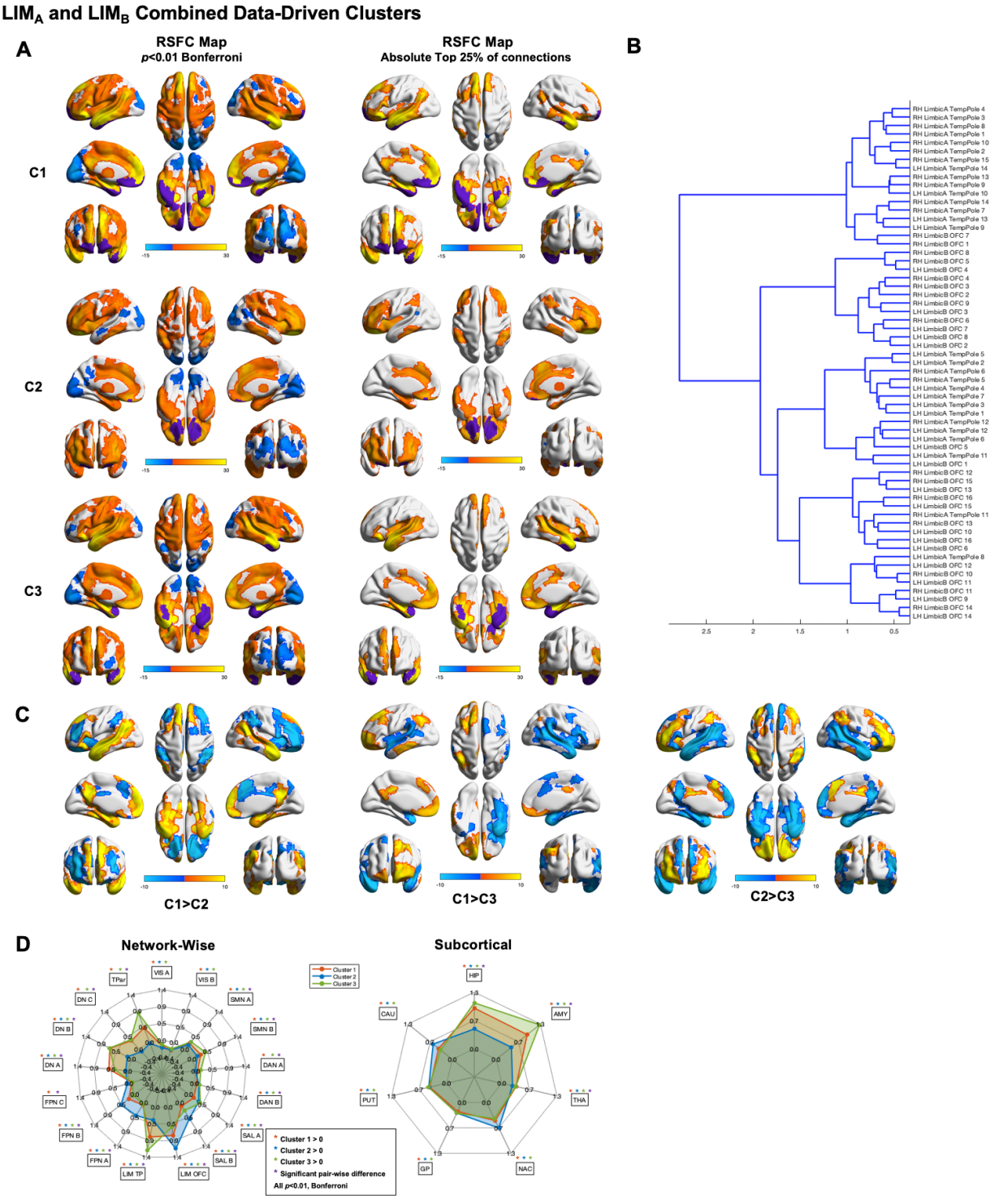

Supplementary Figure 3. Run 2 data-driven clusters revealed by applying Ward clustering to all LIM parcels, spanning both LIM$_A$ and LIM$_B$ **(A) Left:** RSFC maps thresholded at p<0.01 Bonferroni for Cluster 1 (C1; Top), Cluster 2 (C2; Middle), and Cluster 3 (C3; Bottom). **Right:** RSFC maps thresholded at top absolute 25% of connections for Cluster 1 (C1; Top), Cluster 2 (C2; Middle), and Cluster 3 (C3; Bottom). **(B)** Cluster dendrogram. **(C)** Between-cluster contrasts. **(D)** Spider plots displaying network-wise (Left) and subcortical (Right) between-cluster contrasts. Networks are defined based on the Yeo et al. 2011 17 network parcellation.

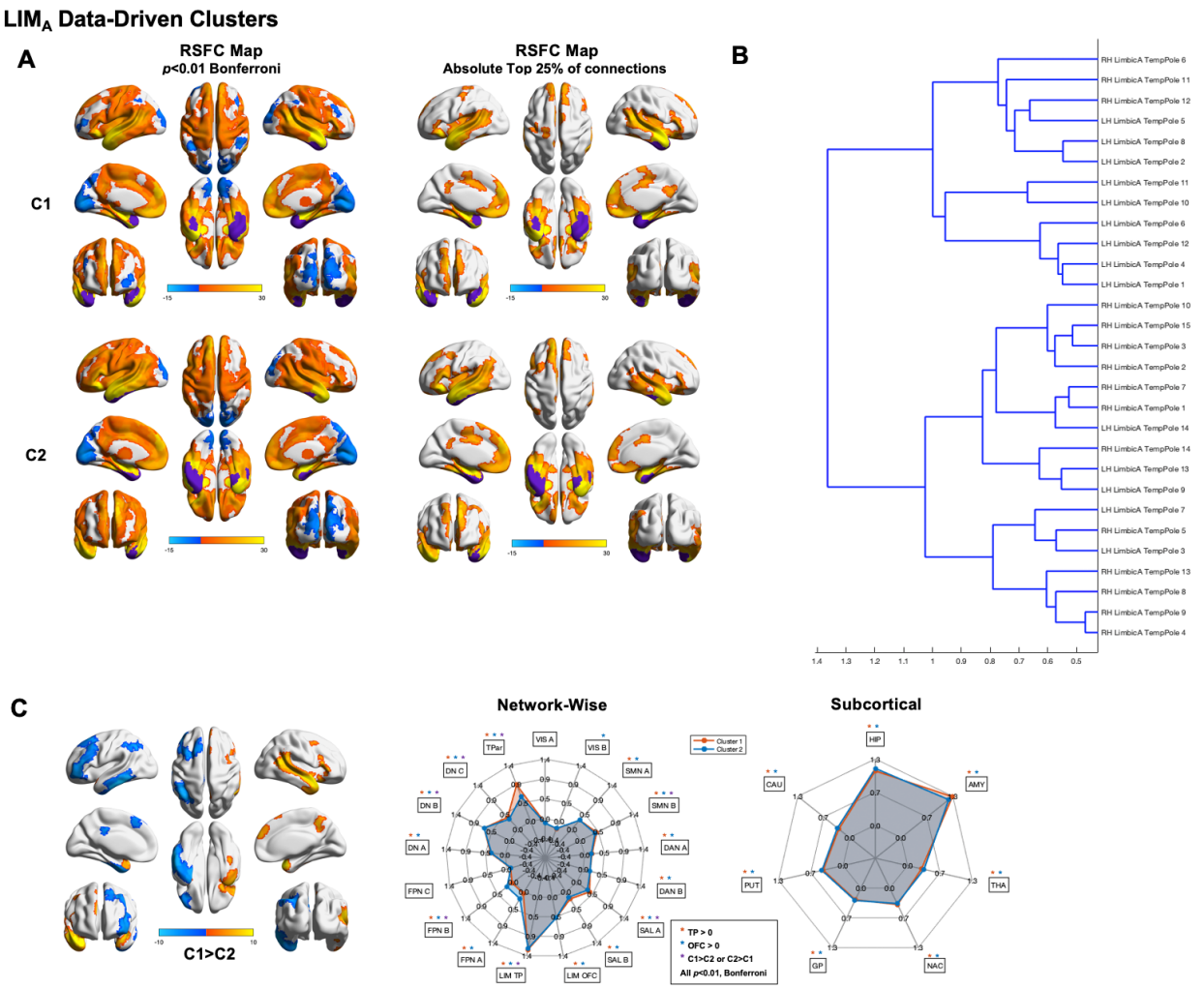

Figure 4. Run 2 data-driven clusters revealed by applying Ward clustering to LIM_A parcels only **(A) Left:** RSFC maps thresholded at p<0.01 Bonferroni for Cluster 1 (C1; Top) and Cluster 2 (C2; Bottom). **Right:** RSFC maps thresholded at top absolute 25% of connections for Cluster 1 (C1; Top) and Cluster 2 (C2; Bottom **(B)** Cluster dendrogram. **(C)** Between-cluster C1>C2 contrast. **(D)** Spider plots displaying network-wise (Left) and subcortical (Right) between-cluster contrasts. Networks are defined based on the Yeo et al. 2011 17 network parcellation.

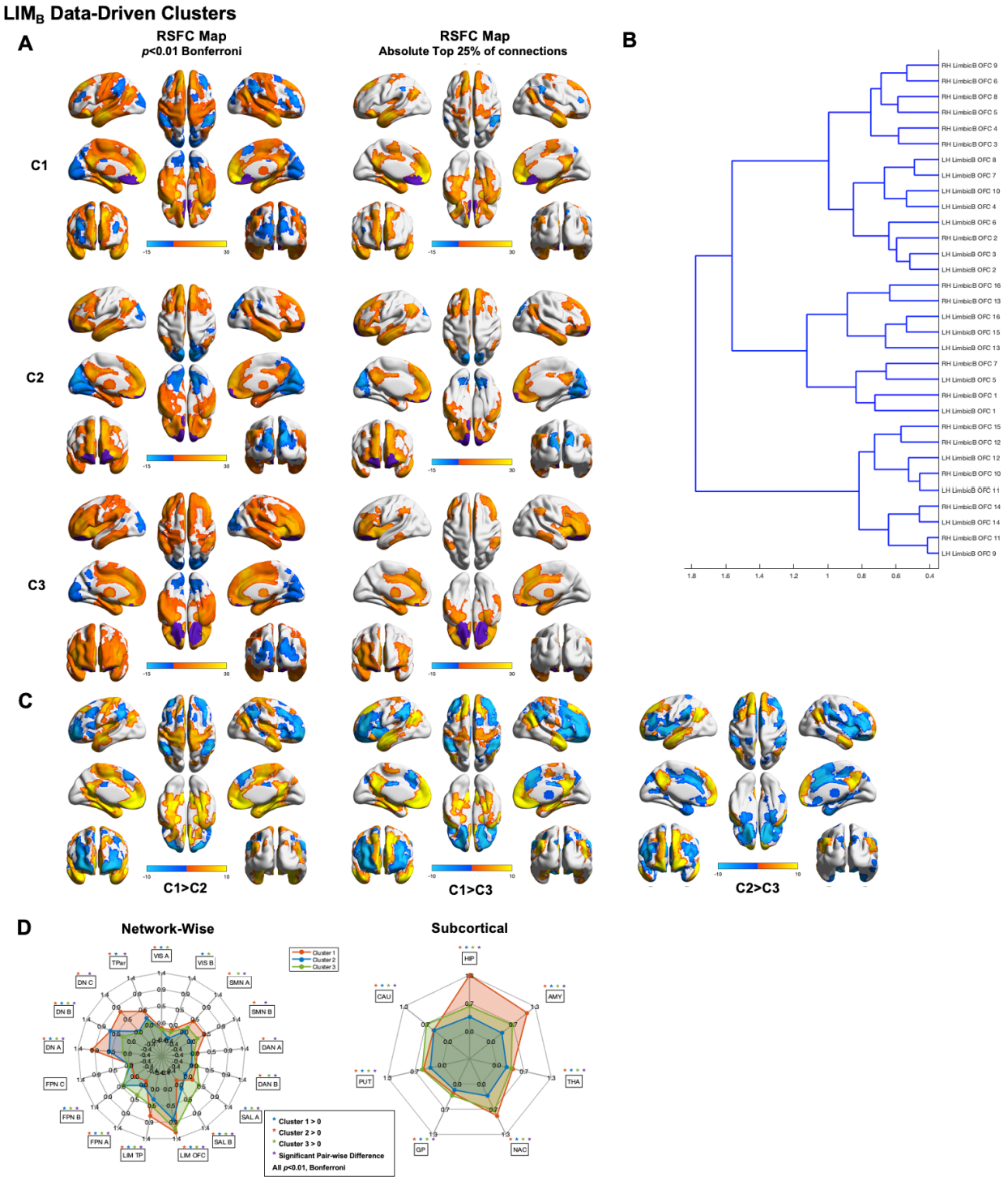

Supplementary Figure 5. Run 2 data-driven clusters revealed by applying Ward clustering to LIM$_B$ parcels **(A) Left:** RSFC maps thresholded at p<0.01 Bonferroni for Cluster 1 (C1; Top), Cluster 2 (C2; Middle), and Cluster 3 (C3; Bottom). **Right:** RSFC maps thresholded at top absolute 25% of connections for Cluster 1 (C1; Top), Cluster 2 (C2; Middle), and Cluster 3 (C3; Bottom). **(B)** Clustering dendrogram. **(C)** Between-cluster contrasts. **(D)** Spider plots displaying network-wise (Left) and subcortical (Right) between-cluster contrasts. Networks are defined based on the Yeo et al. 2011 17 network parcellation.

Appendix B: Supplementary Material to "A multivariate examination of default network subsystem-specific brain-behaviour covariance"

Supplementary Table 1. Variable loadings for all 20 behaviour principal components included in the present analyses.

Behaviour PC Loadings (1-10)	PC 1	PC 2	PC 3	PC 4	PC 5	PC 6	PC 7	PC 8	PC 9	PC 10
Agreeableness-Compassion	-0.05	0.27	0.12	0.01	-0.01	-0.02	-0.02	-0.12	-0.08	0.01
Agreeableness-Politeness	0.01	0.1	0.18	0.24	-0.08	0.15	-0.17	-0.12	-0.05	0.03
AI-External Density	0.01	0.02	-0.08	-0.09	0.09	0.07	0.11	-0.19	-0.16	0.19
AI-Internal Density	-0.02	0.04	-0.07	-0.03	0.13	0.01	0.05	-0.21	-0.19	0.25
ART Fiction	0.05	0.21	-0.11	0.07	-0.06	0.18	-0.06	0.13	-0.09	-0.08
ART Nonfiction	0.02	0.19	-0.17	0	-0.02	0.13	0	0.07	-0.18	0
Beck Depression Inventory	0.16	0.06	0.04	-0.01	0.1	0	0.15	0.05	-0.07	-0.17
BISBAS BAS-Drive	-0.1	0.06	0.06	-0.24	0.15	-0.05	-0.01	-0.11	0.12	-0.18
BISBAS BAS-Fun	-0.02	0.07	0.03	-0.15	0.11	-0.12	-0.06	-0.02	0.18	-0.02
BISBAS BAS-Reward	-0.09	0.12	0.11	-0.04	0.13	-0.1	-0.05	-0.04	0.06	-0.15
BISBAS BIS	0.08	0.1	0.15	0.17	0.12	-0.01	-0.12	0.03	-0.04	-0.05
Conscientiousness-Industriousness	-0.19	-0.04	0.03	0.03	-0.06	0.05	0.07	-0.17	0.08	0.02
Conscientiousness-Orderliness	-0.07	-0.03	0.1	0.12	0.09	0.04	-0.07	-0.1	0.12	0.07
Delayed Gratification	-0.1	0.1	0.07	0.06	0.02	0.19	0.04	-0.09	0.06	0.05
ECR-R Anxiety	0.16	0.04	0.06	-0.05	0.06	0.18	-0.13	-0.17	0.02	0.06
ECR-R Avoidance	0.13	-0.05	0.01	-0.07	0.02	0.19	-0.03	-0.05	0.06	0.05
Education	-0.01	0.01	-0.02	0.12	-0.14	0.03	0.17	0.18	-0.2	0.15
Extraversion-Assertiveness	-0.16	0.08	-0.06	-0.19	0.11	-0.05	0.16	0.01	0.06	-0.12
Extraversion-Enthusiasm	-0.16	0.13	0.08	-0.05	0.12	-0.11	-0.09	0.01	-0.05	-0.15
IRI-Empathic Concern	-0.04	0.17	0.15	0.08	0.02	0.02	0.04	0.08	0.05	-0.11
IRI-Fantasy	-0.03	0.17	0.08	0.1	0.15	-0.13	-0.01	-0.02	0.04	-0.02
IRI-Personal Distress	0.08	0.04	0.13	0.08	0.06	-0.11	-0.2	0	0.1	-0.03
IRI-Perspective Taking	-0.07	0.14	0.1	0.02	0.03	0.25	0.02	-0.01	0.09	0.09
ISEL-Appraisal	-0.15	0.04	-0.05	-0.05	0.05	-0.06	-0.06	0.15	0.1	-0.03
ISEL-Belonging	-0.16	0.01	-0.03	-0.04	0.19	0.03	-0.13	0.06	0.19	-0.11
ISEL-Self Esteem	-0.18	-0.02	-0.06	0	0.06	0.01	-0.07	0.07	0.08	0.06
ISEL-Tangible	-0.09	0.08	-0.12	0	0.15	0.08	-0.05	0.1	0.09	0.03

MFQ-Authority/Respect	-0.06	-0.16	0.19	-0.04	0.12	0.16	0.04	-0.05	-0.07	0.01
MFQ-Fairness/Repricrocity	0.03	0.22	0.07	0.04	0.01	0.12	0.02	-0.05	-0.04	-0.05
MFQ-Harm/Care	-0.03	0.17	0.15	-0.07	0.08	0.14	-0.04	-0.05	-0.1	-0.07
MFQ-In Group Loyalty	-0.06	-0.2	0.18	-0.09	0.1	0.15	0.06	-0.02	-0.08	0.03
MFQ-Purity/Sanctity	-0.06	-0.16	0.24	-0.07	0.12	0.14	0.08	0.05	-0.01	-0.05
MJT-C	0	-0.03	-0.17	0.02	-0.11	-0.02	-0.1	0	0.07	-0.23
MMSE	0.04	0.01	-0.15	0.08	0.01	0.05	0.01	-0.06	0.1	-0.03
Neuroticism-Volatility	0.11	-0.02	-0.03	-0.11	0.12	-0.1	0	0.23	0.09	-0.02
Neuroticism-Withdrawal	0.22	0.08	0.1	0.04	0.11	-0.02	-0.04	0.11	-0.06	0.05
NIHCog_PictureSeqREMOVE	0.03	-0.11	-0.03	0.18	0.26	0	0.25	-0.12	0.15	-0.06
NIHCog-DCCS	-0.04	0	0.04	0.1	-0.01	0.06	0.08	0.23	-0.14	-0.15
NIHCog-Flanker	-0.03	-0.01	0.08	0.11	-0.08	0.03	-0.07	0.11	0.02	0.05
NIHCog-List Sort	-0.02	0.07	-0.2	0.09	0.12	0.06	0.05	-0.01	0.07	-0.01
NIHCog-Pattern Comparison	0.02	0.02	-0.17	-0.1	-0.01	0.06	-0.09	-0.18	0.13	0.01
NIHCog-Picture Sequence	0.03	-0.1	-0.01	0.2	0.25	0	0.25	-0.11	0.15	-0.06
NIHCog-Reading Recognition	0.02	0.13	-0.2	0.11	-0.02	0.25	0.11	0.05	0.02	-0.03
NIHCog-Rey Immediate	0.03	0	-0.07	0.2	0.26	0.05	-0.04	-0.1	-0.18	-0.03
NIHEmo-Anger Affect	0.02	-0.05	0.03	-0.14	0.15	-0.04	-0.15	-0.02	-0.16	0.1
NIHEmo-Anger Hostility	0.16	-0.02	0.08	-0.11	0.17	-0.03	0.03	-0.04	-0.02	0.03
NIHEmo-Anger Physical Aggression	0.01	-0.06	-0.07	-0.23	0.1	-0.04	0.1	0.06	-0.02	0.17
NIHEmo-Emotional Support	-0.21	0	0.04	0.07	0.01	-0.04	-0.11	0.05	-0.05	-0.04
NIHEmo-Fear Affect	0.06	0.03	0.05	-0.04	0.15	-0.16	0.23	0.02	-0.07	-0.03
NIHEmo-Fear Somatic Arousal	0	0.05	-0.06	-0.11	0.21	0.01	-0.07	0.09	-0.08	0.06
NIHEmo-Friendship	-0.19	0.01	-0.02	-0.09	0.12	0.01	-0.12	0.04	-0.02	-0.09
NIHEmo-Instrumental Support	-0.13	-0.04	-0.05	0.01	0.01	0	0.03	0.28	-0.11	-0.04
NIHEmo-Life Satisfaction	-0.17	-0.02	-0.07	0.04	0.06	0.12	-0.06	-0.05	-0.03	0.08
NIHEmo-Loneliness	0.22	0.1	0.02	-0.06	-0.02	-0.02	0.03	-0.08	0.12	0.09
NIHEmo-Meaning and Purpose	-0.17	-0.05	0.11	-0.04	0.08	0.01	0.03	0.02	-0.16	0.07
NIHEmo-Perceived Hostility	0.09	0.07	-0.06	-0.19	0.09	0.22	0.03	0.18	0	0.05
NIHEmo-Perceived Rejection	0.18	0.04	-0.02	-0.17	0.06	0.12	0.03	0.08	0.13	0.01
NIHEmo-Perceived Stress	0.21	0.05	0.1	-0.06	0.04	-0.02	0.1	0.08	0.05	-0.03
NIHEmo-Positive Affect	-0.13	-0.04	0	-0.04	0.04	0.01	-0.1	-0.08	-0.16	0.12
NIHEmo-Sadness	0.04	-0.01	0.02	0.02	0.04	-0.15	0.07	-0.09	-0.14	-0.07
NIHEmo-Self Efficacy	-0.18	0.03	-0.08	-0.17	0.08	0.04	0.19	-0.06	-0.02	0
Openness-Intellect	-0.07	0.18	-0.19	-0.14	0	0.01	0.11	0.01	-0.14	-0.03
Openness-Openness	0	0.27	0.07	-0.06	-0.07	-0.08	-0.06	0.03	0	0.11
Reading the Mind in the Eye	-0.03	0.08	-0.12	0.13	0.16	0.03	-0.07	0.06	-0.08	-0.07
Rey Delay Test H-F	0.05	0.04	0.05	0.16	0.26	0.09	0.03	-0.04	-0.16	0
Ruminative Response Scale	0	-0.05	0.11	0.07	0.06	-0.06	0.08	-0.01	-0.14	0.06

SART Commission Error	-0.05	-0.04	0	0.2	0.03	-0.14	0.02	0.16	-0.03	0.11
SART Omission	0.02	0.06	0	-0.24	-0.06	0.13	-0.15	-0.09	0	-0.09
Satisfaction With Life Scale	-0.21	-0.05	-0.06	0.02	0.01	0.17	-0.08	0.03	0.01	0.04
SDMT Oral	-0.03	-0.06	-0.2	0.09	0.14	0	0.07	-0.19	0.11	-0.06
Shipley Blocks	0	-0.05	-0.13	0.16	0.13	-0.04	0	0.08	0.04	-0.11
Shipley Vocab	0.01	0.21	-0.2	0.03	0.05	0.19	0	-0.05	0	-0.01
SLCSR_Competence	0.04	0.11	-0.04	-0.16	0.08	-0.01	-0.07	0.05	-0.07	0.11
SLCSR-Liking	-0.09	0.01	-0.01	-0.11	-0.03	-0.01	0.3	0.12	-0.05	0.14
SNI-Network Diversity	0.01	0.08	-0.01	0.1	0.13	-0.07	-0.07	0.18	0.2	0.4
SNI-Network Size	0	0.1	-0.01	0.09	0.15	-0.07	-0.07	0.18	0.21	0.39
Spiritual Transcendence Inventory	-0.05	-0.04	0.24	-0.05	-0.03	0.23	0.09	0.16	0.09	0
SWBS-Existential	-0.22	-0.05	0.03	0	0.01	0.03	-0.08	0.03	0.1	0.07
SWBS-Religious	-0.05	-0.08	0.23	-0.05	-0.04	0.18	0.1	0.12	0.06	-0.02
TAS20-DDF	0.15	-0.12	0	0	0.04	0.2	-0.09	0.11	0.1	-0.09
TAS20-DIF	0.14	-0.03	-0.01	-0.05	0.11	0.11	-0.08	0.2	0.08	-0.15
TAS20-EOT	0.05	-0.25	-0.06	0.01	0.04	0.13	-0.07	0.02	0.08	-0.03
Toronto Empathy Questionnaire	-0.04	0.23	0.15	0.02	0.07	-0.11	0.06	0.07	-0.05	-0.08
Trails Test B-A	0.03	0.05	0.11	-0.09	-0.02	-0.08	-0.11	-0.19	0.12	0.15
UCLA Loneliness	0.23	0.06	0.01	-0.02	0	0.04	0.11	-0.06	0.03	0
Wisdom Scale-Affective	-0.08	0.18	0.15	0.09	-0.11	0.07	0.15	-0.06	0.13	-0.08
Wisdom Scale-Cognitive	-0.06	0.16	0.04	-0.01	-0.1	-0.12	0.29	-0.02	0.2	-0.01
Wisdom Scale-Reflective	-0.11	0.09	0.01	0.05	-0.15	0.12	0.19	-0.03	0.22	0.13

Behaviour PC Loadings (11-20)	**PC 11**	**PC 12**	**PC 13**	**PC 14**	**PC 15**	**PC 16**	**PC 17**	**PC 18**	**PC 19**	**PC 20**
Agreeableness-Compassion	0.12	0.03	-0.1	0.09	0.01	0.07	-0.09	0.05	-0.07	0.08
Agreeableness-Politeness	0.09	0.01	0.03	0.01	0.05	0.01	-0.01	0.12	-0.14	0.02
AI-External Density	0.09	0.08	0.19	-0.16	0.14	0.1	0.15	0.15	0.21	0.16
AI-Internal Density	0.1	0.03	0.19	-0.18	0.11	0.12	0.09	0.08	0.18	0.09
ART Fiction	0	0	0.12	-0.11	-0.11	-0.03	0	-0.1	0	-0.12
ART Nonfiction	0.05	0	0.01	-0.04	0.01	0.09	0.06	0.07	-0.07	-0.22
Beck Depression Inventory	-0.03	-0.01	0.02	0.16	-0.06	0.06	0.1	0.05	0.09	-0.01
BISBAS BAS-Drive	-0.05	0.02	0.12	0.02	0.12	-0.05	0.06	-0.12	-0.05	-0.03
BISBAS BAS-Fun	-0.09	0.31	0.11	0	0.13	-0.12	-0.06	-0.04	0.17	-0.03
BISBAS BAS-Reward	-0.13	0.05	0.14	0.06	0.14	0.05	-0.1	-0.16	0.19	-0.22
BISBAS BIS	-0.13	-0.11	0.33	0.01	0.05	0.03	-0.02	-0.08	0.12	0.02
Conscientiousness-Industriousness	0.09	-0.21	0.1	0.08	0.05	0.11	0	-0.04	-0.2	0.07
Conscientiousness-Orderliness	-0.13	-0.31	0.19	0.2	-0.03	0.01	0.07	-0.08	-0.16	0.18

Delayed Gratification	0.05	-0.09	0.02	0.11	-0.07	0.03	-0.11	0.17	-0.08	-0.13
ECR-R Anxiety	0.01	0.07	0.08	0.04	-0.02	-0.06	-0.04	-0.16	-0.01	0.05
ECR-R Avoidance	-0.05	0.12	-0.02	0.03	0.02	0.26	-0.09	-0.19	-0.21	0.07
Education	-0.08	0	0.06	0.04	-0.17	-0.16	-0.2	-0.15	0.01	-0.04
Extraversion-Assertiveness	-0.09	-0.07	-0.01	0.04	0.03	0.07	0.02	-0.11	-0.08	0.03
Extraversion-Enthusiasm	0.05	0.03	0.05	0	0.13	0.02	-0.12	0.11	-0.02	-0.05
IRI-Empathic Concern	-0.17	-0.03	-0.26	-0.18	-0.1	0.14	-0.02	0.06	0.08	0.02
IRI-Fantasy	-0.1	0.04	-0.05	-0.2	-0.04	0.06	-0.2	0.05	0.04	0.15
IRI-Personal Distress	0.04	0.13	0.04	-0.15	0.08	-0.01	0.12	-0.16	0.07	-0.08
IRI-Perspective Taking	-0.05	0.2	-0.05	-0.03	-0.06	-0.08	0.14	0.06	-0.02	0.06
ISEL-Appraisal	0.19	-0.03	0.13	-0.07	-0.06	0.1	0.18	0.25	-0.14	-0.02
ISEL-Belonging	0.2	0.1	0.04	-0.1	-0.05	0.09	0.02	0.03	-0.08	-0.01
ISEL-Self Esteem	-0.07	0.06	-0.08	-0.11	-0.13	0.18	-0.08	-0.06	-0.03	0.07
ISEL-Tangible	-0.13	0.03	0.1	-0.03	-0.09	0.01	0.08	0.21	-0.09	0.09
MFQ-Authority/Respect	-0.05	-0.12	0.02	0.06	-0.06	0.06	-0.13	0.05	0.18	-0.2
MFQ-Fairness/Repricrocity	0.01	-0.19	-0.14	0.04	-0.1	-0.14	0.15	-0.05	0.11	-0.05
MFQ-Harm/Care	-0.03	-0.1	-0.04	-0.03	-0.19	-0.06	-0.09	-0.04	0.14	0.05
MFQ-In Group Loyalty	0.02	-0.06	-0.05	0	0	0.06	-0.16	0.05	0.2	-0.15
MFQ-Purity/Sanctity	-0.01	-0.11	-0.05	-0.03	0.17	0.01	0.07	0	0.08	-0.09
MJT-C	0.04	-0.08	-0.04	0.23	-0.09	0.08	-0.11	0.06	0.25	-0.08
MMSE	0.08	-0.03	0.19	0.2	0.12	0.15	-0.18	-0.02	0.08	0.09
Neuroticism-Volatility	-0.04	-0.18	0.24	-0.2	-0.11	-0.06	0.05	-0.08	0	0.04
Neuroticism-Withdrawal	-0.03	-0.1	0.16	-0.01	-0.09	0	-0.02	0.03	0.07	0.01
NIHCog_PictureSeqREMOVE	0.11	0.07	-0.03	-0.01	-0.08	-0.21	-0.01	0.04	0.02	0.08
NIHCog-DCCS	0.05	0.03	0.16	0.01	0.05	0.01	-0.19	-0.05	-0.1	0.25
NIHCog-Flanker	0.08	0.1	0.14	0	-0.03	-0.11	-0.02	0.27	0.21	-0.03
NIHCog-List Sort	-0.04	-0.16	-0.09	-0.16	0.12	-0.1	-0.1	0.21	0.02	0
NIHCog-Pattern Comparison	-0.21	-0.2	-0.08	-0.03	-0.01	-0.2	-0.09	-0.11	-0.06	-0.08
NIHCog-Picture Sequence	0.09	0.06	-0.04	-0.03	-0.08	-0.23	0	0.06	-0.02	0.08
NIHCog-Reading Recognition	-0.01	-0.11	0.08	0.06	0.14	0.2	0.03	0.01	0.04	-0.03
NIHCog-Rey Immediate	0	0.03	-0.11	-0.08	0.1	-0.12	0.03	-0.14	-0.09	-0.09
NIHEmo-Anger Affect	-0.08	-0.17	-0.02	0	0.01	-0.1	0.15	0.19	-0.14	-0.11
NIHEmo-Anger Hostility	0.17	-0.11	0.09	0.17	-0.06	0.03	-0.08	0.07	-0.1	0.06
NIHEmo-Anger Physical Aggression	0.11	0.01	0.01	0.11	0.01	-0.26	-0.11	0.06	-0.11	0.06
NIHEmo-Emotional Support	0.15	-0.11	0.12	0.08	-0.01	-0.1	0.1	-0.02	0.06	-0.06
NIHEmo-Fear Affect	-0.09	-0.04	-0.03	-0.06	-0.2	0.27	0.04	-0.05	-0.13	0
NIHEmo-Fear Somatic Arousal	-0.22	0.1	-0.11	0.15	-0.08	-0.1	-0.13	0.18	-0.1	0.05
NIHEmo-Friendship	0.27	0.05	0.04	0.06	-0.05	0.07	0.04	-0.04	-0.11	-0.04
NIHEmo-Instrumental Support	0.04	-0.04	0.06	0.02	-0.09	-0.25	0.17	0.01	0.09	0.1

NIHEmo-Life Satisfaction	-0.15	0.11	0.1	-0.11	-0.16	-0.01	0.17	-0.19	-0.02	-0.05
NIHEmo-Loneliness	-0.09	0.02	0.04	-0.03	0.06	0.01	-0.03	0.05	0.06	0.01
NIHEmo-Meaning and Purpose	-0.17	0.04	0.01	0.14	-0.1	0.15	0.02	-0.05	0.06	0.12
NIHEmo-Perceived Hostility	0.14	0.11	0.03	-0.06	0	-0.02	-0.15	0.02	0	-0.11
NIHEmo-Perceived Rejection	0.01	0.04	-0.07	0.01	0.04	0.03	-0.14	0.09	-0.08	-0.07
NIHEmo-Perceived Stress	0.07	-0.12	0.07	0.03	0.01	0.05	0.01	0.04	-0.03	-0.12
NIHEmo-Positive Affect	0.01	0.19	-0.03	0.1	-0.14	0.04	-0.2	-0.06	0.04	0.23
NIHEmo-Sadness	-0.07	0.06	-0.09	0.22	-0.16	0.2	0.31	0.16	0.14	0.08
NIHEmo-Self Efficacy	-0.08	-0.02	-0.03	0.06	-0.02	0	0.05	-0.13	0.05	0.12
Openness-Intellect	0.03	-0.01	-0.14	0.01	0.18	0.01	0.07	-0.18	0.01	0.02
Openness-Openness	-0.09	0.11	-0.05	0.06	0.08	-0.03	-0.02	0.04	-0.01	0.1
Reading the Mind in the Eye	-0.07	-0.05	0.07	0.23	0.11	-0.14	-0.06	-0.08	-0.08	0.06
Rey Delay Test H-F	0.05	0.03	-0.14	-0.01	-0.03	-0.02	0.13	-0.16	-0.09	-0.19
Ruminative Response Scale	0.24	0.27	0.04	0.12	0.05	-0.04	-0.08	-0.18	-0.07	-0.16
SART Commission Error	-0.19	0.08	0.01	0.16	0.27	0.06	0.07	0.06	-0.16	-0.17
SART Omission	0.27	-0.17	-0.07	-0.03	-0.12	-0.08	0.02	-0.13	0.15	0.18
Satisfaction With Life Scale	-0.13	0.06	-0.02	0.01	-0.1	-0.05	0.06	0	0.12	-0.05
SDMT Oral	-0.01	-0.01	-0.02	-0.09	-0.05	0.1	-0.08	0.08	0.06	-0.2
Shipley Blocks	0.01	0	-0.15	0.19	0.16	-0.02	-0.09	-0.01	0.22	0.22
Shipley Vocab	-0.08	0.06	0.11	0.09	0.11	-0.01	0.05	0.05	0	-0.02
SLCSR_Competence	0.01	-0.01	-0.12	0.27	0.11	-0.02	0.03	0.11	0.16	-0.08
SLCSR-Liking	-0.06	0.01	0.17	0.01	-0.07	0.05	-0.11	-0.03	-0.03	-0.22
SNI-Network Diversity	0.14	-0.12	-0.15	0.06	-0.02	0.12	0.02	-0.15	0.12	0.01
SNI-Network Size	0.15	-0.13	-0.16	0.05	-0.02	0.11	0.01	-0.14	0.11	-0.01
Spiritual Transcendence Inventory	0	-0.01	-0.12	-0.04	0.25	-0.02	0.07	-0.03	-0.04	0.09
SWBS-Existential	-0.11	-0.08	-0.03	-0.03	0.07	-0.01	-0.11	0.08	0.08	-0.04
SWBS-Religious	-0.1	-0.03	-0.04	-0.03	0.31	-0.03	0.12	0.05	-0.03	0.16
TAS20-DDF	-0.02	0.19	0	0.12	-0.11	0.04	0.18	-0.07	0.07	-0.02
TAS20-DIF	-0.01	0.13	-0.02	0.15	-0.11	0.06	0.14	0.01	-0.04	0.09
Toronto Empathy Questionnaire	-0.1	0.05	0.08	0	-0.11	0.18	-0.12	0.04	0.01	-0.04
Trails Test B-A	0.01	-0.06	0.06	-0.12	-0.07	-0.04	-0.19	0.02	-0.04	0.04
UCLA Loneliness	-0.14	0.05	0.09	0.19	-0.17	-0.16	0.06	0.08	-0.12	-0.13
Wisdom Scale-Affective	-0.1	0.01	0.06	-0.05	0.02	0.02	0.05	0.03	-0.01	0.16
Wisdom Scale-Cognitive	0.13	0.12	-0.07	0.13	-0.12	0.01	-0.05	0.11	-0.12	-0.04
Wisdom Scale-Reflective	0.05	0.02	0.04	0.11	-0.03	-0.02	0.14	-0.11	0.1	-0.14

Abbreviations. *PC, principal component; AI, Autobiographical Interview; ART, Author Recognition Task; BISBAS, Behavioural Inhibition System Behavioral Activation System; ECR, Experience in Close Relationships; IRI, Interpersonal Reactivity Index; ISEL, Interpersonal Support Evaluation List; MFQ, Mood and Feelings Questionnaire; MJT, Moral Judgement Task; MMSE,*

Mini-Mental State Examination; NIH, National Institute of Health; SART, Sustained Attention to Response Task; SDMT, Symbol Digit Modalities Test; SLCSR, Self-Liking/Competence Scale Revised; TAS, Toronto Alexithymia Scale; DDF, Difficulty Describing Feelings; DIF, Difficulty Identifying Feelings; EOT, Externally-Oriented Thinking; UCLA, University of Los Angeles.

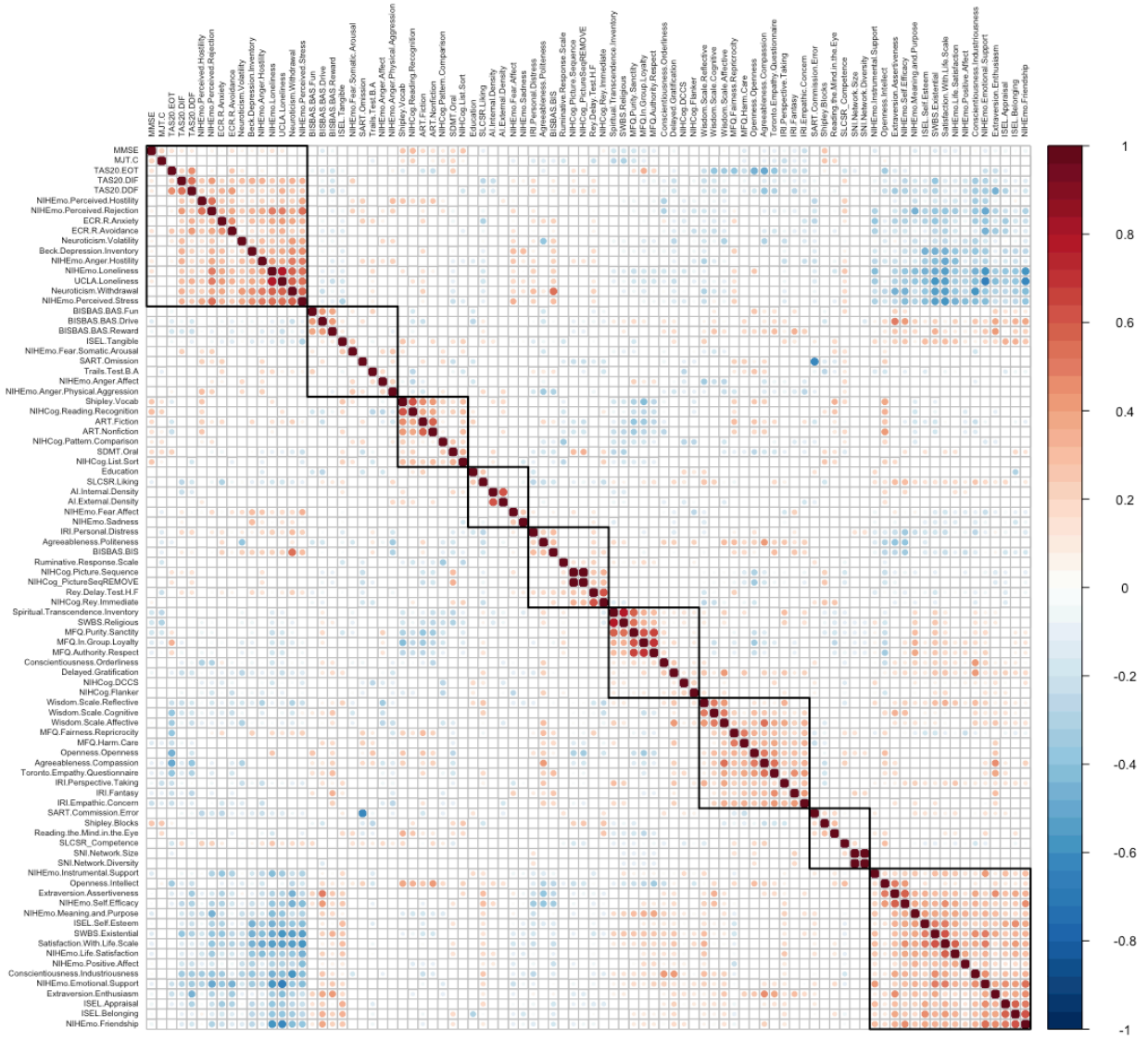

Supplementary Figure 1. Pearson's correlations (r) between all of the included behavioural measures. Correlations are thresholded at $p<0.05$ and ordered based on hierarchical clustering.

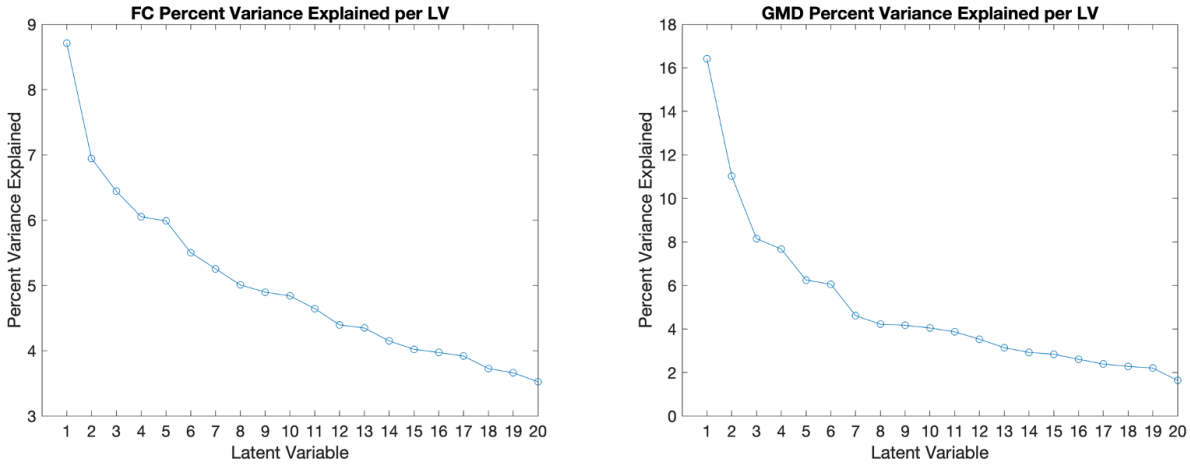

Supplementary Figure 2. Scree plots for each PLS analysis indicating the percent variance explained for each latent variable.

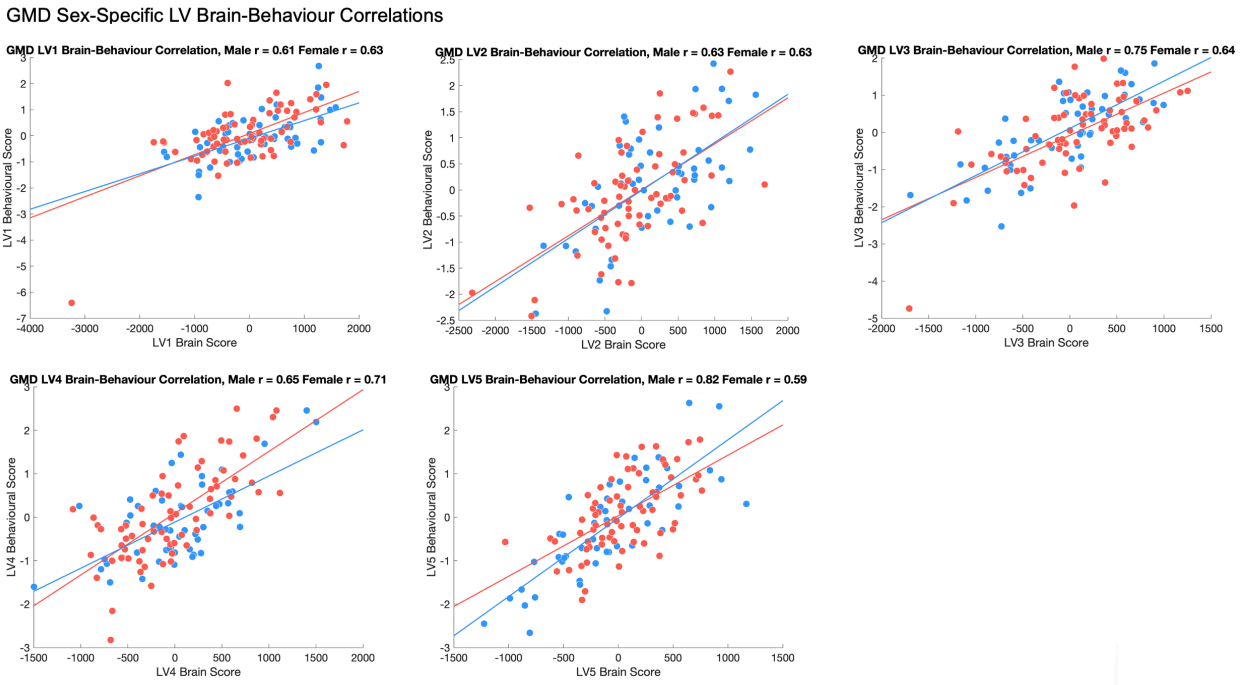

Supplementary Figure 3. Sex-specific correlations for the GMD-behaviour PLS analysis. Correlations are between subject-level neural ('brain scores') and behavioural ('behaviour scores') latent variable loadings. No statistically significant sex differences were found ($p < 0.05$). Red = female, blue = male.

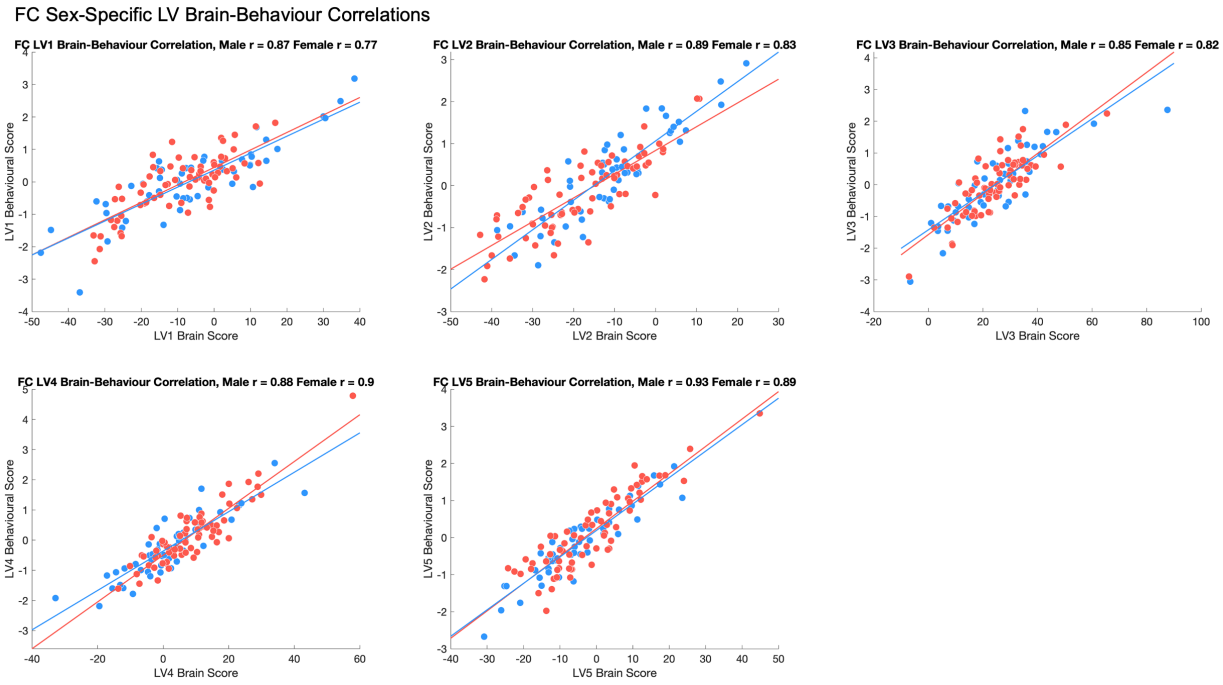

Supplementary Figure 4. Sex-specific correlations for the FC-behaviour PLS analysis. Correlations are between subject-level neural ('brain scores') and behavioural ('behaviour scores') latent variable loadings. No statistically significant sex differences were found ($p < 0.05$). Red = female, blue = male.

Appendix C: Supplemental Material to: "Serotonergic psychedelic drugs reduce the functional differentiation of the default network from sensory cortices"

Supplementary Methods

Neuroimaging Data Acquisition

LSD. Neuroimaging data from an already published dataset (Carhart-Harris, Muthukumaraswamy, et al., 2016) was used for the present analyses. The data acquisition and preprocessing details have been described in detail elsewhere (Carhart-Harris, Muthukumaraswamy, et al., 2016); we outline them in brief here. Subjects participated in two scanning days that were separated by 14 days and which each featured three 7-minute resting-state fMRI scans. On a given scanning day, subjects received either a placebo (10ml saline) or LSD (75 µg) via a bolus intravenous injection. The low-moderate LSD dosage was selected to minimize the potential for intra-scanner anxiety while

ensuring drug effects (Johnson et al., 2008). The order of the conditions was balanced across participants; participants were blind to this order, but the researchers and those analyzing the data were not. The scans on each of the days were as follows: (1) resting-state eyes-closed with no music, (2) resting-state eyes-closed with music, (3) resting-state eyes-closed with no music. Scans featuring no music (scans 1 and 3) were used in the present analyses.

Resting-state BOLD fMRI data were acquired using a gradient echo planar imaging sequence, TR/TE = 2000/35ms, FoV = 220mm, 64×64 acquisition matrix, parallel acceleration factor = 2, 90◦ flip angle. Thirty-five oblique axial slices were acquired in an interleaved fashion, each 3.4mm thick with zero slice gap (3.4mm isotropic voxels). Structural T1w images were acquired on a 3T GE HDx system. These were 3D fast spoiled gradient echo scans in an axial orientation, with field of view = 256 × 256 × 192 and matrix = 256 × 256 × 20 192 to yield 1mm isotropic voxel resolution. TR/TE = 7.9/3.0ms; inversion time = 450ms; flip angle = 20°.

Psilocybin. Neuroimaging data from an already published dataset (Carhart-Harris et al., 2012) was used for the present analyses. The data acquisition and preprocessing details have been described in detail elsewhere (Carhart-Harris et al., 2012) ; we outline them in brief here. Subjects participated in two scanning days that were separated by 14 days and which each featured one 12-minute resting-state scan. Infusion began at 6 minutes following the start of the scan. The post-infusion half of the scan for each condition was used in the present analyses.

Resting-state BOLD fMRI data were acquired using a gradient echo planar imaging sequence, TR/TE 3000/35 ms, field-of-view = 192 mm, 64 × 64 acquisition matrix, parallel acceleration factor = 2, 90° flip angle. Fifty-three oblique- axial slices were acquired in an interleaved fashion, each 3 mm thick with zero slice gap (3 × 3 × 3-mm voxels). A total of 240 volumes were acquired.

Subjective Measures. Subjects completed a number of intra-scanner visual analogue scale (VAS) ratings at the end of each scan for each dataset, reporting on different facets of the psychedelic experience (Carhart-Harris, Muthukumaraswamy, et al., 2016). In addition, subjects completed the 11-factor altered states of consciousness (ASC) questionnaire (Dittrich, 1998; Studerus et al.,

2010) at the end of each scan day. In the present study, we conducted brain-behaviour analysis with two self-report measures which relate to core components of the psychedelic experience: ego dissolution (“I experienced a disintegration of my 'self' or 'ego”) and complex imagery (a composite of “I could see images from my memory or imagination with exceeding clarity”, “I saw whole scenes in complete darkness or with closed eyes”, and “My imagination was extremely vivid”). The former measure was an intra-scanner VAS rating, while the latter measures were ASC measures conducted at the end of the scan day.

Supplementary Figures

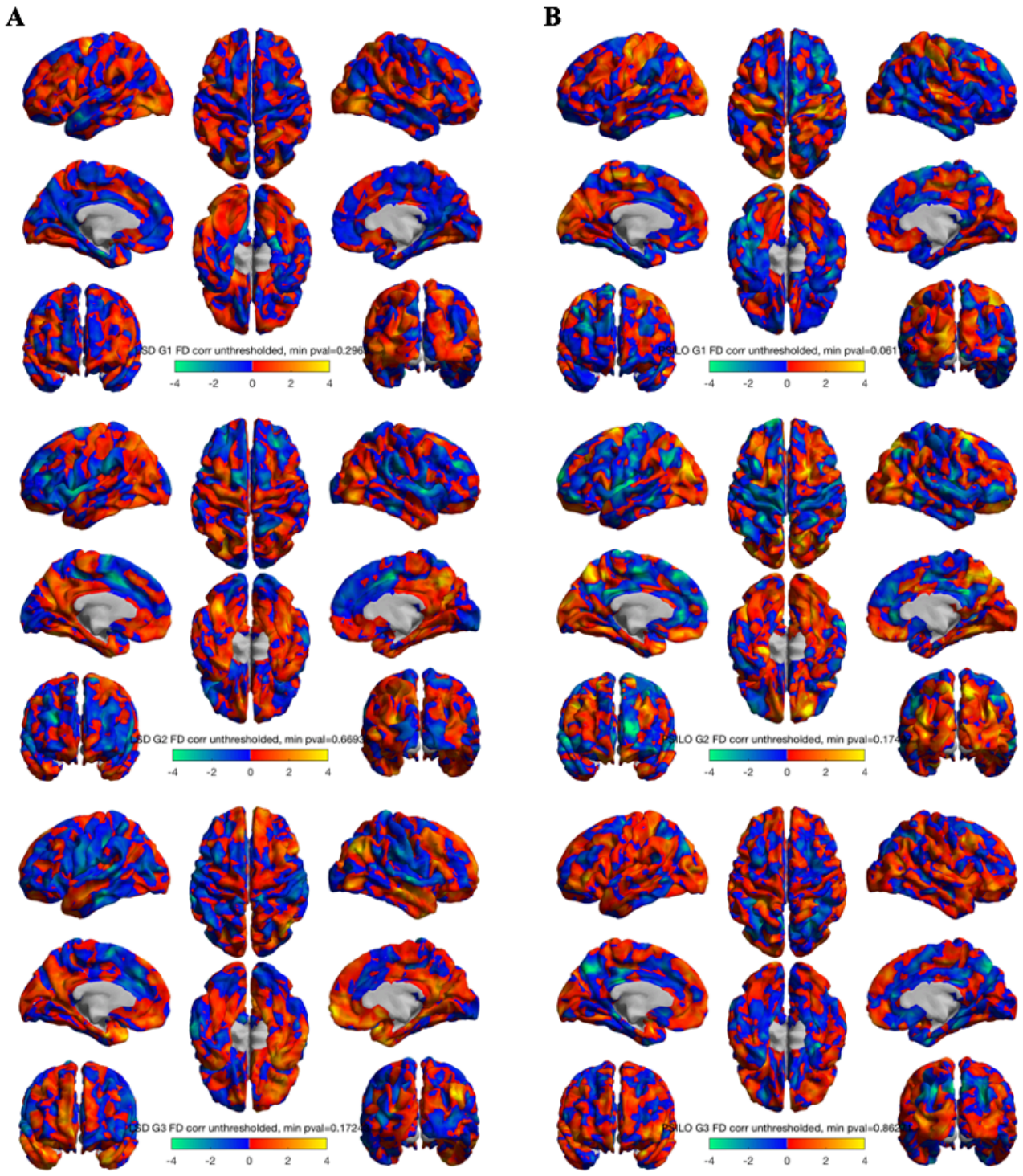

Supp. Figure 1. Unthresholded correlations between difference in mean frame-wise displacement and difference in vertex-wise gradient scores, for each of (A) LSD-Placebo and (B) Psilocybin-

Placebo contrasts. No significant correlations were found. (Top) principal gradient, (Middle) second gradient, (Bottom) third gradient.